UNIVERSITÉ DU QUÉBEC À TROIS-RIVIÈRES

DÉCOUVERTE ET INGÉNIERIE MÉTABOLIQUE DE LA BIOSYNTHÈSE DES ALCALOÏDES AMARYLLIDACEAE DANS *NICOTIANA BENTHAMIANA*

DISCOVERY AND METABOLIC ENGINEERING OF AMARYLLIDACEAE ALKALOID BIOSYNTHESIS IN *NICOTIANA BENTHAMIANA*

THÈSE PRÉSENTÉE

COMME EXIGENCE PARTIELLE DU

DOCTORAT EN BIOLOGIE CELLULAIR ET MOLÉCULAIRE

PAR

BASANTA LAMICHHANE

Mai 2026

Avertissement

L'auteur de ce mémoire ou de cette thèse a autorisé l'Université du Québec à Trois-Rivières à diffuser, à des fins non lucratives, une copie de son mémoire ou de sa thèse.

Cette diffusion n'entraîne pas une renonciation de la part de l'auteur à ses droits de propriété intellectuelle, incluant le droit d'auteur, sur ce mémoire ou cette thèse. Notamment, la reproduction ou la publication de la totalité ou d'une partie importante de ce mémoire ou de cette thèse requiert son autorisation.

UNIVERSITÉ DU QUÉBEC À TROIS-RIVIÈRES

Biologie cellulaire et moléculaire (Doctorat)

Direction de recherche:

Isabel Desgagné-Penix, Ph. D	Université du Québec à Trois-Rivières
Prénom et nom	Directeur de recherche

Co-direction de recherche:

Hugo Germain, Ph. D	Université du Québec à Trois-Rivières
Prénom et nom	Co-directeur de recherche

Jury d'évaluation

Isabel Desgagné-Penix, Ph. D	Directeur de recherche
Prénom et nom	Fonction du membre de jury
Hugo Germain, Ph. D	Co-directeur de recherche
Prénom et nom	Fonction du membre de jury
Marc Germain, Ph. D	Évaluateur interne
Prénom et nom	Fonction du membre de jury
Yang Qu, Ph. D	Évaluateur externe
Prénom et nom	Fonction du membre de jury
Quentin Dudley, Ph. D	Évaluateur externe
Prénom et nom	Fonction du membre de jury

In memory of beloved father Late Rajendra P. Lamichhane

"प्रिय बुबा स्वर्गीय राजेन्द्र प्र. लामिछानेको स्मृतिमा समर्पित"

ACKNOWLEDGEMENTS

I would like to express my sincere gratitude to my supervisor, **Professor Isabel Desgagne-Penix**, for her invaluable support, guidance, and mentorship throughout my doctoral studies. Her expertise, constructive feedback, and encouragement have been instrumental in shaping my research and professional development.

I am also deeply thankful to my co-supervisor, **Professor Hugo Germain**, for his support, guidance, and suggestions throughout my study. His expertise and insights have greatly contributed to the success of this work.

I am profoundly grateful to **Dr. Natacha Merindol**, whose unwavering support, insightful guidance, and boundless patience have been a beacon of light during the most challenging phases of my research journey. Her invaluable contributions have not only enriched the quality of this work but have also shaped me into a more resilient and knowledgeable researcher.

A special acknowledgment is reserved for **Sarah-Eve Gélinas**, whose meticulous attention and resolute dedication in co-working and analyzing the samples have significantly contributed to the depth and precision of this study.

I would like to extend gratitude to **Fatma Meddeb** for her technical and administrative support during my time in the lab along with **Mélodie B. Plourde** for teaching basic laboratory techniques.

I am grateful to all my colleagues and senior researchers who played a vital role in the completion of my research project.

I am thankful to my family for encouragement throughout my Ph.D. journey. I would like to thank my love of life, my wife, **Archana Niraula**, for keeping me motivated and inspired throughout my Ph.D. Especial thanks to my 5 years old and super understanding daughter **Mokshyada Bella Lamichhane**, joining me in lab in weekends and inspiring me with inquisitive questions of science. I extend my deepest gratitude to my mother, **Sushila Lamichhane**, whose unwavering support was the ground beneath my feet and the warmth that carried me through the winter of Canada. I am equally thankful to my brothers, **Shishir** and **Saroj Lamichhane**, who stood beside me like unshakable peak- Mount Everest, shielding me from the harsh winds of doubt and the storms of financial and emotional uncertainty. Their steadfast presence has been my refuge throughout this journey. I extend my heartfelt gratitude to my grandfather, **Ramji P. Lamichhane**, and my uncles and aunts, **Mukunda**, **Prabin**, and **Prashant Lamichhane**, along with my whole family, whose constant communication, mental encouragement, and emotional support have been invaluable throughout my journey.

I feel myself lucky and blessed to have you all during my PhD and you all will be in my deep memory throughout my life.

RÉSUMÉ EN FRANÇAIS

Les alcaloïdes d'Amaryllidaceae (AA) constituent un groupe d'alcaloïdes structurellement divers, isolés de plantes de la famille des Amaryllidaceae. Ils présentent un potentiel pharmacologique très varié et prometteur. La galanthamine est le seul AA produit commercialement, utilisé pour traiter les symptômes légers de la maladie d'Alzheimer. La lycorine, un autre AA, est largement étudiée pour ses puissantes propriété anticancéreuses et antivirales. Leur faible concentration dans les plantes sauvage et la complexité de leur synthèse chimique expliquent la rareté de ces alcaloïdes sur le marché. Leur biosynthèse se fait à partir de la 4′O-méthylnorbelladine (4′OM), elle même produite par condensation de la tyramine et du 3,4-dihydroxybenzaldéhyde (3,4-DHBA) par la norbelladine/norcraugsodine synthase (NBS) et la noroxomaritine/norcraugsodine réductase (NR), puis enfin méthylée par une 4′*O*-méthyltransférase (4′OMT). Les cytochromes P450 de type CYP96 génèrent à partir de la 4′OM une diversité structurale en réalisant trois types de couplage C-C conduisant aux noyaux lycorine, galanthamine et crinine. Bien que certaines enzymes aient été caractérisées, la voie complète n'a jamais été reconstituée et plusieurs étapes restent hypothétiques, notamment en ce qui concerne les différents couplages phénoliques. Nous avons réalisé un profilage métabolique de la Nivéole d'été (*Leucojum aestivum*), confirmant la présence de divers alcaloïdes pharmacologiquement importants. Une recherche d'exploration du transcriptome basée sur l'homologie, une analyse du repliement *in silico* et des études de localisation ont permis d'identifier des gènes candidats. *La*NBS et *La*NR agroinfiltrés ont catalysé la condensation de la tyramine et du 3,4-DHBA en norbelladine *in vivo* chez *Nicotiana benthamiana*. La norbelladine a ensuite été méthylée en 4′OM par *La*4′OMT. La 4′OM a subi un couplage au phénol pour produire tous les produits *ortho-para′*, *para-ortho′* et *para-para′* par *La*CYP96T1 et *La*CYP96T2, qui ont été ensuite réduits par *La*NRII en norgalanthamine, normaritidine, oxomaritinamine et norpluviine comme déterminé par spectrométrie de masse en tandem à haute résolution. Le couplage *para-ortho′* C–C médié par le cytochrome P450 convertit la 4′OM en *N*-déméthylnarwédine. À partir de là, deux voies distinctes ont été proposées : (i) réduction en norgalanthamine, suivie d'une *N*-méthylation pour former de la galanthamine, ou (ii) *N*-méthylation en narwédine, qui est ensuite réduite en galanthamine. Pour élucider ces étapes clés de la *N*-méthylation, nous avons identifié trois candidats *N*-méthyltransférase (NMT) du transcriptome de *Leucojum aestivum* : deux appartenant à la famille des gamma-tocophérol méthyltransférases (TMT) et un à la famille des NMT de la coclaurine. La caractérisation

fonctionnelle chez *Nicotiana benthamiana*, par agroinfiltration avec *La*TMT1, *La*TMT2 et *La*NMT, ainsi que la *N*-déméthylnarwédine ou la norgalanthamine, a démontré que *La*TMT2 était l'enzyme la plus efficace catalytiquement, capable de catalyser à la fois la *N*-méthylation de la *N*-déméthylnarwédine en narwédine et de la norgalanthamine en galanthamine. L'analyse *in vitro* de *La*TMT2 a révélé une préférence pour le substrat de la norgalanthamine par rapport à la nornarwédine. Ces résultats identifient *La*NBS, *La*NRII, *La*N4´OMT, *La*CYP96T1/T2 et *La*TMT2 comme des enzymes clés impliquées dans les multiples étapes de la biosynthèse de la galanthamine, offrant ainsi de nouvelles perspectives sur les voies métaboliques des AA et des stratégies potentielles pour améliorer la production de galanthamine par ingénierie métabolique.

Mots-clés: Métabolites spécialisés, norbelladine, méthyltransférase, cytochrome, couplage phénol

Abstract

Amaryllidaceae alkaloids (AAs) are a group of structurally diverse alkaloids isolated from plants of the Amaryllidaceae family. They display a wide range of vivid pharmacological potential. Galanthamine is the only commercially produced AA, used to treat mild symptoms of Alzheimer's disease. Lycorine is extensively studied for its strong anti-cancer and antiviral activities. As their amount is low in native plants and total chemical synthesis is challenging, the commercial availability of these alkaloids is scarce. Biogenetically, they are formed from 4′*O*-methylnorbelladine (4′*O*M), which is produced by the condensation of tyramine and 3,4-dihydroxybenzaldehyde (3,4-DHBA) by norbelladine/norcraugsodine synthase (NBS) and noroxomaritine/norcraugsodine reductase (NR) and methylated by a 4′*O*-methyltransferase (4′*O*MT). Cyp96-type cytochromes P450 generate structural diversity from 4′*O*M by performing three types of C-C coupling leading to lycorine, galanthamine and crinine cores. Although some enzymes have been characterized, the full pathway has never been reconstituted and several steps remain hypothetical, especially with regards to the different phenol couplings. We performed a metabolic profiling of summer snowflake *(Leucojum aestivum*), confirming the presence of various pharmacologically important alkaloids. Homology-based transcriptome-mining search, *in silico* folding analysis and localization studies enabled the identification of candidate genes. Agroinfiltrated *La*NBS and *La*NR catalyzed the condensation of tyramine and 3,4-DHBA into norbelladine *in vivo* in *Nicotiana benthamiana.* Norbelladine was further methylated into 4′*O*M by *La*4′*O*MT. 4′*O*M underwent phenol coupling to yield all *ortho-para′*, *para-ortho′* and *para-para′* products by *La*CYP96T1 and *La*CYP96T2, which were further reduced by *La*NRII into norgalanthamine, normaritidine, oxomaritinamine, and norpluviine as determined by high-resolution tandem mass spectrometry. Cytochrome P450-mediated *para-ortho′* C–C coupling

converts 4´OM into *N*-demethylnarwedine. From there, two distinct routes have been proposed: (i) reduction to norgalanthamine, followed by *N*-methylation to form galanthamine, or (ii) *N*-methylation to narwedine, which is subsequently reduced to galanthamine. To elucidate these key *N*-methylation steps, we identified three *N*-methyltransferase (*NMT*) candidates from the transcriptome of *Leucojum aestivum*: two belonging to the gamma-tocopherol methyltransferase (GTMT) family and one to the coclaurine NMT family. Functional characterization in *Nicotiana benthamiana*, using agroinfiltration with *LaTMT1*, *LaTMT2*, and *LaNMT*, along with *N*-demethylnarwedine or norgalanthamine, demonstrated that *La*TMT2 was the most catalytically efficient enzyme, capable of catalyzing both the *N*-methylation of *N*-demethylnarwedine to narwedine and norgalanthamine to galanthamine. *In vitro* analysis of *La*TMT2 revealed a substrate preference for nornarwedine over norgalanthamine. These findings identify *La*NBS, *La*NRII, *La*N4´OMT, *La*CYP96T1/T2, and *La*TMT2 as key enzymes involved in multiple steps of galanthamine biosynthesis, offering new insights into AA metabolic pathways and potential strategies for enhancing galanthamine production through metabolic engineering.

Keywords: Specialized metabolites, norbelladine, methyltransferase, cytochrome, phenol coupling

Table of Contents

ACKNOWLEDGEMENTS iv
RÉSUMÉ EN FRANÇAIS v
Abstract vii
List of abbreviations xv
Chapter I 1
1. General Introduction 2
1.1 Alkaloids 2
1.2 Classification of alkaloid 3
1.2.1 Isoquinoline alkaloids 6
1.2.2 Benzylisoquinoline alkaloids (BIA) 7
1.2.3 Amaryllidaceae alkaloids (AAs) 9
1.3 Biological importance of Amaryllidaceae alkaloids 10
1.4 Classification of Amaryllidaceae Alkaloids 13
1.5 Biosynthesis Amaryllidaceae Alkaloids 14
1.6 Enzymatic Players in Amaryllidaceae Alkaloid Biosynthesis: Insights from Benzylisoquinoline Pathways 18
1.7 Metabolic engineering 22
1.8 *Nicotiana benthamiana* as metabolic engineering platform 23
Importance, hypothesis, and objectives 25
Chapter II 27
2.1. Abstract 29
2.2. Introduction 30
2.3. Materials and Methods 32
2.3.1. Database of Amaryllidaceae transcriptomes 32
2.3.2. Phylogenetic analysis 34
2.3.3. Molecular modelling 35
2.3.4. RNA extraction and cDNA synthesis 36
2.3.5. PCR amplification of key candidate genes LaNBS, LaNRII, LaN4´OMT, LaCYP96T1 and LaCYP96T2. 37
2.3.6. Cloning and transformation 38

2.3.7. Transient expression of candidate genes in *N. benthamiana* (*in vivo* assay) 38
2.3.8. Protein expression, and purification.....40
2.3.9. *In vitro* enzymatic assay 41
2.3.10. Thermal unfolding analysis using nanoDSF.....42
2.3.11. Sample preparation for metabolite analysis 42
2.3.12. Instrumentation and chromatographic conditions 43
2.3.13. Subcellular localization study 43
2.4. Results.....44
2.4.1. *In silico* characteristics of pathway candidates 44
2.4.2. Localization assay.....48
2.4.3. Reconstitution of the foundation steps of the AA pathway to produce 4´O-methylnorbelladine *in vivo*.....49
2.4.4. Multiple C-C phenol couplings by a single CYP96T 52
2.4.5. Multiple reduction steps by LaNRII.....55
2.4.6. Full pathway reconstitution with four enzymes 56
2.5. Discussion.....56
2.6. Conclusion 62
2.7. Short legends for Supplementary Information 64
2.9. Supplementary Figures 72
2.10. Supplementary Tables 88
Chapter III.....114
3.1. SUMMARY 116
3.2. Introduction.....117
3.3. Results.....121
3.3.1. Identification and phylogeny of *N*-methyltransferase candidates 121
3.3.2. Identification and phylogeny of aldo-keto reductase candidates.....123
3.3.3. Leaf-specific AA biosynthesis and relative expression of candidate genes in *L. aestivum* 124
3.3.4. *La*TMT1, *La*TMT2, and *La*NMT localize in distinct compartments 126
3.3.5. Docking supports promiscuous biosynthetic machinery from *N*-methylation to carbonyl reduction 128
3.3.6. *La*TMT2 exhibits superior catalytic activity *in vitro* and *in vivo* 130
3.3.7. *La*TMT1 is a putative classical tocopherol methyltransferase.....132

3.3.8. *La*AKR isoforms catalyze reversible redox interconversion 133
3.4. Discussion 136
3.5. Conclusion 140
3.6. Materials and methods 142
3.6.1. Identification of candidates and phylogenetic analysis and Multiple Sequence Alignment 142
3.6.2. Molecular modelling of *La*NMT, *La*TMT1, *La*TMT2, *La*AKR1, *La*AKR2, and *La*AKR3 142
3.6.3. RNA extraction and cDNA synthesis 143
3.6.4. PCR amplification of key candidate genes and RT-qPCR gene expression analysis. 143
3.6.5. Cloning and *Agrobacterium* transformation for *in vivo* characterization 144
3.6.6. Confocal image acquisition 145
3.6.7. Cloning, transformation, and protein purification for *in vitro* characterization ..145
3.6.8. *In vitro* enzymatic assay 146
3.6.9. Transient expression of candidate genes in *N. benthamiana* (*in vivo* assay) 147
3.6.10. Western blotting 148
3.6.11. Substrates and standards preparation 148
3.6.12. Sample preparation for metabolite analysis. 150
3.6.13. Metabolite screening in *Leucojum aestivum* leaf 150
3.6.14. Instrumentation and chromatographic conditions 151
3.6.15. Statistical analysis 152
3.7. References 154
3.8. Supplementary Tables 158
3.9. Supplementary Figures 186
Chapter IV 199
4.1 Overall Discussion 200
4.2 Conclusion 216
4.3 Perspectives 217
4.4 References 219
Annex 1; Research Paper (Co-authorship) 231
Annex 2; Research Paper (Co-authorship) 232
Annex 3; Research Paper (Co-authorship) 233

Annex 4; Research Paper (Co-authorship).....234

List of Figures

Figure 1.1: Overview of pathways of four groups of isoquinoline alkaloids.....8
Figure 1.2 : Biological importance of Amaryllidaceae alkaloids 11
Figure 1.3: Types of Amaryllidaceae alkaloids (Desgagné-Penix, 2021) 14
Figure 1.4: BIA and AA with major class of enzymes.....21
Figure 2.1. Proposed alkaloid biosynthesis pathway in Leucojum *aestivum*. 32
Figure 2.2. Subcellular localization of LaN4´OMT and LaCYP96T1 proteins in *Nicotiana benthamiana* leaves. 49
Figure 2.3. Reconstitution of the foundation steps of the Amaryllidaceae alkaloid pathway to produce 4´-*O*-methylnorbelladine *in vivo*. 51
Figure 2.4. Reconstitution of the branching pathway steps to produce Amaryllidaceae alkaloids *in vivo*.....54
Figure 2.S1. Phylogenetic analysis, multiple sequence alignment and folding of *La*NBS.....73
Figure 2.S2. Phylogenetic analysis, multiple sequence alignment and folding of *La*NRII.....74
Figure 2.S3. Phylogenetic analysis, multiple sequence alignment and folding of *La*N4´OMT. 75
Figure 2.S4. Phylogenetic analysis, multiple sequence alignment and folding of *La*CYP96T1 and *La*CYP96T2. 76
Figure 2.S5. Cellular localization of *La*N4ˈOMT and *La*CYP96T2.....77
Figure 2.S6. Western blot, SDS gel and RT-qPCR analysis 78
Figure 2.S7. HPLC-MS/MS chromatograms of norbelladine and 4´-*O*-methylnorbelladineand *in vitro* detection. 79
Figure 2.S8. Docked structures of candidates *La*CYP96T and *La*NRII.....80
Figure 2.S9. HPLC-MS/MS analysis of *N*-demethylnarwedine, produced upon transient expression of *LaCYP96T1* with 4´-*O*-methylnorbelladineas substrate.....81
Figure 2.S10. HPLC-MS/MS analysis of noroxomaritidine, produced upon transient expression of *LaCYP96T1* with 4´-*O*-methylnorbelladineand *in vitro*.....82
Figure 2.S11. HPLC-MS/MS analysis of oxomaritinamine, produced upon transient expression of *LaCYP96T1* with 4´-*O*-methylnorbelladineas substrates. 83
Figure 2.S12. HPLC-MS/MS analysis of norpluviine produced upon transient co-expression of *LaCYP96T1 and LaNRII* with 4´-*O*-methylnorbelladineas substrates in *N. benthamiana* and *in vitro.* 84
Figure 2.S13. HPLC-MS/MS chromatograms of the *ortho- para'* product lycorine, that was produced upon transient co-expression of *LaCYP96T1* and *LaNRII* with 4´-*O*-methylnorbelladinein *N. benthamiana.* ..85
Figure 2.S14. HPLC-MS/MS chromatograms of the *para- para'* product normaritidine, that was produced upon transient co-expression of *LaCYP96T1 and LaNRII* with 4´-*O*-methylnorbelladinein *N. benthamiana.*.....86
Figure 2.S15. The elucidated alkaloid biosynthesis pathway in *Leucojum aestivum* in this study. 87
Table 2.S2. The accession numbers of the sequences used for phylogenetic analysis for respective protein sequence. 89
Figure 3.1. Proposed galanthamine biosynthetic pathway from 4'-*O*-methylnorbelladine.....120
Figure 3.2. Phylogenetic analysis and sequence alignment of *N*-methyltransferase candidates in Amaryllidaceae alkaloid biosynthesis.....123
Figure 3.3. Tissue-specific expression analysis of genes encoding enzymes involved in galanthamine biosynthesis in *Leucojum aestivum*.....126
Figure 3.4. Subcellular localization of *La*TMT1, *La*TMT2 and *La*NMT proteins in *Nicotiana benthamiana*. 127
Figure 3.5. Docking poses and active site interactions of norgalanthamine within the predicted structures of *N*-methyltransferase candidates.....130
Figure 3.6. *In vitro* and *in vivo* enzymatic assay by candidate N-methyltransferases. 132
Figure 3.7. Reductive and oxidative activities of AKR enzymes in late stage of galanthamine pathway. 134
Figure 3.8. Identified biosynthetic pathway leading to galanthamine. 135
Figure 3.S1. Structural comparison of N-methyltransferase candidates with the reference coclaurine N-methyltransferase (CNMT) from *Coptis japonica* (PDB: 6GKV). 187
Figure 3.S2. Pairwise sequence analysis. 188

Figure 3.S3. Evolutionary analysis by the Maximum Likelihood method and Multiple sequence analysis. ...189
Figure 3.S4. Structural comparison of AKR candidates. 190
Figure 3.S5. Metabolic screening in leaf of *L. aestivum*. 191
Figure 3.S6. GC/MS of nonpolar fraction of leaf extract. 192
Figure 3.S7. Enzymatic activity of dialyzed crude protein extracts. 193
Figure 3.S8. Active site representation for AKR candidates docked with narwedine or nornarwedine and NADPH. 194
Figure 3.S9. SDS gel and western blot 195
Figure 3.S10. Optimization of enzyme concentration, temperature, pH and time for enzymatic reaction of *La*TMT2 with norgalanthamine and *N*-demethylnarwedine. 195
Figure 3.S11. Biochemical characterization of LaTMT1 as a γ-tocopherol methyltransferase. 196
Figure 3.S12. LC–MS/MS analysis of products formed from nornarwedine in AKR-mediated *in vivo* and *in vitro* assays. 196
Figure 3.S13. MS/MS fragmentation profile of the new peaks. 197
Figure 3.S14. HPLC-MS/MS analysis of peaks produced on *in vivo* and *in vitro* enzymatic reaction of narwedine with AKRs. 197
Figure 3.S15. MS/MS fragmentation profile of the new peak. 198
Figure 3.S16. In planta activity of candidate genes in *Nicotiana benthamiana* upon transient expression assays. 198
Figure 4.1. Elucidated known AA pathway at the start of this PhD thesis. 201
Figure 4.2 Elucidated AA pathway at the end of this PhD thesis. 202
Figure 4.3. Biosynthetic network of BIA in blue and AA in purple with several class of enzymes for reaction. 205
Figure 4.4. Structure of few *O*-methylated specialized metabolites catalyzed by *O*-methyltransferase 206
Figure 4.5. Structure showing intramolecular oxidative coupling of 4′-*O*-methylnorbelladine 207
Figure 4.6. Structure showing intramolecular oxidative coupling of *R* and *S* reticuline 208
Figure 4.7. Structure of few specialized metabolites catalyzed by SDRs. 209
Figure 4.8. Structure showing aldo-keto reduction to give rise to specialized metabolites catalyzed by AKRs 210
Figure 4.9. Structure of some *N*-methylated specialized metabolites catalyzed by *N*-methyltransferases 211
Figure 4.10. Schematic diagram of sub-cellular localization of the studied enzymes. 215

List of abbreviations

2,4-D	2,4-Dicholophenoxyacetic acid
4CL	4-hydroxyphenylacetyldehyde
4-HDCA	4-hydroxydihydrocinnamaldehyde
4-HPAA	4-hydroxyphenylpuruvate decarboxylase
AKR	Aldo-keto reductase
AMBER	Assisted Model Building with Energy Refinement
ANOVA	Analysis of Variance
BBE	Berberine bridge Enzyme
BIA	Benzyl Isoquinoline alkaloid
BLAST	Basic Local Alignment Search Tool
BSA	Bovine serum albumin
BUSCO	Benchmarking Universal Single-Copy Orthologs
C3H	*p*-coumarate hydroxylase
C4H	*Trans*-cinnamate hydroxylase
CatOMT	Catechol *O*-methyltransferase
CCoAOMT	Caffeoyl CoA *O*-methyltransferase
CCR	Cinnamoyl-CoA reductase
CES	Shikimate esterase
CFS	Cheilanthifoline synthase
CID	Collision-induced dissociation
C*N*MT	Coclaurine *N*-methyltransferase
CODM	codeine O-demethylase
COMT	Caffeic acid *O*-methyltransferase
COMT	Caffeic acid *O*-methyltransferase
CYP	Cytochrome P450
DBOX	Dihydrosanguinarine oxidase
DFR	Dihydroflavonol 4-reductase
DHBA	3,4-dihydroxybenzaldehyde
DMSO	Dimethyl sulfoxide
DOPA	3,4-dihydroxyphenylalanine

DRR	Dehydroreticuline reductase
DRS	Dehydroreticuline synthase
ECL	Enhanced chemiluminescence
EDTA	Ethylenediaminetetraacetic acid
EGFP	Enhanced Green Fluorescent Protein
ER	Endoplasmic reticulum
ESI	Electrospray Ionization
FAD	Flavin-dependent oxidoreductases
FDA	Food and drug administration
GAM-HRP	Goat anti-mouse-horse radish peroxidase
GAR	Goat anti-rabbit-horse radish peroxidase
GC	Gas chromatography
Ge	*Galanthus elwesii*
GTMT	Gamma-tocopherol methyltransferase
HBS	Hydroxybenzaldehyde synthase
HCT	Hydroxycinnamoyl transferase
HIV	Human immunodeficiency virus
HPLC	High performance liquid chromatography
IPTG	Isopropyl β-D-thiogalactopyranoside
La	*Leucojum aestivum*
LB	Luria Bertani
LC-MS/MS	Liquid chromatography with tandem mass spectrometry
Lr	*Lycoris radiata*
Ly	*Lycoris aurea*
MBP	Maltose binding protein
MEP	methylerythritol phosphate pathway
MES	2-(N-morpholino) ethanesulfonic acid
MIA	Monoterpene indole alkaloid
MRM	Multiple reaction monitoring
MT	Methyl transferase
N4OMT	Norbelladine 4′ *O*-methyltransferase

NADP	Nicotinamide Adenine Dinucleotide Phosphate
NBS	Norbelladine synthase
NCBI	National Center for Biotechnology Information
NCS	Norcoclaurine synthase
NGS	Next-generation sequencing
NMR	Nuclear magnetic resonance
NMCH	N-methylcoclaurine
NMSH	N-methylstylopine 14-hydroxylase
NMT	N-methyltransferase
Nps	*Narcissus* sp. aff *pseudonarcissus*
Np	*Narcissus papyraceus*
NR	Noroxomaritidine reductase
NAA	1-Naphthaleneacetic acid
OMT	*O*-methyltransferase
ORF	Open reading frame
PAL	Phenylalanine ammonium lyase
PCR	Polymerase chain reaction
PDB	Protein Data Bank
PNMT	Pavine *N*-methyl transferase
PVDF	Polyvinylidene difluoride
RFP	Red florescence protein
RIN	RNA Integrity number
RMSD	Root mean square deviation
RT-qPCR	Quantitative reverse transcription polymerase chain reaction
SAM	*S*-adenosyl methionine
SDR	Short chain dehydrogenase/reductase
SDS-PAGE	Sodium dodecyl sulfate-polyacrylamide gel electrophoresis
SM	Specialized metabolites
TBST	Tris-buffered saline (TBS) containing Tween 20
TMT	γ-tocopherol methyltransferases
TYDC	Tyrosine decarboxylase

V11H	Vittatine 11-hydroxylase
*Vp*OMT	*Vanilla planifolia O*-methyltransferase

Chapter I

This chapter contextualizes Amaryllidaceae alkaloids within plant specialized metabolism, reviews their biosynthesis and biological activities, outlines engineering strategies and the *Nicotiana benthamiana* platform, and pinpoints unresolved steps—especially phenol couplings and *N*-methylation—that motivate the hypotheses tested in this thesis.

1. General Introduction

Plants are predominant on earth and form the base of most ecosystems, providing the energy and organic material through photosynthesis that sustains nearly all other life forms. Plants can produce and synthesize countless small-molecule chemical substance which are diverse groups of organic compounds and are divided into two major groups, primary and specialized metabolites (SMs) (Pichersky and Lewinsohn, 2011; Seigler, 2012). Primary metabolites are essential compounds involved in basic cellular processes, such as photosynthesis, respiration, and growth. They include carbohydrates, amino acids, nucleotides, and lipids. On the other hand, SM represent unique, species-specific molecules that facilitate plant adaptation by mediating interactions with biotic and abiotic factors in fluctuating environments (Huang and Dudareva, 2023). The concept of SM was first defined by Albrecht Kossel, Nobel Prize winner for physiology or medicine in 1910 and thirty years later, Czapek described them as end-products (Hussein and El-Anssary, 2019). Recent genetic and chemical investigations are revealing that SMs possess multiple roles; that mediate interactions with the environment while also regulating growth, defense, and metabolic integration across trophic levels (Erb and Kliebenstein, 2020). Plant SMs can be divided into three major groups: terpenoids, alkaloids, and phenylpropanoids/allied phenolic compounds based on their biosynthetic origins and has various therapeutic properties (Kumar and Kumar, 2024). Here we will be discussing on alkaloid and funnel specific type Amaryllidaceae alkaloid in the following section.

1.1 Alkaloids

The term “alkaloid” was introduced by the German chemist Carl Friedrich Wilhelm Meissner in 1819, derived from late Latin root *alkali* (meaning "ashes of plants", referring to the basic or alkaline nature of these compounds) and the Greek-language suffix -οειδής -(meaning "resembling" or "like") (Meißner, 1819). Alkaloids are low-molecular-weight, nitrogen-containing specialized metabolites, typically possessing one or more heterocyclic rings, and are predominantly derived from amino acid precursors (Aniszewski, 2015; Singh et al., 2019). Alkaloids represent the largest and most structurally diverse class of plant secondary metabolites and accounting up to 20% of SMs (Zandavar and Babazad, 2023). To date, more than 12,000 alkaloids have been characterized from a wide range of plant species. These compounds are mostly abundant in higher plants and are distributed across numerous botanical families, including

Apocynaceae, Annonaceae, Amaryllidaceae, Berberidaceae, Boraginaceae, Gnetaceae, Liliaceae, Leguminosae, Lauraceae, Loganiaceae, Magnoliaceae, Menispermaceae, Papaveraceae, Piperaceae, Rutaceae, Rubiaceae, and Ranunculaceae (Zandavar and Babazad, 2023).

In plants, alkaloids play important ecological roles, functioning primarily as chemical defense molecules against herbivores, pathogens, and environmental stresses, while also contributing to plant–environment interactions. Owing to their diverse biological and pharmacological properties, alkaloids have attracted considerable interest in medicine, agriculture, and biotechnology, with many serving as valuable pharmaceutical compounds. Irrespective of their biological origin, alkaloids have been broadly classified based on their chemical structures, particularly the nature of their nitrogen-containing ring systems, giving rise to major groups such as pyrrolidine, tropane, indole, quinolizidine, and isoquinoline alkaloids.

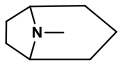
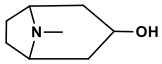
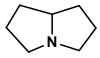
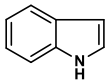
1.2 Classification of alkaloid

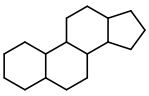
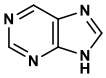
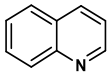
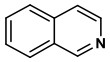
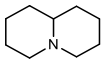
Alkaloids exhibit significant diversity in their botanical origins, structures, and pharmacological actions, leading to various classification systems. They are broadly categorized into three main types: true alkaloids, protoalkaloids, and pseudoalkaloids (Aniszewski, 2015). True alkaloids and protoalkaloids are derived from amino acids, while pseudoalkaloids are not. True alkaloids, which contain a nitrogenous heterocyclic ring, are highly reactive and biologically potent, often forming water-soluble salts. They are typically solid and bitter, with examples including cocaine, morphine, and quinine. Protoalkaloids are alkaloids that contain a nitrogen atom derived from an amino acid, though not part of a heterocyclic ring (de Sousa Falcão et al., 2008; Henriques et al., 2004). They are typically simple in structure, with L-tryptophan and L-tyrosine as key precursors. Examples include yohimbine, mescaline, and hordenine, which are used to treat mental illness, pain, and neuralgia. Pseudoalkaloids, on the other hand, have a carbon skeleton not directly derived from amino acids. They are instead linked to amino acid pathways, forming through amination or transamination, or from non-amino-acid precursors like phenylalanine or acetate. Common pseudoalkaloids include capsaicin, caffeine, and ephedrine (Wink, 2015).

Alkaloids can be classified based on their nuclear ring structures (Table 1.1), which is one of the most widely used systems. Tropane/Tropine alkaloids, found predominantly in the Solanaceae and Erythroxylaceae families, contain a C4N skeleton and include compounds like cocaine, atropine

and hyoccyamine (Kohnen-Johannsen and Kayser, 2019). Pyrrolizidine alkaloids, primarily occurring in the Asteraceae and Fabaceae families, are known for their toxic effects, including liver damage (Robertson and Stevens, 2014). Piperidine alkaloids, characterized by six-membered ring containing five methylene bridges (–CH2–) and one amine bridge (–NH–), with C_5N nucleus and are often neurotoxic and presence of odor is a common feature of these alkaloids (Dey et al., 2020; Strunz and Findlay, 1985). Quinolines, and isoquinoline alkaloids, which include morphine and codeine, are also notable groups with

Table 1.1. Classification of alkaloids based on the ring structure

Alkaloid classification	**Core Nucleus of the structure**	**Plant family**	**Few Examples**	**Precursor/ derived from**	**Reference**
Tropane		Solanaceae and Erythroxylaceae	Atropine, scopolamine, hyoscyamine, cocaine, ecgonine, benzoylecgonine, hydroxytropacocaine, methylecgonine cinnamate, catuabines, scopine	L-ornithine, L-arginine, pyrrolidine alkaloids	(Bravo et al., 2022; Kohnen-Johannsen and Kayser, 2019)
Tropine					
Pyrrolizidine		Asteraceae (tribes Eupatorieae and Senecioneae), Boraginaceae, Fabaceae (mainly the genus Crotalaria), and Orchidaceae	necine base esterified with a necic acid, lycopsamine, amabiline, thesinine, trachelanthamidine, isoretronecanole	L-ornithine, L-isoleucine, L-arginine	(Jayawickreme et al., 2023; Ober and Hartmann, 1999; Schramm et al., 2019)
Piperidine		Aizoaceae	piperine, solenopsin, anabasine, lobeline, coniine, loratadine, droperidol, loperamide	Lysine-derived alkaloids; L-lysine L-leucine L-isoleucine	(Dey et al., 2020; Strunz and Findlay, 1985; Zandavar and Babazad, 2023)
Indole		Apocynaceae (*Alstonia, Aspidosperma, Rauvolfia and Catharanthus*), Rubiaceae, and Loganiaceae	chlorpromazine, reserpine, neostigmine, pyridostigmine, distigmine, yohimbine, ajmaline, rivastigmine, ergometrine, ergotamine,	L-tryptophan	(Dey et al., 2020; Singh and Singh, 2018)

			vinblastine and vincristine		
Steroidal	 It is the backbone; A nitrogen atom (amino group) is essential, either forming part of a heterocyclic ring or attached to the side chain	Apocynaceae, Liliaceae, Solanaceae, Apocynaceaethe, Buxaceae	latifolinin, *Solanum* alkaloids (chaconine, solanine, solasodine, tomatidine, tomatine, and solanidine), veratramine	conanine backbone, amino group or an oxygen compound at the 3rd carbon atom	(Xiang et al., 2022)
Imidazole		Rutaceae, Leucettidae	pilocarpine, cynodine, odiline, cynometrine	L-lysine, histidine, dicarbonyl compounds, aldehydes and ammonia	(Luca, 2006)
Purine		Rubiaceae, Theaceae, Sapindaceae	caffeine, theobromine, theophylline, paraxanthine, 7-methylxanthine, theobromine	glutamine, glycine, aspartate, folic acid derivatives and CO2; xanthosine and xanthine	(Jia et al., 2024)
Pyrrolidine		Erythroxylaceae, Lamiaceae, Boraginaceae, Compositae, Fabaceae	Stachydrine, hygrine, codonopsinine, hyoscyamine, nicotine, cocaine, and cuscohygrine.	L-leucine, L-ornithine	(Poyraz et al., 2023; Yang, 2017)
Quinoline		Rutaceae, Rubiaceae, Asteraceae	Chloroquinine, cinchonidine, quinine, quinidine, strychnine	L-tryptophan, L-anthranilic acid, hemiterpene or a monoterpene	(Shang et al., 2018)
Isoquinoline		Papaveraceae, Berberidaceae, Menispermaceae, Fumariaceae, Ranunculaceae, Amaryllidaceae	Codeine, morphine, papaverine, tetrandrine, thebaine, tubocurarine, berberine	L-tyrosine, L-phenylalanine	(Shamma, 2012)
Quinolizidine derivatives		Leguminosae *Lupinus* (lupins), *Cytisus* (brooms), *Sophora*, *Genista*, *Thermopsis*, and *Baptisia*	Lupinine, cytisine, nupharidin, matrine, oxymatrine, allomatridine	Lysine	(Aniszewski, 2015)

significant medicinal properties. Indole alkaloids, the largest and most diverse group, are derived from tryptophan and include compounds with various biological activities (Singh and Singh, 2018). Steroidal alkaloids, commonly found in higher plants, possess a 1,2-cyclopentane phenanthrene ring structure. Steroidal alkaloids are biosynthesized by the inclusion of one or two nitrogen atoms into a preformed steroid molecule. They are classified into several subtypes, with the most fundamental being various forms of aminopregnanes (Xiang et al., 2022; Zandavar and Babazad, 2023). Imidazole alkaloids, with a characteristic imidazole ring specifically as a diazole, i.e. 1,3-C_3N_2 ring; having a five-membered ring consisting of three carbon atoms and two nitrogen atoms. This ring system ring system is present in important biological building blocks like histidine and the related hormone histamine that has a wide range of biological importance. Purine alkaloids, such as caffeine and theobromine, are derived from nucleotide bases. Finally, pyrrolidine alkaloids, which include hygrine and brevicolline, are known for their distinct C4N skeleton (Dey et al., 2020). Pyrrole alkaloids derived from leucine; pyrrolidine, tropane, and pyrrolizidine alkaloids from ornithine; quinolizidine, and indolizidine alkaloids derive from lysine; catecholamines, isoquinoline, tetrahydroisoquinoline, and benzyltetrahydroisoquinoline alkaloids originate from tyrosine; indolamines, indole, carboline, quinoline, pyrrolindole and ergot alkaloids come from tryptophan; and imidazole alkaloids from histidine (Chiocchio et al., 2021). Among all those classified alkaloids, we will be discussing on isoquinoline alkaloids more on following section.

1.2.1 Isoquinoline alkaloids

Isoquinoline alkaloids make up a major and diverse group of natural substances. Isoquinoline alkaloids constitute a structurally diverse molecule with basic isoquinoline core. Plant isoquinoline alkaloids (PIAs) represent one of the most diverse and pharmaceutically valuable classes of plant-specialized metabolites. PIAs are prevalent in Amaryllidaceae*, Ranunculaceae, Papaveraceae, Berberidaceae, Fumariaceae, Menispermaceae, Rutaceae, Magnoliaeace, Cactaceae,* and *Annonacea* families. PIAs are formed from tyrosine-derived precursors (tyramine or dopamine) that condense with a second substrate to yield core scaffolds such as norcoclaurine, autumnaline, deacetylisoipecoside, or norbelladine (Desgagné-Penix, 2021; Diamond and Desgagné-Penix, 2016). Among PIAs, four groups are very common i.e. benzylisoquinoline alkaloids (BIA), phenethylisoquinoline alkaloids, ipecac alkaloids and AAs (Figure 1.1). Among these, BIAs and

AAs are of particular interest, as their biosynthetic pathways and nuclear core ring structures share notable similarities.

1.2.2 Benzylisoquinoline alkaloids (BIA)

The most studied PIAs are BIAs with more than 2500 known structures, their pharmacological significance spans narcotic analgesics like morphine and codeine, muscle relaxants including tubocurarine and papaverine (Dang et al., 2012), antimicrobials such as sanguinarine and berberine (Li et al., 2018a) and multifunctional agents like noscapine, known for its antitussive and anticancer properties (Aghaali and Naghavi, 2024; Barken et al., 2008). The biosynthetic foundation of most of the BIAs begins with the Pictet–Spengler condensation of dopamine and 4-hydroxyphenylacetaldehyde, catalyzed by the unique enzyme (*S*)-norcoclaurine synthase (NCS), a member of the PR10/Bet v1-type family (Kishimoto et al., 2016; Morris et al., 2021). This reaction produces the tetrahydroisoquinoline and benzyl moieties that form the basic benzylisoquinoline structural unit. The structural diversity of BIAs is achieved through an array of enzymatic transformations that modify the simple BIA backbone into complex frameworks such as aporphine, pavine, protoberberine, benzo[c]phenanthridine, bisbenzylisoquinoline, and morphinan alkaloids. Key contributors to this diversity are cytochromes P450 (CYPs), particularly members of the CYP80 and CYP719 families, which mediate phenol coupling reactions (Meng et al., 2024; Ziegler et al., 2009), and flavoproteins like the berberine bridge enzyme (BBE), which catalyzes oxidative cyclizations (Winkler et al., 2006; Xu et al., 2024). Additional modifications, including hydroxylations, methylations, and demethylations, are mediated by CYPs (Hansen et al., 2021), S-adenosylmethionine (SAM)-dependent methyltransferases (Lee et al., 2024), and dioxygenases (Wang et al., 2021). These enzymatic processes iteratively reconfigure BIA scaffolds, creating vast structural and functional diversity. The evolutionary adaptability of these pathways underscores their role in the ecological and pharmacological functionality of BIAs. While BIAs are primarily found in basal angiosperms of the order ranunculales and eumagnoliids, research has been concentrated on a few model species, such as *Coptis japonica* and *Eschscholzia californica*. Although their precise roles in plant defense against herbivores and pathogens remain speculative, the pharmacological applications of BIAs have been extensively studied, offering insights into their ecological significance and their potential in sustainable drug development (Tuzimski and Petruczynik, 2023).

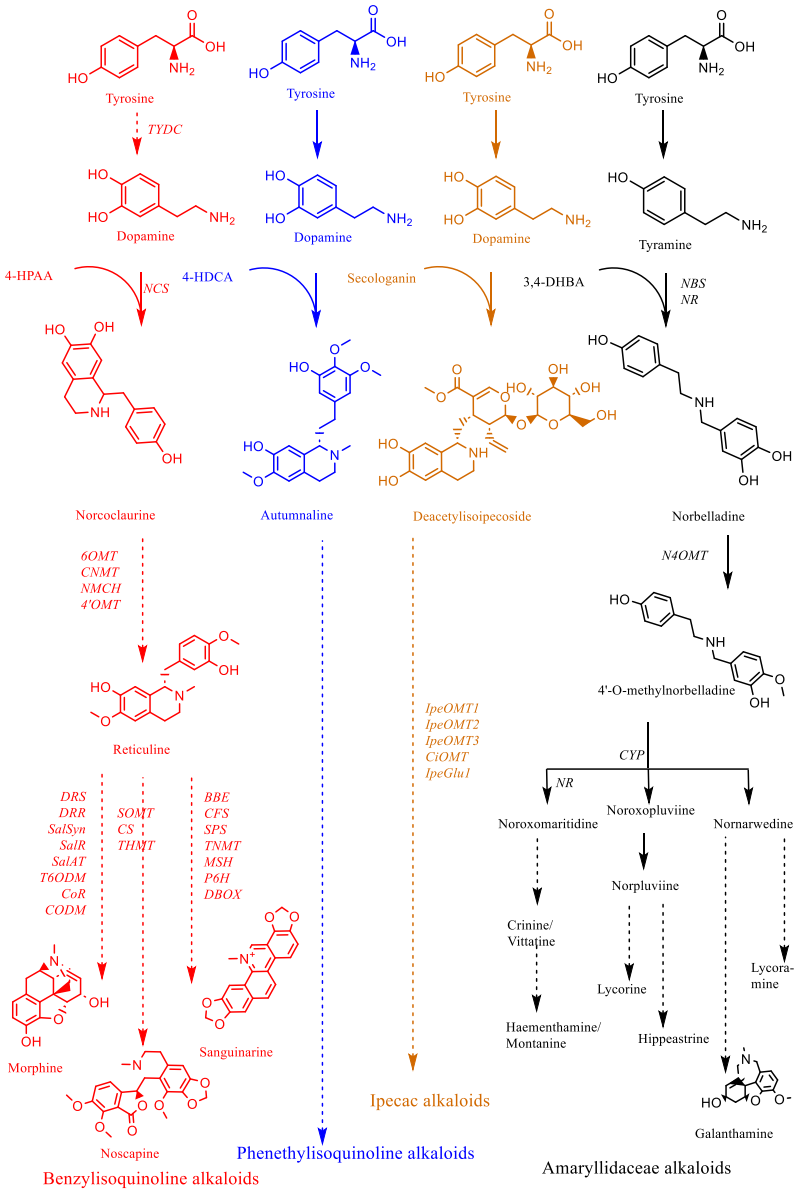


Figure 1.1: Overview of pathways of four groups of isoquinoline alkaloids.

Each color represents individual pathway and particular enzyme's corresponding genes are represented in italics. 4-HPAA, 4-hydroxyphenylacetaldehyde; 4-HDCA, 4-hydroxydihydrocinnamaldehyde; 3,4-DHBA, 3,4-dihydroxybenzaldehyde; TYDC, tyrosine decarboxylase; NCS, norcoclaurine synthase; 6OMT, norcoclaurine 6-*O*-methyltransferase; CNMT, coclaurine *N*-methyltransferase; NMCH, *N*-methylcoclaurine; 4′OMT, 4′-*O*-methyltransferase; SalSyn, salutaridine synthase; SalR, salutaridine reductase; SalAT, salutaridinol 7-*O*-acetyltransferase; T6ODM, thebaine 6-Odemethylase; CoR, codeinone reductase; CODM, codeine O-demethylase; BBE, berberine bridge enzyme; CFS, cheilanthifoline synthase; SPS, stylopine synthase; TNMT, tetrahydroprotoberberine *N*-methyltransferase; MSH, *N*-methylstylopine 14-hydroxylase; P6H, protopine 6-hydroxylase; DBOX, dihydrosanguinarine oxidase; SOMT, scoulerine-*O*-methyltransferase; CS, canadine synthase; THMT, thiopurine methyltransferase; IpeOMT1,2,3, Ipecac O-methyltransferase-1, -2, -3; IpeGlu1, Ipecac glycosidase-1; CiOMT, Carapichea ipecacuanha O-methyltransferase; NBS, norbelladine synthase; NR, noroxomaritidine reductase; N4OMT, norbelladine 4-*O*-methyltransferase; CYP, cytochrome p450.

1.2.3 Amaryllidaceae alkaloids (AAs)

AAs are a large group of over 650 structurally diverse isoquinoline alkaloids derived from a common intermediate norbelladine or 4′O-methylnorbelladine that are found exclusively in plants of the Amaryllidaceae family. The Amaryllidaceae family consists of monocotyledonous, herbaceous perennial plants that belongs to the order Asparagales and this family was further divided into three sub-families i.e. Amaryllidoideae, Agapanthoideae, and Allioideae. This family encompasses approximately 1,600 species across 75 genera, which are broadly distributed across tropical, subtropical, and warm regions worldwide (Desgagné-Penix, 2021). These plants are known for their considerable economic and medicinal importance as it includes many ornamental garden plants and has been used traditionally in several illness (Fennell and Van Staden, 2001). For instance, daffodils (*Narcissus*) are among the most popular ornamental varieties, making them highly valuable to the floriculture industry (Bastida et al., 2006).

The Amaryllidaceae family has a long and enduring history of use in traditional medicine across different cultures and eras, largely due to the presence of structurally diverse alkaloids with notable biological and pharmacological activities. Records trace their use back to Hippocrates of Cos in the 4th century before common era/before Christ (BCE), who employed oil from *Narcissus poeticus* L. (daffodil) to treat uterine tumors, a practice later continued by physicians such as Soranus of Ephesus and endorsed by Gaius Plinius Secundus for topical treatments, with similar references appearing in medieval Europe, where Henri de Mondeville advocated their use against cancer in 14th-century (Bostock and Riley, 1855; Manolov et al., 2015; Riddle, 1985). Beyond Europe, archaeological evidence from Inca ruins depicts genera such as *Ismene*, *Pyolirion*, and *Stenomesson* on ceremonial drinking vessels, suggesting their role in cultural practices (Vargas, 2008),while San rock paintings in South Africa portrayed *Boophone* and *Brunsvigia*, demonstrating early indigenous use (Nair and van Staden, 2014). In West Africa, the bulbs of *Crinum jagus* remain part of ethnomedicine, traditionally used to treat memory loss and mental illnesses (Houghton et al., 2004). Across the Mediterranean and Eastern Europe, extracts from *Galanthus nivalis* (snowdrop) were valued in folk medicine for alleviating senile tremors, vision problems, and fatigue, with Bulgarian traditions even employing snowdrop brandy for such ailments (Stanilova et al., 2010). Interestingly, it has been speculated that the mythical “Moly” antidote from Homer’s *Odyssey* could have been a snowdrop, highlighting its early recognition for

cholinergic activity (Plaitakis and Duvoisin, 1983). Today, traditional knowledge continues to inform the medicinal applications of Amaryllidaceae plants, with modern accounts recommending species such as *Galanthus* and *Leucojum aestivum* (summer snowflake) for conditions ranging from fever, sore throat, and cold to plexitis and even leukemia (Heinrich, 2010).

1.3 Biological importance of Amaryllidaceae alkaloids

Amaryllidaceae alkaloids represent a structurally diverse group of specialized plant metabolites that have attracted considerable scientific and pharmaceutical interest because of their broad spectrum of biological activities. Over the past several decades, extensive phytochemical, pharmacological, and clinical investigations have demonstrated that these compounds possess significant therapeutic potential, including neuroprotective, anticancer, antimicrobial, antiviral, anti-inflammatory, analgesic, and enzyme-inhibitory properties. The unique chemical scaffolds of AAs enable interactions with diverse molecular targets, making them valuable not only as naturally occurring bioactive compounds but also as promising lead molecules for drug discovery and development.

Some of the key biological importance of AAs supported by research has been illustrated below (Figure 1.2), followed by a short explanation and selected examples of supporting evidence.

●**Acetylcholinesterase (AChE) Inhibition**: It is a process of blocking the acetylcholinesterase enzyme's ability to break down the neurotransmitter acetylcholine (ACh) which results in enhanced cholinergic signaling in brain and at neuromuscular junctions. The most notable biological activity of AAs is their ability to inhibit AChE. This property is significant in the treatment of neurological disorders like Alzheimer's disease. Galanthamine, a well-known AA, under the generic name Reminyl, is the first AA to be approved as a prescription drug by FDA due to its high inhibitory efficacy and both reversible and selective activity on AChE (He et al., 2015; Wilkinson et al., 2001). Other alkaloids in this family, such as lycoramine, epinorlycoramine, narwedine, haemanthamine and lycorine, also show varying degrees of AChE inhibitory activity (Berkov et al., 2022; Jayawardena et al., 2024; Kiris et al., 2021). New research is also being published for butyrylcholinesterase (Girard et al., 2022) as well as prolyl oligopeptidase inhibitory potential of AA (Al Mamun et al., 2020).

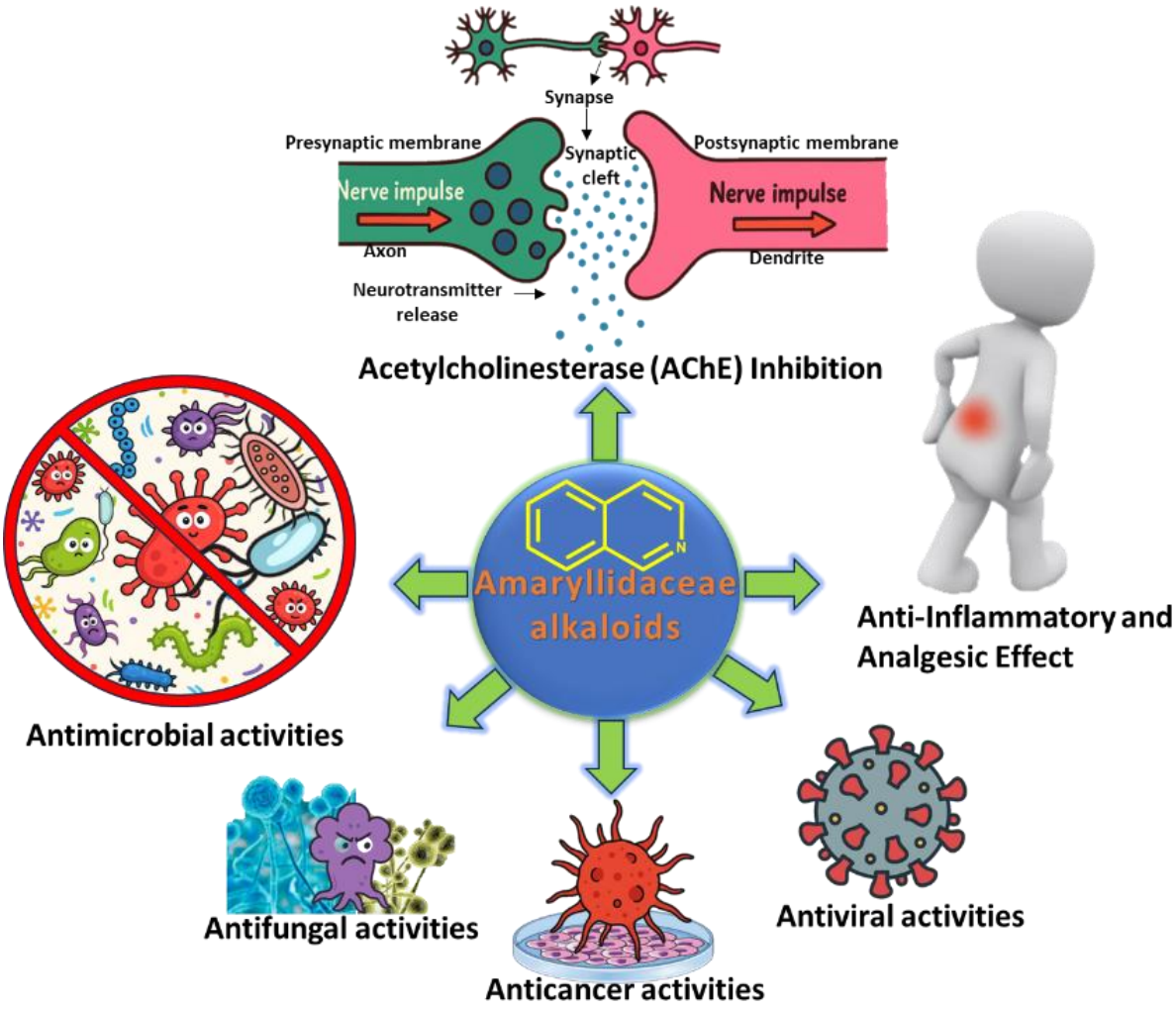


Figure 1.2 : Biological importance of Amaryllidaceae alkaloids

●**Cytotoxic and Antitumor Activity**: Cytotoxic activity refers to the ability to kill cells, while antitumor activity specifically describes the capability of a substance or treatment to inhibit or destroy tumor cells, thereby reducing tumor growth and spread. Many AAs demonstrate potent cytotoxic and antitumor activities, making them potential candidates for anticancer therapies. Lycorine, a prominent alkaloid, inhibits cell growth, division, and organogenesis in various organisms, including tumor cells (Chen et al., 2018; Zhang et al., 2024). Narciclasine and pancratistatin are potent antitumor agents that induce apoptosis in cancer cells (Griffiths, 2015). Crinine alkaloids have shown promising antiproliferative profiles, suggesting their potential as anticancer agents (Ka et al., 2020). Alkaloids derived from *Galanthus* species exhibited dose-

dependent growth suppression in cancer cell line models like breast (MCF-7), prostate (PC-3), and colon (HCT116) cancer cell lines. Similarly, lycorine, a well-characterized alkaloid from *Lycoris* species, showed pronounced antiproliferative activity against lung cancer cells (A549) and leukemia cells (K562) (Li et al., 2012). Lycorine hydrochloride (LH), an alkaloid extracted from the bulb of the *Lycoris radiata* reported to have anti-tumorous effect against gastric cancer as well as the recurrence and metastasis of different kinds of tumors (Li et al., 2020; Lv et al., 2022). The precursor of several derivatives of AA, norbelladine, is cytotoxic to hepatocarcinoma cells(Girard et al., 2022).

●**Antiviral Activity**: Antiviral activity is a property of a substance or its capability to inhibit the replication and proliferation of viruses, often by disrupting specific stages of the viral life cycle, such as attachment, entry, uncoating, replication, assembly, or release of new viral particles. Several AAs have demonstrated antiviral activity against a range of viruses. Lycorine, pancratistatin, narciclasines, pseudolycorine and their derivatives gives exhibits broad-spectrum antiviral activity against RNA and DNA viruses, including flaviviruses, bunyaviruses, poliomyelitis, coxsackie, herpes type 1, and SARS-CoV (Merindol et al., 2024). Amaryllidaceae alkaloids lycorine, hippeastrine, haemanthamine and their analogous shows anti influenze A virus N5H1 *in vitro*. The antiviral activities of AAs make them potential candidates for the development of new antiviral drugs (Masi et al., 2022; Nair and van Staden, 2023; Shen et al., 2024). Furthermore, lycorine and haemanthidine, haemanthamine and pancracine also possess antiretroviral abilities, inhibiting pseudotyped human immunodeficiency virus (HIV)−1 (Masi et al., 2022).

●**Antibacterial Activity**: Antibacterial activity describes a substance's ability to kill bacteria (bactericidal) or inhibit their growth and reproduction. This activity can stem from various mechanisms, such as damaging the bacterial cell wall or membrane, interfering with DNA or protein synthesis, or producing antimicrobial metabolites. AAs like phenanthridone alkaloids possess antibacterial properties (Nair et al., 2017). Pancracine exhibits activity against *Staphylococcus aureus* and *Pseudomonas aeruginosa* (Nair et al., 2017; Othman et al., 2019). Likewise, AA from *Pancratium trianthum* has shown antibacterial activity against *P. aeruginosa, Staphylococcus aureus,* and *E. coli* (Ka et al., 2021). AA from *Crinum glaucum*, ungeremine was shown to be active against *Enterococcus faecalis* and *P. aeruginosa* (Kianfe et al., 2020). Many

Crinine- and lycorine-types have studied in association with potent antibacterial properties (Adesanya et al., 1992; Evidente et al., 2004; Tan et al., 2011).

●**Antifungal Activity**: Certain AAs have shown antifungal activity, contributing to the traditional use of Amaryllidaceae plants to treat fungal infections (Cahlíková et al., 2021; He et al., 2015). Phenanthridone alkaloids, a small group within the Amaryllidaceae, characterized by their basic phenanthridine nucleus which is highly oxidized in ring-C, showed inhibitory activities against *Candida albicans* and *Candida parapsilosis* (Nair and van Staden, 2018).

●**Anti-Inflammatory and Analgesic Effects**: Amaryllidaceae plants are traditionally used for their anti-inflammatory and analgesic properties. Lycorine has been shown to possess analgesic effects, even stronger than aspirin (Çitoğlu et al., 2012). 15 Amaryllidaceae alkaloids isolated from *Crinum bulbispermum* and *C. moorei* showed low inhibitory activity for anti-inflammatory activity tested using cyclooxygenase assay (COX-1 and COX-2) (Elgorashi et al., 2003).

The biological importance of AA lies in their diverse range of activities that make them potential therapeutic agents for a variety of diseases. Currently, only galanthamine is commercially available as a drug, but ongoing research into the pharmacological properties of other AAs may lead to the development of new drugs for treating various conditions, including Alzheimer's disease, cancer, and viral infections.

1.4 Classification of Amaryllidaceae Alkaloids

Researchers have employed multiple approaches to classify AA, considering factors such as their biosynthetic pathways, underlying carbon skeletons, and characteristic ring systems. Previous studies have proposed various classification systems for such as 9-, 11-, and 12-ring types (Desgagné-Penix, 2021; He et al., 2015; Ka et al., 2020; Kornienko and Evidente, 2008). However, these schemes have undergone continuous revision as new alkaloids are discovered, structural overlaps between groups emerge, and inconsistencies arise among different researchers. Consequently, establishing a universally accepted classification system remains challenging, largely due to the vast diversity of compounds and the constantly expanding discoveries in natural product chemistry. Despite those challenges, we have categorized into 8 distinct types of AA based on their molecular skeletons derived from the same precursor molecule norbelladine (Figure 1.3). They are lycorine, homolycorine, crinine, haemanthamine, narciclasine, tazettine, montanine, and

galanthamine types. More categories have been reported in the literature too like fifteen, eighteen or twenty types (Jin, 2007; Li et al., 2021).

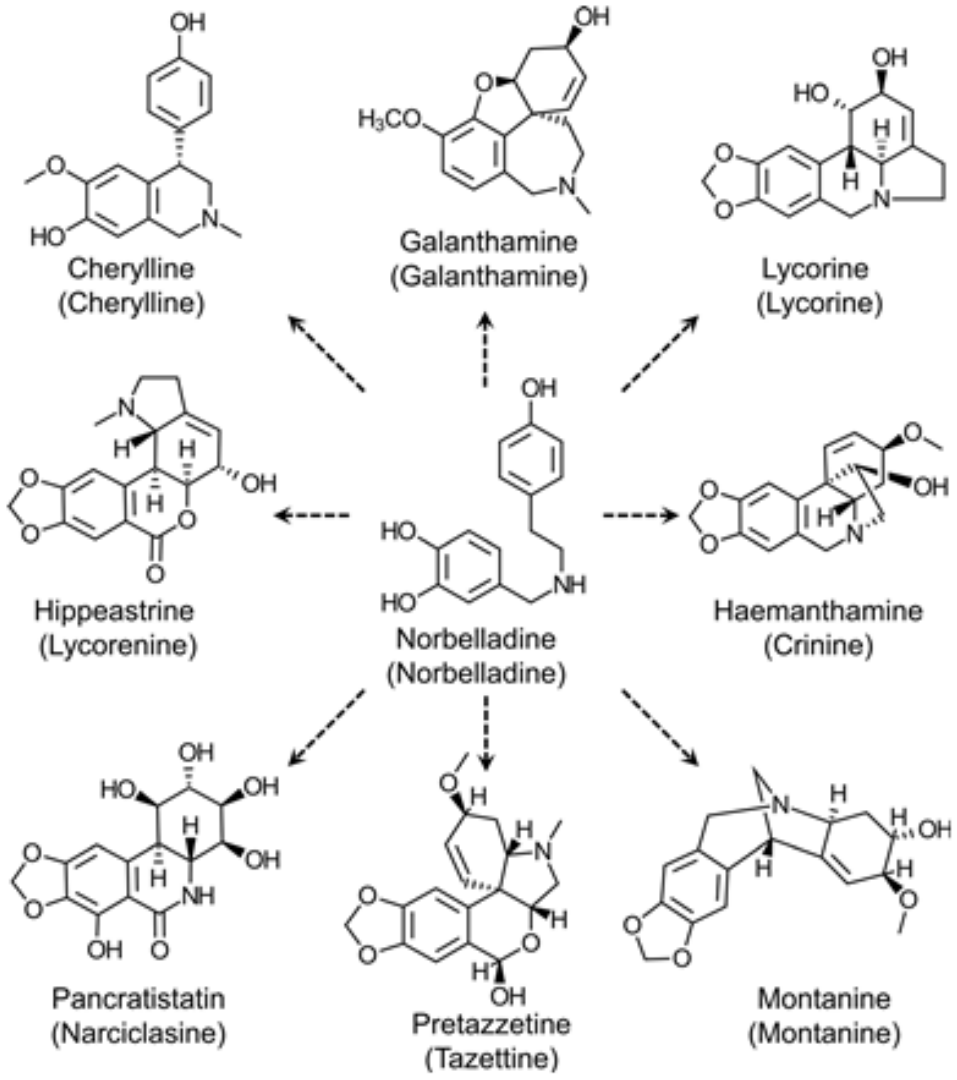


Figure 1.3: Types of Amaryllidaceae alkaloids (Desgagné-Penix, 2021)

1.5 Biosynthesis Amaryllidaceae Alkaloids

Significant progress has been made in studying the therapeutic potential of AAs, however, a comprehensive understanding of their biosynthetic pathways and the enzymes catalyzing various biosynthetic reactions still requires investigation. The combination of early labeling studies and omics approaches has greatly advanced the discovery of AA biosynthetic enzymes (Eichhorn et

al., 1998; El Tahchy et al., 2011). Following the identification of biosynthetic routes for various intermediates, numerous biosynthetic enzymes have been predicted based on the nature of their biochemical reactions and their similarity to enzymes involved in alkaloid biosynthesis from other plant families (Desgagné-Penix, 2021; Kilgore and Kutchan, 2016b). Transcriptomic and metabolic databases generated from several Amaryllidaceae species further confirm the presence of enzyme families responsible for catalyzing distinct biochemical reactions within the AA biosynthetic pathway (Ferdausi et al., 2021; Hotchandani et al., 2019; Kilgore et al., 2016a; Koirala et al., 2023; Singh and Desgagné-Penix, 2017; Tousignant et al., 2022).

Plastids are the birth centre of all aromatic amino acids which are exported in cytosol so that they can be utilized for specialized metabolism, protein synthesis, or other processes. Few investigations have identified shikimate enzymes in the cytosol, despite most studies demonstrating that enzymes from the shikimate pathway in higher plants are often produced as precursors with a plastid transit peptide that guides them to the plastid (Schenck and Maeda, 2018; Shende et al., 2024). It is hypothesized that the shikimate pathway's intermediates and/or end products are carried from the plastid to the cytosol in the AA biosynthesis pathway. Thus, the formation of AA requires the involvement of the shikimate pathway followed by two major routes, namely the tyramine and the phenylpropanoid pathways (Desgagné-Penix, 2021).

Tyramine formation begins with the decarboxylation of L-tyrosine by tyrosine decarboxylase (TYDC), a key enzyme linking primary and specialized metabolism. This reaction is foundational to the synthesis of diverse metabolites, such as phenylethanoid glycosides, protoalkaloids, and BIAs (Hagel and Facchini, 2005). TYDC plays a regulatory role in AA biosynthesis, with its expression varying by development, tissue, and external stimuli. *TYDC* genes exhibit diversity across species, with *Arabidopsis* having one gene, lotus five, and opium poppy around 15, which are differentially regulated. These enzymes specifically decarboxylate L-tyrosine and L-DOPA, but not L-phenylalanine or L-tryptophan (Deng et al., 2018; Desgagné-Penix and Facchini, 2011; Facchini and De Luca, 1994). Genetic engineering studies have leveraged *TYDC* genes to explore tyrosine-derived metabolite regulation. Plant TYDCs, characterized by structural and functional similarities, have been identified in several Amaryllidaceae species, such as *Narcissus pseudonarcissus*, *N. papyraceus* and *Lycoris radiata* (Hotchandani et al., 2019; Hu et al., 2021).

The phenylpropanoid pathway is involved in the conversion of L-phenylalanine to the aldehyde precursor 3,4-dihydroxybenzaldehyde (3,4-DHBA), as suggested by studies on vanillin biosynthesis in *Vanilla planifolia* and its presence in Amaryllidaceae plants (Benedec et al., 2018). Radiolabeled precursor feeding studies in *N. pseudonarcissus* identified a pathway involving phenylalanine, *trans*-cinnamic acid, 4-hydroxycinnamic acid, 3,4-dihydroxycinnamic acid, and 3,4-DHBA (Suhadolnik et al., 1963). Limited data exist on phenolic metabolites in Amaryllidaceae, but compounds like protocatechuic, vanillic, and ferulic acids have been detected. This supports the role of phenylpropanoid pathway enzymes in 3,4-DHBA synthesis.

Phenylalanine ammonia-lyase (PAL) initiates the pathway by converting phenylalanine to *trans*-cinnamic acid, directing carbon from the shikimate pathway to phenylpropanoid metabolism. PAL is encoded by multi-gene families, with Amaryllidaceae species expressing distinct *PAL* transcripts. For instance, *Lycoris radiata* expresses *LrPAL1* in roots and bulbs, correlating with galanthamine content, while *LrPAL2* in aerial parts. Phylogenetic analysis divides Amaryllidaceae PALs into PAL1 and PAL2 clusters, suggesting functional specialization (Jiang et al., 2013; Jiang et al., 2011). In *N. papyraceus*, *NpPAL1* is ubiquitously expressed, while *NpPAL2* predominates in bulbs similar like in *N. pseudonarcissus*, indicating distinct roles in phenylpropanoid branches (Hotchandani et al., 2019; Singh and Desgagné-Penix, 2017).

Following PAL, cinnamate-4-hydroxylase (C4H), a cytochrome P450 enzyme, converts *trans*-cinnamic acid to *p*-coumaric acid. A single *C4H* gene was identified in *N. pseudonarcissus* and *N. papyraceus*, with expression highest in bulbs during dormancy and germination. Functional studies of *C4H* from *L. aurea and L. aestivum* confirmed its role in conversion of *trans*-cinnamic acid to *p*-coumaric acid (Karimzadegan et al., 2024; Li et al., 2018b). C4H has also been used in synthetic biology for specialized metabolite production, such as assembling *L. aurea Ly*C4H with *A. thaliana At*PAL1 in *E. coli* to produce *p*-coumaric acid (Li et al., 2018c).

Downstream, enzymes like 4-coumarate CoA ligase (4CL), hydroxycinnamoyl CoA shikimate transferase (HCT), and caffeoyl shikimate esterase (CES) convert p-coumaric acid to caffeic acid. Transcripts for these enzymes have been identified in *Narcissus* species, with differential expression patterns suggesting tissue-specific roles. For example, *Np*HCT1 highly expressed in aerial parts (Hotchandani and Desgagne-Penix, 2017). CYP450 C3H enzymes, which hydroxylate

p-coumaric acid to caffeic acid, have also been characterized in Amaryllidaceae, with expression highest in bulbs during early development (Karimzadegan et al., 2024).

The chain-shortening reaction from caffeic acid to 3,4-DHBA remains unknown but may resemble vanillin biosynthesis. Enzymes like vanillin synthase (*Vp*VAN) and phenylpropanoid 2,3-dioxygenase (PPDiox) have been implicated in similar reactions in Vanilla planifolia (Negishi and Negishi, 2017). It is possible that related enzymes catalyze 3,4-DHBA formation in AA biosynthesis. Further studies are needed to identify and confirm these enzymatic roles.

The series of biochemical reactions giving key amine precursor tyramine and aldehyde building blocks 3,4-dihydroxybenzylaldehyde (3,4-DHBA), synthesized from L-tyrosine and L-phenylalanine, respectively is the root of major AA biosynthesis pathway (Desgagné-Penix, 2021). The condensation of amine and aldehyde precursor tyramine and 3,4-DHBA gives norbelladine and is carried out by an enzyme norbelladine synthase (NBS) (Singh and Singh, 2018). However, later other research shows that condensation of tyramine and 3,4-DHBA into norbelladine was catalysed by NBS and noroxomaritidine/norcraugsodine reductase (NR) (Kilgore et al., 2016; Majhi et al., 2023). Despite having a remarkable diversity in structure and biological activity, norbelladine is considered as first common intermediate of all AAs. Further NBS and NR are shown to be localized in the cytosol and their observed physically interaction in yeast and planta, indicates that both NR and NBS are involve in biosynthesis of norbelladine (Majhi et al., 2023; Tousignant et al., 2022). Recently, a group of scientists checked for various substrate flexibilities and concluded that norbelladine is formed through the condensation/reduction reaction of 3,4-dihydroxybenzaldehyde with tyramine (Hnin et al., 2024).

Conversion of norbelladine to its *O*-methylated counterpart by a *S*-adenosyl-L-methionine (SAM) dependent *O*-methyltransferase (*O*MT) enzymes catalyse the transfer of methyl group from methyl-donor (SAM) to free hydroxyl group acceptor of substrate (Koirala et al., 2024). Based on the amino acid sequence alignment, substrate and size, plant *O*MTs can be broadly classified into two group *i.e* class I *O*MTs (23-27 KDa) and class II *O*MTs (38-43 KDa). Class I *O*MTs require divalent cation for methylation reaction and class II *O*MTs are metal independent. In AAs pathway, class I *O*MTs involved in *O*-methylation of norbelladine has been characterized in *Narcissus papyraeus, Narcissus* sp. *aff. pseudonarcissus*, *Lycoris aurea* and *Lycoris radiata*, catalyzes the

methylation of norbelladine *in vitro* (Kilgore et al., 2014; Koirala et al., 2024; Li et al., 2019; Sun et al., 2018). Therefore, *O*-methylated norbelladine was considered as key intermediate of AAs pathway. However, the structural feature of cherylline-type of AAs suggests the occurrence of 3'-*O*-methylation during the biosynthesis of these types of AAs, although it remains to be experimentally elucidated. According to Kilgore et al.'s characterization of norbelladine *O*-methyltransferase from *Narcissus sp.* aff. *pseudonarsissus* (*Np*N4*O*MT), the enzyme catalyzed the transfer of a methyl-group from SAM to an alkaloid substrate at the 4' -*O* position of norbelladine and its *N*-methylated form (Kilgore et al., 2014). Future research on homologous norbelladine *O*MT from *L. radiata*, *L. aurea*, and *Galanthus elwesii* showed that methylation can take place in the 3-*O* and 4-*O* positions of norbelladine, as well as in the 3-*O* and 4-*O* positions of precursors, 3,4-DHBA or caffeic acid *vitro* (Kilgore et al., 2014; Koirala et al., 2024; Li et al., 2019; Sun et al., 2018).

Radiolabeling studies in *L. aestivum* revealed that deuterium-labelled 4′*O*M was further incorporated into galanthamine and lycorine through a C-C coupling cyclization step, as observed in the biosynthesis pathway of berberine-type alkaloids (Cui et al., 2007; El Tahchy et al., 2010; Iwasa and Kim, 1997). Later studies uncovered that a new class of cytochrome P450, CYP96T1 catalyzes mainly *para-para´* (*p-p'*) C-C oxidative coupling of 4′*O*M in *N.* sp. *aff. pseudonarcissus* but also yields the *para-ortho´* (*p-o'*) product *N*-demethylnarwedine as a minor product (Kilgore et al., 2016a). Recently, scientist uncovered three different homologs of cytochrome P450 that does distinct coupling from *N. tête-à-tête* (Mehta et al., 2024). However, no definitive success had been achieved on AA pathway prior to the commencement of my PhD in 2021, thereby highlighting a critical gap that my research aimed to address.

1.6 Enzymatic Players in Amaryllidaceae Alkaloid Biosynthesis: Insights from Benzylisoquinoline Pathways

The benzylisoquinoline alkaloid (BIA) pathway serves both as an inspiration and a model framework for elucidating the steps and enzymes involved in the Amaryllidaceae alkaloid pathway. Both pathways originate from L-tyrosine and are driven by a complex network of enzymes that generate remarkable structural diversity. Insights from the well-characterized BIA pathway can therefore provide valuable guidance for deciphering the AA pathway, as many of its predicted steps can be correlated with those already elucidated in BIA biosynthesis. Among plant alkaloid

pathways, the BIA pathway has been the most extensively studied, and its enzymatic machinery encompasses several major enzyme families (Figure 1.4), the most common and functionally important of which are summarized below.

PR10 like proteins: The initial scaffolding of BIAs begins with condensation carried out by enzyme norcoclaurine synthase (NCS), a member of the pathogenesis-related protein 10 (PR10) family, which catalyzes the stereoselective Pictet-Spengler condensation of dopamine and 4-hydroxyphenylacetaldehyde to yield a common intermediate (S)-norcoclaurine (Beaudoin and Facchini, 2014; Samanani et al., 2004). In AA pathway, norbelladine synthase, protein of same PR10 family catalyzes the condensation reaction to give rise to common intermediate norbelladine (Majhi et al., 2023; Singh and Singh, 2018).

Methyltransferases (MTs): These enzymes that introduce methyl groups and more often two class are involved in alkaloid pathway, i.e. *N*-methyltransferases (*N*MTs) and *O*-methyltransferases (*O*MTs). *N*MTs, such as coclaurine *N*-methyltransferase (C*N*MT), thiopurine methyltransferase (THMT), tetrahydroprotoberberine *N*-methyltransferase (T*N*MT) and reticuline *N*-methyltransferase (R*N*MT) methylate nitrogen atoms (Choi et al., 2002; Desgagné-Penix and Facchini, 2012), while *O*MTs like norcoclaurine 6-*O*-methyltransferase (6*O*MT) and 3'-hydroxy-*N*-methylcoclaurine 4′-*O*-methyltransferase (4′*O*MT) methylate oxygen atoms (Gurkok et al., 2016). Couple of 4′*O*MT transcript and a C*N*MT like *N*-methyl transferase transcripts has been identified in Amaryllidaceae species (Koirala et al., 2024; Liyanage et al., 2025).

Cytochromes P450 (CYPs): These heme-thiolate enzymes are predominantly anchored to the endoplasmic reticulum and catalyze a wide range of oxidative reactions, including hydroxylations, methylenedioxy bridge formations, and carbon-carbon bond formations. In BIA, P450 monooxygenase like (S)-*N*-methylcoclaurine 3'-hydroxylase (CYP80B3) (Liu et al., 2021), berbamunine synthase (CYP80A1) (Stadler and Zenk, 1993), and salutaridine synthase (CYP719B1) (Gesell et al., 2009; Wijekoon and Facchini, 2012), which contribute to diverse BIA structures from the 1-benzylisoquinoline backbone. In Amaryllidaceae, a cytochrome P450 enzyme (CYP96T1) in *Narcissus* aff. *pseudonarcissus* was identified to catalyze the *para-para´* C-C phenol coupling of 4′-*O*-methylnorbelladine in alkaloids biosynthesis, including

haemanthamine- and crinamine-type alkaloids (Kilgore et al., 2016a). Similar enzymes might be involved in the formation of cherylline and rystilline too.

Flavin-dependent oxidoreductases (FADOXs): These enzymes facilitate oxidoreductive reactions without incorporating oxygen atoms into the substrate. Notably, the berberine bridge enzyme (BBE) catalyzes a unique intramolecular C-C bond formation to yield the protoberberine backbone, (S)-scoulerine (Kutchan and Dittrich, 1995). Other FADOXs like (S)-tetrahydroprotoberberine oxidase (TPOX) and dihydrobenzophenanthridine oxidase (DBOX) are involved in terminal oxidations leading to quaternary alkaloids (Hagel and Facchini, 2013). BBE and STOX are notably found in distinct cellular vesicles, highlighting specific compartmentation (Jiao et al., 2024). In AA, similar enzyme can catalyze the conversion of norpluviine to caranine or normaritidine to vittatine.

2-Oxoglutarate-dependent dioxygenases (2-ODDs): These enzymes are responsible for critical *O*-demethylation and *O*,*O*-demethylation steps, such as those performed by thebaine 6-*O*-demethylase (T6ODM) and codeine *O*-demethylase (CODM) in morphine biosynthesis (Hagel and Facchini, 2010). In AA, we can predict the similar enzyme occurrence in conversion of vittatine to 11-hydroxyvittatine or the hydroxylation of intermediate of cherylline pathway.

NADPH-Reductases: This group includes short-chain dehydrogenases/reductases (SDRs) and aldo-keto reductases (AKRs), which catalyze various reduction reactions. Examples include salutaridine reductase (SalR) (Ziegler et al., 2009) in morphine biosynthesis and codeinone reductase (CoR) (Dastmalchi et al., 2018; Unterlinner et al., 1999). In AA biosynthesis, same family of enzyme norcraugsodine reductase (NR) is shown to be involved in initial step (Majhi et al., 2023). Similar enzyme, noroxomaritidine reductase reduce noroxomaritidine to normaritidine (Kilgore et al., 2016). Other predicted similar enzymes could be nornarwedine reductase or narwedine reductase in galanthamine pathway and caranine reductase in lycorine pathway.

This modular and repetitive recruitment of a limited number of ancestral enzyme families, coupled with their specific subcellular localization, underlies the remarkable diversity and complexity of the alkaloid biosynthetic network.

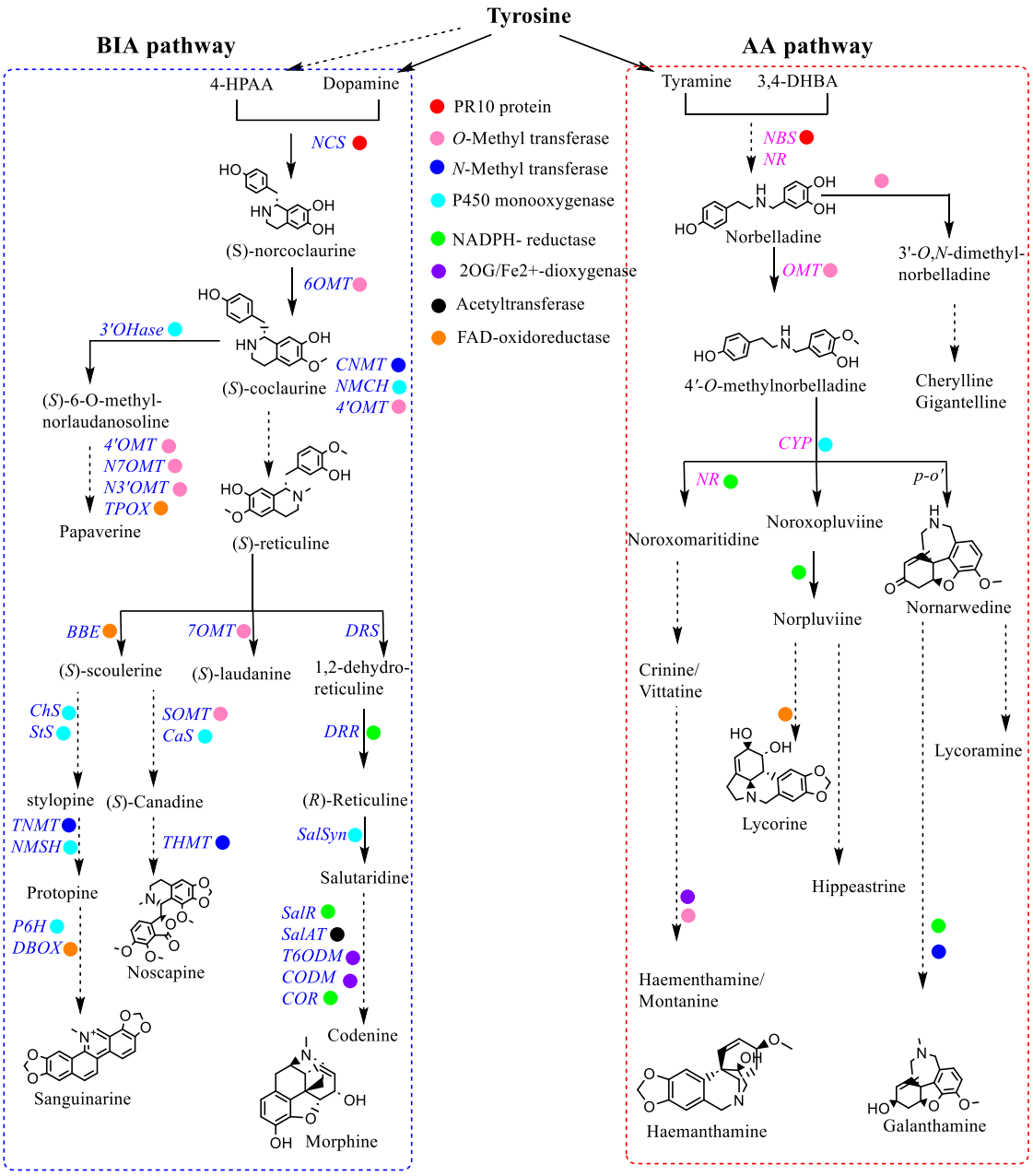


Figure 1.4: BIA and AA with major class of enzymes.
4-HPAA, 4-hydroxyphenylacetaldehyde; 4-HDCA, 4-hydroxydihydrocinnamaldehyde; 3,4-DHBA, 3,4-dihydroxybenzaldehyde; NCS, norcoclaurine synthase; 6OMT, norcoclaurine 6-*O*-methyltransferase; CNMT, coclaurine N-methyltransferase; NMCH, N-methylcoclaurine; 4′OMT, 4′-*O*-methyltransferase; SalSyn, salutaridine synthase; SalR, salutaridine reductase; SalAT, salutaridinol 7-*O*-acetyltransferase; T6ODM, thebaine 6-Odemethylase; CoR, codeinone reductase; CODM, codeine O-demethylase; BBE, berberine bridge enzyme; ChS, cheilanthifoline synthase; StS, stylopine synthase; TNMT, tetrahydroprotoberberine N-methyltransferase; NMSH, N-methylstylopine 14-hydroxylase; P6H, protopine 6-hydroxylase; DBOX, dihydrosanguinarine oxidase; SOMT, scoulerine-*O*-methyltransferase; CaS, canadine synthase; THMT, thiopurine methyltransferase;DRS, dehydroreticuline synthase; DRR, dehydroreticuline reductase; NBS, norbelladine synthase; NR, noroxomaritidine reductase; N4OMT, norbelladine 4-*O*-methyltransferase; CYP, cytochrome p450

1.7 Metabolic engineering

Metabolic engineering is the science of reprogramming cell metabolism to improve the production of natural compounds or enable cells to make new products, with applications in fuels, chemicals, food, feed, and pharmaceuticals (Nielsen and Keasling, 2016). Metabolic engineering begins with identifying and reconstructing a biosynthetic pathway often in model hosts like *E. coli, S. cerevisiae, Arabidopsis thaliana, Nicotiana. benthamiana* or algae like *Chlamydomonas* or *Phaeodactylum tricornutum.* Through precise genetic manipulation and systems-level analysis, metabolic engineering can revolutionize biomanufacturing processes, enabling cost-effective production of complex molecules with applications in healthcare, agriculture, and environmental sustainability.

Recent advancements in synthetic biology tools, omics technologies, computational modeling and artificial intelligence have further accelerated progress in this field, offering new avenues for the rational design and optimization of cellular metabolism for diverse industrial and therapeutic applications (Helmy et al., 2020). The elucidation of SM pathways by integrating genetic manipulation techniques has led in the identification and optimization of key biosynthetic steps (O'Connor, 2015). Pathways such as colchicine and monoterpene indole alkaloids are being elucidated (Guo et al., 2024; Nett et al., 2020; Salim and De Luca, 2013) and synthetic biology now allows their reconstitution in microbial hosts like *Saccharomyces cerevisiae* (Cravens et al., 2019). Using advanced enzyme expression, pathway optimization, and high-throughput methods, researchers have achieved microbial production of BIAs including reticuline, codeine, and morphine (Fossati et al., 2015; Pyne et al., 2016). Similar progress has been made with tropane alkaloids, where the full biosynthetic routes of hyoscyamine and scopolamine have been elucidated and successfully produced in yeast and *N. benthamiana* (Srinivasan and Smolke, 2020; Wen et al., 2024). Similarly, mevalonate pathway–derived sesquiterpenes such as costunolide (Liu et al., 2011), parthenolide (Liu et al., 2014), valencene (Cankar et al., 2015), artemisinic acid (van Herpen et al., 2010) and artemisinin (Wang et al., 2016) or methylerythritol phosphate pathway (MEP)-derived monoterpenes like Geraniol (Dong et al., 2016), diterpene like taxadiene (Hasan et al., 2014) or cembratrienol (Brückner and Tissier, 2013) has been produced through transient expression in *N. benthamiana*. While numerous alkaloids have been extensively studied and reported in the context of plant metabolic engineering, AA remain largely unexplored. For applying

metabolic engineering approaches to this class, the elucidation of key biosynthetic genes is essential, and this thesis specifically addresses that gap.

1.8 *Nicotiana benthamiana* as metabolic engineering platform

Nicotiana benthamiana is widely used as a model plant in plant biology for several reasons. It is highly amenable to *Agrobacterium tumefaciens*-mediated transformation, making it an excellent system for transient gene expression and genetic studies. The plant is highly susceptible to viruses, which has been leveraged for virus induced gene silencing (VIGS), a tool used to study gene function by silencing specific genes (Velásquez et al., 2009). It grows quickly and is easy to maintain under controlled conditions, which allows for rapid experimentation and multiple generations within a short time frame. It has large leaves and provides a substantial surface area for experiments involving infiltration, such as transient expression studies. Moreover, the genome of *N. benthamiana* has been sequenced and annotated, providing a wealth of information for functional genomics studies (Kurotani et al., 2023).

The foundation of plant molecular farming was established in 1989 when Hiatt, Cafferkey, and Bowdish successfully expressed mammalian antibodies in tobacco (Hiatt et al., 1989). This pioneering work led to the development of plant-based platforms that produce recombinant proteins, therapeutic antibodies, and vaccine antigens. Over the years, plant molecular farming has evolved into a viable biotechnology discipline, with *N. benthamiana* emerging as a critical model organism. The transient expression system using *A. tumefaciens* has become a standard for producing high quantities of recombinant proteins, taking advantage of the ability of *A. tumefaciens* to transfer DNA into the host genome.

N. benthamiana, has shown considerable potential in the engineering of complex alkaloids and recombinant proteins. This system has enabled numerous advancements in the field, with significant research focused on improving recombinant protein yield, enhancing product quality, and discovering new metabolites (Boccia et al., 2022; Nett et al., 2020). As more studies report successful applications of *N. benthamiana*, its importance in both scientific research and commercial biotechnology continue to grow, solidifying its role in the production of valuable bioactive compounds and pharmaceuticals (Golubova et al., 2024).

These systems offer substrates, cofactors, and subcellular compartmentalization that support biosynthetic processes (Reed, 2016). A key method utilized in this field is agroinfiltration, a scalable technique for transient gene expression, allowing to produce valuable compounds such as terpenoids and alkaloids. This plant is emerging as a preferred heterologous host to investigate and manipulate metabolic pathways (Boccia et al., 2022; Miettinen et al., 2014; Nett et al., 2020; Reed and Osbourn, 2018). Although there is countable research on BIA using *N. benthamiana* as heterologous host, in this study we used this model system for all our *in vivo* experiments.

Importance, hypothesis, and objectives

Medicinal plants have long been a source of therapeutic agents, and many modern drugs are plant-derived (Atanasov et al., 2015). Among them, AAs represent a structurally diverse and pharmacologically rich class of compounds. One of the AA galanthamine-an FDA-approved drug for the symptomatic treatment of Alzheimer's disease—has reached top commercial use, predominantly sourced from *Narcissus* and *Leucojum* species (Heinrich and Teoh, 2004; Hotchandani and Desgagne-Penix, 2017). However, galanthamine accumulation in plants is low and variable, and its purification is laborious, resulting in scarce availability in the global market. With dementia and Alzheimer's disease cases rising rapidly worldwide, the demand for galanthamine far exceeds current supply. This scarcity underscores an urgent need for alternative and sustainable production systems. Yet, progress has been hindered by limited knowledge of the intermediate metabolites and genes involved in AA biosynthesis. Elucidating the galanthamine pathway is therefore critical not only to advance fundamental understanding of AA metabolism but also to enable metabolic engineering strategies for scalable, reliable, and cost-effective production of this vital drug.

To formulate a working hypothesis and design experiments, it is essential to first consider the current state of knowledge, which is summarized in section 1.5. Shortly, the proposed biosynthetic pathway of galanthamine has been largely inferred from isotope feeding studies and structural analyses of AAs. These studies suggest that L-phenylalanine and L-tyrosine are converted into 3,4-dihydroxybenzaldehyde and tyramine, which subsequently condense to form norbelladine via the action of norbelladine synthase and noroxomaritidine reductase —the only steps characterized to date in *Leucojum aestivum*. In *Narcissus*, norbelladine has been shown to undergo *O*-methylation by N4′*O*MT to yield 4′-*O*-methylnorbelladine. Beyond this point, the enzymatic steps leading to galanthamine remained unresolved when I initiated the PhD project in 2021.

On basis of drawing on parallels with the BIA pathway and knowledge-based predictions in AA pathway, several steps were proposed that involve enzyme families such as cytochrome P450 monooxygenases, NADPH-dependent reductases, and *N*-methyltransferases to give galanthamine. Candidate genes encoding putative enzymes for these reactions have been identified from the

transcriptomes of *L. aestivum* (Tousignant et al., 2022) and efforts were undertaken to functionally characterize them.

Based on this framework, we formulated the following hypotheses.

I. Tyramine and 3,4-DHBA co-infiltrated with *LaNBS* and *LaNRII* yields norbelladine which is catalyzed by *LaN4′OMT* to yield 4′-*O*-methylnorbelladine.

II. 4′-*O*-methylnorbelladine undergoes phenol coupling by cytochrome enzyme *La*CYP96T1 and *La*CYP96T2 and gets reduced to subsequent compounds by NADPH dependent reductase.

III. *N*-demethylnarwedine yield narwedine and norgalanthamine is catalyzed to galanthamine by *N*-methyltransferase.

The objective of this study is to functionally characterize candidate enzymes of the galanthamine biosynthesis pathway and reconstruct the sequential steps in *N. benthamiana*, thereby validating their roles and advancing metabolic engineering strategies for sustainable galanthamine production.

Chapter II

Chapter II contains a study that presents an enzyme network driving Amaryllidaceae Alkaloids Biosynthesis in *Leucojum aestivum*.

The manuscript was published in March 2025 in Plant biotechnology journal.

Contributions: Basanta Lamichhane designed and constructed the biosynthetic pathway, performed both *in vivo* and *in vitro* enzymatic assays, and was responsible for drafting, revising, and finalizing the manuscript. Sarah-Eve Gélinas carried out metabolite analyses using LC–MS/MS. Natacha Merindol performed molecular docking studies and assisted in revising the manuscript. Karen prepared Table 2.1. Hugo Germain co-supervised the project and contributed to data interpretation, figure preparation, and manuscript revisions. Isabel Desgagné-Penix supervised the project, provided funding and research materials, and contributed to manuscript writing and critical revisions."

Plant Biotechnology Journal
Open Access

Plant Biotechnology Journal (2025), pp. 1–18 doi: 10.1111/pbi.70026

Elucidating the enzyme network driving *Amaryllidaceae* alkaloids biosynthesis in *Leucojum aestivum*

Basanta Lamichhane[1], Sarah-Eve Gélinas[1], Natacha Merindol[1], Manoj Koirala[1], Karen Cristine Gonçalves dos Santos[1], Hugo Germain[1,2] and Isabel Desgagné-Penix[1,2,*]

[1]*Department of Chemistry, Biochemistry and Physics, Université du Québec à Trois-Rivières, Trois-Rivières, QC, Canada*
[2]*Plant Biology Research Group, Trois-Rivières, QC, Canada*

Received 12 September 2024;
revised 28 January 2025;
accepted 14 February 2025.
**Correspondence* (Tel 1-819-376-5011; fax 1-819 376-5012; email isabel.desgagne-penix@uqtr.ca)

Keywords: specialized metabolism, cytochrome P450, phenol coupling, biosynthetic pathway, pharmaceuticals, metabolic engineering.

Summary

Amaryllidaceae alkaloids (AAs) are diverse bioactive metabolites with significant pharmaceutical potential, derived from 4′-O-methylnorbelladine (4′OM). The biosynthesis of these compounds involves the condensation of tyramine and 3,4-dihydroxybenzaldehyde by norbelladine synthase (NBS) and/or noroxomaritidine/norcraugsodine reductase (NR), followed by *O*-methylation. Cytochrome P450 enzymes, particularly the CYP96T family, introduce further structural diversity through C–C couplings, resulting in lycorine, galanthamine and crinine cores. Despite their importance, the exact biosynthetic pathways remain poorly defined. In this study, we describe key enzymes from *Leucojum aestivum* (*La*), providing crucial insight into AA biosynthesis. Transient expression in *Nicotiana benthamiana* demonstrated that *La*NBS and *La*NRII catalyse the conversion of tyramine and 3,4-dihydroxybenzaldehyde to norbelladine, which is subsequently *O*-methylated by a norbelladine-4′-*O*-methyltransferase (*La*N4′OMT) *in planta*. Co-agroinfiltration of *La*NBS, *La*NRII, *La*N4′OMT and *La*CYP96T1 resulted in the production of various phenol-coupled products, with lycorine as the predominant compound, alongside haemanthamine, crinine/vittatine and norgalanthamine. This study identifies *La*CYP96T1 and *La*CYP96T2 as the first monocot enzymes capable of catalysing all three regioselective C-C phenol couplings and also highlights the substrate promiscuity of *La*NRII. The findings not only elucidate critical steps in AA biosynthesis but also open new avenues for biotechnological application in producing valuable alkaloids, offering potential for novel drug development.

Elucidating the enzyme network driving Amaryllidaceae Alkaloids Biosynthesis in *Leucojum aestivum.*

Basanta Lamichhane[1], Sarah-Eve Gélinas[1], Natacha Merindol[1], Manoj Koirala[1], Karen Cristine Gonçalves dos Santos[1], Hugo Germain[1,2], Isabel Desgagné-Penix[1,2*]

[1]Department of Chemistry, Biochemistry and Physics, Université du Québec à Trois-Rivières, Trois-Rivières, QC, Canada

[2]Plant Biology Research Group, Trois-Rivières, Québec, Canada

BL: Basanta.Lamichhane@uqtr.ca

SEG: Sarah-Eve.Gelinas@uqtr.ca

NM: natacha.Merindol@uqtr.ca

MK: Manoj.Koirala@uqtr.ca

KCGS: cris.kgs@gmail.com

HG: Hugo.Germain@uqtr.ca

IDP: Isabel.Desgagne-Penix@uqtr.ca

*Corresponding author's email address: Isabel.Desgagne-Penix@uqtr.ca ; Tel.: 1-819-376-5011 ext. 3316

2.1. Abstract

Amaryllidaceae alkaloids (AAs) are diverse bioactive metabolites with significant pharmaceutical potential, derived from 4′-*O*-methylnorbelladine (4′*O*M). The biosynthesis of these compounds involves the condensation of tyramine and 3,4-dihydroxybenzaldehyde by norbelladine synthase (NBS) and/or noroxomaritidine/norcraugsodine reductase (NR), followed by *O*-methylation. Cytochrome P450 enzymes, particularly the CYP96T family, introduce further structural diversity through C-C couplings, resulting in lycorine, galanthamine, and crinine cores. Despite their importance, the exact biosynthetic pathways remain poorly defined. In this study, we describe key enzymes from *Leucojum aestivum* (*La*), providing crucial insight into AA biosynthesis. Transient expression in *Nicotiana benthamiana* demonstrated that *La*NBS and *La*NRII catalyze the conversion of tyramine and 3,4-dihydroxybenzaldehyde to norbelladine, which is subsequently *O*-methylated by a norbelladine-4′-*O*-methyltransferase (*La*N4′*O*MT) *in planta*. Co-agroinfiltration of *La*NBS, *La*NRII, *La*N4′*O*MT, and *La*CYP96T1 resulted in the production of various phenol-coupled products, with lycorine as the predominant compound, alongside with haemanthamine, crinine/vittatine, and norgalanthamine. This study identifies *La*CYP96T1 and *La*CYP96T2 as the first monocot enzymes capable of catalyzing all three regioselective C-C phenol couplings, and also highlights the substrate promiscuity of *La*NRII. The findings not only elucidate critical steps in AA biosynthesis but also open new avenues for biotechnological application in producing valuable alkaloids, offering potential for novel drug development.

Keywords: specialized metabolism; cytochrome P450; phenol coupling; reductase; microsome; biosynthetic pathway; biotechnological applications; pharmaceuticals

2.2. Introduction

Amaryllidoideae from the Amaryllidaceae family produce a class of diverse specialized metabolites (SMs) with potent biological and therapeutic effects, known as the Amaryllidaceae alkaloids (AAs). Although galanthamine is the only AA commercialized as a treatment of mild symptoms of Alzheimer's disease owing to its acetylcholinesterase inhibitory properties, many other AAs have potential pharmacological applications. For instance, lycorine is extensively studied for its strong antiviral activities, and haemanthamine is known for its anticancer properties (Cahlikova et al., 2020; Girard et al., 2022).

However, the potential exploitation of AAs is hindered by their limited commercial availability (Takos and Rook, 2013). On the one hand, the current supply relies on AAs extracted from wild plants, such as *Leucojum aestivum* (summer snowflake), with varying yields (Georgievaa et al., 2007). On the other hand, total chemical synthesis is challenging due to the intricate carbon ring structures of these metabolites, compounded by environmentally unsustainable purification processes. *In vitro* culture of galanthamine-producing species, primarily *Narcissus confusus* and *L. aestivum*, have gained attention as an alternative strategy (Berkov et al., 2009; Kohut et al., 2007; Koirala et al., 2022; Pavlov et al., 2007) but are not widely used to date due to the resulting limited accumulation of AAs.

Metabolic engineering presents a promising alternative avenue for future AA production, contingent upon a thorough understanding of the biosynthetic pathway. Yet, while our comprehension of the chemistry and pharmacological properties of AAs is rapidly advancing, there remains a scarcity of knowledge regarding their synthesis (Desgagné-Penix, 2021; Kilgore and Kutchan, 2016b; Liyanage et al., 2024; Takos and Rook, 2013).

Roughly, the biosynthesis of AAs is governed by an extensive network of genes that code for enzymes, orchestrating a cascade of biochemical transformations starting from basic amino acid precursors to yield the structurally complex alkaloids characteristic of *Amaryllidoideae* (Figure 2.1). Specifically, from the plastidic aromatic amino acids pathway, L-tyrosine undergoes decarboxylation to yield tyramine (Xu et al., 2020), while L-phenylalanine, is converted to 3,4-dihydroxybenzaldehyde (3,4-DHBA) most likely through the phenylpropanoid pathway (Desgagné-Penix, 2021; Koirala et al., 2022). Previous *in vitro* studies using norbelladine/norcraugsodine synthase (NBS) and noroxomaritidine/norcraugsodine reductase

(NR) from *Narcissus pseudonarcissus, N. papyraceus* and *L. aestivum* suggested that the condensation of tyramine and 3,4-DHBA yields norcraugsodine, further reduced to form norbelladine (Figure 2.1) (Hnin et al., 2024b; Liu et al., 2023; Majhi et al., 2023a; Singh et al., 2018; Tousignant et al., 2022a). A 4′-*O*-methyltransferase, identified in *Narcissus* sp. *aff. pseudonarcissus*, *N. papyraceus*, *Lycoris aurea* and *Lycoris radiata*, catalyzes the methylation of norbelladine *in vitro* into the metabolic intermediate of AAs, 4′-*O*-methylnorbelladine (4′*O*M) (Kilgore et al., 2014; Li et al., 2019; Sun et al., 2018). Isotope labeling studies in *L. aestivum* revealed that deuterium-labelled 4′*O*M was further incorporated into galanthamine and lycorine through a C-C coupling cyclization step, as observed in the biosynthesis pathway of berberine-type alkaloids (Cui et al., 2007; El Tahchy et al., 2010; Iwasa and Kim, 1997). Later studies uncovered that a new class of cytochrome P450, CYP96T1 catalyzes mainly *para-para'* (*p-p´*) C-C oxidative coupling of 4′*O*M in *N.* sp. *aff. pseudonarcissus* but also yields the *para-ortho'* (*p-o´*) product *N*-demethylnarwedine as a minor product (Kilgore et al., 2016a). Recently, three homologs identified from *Narcissus* cv. Tête-à-Tête were shown to exhibit specific catalytic activity towards *o-p´*, *p-o´* or *p-p´* coupling reactions (Mehta et al., 2024), and four CYP96T1 homologs from *L. aurea* catalyzed exclusive *p-p´* or *p-o´* scaffold formation (Liu et al., 2024). These recent discoveries have led to the reconstitution of a partial galanthamine pathway starting from the C-C oxidative coupling of 4′*O*M in *Nicotiana benthamiana*. While they provided meaningful insight into galanthamine and haemanthamine scaffold formation, the functionality of orthologous *Amaryllidoideae* CYP96T, especially towards the *o-p´* coupling remains unclear. Moreover, the reconstitution of a complete pathway, i.e. starting from precursors, rather than *Amaryllidoideae*-restricted 4'OM is crucial both for elucidation purposes and for synthetic biology applications.

Nicotiana benthamiana contains all necessary cofactors, intracellular compartments along with protein-folding mechanisms essential for efficient synthesis of plant proteins (Reed and Osbourn, 2018). It has been extensively used to investigate plant metabolic pathways, from characterization of enzymes to elucidation of pathway, such as the monoterpene indole alkaloids (Boccia et al., 2022; Miettinen et al., 2014), strictosidine (Dudley et al., 2022), or colchicine (Nett et al., 2020), to name but a few.

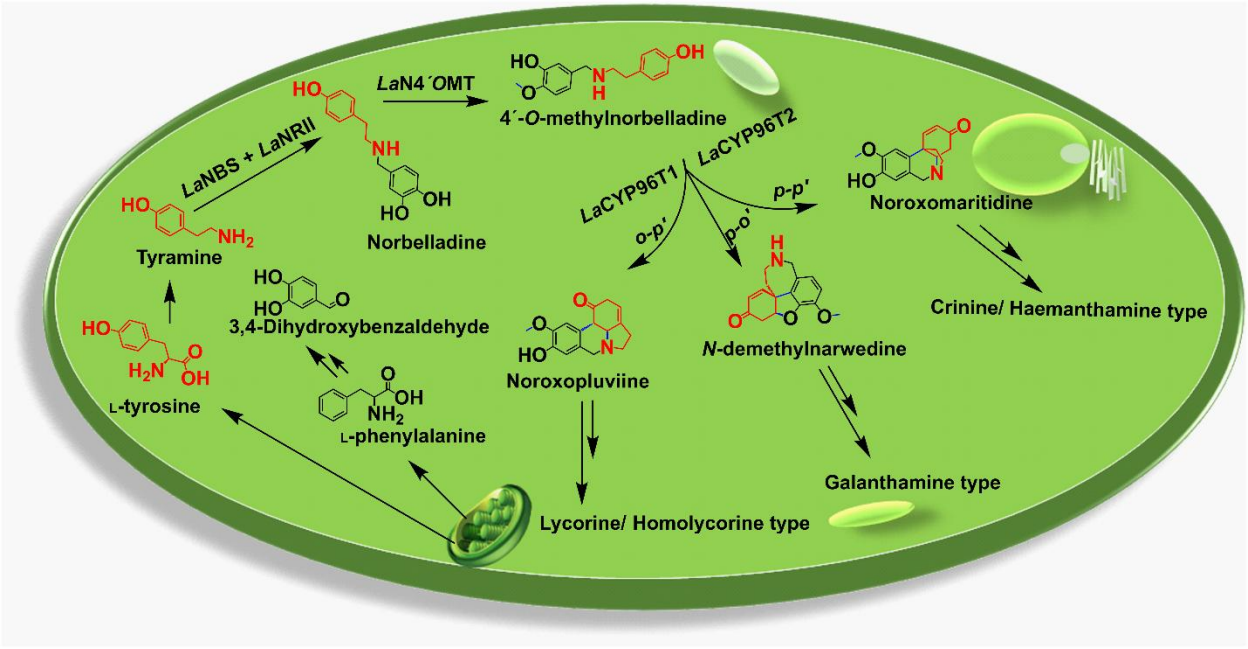


Figure 5 Proposed alkaloid biosynthesis pathway in *Leucojum aestivum.*

The diagram illustrates the hypothesized sequence of biochemical reactions leading to the synthesis of galanthamine, lycorine/homolycorine and crinine/haemanthamine-types of alkaloids in *Leucojum aestivum*, highlighting key enzymatic steps and intermediate compounds. *p-p´: para-para´* coupling, *p-o´: para-ortho´* coupling, *o-p´: ortho-para´* coupling.

In this study, we reconstituted the biosynthetic pathways of AAs through heterologous expression in *N. benthamiana* using *Agrobacterium*-mediated transient T-DNA expression. By leveraging the genetic tractability of *N. benthamiana*, we hypothesize that it is possible to produce therapeutically valuable AAs. This research provides insights into the complex biosynthetic pathways of these alkaloids and facilitates the development of a metabolic engineering platform.

2.3. Materials and Methods

2.3.1. Database of Amaryllidaceae transcriptomes

We constructed a database of Amaryllidaceae transcriptomes by downloading either raw read files (fastq) or assembly files (fasta) publicly available. If multiple datasets were available for the same species and cultivar, we selected the one for the assembly file was available. For species with multiple transcriptome assemblies available in NCBI Transcriptome Shotgun Assembly, we used the following criteria to select the assembly to include in the database: most recent, publication information available, best assembly statistics (i.e. lowest contig count, longest N50 length). If

only the raw datasets were available, we selected the one associated with a peer review publication, and used all data available if all were peer reviewed. Species, accession numbers and, when available, links to the original assembly files are provided in Table 2.1.

The raw reads were first processed with Fastp (v0.23.1) (Chen et al., 2018) software with cut front mean quality 20, cut tail mean quality 20 and length required 50. The resulting clean reads were assembled with Trinity version 2.14.0 (Grabherr et al., 2011) using default parameters. The completeness of the transcriptome assembly was assessed with BUSCO (v5.2.2) (Simao et al., 2015) using liliopsida_odb10. To limit the technical differences between the assemblies, all annotations were done using the same pipeline, even when predicted protein sequences and annotations were available. We used the Trinotate pipeline version 4.0.0 (http://trinotate.github.io/) (Bryant et al., 2017) with: TransDecoder version 5.5.0 (http://transdecoder.github.io/) was used for prediction coding sequences; HMMer version 3.2.2 (Eddy, 2008; Eddy, 2011) with Pfam-A database v3.1b2 was use to find protein family domains; prediction of transmembrane domains was done with TmHMM version 2.0c (Krogh et al., 2001); identification of noncoding RNA was performed with Infernal version 1.1.4 (Nawrocki et al., 2009); and Blast+ version 2.13 (Camacho et al., 2009) against the UniProt Swiss-Prot database (release 2024_04). Parameters for each software were set following Trinotate suggestions. For further analysis, only sequences with no hits blast hits (against UniProt Swiss-Prot) or with hits to Viridiplantae proteins were kept in the database, the remaining were considered contaminants.

Table 2.1. List of species included in database
List of species included in database with accession numbers for raw data in BioProject or BioSample and, when available, accession numbers or names of assembly files. [i]http://gigadb.org/dataset/100910; [ii]https://medplantrnaseq.org/; [iii] downloaded from the China National Center for Bioinformatics https://download.cncb.ac.cn/gsa/; [iv] assembly available for download at NCBI Gene Expression Omnibus.

Species	Reference	Raw data accession	Assembly accession
Amaryllis belladonna	One Thousand Plant Transcriptomes Initiative (2019)	ERS1829785	LDME[i]
Clivia miniata	Y. Li, R. Gao, et al. (2022); Wang et al. (2018)	PRJNA480383, PRJNA813401	
Crinum x powellii	M. Koirala et al. (2023)	PRJNA962562	
Galanthus elwesii	Matthew B. Kilgore, Megan M. Augustin, et al. (2016)	PRJNA306273	G_elwesii_Trinity.tar.gz[ii]
Galanthus sp. MBK-2015	Matthew B. Kilgore, Megan M.	PRJNA306697	Galanthus_Trini

	Augustin, et al. (2016)		ty.tar.gz[ii]
Hippeastrum vittatum	Zeng et al. (2024)	PRJNA862291	
Hippeastrum x *hybridum*	X. Li et al. (2022)	PRJNA608969	
Leucojum aestivum	Tousignant et al. (2022)	PRJNA720900	
Lycoris chinensis	F. Zhang et al. (2022)	PRJNA847051	
Lycoris longituba	Q. Li et al. (2020)	PRJNA590043	
Lycoris radiata	N. Wang et al. (2021)	PRJCA006232	CRA004779[iii]
Lycoris sprengeri	Yang et al. (2021)	PRJNA714286	
Narcissus papyraceus	T. Hotchandani et al. (2019)	PRJNA407433	
Narcissus pseudonarcissus cv King Alfred	Singh and Desgagné-Penix (2017)	PRJNA392294	
Narcissus aff. *pseudonarcissus*	Matthew B. Kilgore, Megan M. Augustin, et al. (2016)	PRJNA301357	narcissus_9-20101112.tar[ii]
Narcissus tazetta var. *chinensis*	He et al. (2020)	PRJNA523125	GSE126727[iii]
Narcissus viridiflorus	One Thousand Plant Transcriptomes Initiative (2019)	ERS1829787, ERS1829786	TRRQ[i]
Phycella aff. *cyrtanthoides*	One Thousand Plant Transcriptomes Initiative (2019)	ERS3670342	DMIN[i]
Rhodophiala pratensis	One Thousand Plant Transcriptomes Initiative (2019)	ERS1829788	JDTY[i]
Traubia modesta	One Thousand Plant Transcriptomes Initiative (2019)	ERS1829789	ZKPF[i]
Zephyranthes candida	C. H. Zhang et al. (2022)	PRJNA796382	
Zephyranthes treatiae	One Thousand Plant Transcriptomes Initiative (2019)	ERS1829790	DPFW[iv]

2.3.2. Phylogenetic analysis

The candidate transcripts of *L. aestivum* selected in this study include homologous (norbelladine/norcraugsodine synthase [NBS] and noroxomatidine/norcraugsodine reductase [NR], (Majhi et al., 2023b)) and orthologous sequences (4'-*O*-methyltransferase [N4'*O*MT] and noroxomaritidine synthase CYP96Ts, (Hnin et al., 2024a; Kilgore et al., 2016a; Koirala et al., 2024) of previously characterized enzymes pulled from transcriptome database. To find putative NBS, NR, N4'*O*MT and CYP96 in *L. aestivum*, we used the sequences of the enzymes characterized previously in *Papaver somniferum*, *N. pseudonarcissus* and *N.* aff. *pseudonarcissus* (UniProt accessions: NCS_PAPSO, NR_NARAP, NOMT_NARAP and C96T1_NARAP, respectively) as query in BLAST searches (blast+/2.14.0 (Camacho et al., 2009), e-Value < 0.001, identity > 30%) of the transcriptome of *L. aestivum*. Predicted sequences contained both start and stop codons. The candidate transcripts of *L. aestivum* were aligned against PR10/BetIV family

proteins (in the case of *La*NBS), short chain dehydrogenase/reductases (for *La*NRII), *O*-methyltransferases (for *La*N4′*O*MT) and cytochrome P450 proteins (for *La*CYP96T) obtained from UniProt, SwissProt, or the National Center for Biotechnology Information (NCBI) databases (accession numbers available in Table 2.S1) using ClustalW (Sievers et al., 2011) (default parameters). Catalytic sites and conserved motifs were identified on basis of published literature or NCBI conserved domain search tool or InterPro database following the alignment (Paysan-Lafosse et al., 2023). The percentage identity matrix was calculated in UGENE software (Okonechnikov et al., 2012) and the multiple sequence alignment was viewed in Jalview software (Waterhouse et al., 2009). Phylogenetic trees were constructed using ModelRevelator software tool "Iqtree" with 1000 ultrafast bootstraps, 1000 branch test, as well as 1000 with minimum correlation coefficient 0.99, followed by standard IQ tree search parameters (Hoang et al., 2018; Kalyaanamoorthy et al., 2017; von Haeseler et al., 2014). ModelRevelator is a model selection tool underpinned by two deep neural networks. The models resulting from neural network estimates are closer to the ground truth than maximum likelihood trees (Burgstaller-Muehlbacher et al., 2023). iTOL was used for tree visualization and representation (Letunic and Bork, 2021).

2.3.3. Molecular modelling

Structural prediction of *L. aestivum* enzymes including norbelladine 4ˈ-*O*-methyltransferase (*LaN4'O*MT), norbelladine/norcraugsodine synthase (*La*NBS), noroxomaritidine/norcraugsodine reductase (*La*NR), and cytochrome P450 *La*Cyp96T1 and cytochrome P450 *La*Cyp96T2 was performed using CollabFold v1.5.3 (AlphaFold2 via MMseqs2) (Mirdita et al., 2022). Models were visualized and superimposed using Pymol 3.0.0 (Schrödinger). MOE2022.09 software (Chemical Computing Group) was employed for analyzing model conformations and preparing receptors for docking, as outlined in (Majhi et al., 2023b). Pocket residues of predicted enzymes were superimposed with reference crystal structures in MOE. Crystal structures of *Rattus norvegicus* and *Homo sapiens* Cat*O*MTs (PDB:1H1D (Bonifacio et al., 2002) and 3A7E, respectively) were used as references for *La*N4′*O*MT, norcoclaurine synthase from *Thalictrum flavum* for *La*NBS (PDB:2VQ5; (Ilari et al., 2009)), *N. pseudonarcissus* King Alfred noroxomaritidine/norcraugsodine reductase for *La*NR (PDB:5FF9; (Kilgore et al., 2016)), and *Priestia megaterium* CYP102A1 (PDB:6JMH; (Stanfield et al., 2020)) and *Mycobacterium*

tuberculosis cyclo(l-Tyr-l-Tyr) C-C coupling CYP121 (PDB:3G5H; (Belin et al., 2009; Dumas et al., 2014; Peng et al., 2023)) for *La*CYP96T1 and for *La*CYP96T2. Methyl donor *S*-adenosylmethionine (SAM for *La*N4′*O*MT), metal ion (Mg^{2+} for *La*N4′*O*MT), cofactor nicotinamide adenine dinucleotide phosphate (NADPH for *La*NR), as well as heme and two vicinal H_2O (*La*Cyp96T1 and 2) were included in the active sites at coordinates of orthologous crystal structures. Structures underwent preparation including correcting issues, capping, charging termini, selecting appropriate alternate, protonation, calculating optimal hydrogen position and charges, and energy minimization with tethered active site residues and fixed NADPH, H_2O and heme, SAM and Mg^{2+}, in corresponding enzymes, before docking. The docking site was predicted based on residues in interaction with ligands of orthologous crystal structures, as described in (Majhi et al., 2023b), or using dummies atoms added to the receptor with MOE Site Finder tool. The docking site included Mg^{2+} and SAM, H_2O and heme, or NADPH, where applicable. Ligands (3,4-DHBA, tyramine (*La*NBS), norcraugsodine (*La*NRII), norbelladine (*La*N4′*O*MT), and 4'-*O*-methylnorbelladine (*La*CYP96T1 and *La*CYP96T2)) isomeric smiles codes were retrieved from PubChem and submitted to the ZINC20 database to download 3D data files (Irwin et al., 2020). Every protomer predicted at pH=7 was included as a possible ligand.

The AMBER10:EHT force field was employed. Triangle Matcher was used as the placement method for 200 poses and flexible docking was performed with tethered induced fit refinement, yielding 10 best poses. Docking poses were analyzed by comparison with crystalized protein-ligand complexes, and the first pose (with the best docking score) coherent with crystalized enzymes ligand positioning and with the catalyzed reaction was selected for each ligand. PLIP was utilized to analyze the interactions between ligands and receptor residues (Adasme et al., 2021), and the images were further processed using PyMOL along with prediction of hydrogen bonds between the metal ion or the water molecules and the docked ligand, where applicable.

2.3.4. RNA extraction and cDNA synthesis

L. aestivum bulbs were purchased from The Seed Company, Canada and grown in the laboratory plant room. 4 cm of the apical part of a one-month-old newly emerging leaf was cut, immediately grinded in liquid nitrogen by mortar and pestle, and stored at -80 °C. 50 mg of grinded leaf tissue was used for targeted metabolite analysis with a HPLC-MS/MS to identify key metabolites, i.e.,

4'-*O*-methylnorbelladine, norgalanthamine, and galanthamine. The remaining leaf tissue was used for subsequent RNA extraction. RNA was extracted from 80 mg snap frozen tissue with the RNeasy® Plant Mini Kit (Qiagen) following the manufacturers protocol without the optional steps. cDNA synthesis was performed using the SensiFAST cDNA synthesis kit by Meridian Bioscience. Briefly, the SensiFAST cDNA Synthesis Mix containing random hexamers and anchored oligo-dT primers was mixed with RNA, followed by the addition of reverse transcriptase and reaction buffer, to be then incubated at 42 °C. After the reaction, the enzyme was inactivated by heating at 85 °C for 5 minutes. The resulting cDNA was then stored at -80 °C.

2.3.5. PCR amplification of key candidate genes LaNBS, LaNRII, LaN4´OMT, LaCYP96T1 and LaCYP96T2.

The coding sequences of norbelladine synthase (*LaNBS*), noroxomaritidine reductase (*LaNRII),* 4´*O*-methyltransferase (*LaN4´OMT)* and cytochrome P450 (*LaCYP96T1* and *LaCYP96T2*) of *L. aestivum* were amplified using primers designed with *att*B1 and *att*B2 overhangs for Gateway cloning in expression vector pK7WG2 (Karimi et al., 2007). Primers for *LaNBS, LaNRII*, *LaN4´OMT, and LaCYP96T1/2* were designed for expression with x3 AU1, x3 FLAG, x3 AU5, and x3 Myc tag at their C-terminal, respectively, tag sequences were included in the reverse primers (Table 2.S2). Primers for localization study of the candidate gene *LaN4´OMT* were designed for cloning into expression vectors pB7WGF2 (N-terminal EGFP fusion) and pB7FWG2 (C-terminal EGFP fusion) vectors, while *LaCYP96T2* primers were designed to clone into pB7FWG2 (C-terminal EGFP fusion) (Table 2.S2). The coding sequences of *LaNBS*, *LaNRII, LaN4´OMT* were also amplified with primers containing restriction sites BamHI and HindIII to clone into pMAL-c2X plasmid. PCR amplifications were conducted PrimeStar GXL premix (TaKaRa Bio) in T100 Thermal cycler of Bio-Rad. PCR program parameters were 5 min 98 °C 1 cycle, 10 s 98 °C, 30 s (55 °C - 65 °C; primer specific), 1-min/kb 72 °C for 34 cycles, 5 min 72 °C 1 cycle, and final infinite hold at 4 °C. Amplification was checked by running 2 µl of PCR product in 0.9% agarose gel and images were taken in Bio-Rad ChemiDoc Imaging system. PCR clean-up and gel purification was done according to manufacturer's protocol by GeneAid-PCR & Gel Kit.

2.3.6. Cloning and transformation

Amplified PCR fragments with attb1 and attb2 were cloned with Gateway cloning according to manufacturer's protocol (Thermo Fisher scientific). Briefly, the Gateway-adapted *att*P-flanked pDONR 221 vectors with kanamycin resistance gene was used for BP recombination reaction to generate an *att*L-flanked entry clone with *att*B-flanked-*LaNBS*, -*LaNRII*, -*LaN4´OMT*, -*LaCYP96T1*, -*LaCYP96T2,* -*LaN4´OMT* (C-terminal EGFP fusion)*,* -*LaN4´OMT* (N-terminal EGFP fusion) and -*LaCYP96T2* (C-terminal EGFP fusion) DNA fragment. These entry vectors were transformed into *E. coli* DH5α chemicompetent cells, subsequently grown on a kanamycin (50 µg/mL) LB agar plate. Following colony PCR, Miniprep of positive clones were performed according to the manufacturers protocol of Presto Mini Plasmid Kit from Geneaid. A positive entry clone of each construct was sent for Sanger sequencing (Genome Quebec). Once integrity was confirmed, the selected plasmids were incubated overnight with LR reagents to perform a LR recombination reaction between an *att*L containing entry clone and *att*R-containing destination vectors (pK7WG2, pB7FWG2 and pB7WGF2 vectors). The LR reaction mix was transformed into *E. coli* DH5α chemicompetent cells and grown in spectinomycin (50 µg/mL) agar plates. The positive clones were confirmed by colony PCR, and plasmid extraction was done as mentioned above, growing positive colonies in 5 mL LB broth with spectinomycin 50 µg/mL. These expression clones were transformed in *Agrobacterium* GV3101. After 48 hours of incubation in LB plates at 28 °C, the presence of insert in the construct was once again confirmed with colony PCR.

Amplified PCR fragments of *LaNBS*, -*LaNRII*, -*LaN4´OMT* along with the vector pMALc2X were digested by BamHI and HindIII. Fragments were ligated using T4-DNA ligase (New England Biolabs) and transformed in chemically competent *E. coli* DH5α cells leaving them to grow in ampicillin (100 µg/mL) agar plates for each gene. Colony PCR and sequencing was carried out for verification of integrity of each gene in the plasmid. Plasmids were further transformed in *E. coli* Rosetta (BL21) and grown on ampicillin (100 µg/mL) and chloramphenicol (34 µg/mL) agar plate.

2.3.7. Transient expression of candidate genes in *N. benthamiana* (*in vivo* assay)

Individual *Agrobacterium* GV3101 colonies, carrying the desired gene constructs (*LaNBS*, *LaNRII*, and *LaN4´OMT*, *LaCYP96T1* and *LaCYP96T2*), were streaked on LB plates with 50

µg/mL spectinomycin, 50 µg/mL rifampicin and 30 µg/mL gentamicin, and grown at 28 °C for 2 days. With the cell scraper, colonies were scraped from plate, resuspended in *Agrobacterium* induction buffer (10 mM MES, pH 5.6, 10 mM $MgCl_2$, and 150 µM acetosyringone) and incubated for 2 hours at room temperature. 4–5-week-old *N. benthamiana* grown in growth chamber with 22 °C temperature and 16 h of light/8 h of dark conditions were used for the experiments. *N. benthamiana* leaves were infiltrated or co-infiltrated with *Agrobacterium* suspensions of 0.6 of optical density at 600 nm (OD_{600}) on the leaf abaxial side using a needleless syringe. Unless otherwise mentioned, three leaves each of three independently infiltrated plants of each experimental condition were used to test the hypothesis. At first, *Agrobacterium* suspensions harboring the genes were infiltrated in the plant leaves and incubated for 48 hours. In the second step, leaves were infiltrated with 100 µM substrates. Following an incubation of 24 hours, the leaves were harvested, snap-frozen and preserved at -80 °C for further analysis. The snap-frozen samples were crushed into powder using 5-mm diameter stainless steel beads, shaking at 25 Hz for 1.5 min in TissueLyser II (Qiagen).

The expression of enzymes after agroinfiltration of genes of interest in *N. benthamiana* leaves was verified by RT-qPCR and western blot. Briefly, 100 mg of tissue was resuspended in 0.5 mL of lysis buffer (100 mM Tris-HCl, pH 7.5, 1 mM phenylmethylsulfonyl fluoride, 10% glycerol, 10 mM β-mercaptoethanol and 2% polyvinylpolypyrrolidone) and incubated for 30 min on ice with periodic, gentle inversion. Extracts were centrifuged at 12,000 *g* at 4 °C for 30 min to pellet debris, after which the supernatant were collected in 3 tubes and preserved at -80 °C for future experiments. Specific primary antibodies were used to verify expression on PVDF membranes after semi-dry transfer and blocking by 5% milk overnight at 4 °C. For *La*NBS and *La*N4′*O*MT, goat anti-AU1 and anti-AU2 polyclonal antibodies from Thermo Fisher Scientific were employed, respectively. A rabbit anti-FLAG monoclonal antibody from Cell Signaling Technology (NEB) was used for *La*NRII, while an anti-Myc polyclonal antibody raised in rabbit from Millipore Sigma Aldrich was applied for *La*CYP96T1 and T2. For the *La*N4′*O*MT-EGFP fusion protein and *La*CYP96T2-EGFP fusion protein, a primary anti-GFP/CFP/YFP monoclonal antibody raised in mouse was used. Host specific secondary antibodies conjugated with Horseradish peroxidase (HRP) were utilized to detect the bands in the membrane, i.e., Immun-Star goat anti-mouse (GAM)-HRP conjugate and Immun-Star goat anti-rabbit (GAR)-HRP conjugate from BioRad, and anti-goat-HRP from Jakson Immuno Research Laboratories.

Further validation of each gene expression was conducted by RT-qPCR. RNA was isolated from 200 mg of snap frozen samples. 700 µL of Trizol were added and samples vortexed. 300 µL chloroform were added, samples were vigorously shaken, and incubated on ice for 3 minutes, then centrifuged at 12,000 x g at 4 °C. The mixture separated into a lower red phenol-chloroform and interphase, and a colourless upper aqueous phase. The upper phase was transferred to a new tube containing 35 µL of NaCl (5M) and 400 µL Isopropanol and incubated at -20 °C for 10 minutes. The mixture was centrifuged at 12,000 x g at 4 °C, and the supernatant discarded, leaving the total RNA pellet at bottom. The pellet was washed twice with 1mL of 75% ethanol, centrifuged at 7,500 x g at 4 °C, and air dried for 10 minutes. DNAse treatment was performed using TurboDNAse according to the standard protocol from supplier (Invitrogen TURBO DNA-*free* Kit). RT-qPCR was conducted using Luna® Universal One-Step RT-qPCR Kit Protocol (NEB). The threshold cycle (Ct) value of each gene was normalized against the Ct value of the reference gene *histone 3*. The relative gene expression levels were determined using the comparative $\Delta\Delta^{Ct}$ method by calculating the average Ct values obtained from technical triplicates of pooled biological triplicate samples. The obtained results were analyzed and visualized in Prism.

2.3.8. Protein expression, and purification

E. coli Rosetta (BL21) cells harboring pMAL-c2X-*LaNBS*, pMAL-c2X-*LaNRII* and pMAL-c2X-*LaN4'OMT* were grown in LB broth with ampicillin (100 µg/mL) and chloramphenicol (34 µg/mL) overnight as seed culture. The next morning, 200 mL of medium was added, and bacteria grown at 37 °C with 210 rpm till the OD_{600} reached at 0.5-0.6. For induction of protein, 0.25 mM isopropyl-b-D-thiogalactopyranoside (IPTG), 50 µM zinc chloride ($ZnCl_2$) and 50µM magnesium chloride ($MgCl_2$) were added and cultures further incubated at 18 °C, 150 rpm. After 16 hours, cells were harvested at 5,000g and protein extraction was performed following sonication by adding ice chilled protein extraction (PE) buffer [30 mM Tris-HCl (pH:8), 150 mM NaCl, 1 mM EDTA, 10% Glycerol, 1 mM PMSF and 0.1% protease inhibitor cocktail (Cell Signaling Technology, NEB)]. Sonication parameters was 40% amplitude for a total of 8 min with 15 sec run and 30 sec pause. The lysates were centrifuged for 60 min at 16,000g at 4 °C. Supernatant was mixed with 1 mL of three times pre-washed amylose resin, kept on a rocking shaker for two hours and subsequently passed through filter column to isolate resin. Resin was washed three times with

PE buffer under gravity at 4ºC and the flowthrough was discarded. 1 mL of PE buffer containing 25 mM maltose was added to resin and pure protein was collected. Purified proteins were further washed three times with buffer containing Tris-HCl (pH:8) and 20% glycerol using Amicon® Ultra Centrifugal Filter (Millipore), 10 kDa at 2,000 g for 10-15 minutes at 4 °C. Finally, the pure, concentrated, and desalted proteins were aliquoted in individual tubes and preserved in -80 °C.
For the *in vitro* reaction of cytochrome enzymes, microsomes were isolated from *N. benthamiana*. As aforementioned in 2.6, CYP96T1/2 were extracted from 9 leaves of 3 biological triplicates of *N. benthamiana*. The 20 mL of supernatant were kept in Beckman Coulter polycarbonate centrifuge tube (25 x 89 mm) and ultracentrifugation performed at 100,000 g for 90 minutes. Supernatant were removed slowly and the microsomes on the bottom of the tubes were washed by softly resuspending in 20mL ice chill Tris-HCl (pH 8) and 20%glycerol. After repeating the centrifugation and wash twice, the supernatant was discarded and the pelleted microsomes were resuspended in pre weighted tube with 1 mL of Tris-HCl (pH 8) with 20% glycerol, aliquoted in individual tubes and preserved in -80 °C.

2.3.9. *In vitro* enzymatic assay

In vitro reaction for purified *La*NBS, *La*NRII, was carried out using 80 µg of purified NBS enzyme, 60 µg of purified NR enzyme, 10 µM tyramine, 300 µM 3,4-DHBA, and 1 mM NADPH in 50 mM potassium phosphate buffer (pH 7.8), in a total volume of 50 µL, incubated at 35 °C for 2 hours, and quenched at 65 °C for 20 min. The reaction was aternatively conducted using 200 µg of crude enzyme extracted from *N. benthamiana* leaves along with 100 µM tyramine, 100 µM 3,4-DHBA, and 1 mM NADPH in 50 mM potassium phosphate buffer (pH 7.8). To illustrate the formation of 4´OM, 5 µM of *La*N4'OMT enzyme and 2 mM SAM along with 1 mM nickel or magnesium were incubated with 100µM norbelladine in a total reaction volume 200 µL of sodium phosphate buffer (pH 7.4) at 45 °C for half hour or as indicated, and quenched by equal volume of 100% methanol (Koirala et al., 2024). Similar reaction with 100 µM 3,4-DHBA as substrate was also performed to check promiscuity of *La*N4'OMT enzyme in presence of Mg^{2+} ions. Enzymatic assay for cytochrome enzyme was carried out using the microsomal fractions prepared from *N. benthamiana* leaves. Reaction was carried out in a total volume of 150 µl with 50mM phosphate buffer (pH 7.8), using approximately 100 µg of microsomes, 1 mM NADPH, and 50 µM 4´OM, incubated at 30 °C

for time course followed by quenching with equal volume of 100% acetonitrile. To obtain the reduced product, same reaction condition was carried out in a total volume of 150 µl in addition with 75 µg of pure reductase enzyme (*La*NRII) obtained from *E. coli*. Papaverine was added after quenching the *in vitro* reactions in such way to obtain 1 ppm of final concentration while mixing with mobile phase before injection in LC-MS/MS.

2.3.10. Thermal unfolding analysis using nanoDSF

For melting temperature measurements, 500 µg/mL of purified MBP tagged *La*NBS was mixed with 100 µM of tyramine and 100 µM of 3,4-DHBA in 50mM HEPES (pH 6) buffer with 20% glycerol. For *La*NRII, 1 mM of NADPH was used in addition to the substrates, and the reaction was carried out in sodium citrate buffer. Similarly, enzymes without substrates, as well as purified MBP alone, and with substrates were used as negative control for the experiment. The samples were incubated at room temperature for 5 minutes before being introduced into high-sensitivity capillaries, each containing 10 µL of sample. Excitation light settings were configured to autodetect, and measurements were conducted across a temperature range of 25 to 95 °C, with a controlled temperature increase of 1 °C/min, using the Prometheus Panta instrument (NanoTemper Technologies GmbH, Munich, Germany). The protein melting temperature (Tm) was determined by plotting the fluorescence intensity ratio at 350 nm and 330 nm (F350/F330), which reflects changes in the local chemical environment of tryptophan and tyrosine residues. The thermal unfolding profile was analyzed using Panta analysis software (NanoTemper Technologies GmbH, Munich, Germany), and the derivatives of the experimental value were plotted to enhance data visualization by Prism.

2.3.11. Sample preparation for metabolite analysis

Metabolites were extracted from crushed snap-frozen leaf tissues using methanol-water extraction solvent (8:2, *v/v*) with a constant ratio of 20 µL/mg of the samples. Samples were placed on a shaker at 200 rpm overnight and then heated at 65ºC for 20 minutes with closed lid. Supernatants were collected after centrifuging at 16,000g for 10 minutes and dried using a rotary evaporator. Sample extracts were reconstituted in the mobile phase (Milli-Q water and methanol, both containing formic acid 0.1% (90:10)) at a constant ratio of 20 µL/mg unless stated, vortexed and filtered through 0.22 µm PTFE filter prior analysis conducted by High-performance liquid

chromatography coupled with tandem mass spectrometry (HPLC-MS/MS). Papaverine was added as internal standard prior to extraction, ensuring a final concentration of 1 ppm upon reconstitution in the mobile phase. Relative quantification was subsequently performed by normalizing metabolite signal intensities to the area under the curve of the internal standard.

2.3.12. Instrumentation and chromatographic conditions

HPLC-MS/MS system equipped with an Agilent Jet Stream ionization source, a binary pump, an autosampler and a column compartment were used for the analysis (Agilent Technologies, Santa Clara, California, USA). Compounds separation was achieved using a Kinetex EVO C18 column (150 × 4.6 mm, 5 mm, 100 Å; Phenomenex, Torrance, USA). Five µL of each sample were injected onto the column that was set at 30 °C. A gradient method made of (A) formic acid 0.1% v/v in Milli-Q water and (B) formic acid 0.1% v/v in methanol with a flow rate of 0.4 mL/min was used to achieve chromatographic separation. The HPLC elution program was the following: 0 min, 10% B; 10.0 min, 10% B; 20.0 min, 100% B; 25.0 min, 100% B; 26.0 min, 10% B. The total run time was 30 min per sample to allow the reconditioning of the column prior to the next injection. The parameters used in the MS/MS source were set as follows: gas flow rate 10 $L.min^{-1}$, gas temperature 300 °C, nebulizer 45 psi, sheath gas flow 11 $L.min^{-1}$, sheath gas temperature 300 °C, capillary voltage 4000 V in ESI+ and 3500 V in ESI- and nozzle voltage 500 V. Agilent MassHunter Data Acquisition (version 1.2) software was used to control the HPLC-MS/MS. MassHunter Qualitative Analysis (version 10.0) and MassHunter Quantitative QQQ Analysis (version 10.0) softwares were used for data processing. Compounds identification was performed using authentic reference standards or by employing collision-induced dissociation (CID) mass spectra published in literature (Kilgore et al., 2016a; Kilgore et al., 2016c; Mehta et al., 2024), in cases where reference standards were not available. MRM transitions and instrument parameters used for identifications in N4′OMT and in CYP96T experiments are included in Table 2.S3 and Table 2.S4, respectively. Instrument parameters used in Product Ion Analysis mode to obtain the full CID mass spectra of signals detected in MRM mode are presented in Table 2.S5.

2.3.13. Subcellular localization study

Subcellular localization of *LaN4′O*MT and *La*CYP96T2 was determined using confocal microscopy by infiltrating culture of *A. tumefaciens* (GV3101) harboring pB7FWG2-*LaN4′OMT*,

pB7WGF2-*LaN4′OMT,* or pB7FWG2-*LaCYP96T2* into 3-4 weeks old *N. benthamiana* plants. *Agrobacterium* suspensions were prepared and infiltrated as described above. For co-localization assay, co-infiltration of the suspensions aforementioned, along with *Agrobacterium* harbouring RFP or ER-mCherry plasmids (Nelson et al., 2007) were mixed to a final OD_{600} of 0.6, and infiltrated. After 48 hours of infiltration, the abaxial epidermis of leaf discs was placed on a microscopic slide in a water drop, shielded by a cover slip, and photographed immediately. A confocal laser scanning microscope (Leica TCS SP8; Leica Microsystems) with a 40X/1.30 oil immersion objective was used to observe protein localization. Las X software was used to create the composite photos (Leica Microsystems). Colocalization graph was created using florescence intensity.

2.4. Results

2.4.1. *In silico* characteristics of pathway candidates

We initially examined the sequences of the proposed enzymes involved in the pathway of AAs (Figure 2.1), focusing on the candidates identified in the *L. aestivum* transcriptome (Tousignant et al., 2022b). Prospects for norbelladine synthesis included *La*NBS and *La*NRII. *La*N4′*O*MT was proposed to catalyze the formation of 4′-*O*-methylnorbelladine, and CYP96Ts were candidates for further diversification of SMs through oxidative phenol couplings.

*La*NBS belonged in the PR10/Bet v1-like protein superfamily, similar to previously characterized norcoclaurine synthase (NCS) (Figure 2.S1a). One candidate transcript of NBS was identified from the transcriptome and sequencing of the amplified candidate revealed a single alteration c.23A>G (Glu8Gly) (Figure 2.S1b). *La*NBS subclustered with orthologous *Narcissus papyraceus* NBS (*Np*NBS) sequences within a larger clade containing characterized NCS enzymes, distinct from the non-NCS PR10 enzyme clade. The 159 amino acids long *candidate* shared almost 100% identity with the previously described *La*NBS by Tousignant et al., Majhi et al., along with 87% and 86% similarity with orthologs from *Narcissus pseudonarcissus*, *N. papyraceus* respectively, and 38%, 36% and 31% with NCS from *Coptis japonica, Thalictrum flavum* subsp. *glaucum* and *Papaver somniferum,* respectively (Table 2.S6a). Its sequence and structure included a conserved

glycine-rich P-loop, proximal to the entrance of the ligand-binding pocket, a characteristic feature of the Bet v1 protein (Figure 2.S1b and 1c). Eight ligand-binding residues were conserved in all Bet v1 transcripts from various species (Figure 2.S1b), including hydrophobic residues Tyr68, Tyr100 for wider opening of substrate binding tunnel and Lys83 for intercepting the carbonyl group of the substrate. Modeling of *La*NBS revealed a seven-stranded antiparallel β-sheets with two long N- and C-terminal helices surrounding a cleft with a core of hydrophobic residues, confirming its Bet v1-like structure and resemblance with *Tf*NCS (Figure 2.S1c). Previously proposed interacting residues Ser31 (Leu31 in homologous *La*NBS), Leu34, Tyr59, Tyr68, Glu71, Phe73, Lys83, Val85, Leu104, Pro139, and Ile143 formed the binding pocket of the enzyme (Figure 2.S1b, Table 2.S7) (Hnin et al., 2024c; Majhi et al., 2023b). The similarity in sequence and structures with functional NBSs and characterized NCSs, the latter catalyzing the condensation of dopamine and 4-hydroxyphenylacetaldehyde (4-HPAA), supports the hypothesis that the putative *La*NBS homolog performs the condensation of 3,4-DHBA and tyramine (Figure 2.1).

Eleven sequences and two previously reported transcripts were identified as candidates for the reduction of norcraugsodine and other AAs, from the transcriptome and from the NCBI database, respectively. They clustered with the tropinone reductase (TR) sub-family of the short-chain dehydrogenase/reductase (SDR) family (Figure 2.S2a). Transcripts 'NR1', 'NR2' and 'Red.8' clustered with *Narcissus* cv *Tête-à-Tête Nt*SDR1, *N.* aff. *pseudonarcissus (Nps*NR*)*, *N. pseudonarcissus* and *N. papyraceus (Np*NR) clade. *Np*NR and *Nps*NR catalyze norbelladine synthesis and/or norcraugsodine reduction, while *Nt*SDR1 accepts noroxopluviine as substrate. Amplification led to the identification of *LaNRII* matching uncharacterized NR2 in NCBI (UIP35235.1). *La*NRII 269 aa sequence corresponded to a classical SDR having TGXXXGXG cofactor binding motif in position 29-33 and YXXXK active site motif in 173-177 position, as well as a conserved NNAG domain required for stabilization of central ß-sheets and reductase activity (Filling et al., 2002), and PGxxxT that is suggested to play a structural role (Figure 2.S2b and c). *La*NRII predicted folding was arranged as a seven-stranded parallel β-sheet embedded between a pair of three α-helices (Figure 2.S2c).

The candidate included conserved Asn132 and Ser160, necessary for the activity of other reductase, such as SDR hsdA from *Comamonas testosterone* (corresponding residues Asn111 and Ser138) (Filling et al., 2002). *La*NRII also displayed Tyr173, aligning with Tyr209 from tropinone reductase SDR of *Cochlearia officinalis* (*Co*TR), essential for the reduction of tropinone and

nortropinone (Brock et al., 2008). *La*NRII shared 98%, 93%, 91% and 77% sequence similarity with previously characterized *La*NRI, *Np*NR, *Nt*SDR1, and *Nps*NR sequences, respectively (Table 2.S6b). Comparison with these reductases revealed the conservation of a total of 49 active site residues with *Nt*SDR1 and *Np*NR1 (Table 2.S7 and 2.S8), 15 of which differed with crystalized *Nps*NR. Conserved residues included Lys33, Ile35, Gly36, Cys53, Arg55, Cys79, Asn108, Ala109, Gly110, Thr111, Leu114, His170, Tyr173, Lys177, Ile205, Thr206, Thr208, Val209, Gln210, Phe214, Leu215, Glu224, and Arg265, previously predicted to interact with ligands. The only active site residue that was distinct in *La*NRII compared to *Nt*SDR1 was Ile *vs* Met239. Additional mutations could be noted in surrounding residues and in the N-terminal tail. Together, these results suggest that *La*NRII contains the required features to carry out the reduction catalysis of imine and/or alkaloid substrates.

Six candidate OMTs were identified in *L. aestivum* transcriptome (Figure 2.S2c). On the basis of maximum likelihood and consensus (not shown) trees, a putative *O*-methyltransferase (*LaN4′OMT)* was selected for primer design and amplification. There were 2 amino acid differences compared to the transcriptome sequence, *i.e.* c.52G>A (p.Gly18Ser) and c.299T>C (p.Met100Thr). The identified transcript clustered with class I OMT encompassing other previously characterized enzymes from different species like *C. japonica*, *P. somniferum*, *Lycoris* and *Narcissus* species (Figure 2.S3a). The distance matrix showed > 95% similarity with six orthologous enzymes, but only 12% with *Nt*OMT1 (Table 2.S6c). Except for *Nt*OMT1, which catalyzed *O*-methylation of 11-hydroxyvittatine, all reference *Amaryllidaceae* OMT were shown to catalyze *O*-methylation of norbelladine and phenylpropanoid precursors. Class I OMTs are metal-dependent enzymes characterized by a distinctive feature: a Rossmann fold-binding site for S-adenosyl-$_L$-methionine (SAM), as the methyl donor (Figure 2.S3b and c). 239 amino acid-long *LaN4′OMT* displayed conserved residues involved in interactions with SAM such as Val55, Glu77, Gly79, Val80, Tyr84, Ala132A, and Asp157 (Li et al., 2019). Conserved Asp155, Asp181, and Asn182 are involved in metal ion binding in orthologous enzymes. Asn182 is also implicated in the methyl transfer catalysis together with Lys158 and Asp230 (Li et al., 2019) (Figure 2.S3b). The predicted *La*N4′OMT candidate folded similarly to a catechol OMT, with 7 β-sheets encompassed between α-helices and loops (Figure 2.S3c).

Previous studies have suggested the involvement of 19 amino acids in substrate specificity of *Amaryllidaceae* OMT (Hnin et al., 2024a; Koirala et al., 2024). *La*N4'OMT displayed two residues

that were proposed to be associated with a preference towards 3'-*O*-methylation catalysis of norbelladine (Val30, Gln141), but most were suggestive of 4'-*O*-methylation (Ala179, Tyr186, Ser188. Tyr191, Leu206, Thr213, Val232) (Table 2.S9). Other variations in residues (N-terminal loop) are surface-exposed and unlikely to interact directly with ligands but could be involved in a catalytic network to support substrate interaction. Overall, this analysis supports that the *La*N4'OMT candidate could catalyze the 4'-*O*-methylation of norbelladine.

Two transcripts were previously reported for CYP96T1 and CYP96T2 (GenBank: UIP35232.1 and UIP35233.1) and in *L. aestivum* transcriptome nine additional candidates were identified (Figure 2.S4a). *La*CYP96T candidates clustered with orthologous *p-p´*, *p-o´*, *o-p´* couplings catalyzing enzymes, and formed a clade distinct from the CYP80, CYP71, and CYP76 subfamilies (Figure 2.S4a and b). Following amplification, the 512 amino acid-long candidates included a signal peptide (residue 7-29 predicted by IntelPro) to embed the protein in the membrane at the cytosolic surface of the ER. *La*CYP96T1 displayed 17 bases alterations resulting in 4 amino acids differences compared to the GeneBank sequence, while *La*CYP96T2 had 36 bases differences resulting in a change of 12 amino acids. They both subclustered with the recently uncovered *o-p´* coupling catalyzing *Nt*CYP96T5 (Mehta et al., 2024). *La*CYP96T1 and *La*CYP96T2 proteins shared 98% identity and exhibited 92% similarity with *Lau*CYP96T1-like-2 from *Lycoris aurea*, 90% with both *Lau*CYP96T1-like-3 and *Nt*CYP96T5, and 72% with *Nps*CYP96T1 (Table 2.S6d). The predicted α-helix-rich shape of *La*CYP96T1 and *La*CYP96T2 was characteristic of CYPs (Figure 2.S4c and d), which bind their diverse ligands within a buried, hydrophobic active site accessed through a substrate channel formed by two flexible helices and their connecting loop (Figure 2.S4c). The N-terminal ER-membrane-anchoring α-helix domain (at the left in Figure 2.S4c and d), and the heme pocket buried inside the enzyme large cavity were apparent in the folded proteins (at the center of each prediction).

The oxygen binding and activation motif (A/G)GX(D/E)TT was substantially different between *La*CYP96T1 and its variants when compared to CYPs that catalyze hydroxylation reactions. *La*CYP96T1 and *La*CYP96T2 also contained the heme binding domain (FXXGXRXCXG) that secures the heme in the active site by a strongly preserved thiolate residue (Cys457) which interacts with two molecular oxygens, one oxygen molecule oxidizing the substrate and the other being reduced to form water (Porter and Coon, 1991) (Figure 2.S4b). Ala219, Leu220, Thr303, Leu306, Val307, Thr311, and Pro382-Ile385 are predicted to be involved in substrate binding pocket along

with 25 other residues conserved throughout various species (Figure 2.S4b and c, Table 2.S1). Out of 47 active site residues predicted by MOE (Table 2.S7), 11 differed from *Nps*CYP96T1, while they matched with *Lau*CYP96T1-like2 sequence catalysing *p-p´* coupling and with *Nt*CYP96T5 *(o-p´* coupling) (Table 2.S10) (Kilgore et al., 2016a; Liu et al., 2024; Mehta et al., 2024). Furthermore, *La*CYP96T1 and T2 encoded for Leu123 and Phe124, a combination that was specifically detected in enzymes performing *o-p´* or *p-p´* couplings, but not *p-o´*. This suggested that the *La*CYP96T candidates could preferentially catalyze *o-p´* and/or *p-p´* reactions.

Taken together, phylogenetic analysis, multiple sequence alignment, and folding prediction of the five candidates provide evidence to support their capability in executing the proposed biosynthetic pathway (Figure 2.1).

2.4.2. Localization assay

We previously showed that *La*NBS and *La*NR both localize in the cytoplasm (Majhi et al., 2023b; Tousignant et al., 2022b). To further investigate the spatial organization of the AA pathway and its potential impact on metabolite flux, we studied the subcellular localization of *La*N4´OMT and *La*CYP96T2 following agroinfiltration in *N. benthamiana* (Figure 2.2). The red fluorescent protein (RFP), which localizes to the cytoplasm and nucleus, and ER_M-cherry that is restricted to the endoplasmic reticulum (ER), were used as controls.

Both N- and C-terminal *La*N4´OMT-EGFP accumulated in the cytoplasm (Figure 2.2a, Figure 2.S5), while *La*CYP96T2 localized in the ER (Figure 2.2b, Figure 2.S5). Expression of the fusion proteins was verified by western blot. Both amino and carboxy terminal tagged EGFP fusion *La*N4´OMT proteins were observed at around 54 kDa in blot, and C-terminal-EGFP fusion *La*CYP96T2 at around 87kDa consistent with a GFP fusion (Figure 2.S6a and b). These results suggest that *La*N4´OMT resides in the cytosol, the same compartment as *La*NBS and *La*NR, while *La*CYP96T localizes to the ER, confirming the expected subcellular localization of the candidates.

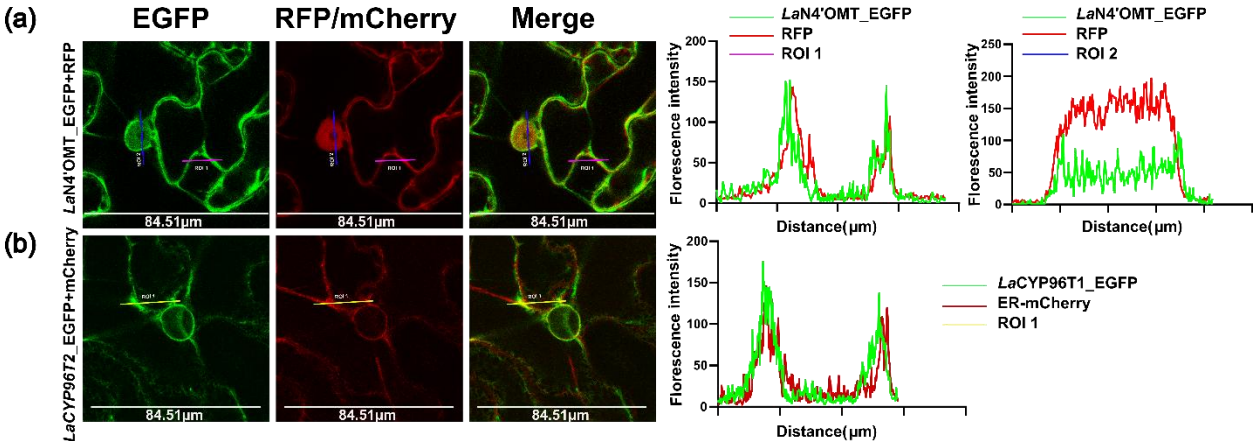


Figure 6. Subcellular localization of LaN4´OMT and LaCYP96T1 proteins in *Nicotiana benthamiana* leaves. Agroinfiltrated C-terminal-EGFP-fusion-*La*N4´OMT and C-terminal-EGFP-fusion-*La*CYP96T1. The histogram of the right panel shows fluorescence intensity profile of respective panel. Scale bars resemble 84.51 µm.

2.4.3. Reconstitution of the foundation steps of the AA pathway to produce 4´O-methylnorbelladine *in vivo*.

The proposed pathway entails the condensation of 3,4-DHBA and tyramine by *La*NBS to yield norcraugsodine, which is subsequently reduced by *La*NRII and *O*-methylated by *La*N4´OMT, as crucial initial steps (Figure 2.1). Having established the candidates' phylogeny and localization, we proceeded to characterize the interaction of enzymes with their suggested ligands, both *in silico* and *in vivo* (Figure 2.3).

Tyramine and 3,4-DHBA were docked into the active site of *La*NBS with binding scores of -5.1 and -5.5 kcal/mol, respectively. In their predicted calculated position, the ligands faced each other, 3,4-DHBA forming hydrogen bonds with catalytic residues Glu71 and Lys83, and tyramine with Ile39, Tyr59, and Glu71. Additionally, both engaged in hydrophobic interactions with surrounding residues: tyramine interacted with Ile39, Pro139, Ile143, and Val85, while 3,4-DHBA interacts with Leu104 and Leu140 (Figure 2.3a, right panel, Table 2.S1). The near-parallel orientation of the aromatic rings of the two ligands, and the carbonyl group of 3,4-DHBA facing tyramine's amine group are reminiscent of dopamine and hydroxybenzaldehyde positioning in *Tf*NCS (Samanani and Facchini, 2002). Hence, the docking analysis was consistent with Lys83- and Glu71-assisted condensation to form norcraugsodine. The latter is proposed to be further reduced by the noroxomaritidine/norcraugsodine reductase *La*NRII.

Norcraugsodine docked with a score of -6.3 kCal/mol in the active site of *La*NRII, its N-C double bond laid closest to the nicotinamide ring of the electron donor NADPH and to Tyr173, interacting

with Leu114, Val161, Val211, Phe214, and Tyr173 of the enzyme active site (Table 2.S1, Figure 2.3b). This positioning aligns with the proposed NADPH-dependent reduction of norcraugsodine to produce norbelladine assisted by Tyr173. In the next step yielding to 4′OM, norbelladine docked in *La*N4′OMT active site with a score of -8.8 kCal/mol, forming interactions with Mg^{2+}, Lys158, as well as Ile11, Ser52, Asp155, Trp185, Glu200 and Glu201. Mg^{2+} was positioned between the ligand 3′ and 4′OH groups, the 4′OH located proximal to the SAM methyl group (Table 2.S1, Figure 2.3c). The docking results are consistent with the catalysis of a 4′-*O*-methylation of norbelladine, in interaction with Lys158, Asn182, and Mg^{2+}.

To achieve the reconstitution of the original steps of the *Amaryllidaceae* pathway, we agroinfiltrated the genes encoding the candidate enzymes into *N. benthamiana*. Forty-eight hours post-agroinfiltration, we injected the substrates and harvested the leaves for metabolite analysis 24 hours later. First, we confirmed protein accumulation by western blotting (Figure 2.S6c-f), detecting bands corresponding to the expected sizes (~20 kDa for *La*NBS, ~30 kDa for *La*NRII and the EGFP control, ~35 kDa for *La*N4′OMT, and ~60 kDa for *La*CYP96T1, as well as *La*CYP96T2). The expression level was further validated by RT-qPCR, which showed the relative expression of each gene while infiltrated alone or co-infiltrated together (Figure 2.S6h-k). Previous *in vitro* studies suggested that norcraugsodine is unstable and that the yield of norbelladine synthesis increases when *La*NBS and *La*NR interact (Majhi et al., 2023b). Therefore, we co-agroinfiltrated *LaNBS* and *LaNRII* with tyramine and 3,4-DHBA (Figure 2.3d, Figure 2.S7a). Under these conditions, norbelladine was detected in the metabolite extracts. In contrast, feeding EGFP-infiltrated leaves with the substrate, feeding substrates to leaves alone, or non-fed *LaNBS* and *LaNRII*-infiltrated leaves did not produce detectable levels of norbelladine.

Subsequently, agroinfiltration of *LaN4′OMT* with norbelladine confirmed the production of 4′-*O*-methylnorbelladine *in planta* (Figure 2.3e, Figure 2.S7b). Finally, co-infiltration of the genes encoding the three enzymes *La*NBS, *La*NRII and *La*N4′OMT with tyramine and 3,4-DHBA as substrates led to the production of both norbelladine and 4′-*O*-methylnorbelladine, which were undetected in the negative controls (Figure 2.3f).

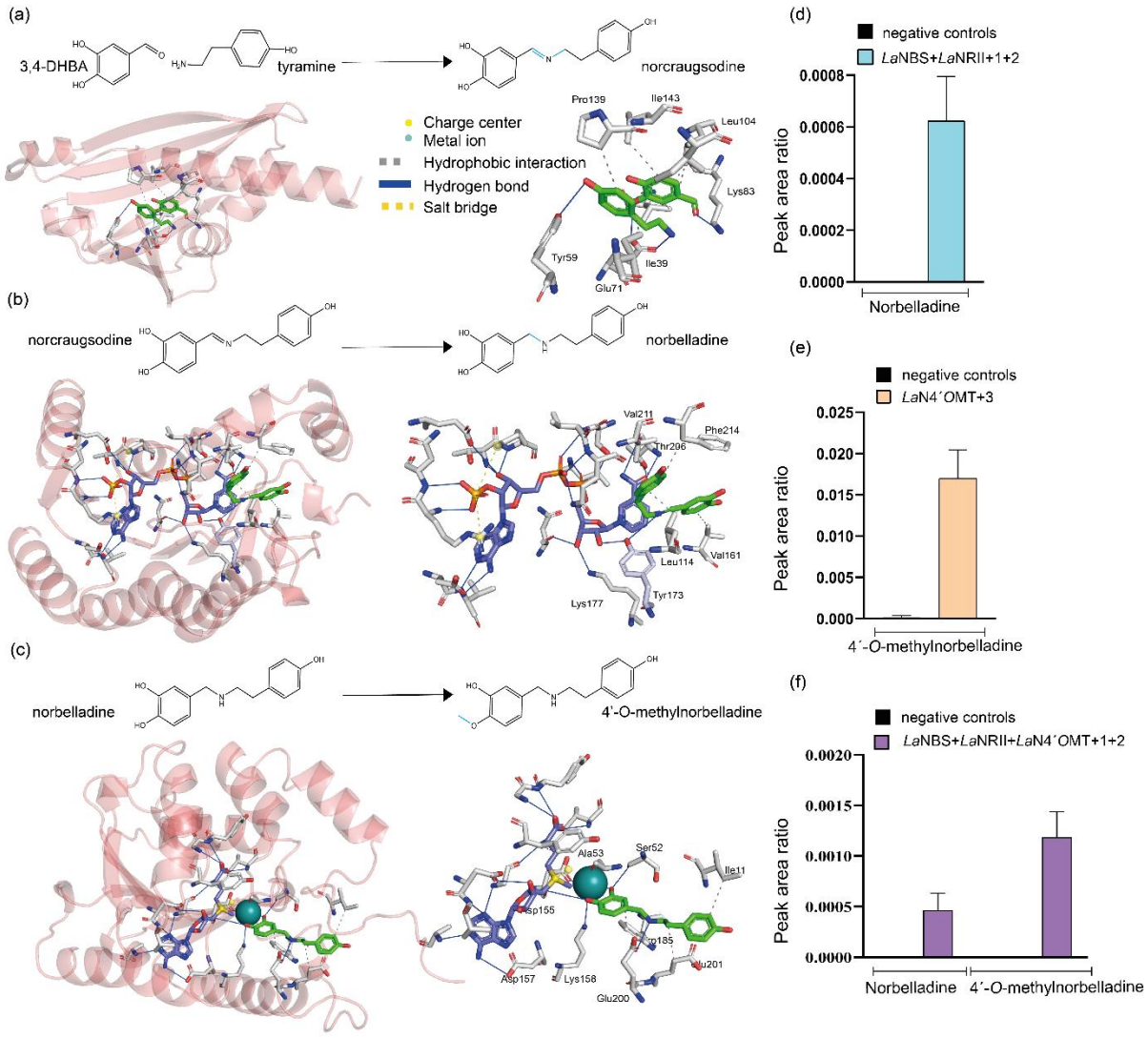


Figure 7. Reconstitution of the foundation steps of the Amaryllidaceae alkaloid pathway to produce 4´-*O*-methylnorbelladine *in vivo*.

a *ca*talyzed condensation of 3,4-DHBA and tyramine. **b** *La*NRII-catalyzed reduction of norcraugsodine. **c** *La*N4´OMT-catalyzed 4´*O*-methylation of norbelladine. Ligands were docked in the candidate enzyme active site and are shown as green sticks. The AlphaFold2 predicted structure are shown as a transparent deep salmon cartoon (left) and active site residues are shown as light grey sticks. NADPH and SAM are shown as violet sticks. Mg^{2+} is displayed as a blue sphere. A specific view on the active site residues and ligands positioning with interaction is shown (right). The blue bonds in the schemes display the catalyzed reactions. **d** Relative quantification of norbelladine production *in planta* following agroinfiltration with *LaNBS* and *LaNRII* and feeding with 3,4-DHBA and tyramine. **e** Relative quantification of 4´-*O*-methylnorbelladine production upon agroinfiltration of *La*N4´OMT and feeding with norbelladine. **f** Relative quantification of norbelladine and 4´-*O*-methylnorbelladine production by agroinfiltrated *La*NBS, *La*NRII and *La*N4´OMT upon feeding with 3,4-DHBA and tyramine. The product profiles obtained in different assays were analyzed by HPLC-MS/MS. The area ratio of each detected analyte was obtained by dividing the peak area of the targeted compound by the one of the internal standard papaverine. Relative quantification was performed using the area ratio of each analyte produced in the assay. Data are the means ± SE of three biological repeats with background subtracted. 1 is denoted for tyramine, 2 for 3,4-dihydroxybenzaldehyde and 3 is for norbelladine. *N. benthamiana* infiltrated with *Agrobacterium* harboring EGFP and respective substrate/s are the negative controls in bar plots. Representative detection of at least three independent experiments with three leaves infiltrated in each replicate.

To validate the functionality of the candidates in this premise pathway, the activity of *La*NBS, *La*NRII, and *La*N4'OMT was verified *in vitro* by using crude enzymes from *N. benthamiana* or purified N-terminal MBP tagged proteins (Figure 2.S6g). First, crude extracts from *N. benthamiana* leaves agroinfiltrated with *La*NBS and *La*NRII led to the detection of the condensed product norbelladine upon feeding with tyramine and 3,4-DHBA (Figure 2.S7c). *E. coli* harvested purified MBP-tagged enzymes also led to the synthesis of norbelladine *in vitro,* as detected in two out of three samples. Of note, the amount yielded from purified enzymes expressed in bacteria was almost three times lower compared to crude enzymes from plant leaves (Figure 2.S7c). To get additional insight on the interaction of the substrates with the two purified enzymes, we compared the thermal unfolding profiles of pure *La*NBS and *La*NRII with and without ligands using a Prometheus. We observed differences in the melting temperature (Tm) of both enzymes when bound to their ligand, whereas ligand addition to pure MBP did not impact its Tm. The thermal shift resulted in a decrease of the F350/F330 ratio above the threshold limit (>0.2), confirming significant changes in *La*NBS and *La*NRII folding upon interaction with 3,4-DHBA and tyramine (Figure 2.S7d-f). Furthermore, we observed that 4´*O*M is produced from norbelladine *in vitro* upon incubation with purified *La*N4'OMT and Mg^{2+}. 4´*O*M levels increased constantly during the 60 minutes of the reaction, reaching up to ~28 µg/mL (Figure 2.S7g) and no dimethylnorbelladine was detected. As previous studies showed that metal ion can impact OMTs regioselectivity (Su et al., 2022b), we tested the reaction in presence of Ni^{+2} instead of Mg^{+2}. This led to the detection of 4´*O*M as major product, along with 3',4'-*O*-dimethylnorbelladine (Figure 2.S7h). *La*N4'OMT also showed promiscuity by methylating 3,4-DHBA yielding 7602 ng/mL vanillin as major product along with 526 ng/mL isovanillin (Figure 2.S7i).

Overall, these results corroborate the proposed grounds of the biosynthetic pathway *in vivo* and *in vitro*.

2.4.4. Multiple C-C phenol couplings by a single CYP96T

In the subsequent steps of the proposed biosynthetic pathway (Figure 2.1), 4´*O*M undergoes significant transformations (Figure 2.4), leading to the generation of a diverse array of alkaloid structures catalyzed by CYP96T isoforms (Figure 2.4a). The active site of these enzymes includes

a heme group and two water molecules, essential for correct ligand positioning and catalysis. 4′*O*M docked with its 4-OH in the vicinity of the iron-bonded water molecule (Figure 2.4b). The ligand interacted with Lys109, Leu112, Phe116, Phe124, Leu224, Val307, Val381, and Leu495, in CYP96T1, and with Lys109, Phe116, Phe124, Leu220, Val307, and Leu495 in CYP96T2, with the *O*-methylated ring stabilized by aromatic residues (Table 2.S1, Figure 2.4b, Figure 2.S8a and b). Phe124 was suggested to be involved in *o-p′* and *p-p′* coupling reactions, while Val307 was detected in all *o-p′, p-o′,* and *p-p′* catalyzing enzymes. This positioning supports the catalysis of a C-C-phenol coupling reaction, leading to the synthesis of noroxopluviine, noroxomaritidine, and possibly *N*-demethylnarwedine, in both enzymes active site (Figure 2.4b).

To validate enzyme activity *in vivo*, we expressed *LaCYP96T1* or *LaCYP96T2 and* fed 4′*O*M as the substrate. Although we did not detect the *o-p′* phenol coupled product noroxopluviine, lycorine was intriguingly detected with *La*CYP96T2 and 4′*O*M (Figure 2.4f). In leaves agroinfiltrated with *LaCYP96T1* or *LaCYP96T2* and 4′*O*M as substrate, we also observed the *p-o′* coupled product *N*-demethylnarwedine (Figure 2.4g, Figure 2.S9a and b), which was absent in all five negative controls. The accumulation of *N*-demethylnarwedine was nearly twice as high with *LaCYP96T1* compared to *LaCYP96T2* ($p<0.0001$, Tukey's multiple comparison post hoc test, one way ANOVA). Additionally, we detected the *p-p′* phenol coupled product noroxomaritidine and its reduced form oxomaritinamine in leaves agroinfiltrated with *LaCYP96T1* or *LaCYP96T2* gene and 4′*O*M (Figure 2.4h, Figure 2.S10a and b, Figure 2.S11a and b), whereas these products were undetectable in leaves agroinfiltrated with *EGFP* and 4′*O*M. Therefore, *La*CYP96T1 and *La*CYP962 catalyzed the synthesis of the three types of phenol coupled products, namely, *p-o′* (galanthamine-type), *p-p′* (crinine-type) *and o-p′* (lycorine-type) involved in AAs biosynthesis pathway *in planta. p-p′* coupling activity *of La*CYP96T1 was verified *in vitro*, using microsomes isolated from agroinfiltrated *N. benthamiana* leaves which led to the formation of noroxomaritidine from 4′*O*M (Figure 2.S10d).

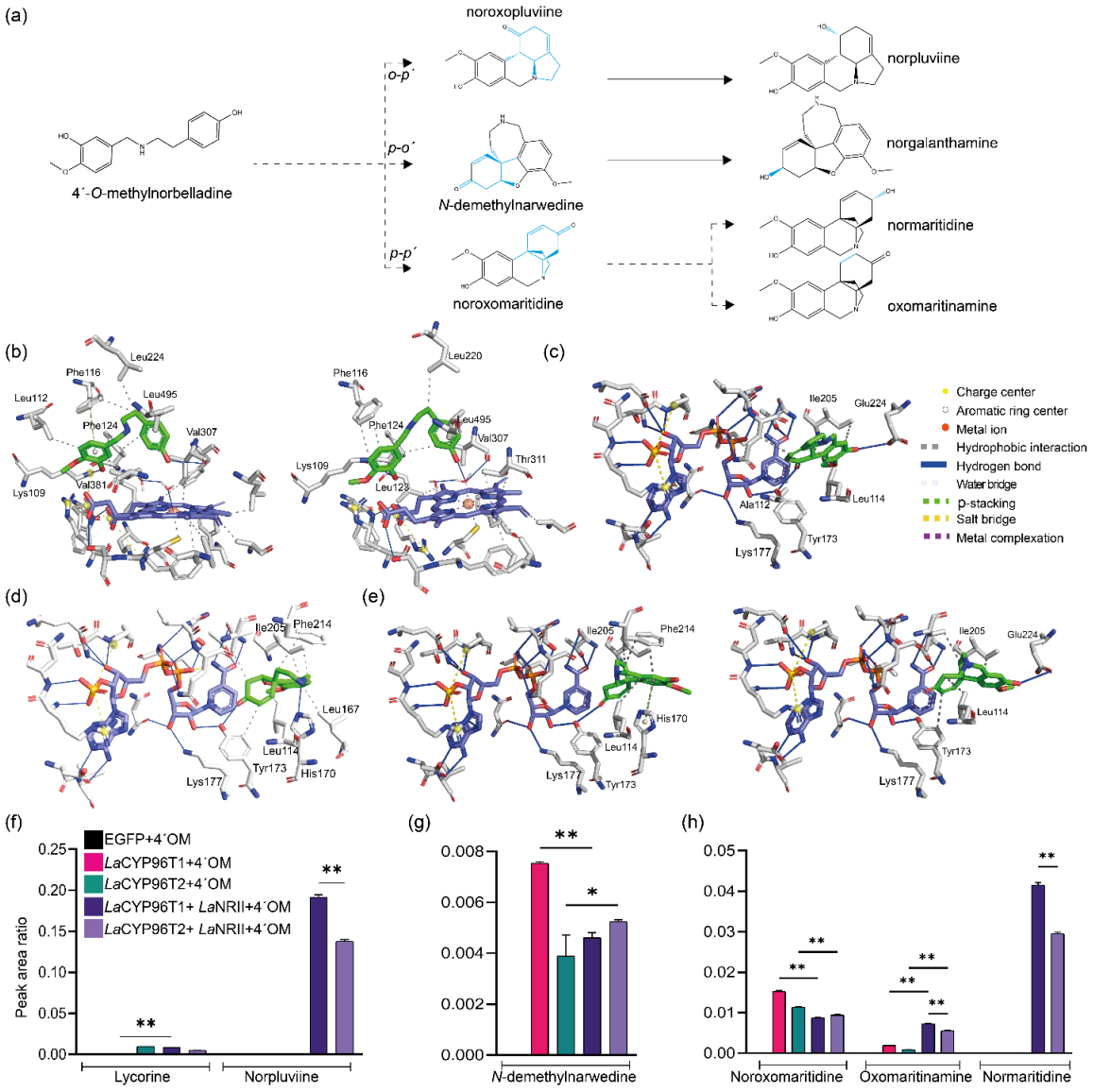


Figure 8. Reconstitution of the branching pathway steps to produce Amaryllidaceae alkaloids *in vivo*.
a Scheme of the proposed *La*CYP96T-catalyzed phenol couplings of 4´-*O*-methylnorbelladine yielding noroxopluviine, *N*-demethylnarwedine, noroxomaritidine, further reduced by *La*NRII into norpluviine, norgalanthamine, normaritidine and oxomaritinamine. Blue bonds are the results of the proposed catalyzed reactions. **b** Docked 4´-*O*-methylnorbelladine in the active site of CYP96T1 (left) and CYP96T2 (right). **c** Docked noroxopluviine in the active site of *La*NRII to yield norpluviine. **d** Docked *N*-demethylnarwedine in the active site of *La*NRII to yield norgalanthamine. **e** Docked noroxomaritidine in the active site of *La*NRII to yield normaritidine (left) or oxomaritinamine (right). Candidate active site residues are shown as grey sticks and ligands as green sticks. Heme and NADPH are shown as purple sticks. Iron as a red sphere. Interactions are shown as lines as displayed in the legend. **f** Relative quantification of *ortho-para´* products norpluviine and lycorine. **g** Relative quantification of *para-ortho´* product *N*-demethylnarwedine. **h** Relative quantification of *para-para´* products noroxomaritidine, oxomaritinamine and normaritidine. The area ratio of each detected analyte was obtained by dividing the peak area of the targeted compound by the internal standard papaverine. Relative quantification was performed using the area ratio of each analyte produced in the assay. Data are the means ± SE of three biological repeats with background subtracted. *N. benthamiana* infiltrated with *Agrobacterium* harboring EGFP and respective substrate/s is the negative control in each bar plot. ** and * represent the statistically significant differences among means with $p<0.0001$ and $p<0.05$, respectively.

2.4.5. Multiple reduction steps by LaNRII.

The reduction step is key for stabilizing metabolites and producing end-of-pathway AAs. We hypothesized that *La*NRII could accept *N*-demethylnarwedine, noroxopluviine and noroxomaritidine as substrates. Docking results supported this hypothesis, showing noroxopluviine and *N*-demethylnarwedine positioned to reduce their C-O double bonds through interaction with catalytic Tyr173 near the nicotinamide ring of NADPH at the enzyme's active site (Table 2.S1, Figure 2.4c and d, Figure 2.S8d and c). Noroxomaritidine docked in two distinct orientations, favoring the reduction of the C-O or the C-C double bond, in interaction with Tyr73 (Table 2.S1, Figure 2.4e, Figure 2.S8e and f).

To further investigate the pathway reconstitution, we co-expressed *LaCYP96T1* or *LaCYP96T2* with *LaNRII,* and fed 4′*O*M as substrate. This resulted in the detection of the reduced *o-p′* phenol coupled product norpluviine **(**Figure 2.4f). The norpluviine signal was significantly higher in leaves infiltrated with *LaCYP96T1* and *LaNRII* (~1.4 times, $p<0.0001$) compared to *LaCYP96T2* and *LaNRII* (Figure 2.4f, right panel, Figure 2.S12a and b). Norpluviine was not detected in any negative controls or samples lacking the reductase enzyme. Lycorine was also detected in samples infiltrated with either of the *LaCYP96T* and the *reductase* (Figure 2.4f, Figure 2.S13). Interestingly, co-infiltrating *LaCYP96T1* and *LaNRII* resulted in a decreased accumulation of *N*-demethylnarwedine to the level of *LaCYP96T2* ($p<0.0001$, Tukey's multiple comparison post-hoc test, one way ANOVA, Figure 2.4g). On the other hand, the yield of *N*-demethylnarwedine rose slightly (by 1.3-fold), but significantly ($p=0.0105$) when *LaNRII* was co-infiltrated with *LaCYP96T2*.

Co-infiltrating *LaCYP96T1* or *LaCYP96T2* and *LaNRII* also led to an increase in oxomaritinamine by nearly 4- and 6-fold respectively, compared to when infiltrated without *LaNRII* ($p<0.0001$, Tukey's multiple comparison test by ordinary two-way ANOVA, Figure 2.4h). Strikingly, agroinfiltration of *LaCYP96T1* or *LaCYP96T2* with *LaNRII* resulted in a strong signal of normaritidine, which had not been detected in samples with *LaCYP96T1* or *LaCYP96T2* alone (Figure 2.4h, Figure 2.S14). Normaritidine accumulated significantly more following the infiltration of *LaCYP96T1* compared to *LaCYP96T2* (1.4-fold, $p<0.0001$). Noroxomaritidine, oxomaritinamine, and normaritidine were not detected in any negative controls. Thus, in addition

to norbelladine biosynthesis, *La*NRII catalyzes the reduction of all phenol coupled products *in planta.*

To further substantiate the enzymes activity, we conducted *in vitro* assays using microsomes isolated from *Nicotiana benthamiana* leaves expressing *La*CYP96T1, in conjunction with the purified reductase enzyme (*La*NRII) expressed in *E. coli*. These assays with 4′*O*M as substrate, revealed norpluviine as the predominant product, accompanied by the formation of normaritidine and noroxomaritidine (Figure 2.S12d, e). These results confirmed the ability of *La*CYP96T1 and *La*NRII to yield *o-p′* and *p-p′* reduced products *in vitro*.

2.4.6. Full pathway reconstitution with four enzymes

To confirm that the four candidates could reconstitute the complete pathway, from aromatic amino acid and phenylpropanoid precursors, we infiltrated *LaNBS*, *LaNRII*, *LaN4′OMT*, and *LaCYP96T1* or *LaCYP96T2*, and supplemented with tyramine and 3,4-DHBA. This resulted in the detection of norbelladine, 4′*O*M, the *o-p′* coupled products norpluviine and lycorine, the *p-p′* products noroxomaritidine, normaritidine, haemanthamine, and vittatine/crinine, and the *p-o′* products *N*-demethylnarwedine and norgalanthamine (Table 2.S11). Lycorine was the major product formed by both *La*CYP96T enzymes, with production nearly three times higher for *La*CYP96T1 compared to *La*CYP96T2 (1.16 ± 0.077 ng/mg and 0.41 ± 0.016 ng/mg of biomass, respectively).
While noroxomaritidine and normaritidine were consistently detected in all samples, vittatine and haemanthamine were only confirmed when *LaCYP96T1* was included, with a production of 4.85 ng/mL. Norgalanthamine was detected, but only confirmed in 1 out of 3 samples for *LaCYP96T1*, and 2 out of 3 samples for *LaCYP96T2* (Table 2.S11), indicating that *La*CYP96T2 more efficiently yielded norgalanthamine compared to *La*CYP96T1. In summary, the results support the previous stepwise findings and validate the reconstructed pathway with the four enzymes, as illustrated in Figure 2.S15.

2.5. Discussion

In this study, we identified and characterized the functionality of the key enzymes involved in the biosynthesis of the pharmaceutically potent AA using a multifaceted approach that included

homology-based sequence comparison, phylogenetic reconstruction, subcellular localization studies, docking, and *in planta* assays. The synthesis of norbelladine, the first AA of the pathway, is a critical biosynthetic step. The identified *La*NBS candidate belongs to the pathogenesis-related 10 (PR10)/Bet v1 protein superfamily, which has gained significant attention for its role in condensation reactions in the initial steps of benzylisoquinoline alkaloids (BIA) and AA biosynthesis pathways. A proeminent member of this superfamily, (*S*)-norcoclaurine synthase (NCS) catalyzes condensation of dopamine and 4-HPAA to produce (*S*)-norcoclaurine, the first committed step in the biosynthesis of BIA such as morphine and codeine (Samanani and Facchini, 2002; Samanani et al., 2004). A truncated NCS gene from *C. japonica* condensed 4-hydroxydihydrocinnamaldehyde (4-HDCA) and dopamine, derived from L-phenylalanine and L-tyrosine respectively, to yield 1-phenethylisoquinoline, a precursor in the colchicine alkaloid biosynthetic pathway (Nett et al., 2020; Qiao et al., 2023). Similarly, *LaNBS* encodes an enzyme catalyzing the condensation of tyramine and 3,4-DHBA into norbelladine (Singh et al., 2018; Tousignant et al., 2022a). Although a norcraugsodine/noroxomaritidine reductase has also been shown to catalyze this step (Kilgore et al., 2016), the condensation of tyramine and 3,4-DHBA to yield norbelladine in yeast requires both NBS and NR enzymes (Majhi et al., 2023b), suggesting that NBS catalyzes the condensation to form norcraugsodine, which is then reduced to norbelladine by NR. Thermal unfolding analysis further strengthened the evidence of interaction of the substrates 3,4-DHBA+tyramine with *La*NBS and *La*NRII. Docking analysis indicates that the condensation of the amine and the aldehyde is facilitated by catalytic residues Tyr59, Glu71 and Lys83, and stabilized by hydrophobic interactions, consistently with previous studies on *Np*NBS, *La*NBS, and *Nps*NBS (Hnin et al., 2024c; Majhi et al., 2023b). Norcraugsodine was positioned in a bended position in the active site of NR to expose its C-N double bond to Tyr173 and to NADPH. Similarly to tyramine and piperonal in *Nps*NR crystals, the ligand was further stabilized by interactions with Ile205 (Ala207 in *Nps*NR) and His170 (His172) (Kilgore et al., 2016). While mutagenesis studies are required to validate the role of these residues, the results emphasize the critical importance of these key amino acids in NBS and NR biosynthesis of norbelladine. Consistent with previous *in vitro* findings and with the current docking analysis, we confirmed the catalysis of norbelladine formation in *in vivo* as well as *in vitro* reactions, as detected by LC-MS/MS. However, the low quantities produced suggest that this step in the AA pathway may be rate limiting, warranting further optimization to enhance its efficiency.

Norbelladine then undergoes 3′ or 4′*O*-methylation as a critical step for diversification into various AAs (Figure 2.1). Some plant OMTs, particularly those involved in phenylpropanoid and flavonoid biosynthesis, often exhibit substrates versatility (Liscombe et al., 2012). *In vitro* studies in *N.* sp. *aff. pseudonarcissus* have shown that OMT regiospecifically methylates norbelladine at the 4′O position (Kilgore et al., 2014). However, the OMT from *N. papyraceus, Galanthus elwesii* and *Lycoris* species are promiscuous, methylating at the 3′ or 4′ position depending on the ligand, and on the metal ion (Koirala et al., 2024; Li et al., 2019; Su et al., 2022b; Sun et al., 2018). Sequence comparison and docking analysis suggest that the *LaN4′OMT* candidate identified in this study likely yields 4′-*O*-methylnorbelladine (4′OM), with norbelladine 4′O to face the SAM methyl group in interaction with Mg^{2+}, Asp155 and Lys158. *In planta* agroinfiltration confirmed the regiospecificity, yielding 4′*O*M as sole product and similar results were obtained *in vitro* while using Mg^{2+} as ion. Intriguingly, *La*N4′OMT enzyme also contained specific residues that were previously associated with 3'-*O*-methylation of norbelladine (Val30, Gln141). As Ni^{2+} was shown to reverse regioselectivity of *G. elwesii* class I OMT triple mutant (Su et al., 2022a), this ion was selected for further *in vitro* experiments. Its addition instead of Mg^{2+}, Ni^{2+} resulted in the formation of 3′,4′-*O*-dimethylnorbelladine from norbelladine catalyzed by *La*N4′OMT, although its level was 250-fold lower than 4′*O*M. Additionally, *para*- and *meta*-methylated derivatives of 3,4-DHBA, yielding vanillin and isovanillin, were observed. Mutagenesis studies revealed that Ser52 and Tyr186 play pivotal roles in determining *para* versus *meta*-*O*-methylation preferences (Hnin et al., 2024a). Further exploration of combinations of mutations and divalent metal ions is needed to gain insight on regioselectivity to increase dimethylated product yields. For the first time, co-infiltration of *LaNBS*, *LaNRII*, *LaN4′OMT*, along with supplementation of tyramine and 3,4-DHBA, led to the detection of norbelladine and 4′OM, reconstituting the foundational steps of the pathway *in vivo*.

At this critical branching point in the biosynthetic pathway, 4′*O*M undergoes three potential phenol couplings to generate skeletal frameworks that give rise to over 650 known AAs. Phenol couplings catalyzed by CYPs in BIA pathway of several plants, such as *Gloriosa superba*, *Berberis stolonifera*, *C. japonica*, *P. somniferum*, and *Argemone mexicana* lead to the production of pharmaceutically potent compounds. The discovery of *Nps*CYP96T1 in *N.* sp. *aff. pseudonarcissus* marked a significant advancement in AA biosynthesis, as it represented the first enzyme of its kind identified in a monocot. *Nps*CYP96T1 catalyzes the ring closure 4′OM, strongly favoring the

formation of the *p-p´* coupled product, noroxomaritidine, over the *p-o´* product, *N*-demethylnarwedine (Kilgore et al., 2016a). Further studies uncovered other *Amaryllidaceae* CYP96Ts with specific coupling preferences (Liu et al., 2024; Mehta et al., 2024). In this study, we identified and examined orthologs *La*CYP96T1 and *La*CYP96T2, which were localized to the ER membrane. Membrane-bound proteins, including cytochromes P450, are proposed to act as nucleation factors that orchestrate the assembly of metabolons at the endoplasmic reticulum membrane interface (Bassard et al., 2012). Consistently, our localization results suggest that *La*CYP96T1 and *La*CYP96T2 may recruit additional cytosolic metabolic enzymes, such as *La*NBS, *La*NRII and *LaN4´OMT*, to form a metabolon, although further studies are required to confirm this hypothesis.

Phylogenetic analysis indicated that the candidates clustered with the *o-p´* coupling enzyme *Nt*CYP96T5 (Mehta et al., 2024). Docking studies revealed that heme interacted with Leu123 and 4´OM with Phe124, and Val307 among other key residues in the enzyme catalytic pocket. Leu123 and Phe124 have been associated with either *p-p´* or *o-p´* coupling (Liu et al., 2024). Mutations of residues at both positions were shown to impact coupling specificity, with Ile123 and Leu124 specific to *p-o´* and *p-p´* coupling catalysis, but absent from *o-p´* coupling enzymes, while Leu123 and Phe124 could not yield *p-o´* coupled products (Liu et al., 2024). By contrast, Val307, predicted to interact with water or with the oxygen of the substrate phenol ring, seems to be compatible with the three types of couplings. The analyses of the active site sequence and docking of the candidates suggested that the enzymes could catalyze *o-p´* and *p-p´* reactions. Intriguingly, like *Nt*CYP96T5 from Mehta *et al*, *La*CYP96T1 and *La*CYP96T2 were not active *in vitro* when expressed in yeast (data not shown). While *Nt*CYP96T5 activity has not been verified *in vitro*, the isolation of microsomes from *N. benthamiana* leaves agroinfiltrated with *La*CYP96T1 was successful and resulted in the formation of minor *p-p´* and major *o-p´* products from 4'OM, when co-incubated with the reductase (*La*NRII) purified from bacteria. This *in vitro* assay confirmed the *in silico* predictions, demonstrating that *La*CYP96T1 and *La*CYP96T2 can yield various coupled products, although *p-o´* derived alkaloids were not detected.

In planta, upon feeding 4´OM, *La*CYP96T1 and *La*CYP96T2 catalyzed the formation of noroxomaritidine and *N*-demethylnarwedine. *La*CYP96T2 yielded detectable amount of lycorine as well. The addition of a reduction steps showed that both enzymes could yield the three coupled

products, suggesting that they are promiscuous with regards to the product they can form. There is growing evidence that CYPs exhibit significant substrate and product promiscuity (Hansen et al., 2021). However, this notion of multifunctionality appears somewhat contradictory to recent studies by Mehta *et al* and Liu *et al* (Liu et al., 2024; Mehta et al., 2024), where specific amino acid sequences were reported to be associated with exclusive coupling patterns. In these studies, the residues involved in substrate binding were consistent with those found in *Lau*CYP96T1-like2 and *Nt*CYP96T5 transcripts, which yielded *p-p´* coupled product (haemanthamine pathway) and *o-p´* coupled products (lycorine pathway), respectively. Despite these similarities, *La*CYP96T1 and *La*CYP96T2 catalyzed the formation of all three couplings, with *o-p´* as major reaction product. Mehta *et al* suggested Ala308 in *Nt*CYP96T1 was required for *p-p´* coupling and Leu308 for the *p-o´* coupling by *Nt*CYP96T6 by performing mutagenesis study where as *o-p´* coupling *Nt*CYP96T5 contained Val308. This requirement, however, may be context-dependent and not applicable to sequences from other species as demonstrated by *Lau*CYP96T1-like2, *Lau*CYP96T1-like3 and their mutants, which catalyzed *p-p´* and *p-o´* products formation, despite displaying a valine (Val307) at the corresponding position (Table 2.S10) (Liu et al., 2024). Docking studies further highlighted the relevance of conserved Lys109, Leu112, Phe116, Leu220, Leu224, Thr311, and Leu495 in substrate stabilization. However, complementary residues that enable promiscuity in product formation for *La*CYP96T1 and T2 remain unknown at this stage. Notably, the cloned sequences displayed a unique glutamine at position 251 in the vicinity of the catalytic site compared to all other characterized CYPs, which could play a role (Figure 2.S4b). Further mutagenesis studies that explore single and combinations of amino acids will be necessary to reveal the precise requirements for substrate positioning to yield the different couplings.

The current results also highlight the promiscuity of *La*NRII. Docking studies suggested that *La*NRII, which previously reduced norcraugsodine to norbelladine accepted noroxopluviine, *N*-demethylnarwedine, and noroxomaritidine (in two positions) with similar scores in its active sites, conserving the key interaction with Tyr173. Co-infiltration of *LaCYP96T1* or *LaCYP96T2* with *LaNRII* supplemented with 4´OM yielded six detectable products from the three coupling branches, namely *p'-o N*-demethylnarwedine, the *p-p´* coupled product, noroxomaritidine, oxomaritinamine and normaritidine, together with the *o-p´* phenol coupling norpluviine and lycorine. These results, confirmed by *in vitro* assays, revealed that *La*NRII is involved in the

synthesis of all three types of phenol coupled products in the AA biosynthetic pathway. The ability of *La*NRII to reduce all three phenol-coupled products at different positions is novel, but consistent with findings for *Nps*NR from *N.* sp. *aff. pseudonarcissus*, and *Zt*SDR from *Zephyranthes treatiae*, which reduced imines and ketones (Kilgore et al., 2016; Roth et al., 2018). Similarly, in tropane alkaloid biosynthesis, SDR presented substrate flexibility, as seen in *Cochlearia officinalis* SDR (*Co*TR) and*Th*TRL from *Tarenaya hassleriana* (Li et al., 2022; Reinhardt et al., 2014).

SDR catalyze the interconversion of hydroxyl and oxo groups in substrates using a conserved Ser-Tyr-Lys catalytic triad (Jornvall et al., 1995). Tyrosine functions as the central acid-base catalyst in its deprotonated tyrosinate state, supported by lysine, which lowers tyrosine's pKa and aligns NADP+ for hydride transfer (Benach et al., 1999). The serine stabilizes the substrate and intermediates via hydrogen bonding. (Brock et al., 2008; Chen et al., 1993; Gani et al., 2008; Kavanagh et al., 2008). In *La*NRII enzyme, Ser159, Tyr173 and Lys177 are predicted to form the catalytic triad and surrounds the NADP ring. Moreover, Tyr173 directly interacted with the ligands. The role of additional residues, such as His170 and Glu224 in various substrates reduction requires further investigation. Compared to *Nps*NR and *Nt*SDR1, *La*NRII encodes an alanine instead of Ser174, between residues of the catalytic triad, along with a 9% and 29% difference in amino acids, respectively. While the promiscuity of *Nt*SDR1 has not been assessed, these sequence differences may contribute to variations in substrate specificity. However, further mutagenesis studies are recommended to explore the promiscuity of *La*NRII.

Finally, whole pathway co-infiltration (*LaNBS, LaNRII, LaN4´OMT,* and *LaCYP96T1* or *LaCYP96T2),* along with precursors tyramine and 3,4-DHBA, yielded lycorine as the major product, with *La*CYP96T1 being almost three times more efficient than *La*CYP96T2. While norpluviine likely resulted from noroxopluviine reduction by *La*NRII, the synthesis of lycorine requires, in theory, more enzymatic steps, such as oxygen bridging and hydroxylation (Desgagné-Penix, 2021; Jayawardena et al., 2024), possibly carried out by endogenous enzymes in *N. benthamiana* as observed in other studies (Boccia et al., 2022; Caputi et al., 2018; Dong et al., 2013; van Herpen et al., 2010). In addition to lycorine, Norgalanthamine was observed in leaves co-infiltrated with *LaNBS, LaNRII, LaN4´OMT, LaCYP96T1* or *LaCYP96T2,* supplemented with tyramine and 3,4-DHBA, confirming the possible reduction of *N*-demethylnarwedine.

Infiltration of the entire pathway also resulted in the detection of trace amounts of crinine and haemanthamine when *LaCYP96T1* was included, whereas these products were not detected with *LaCYP96T2*. This finding suggests that *La*CYP96T1 is more efficient not only in producing lycorine but also in driving the biosynthesis of crinine/haemanthamine, whereas *La*CYP96T2 primarily yielded lycorine and norgalanthamine. The proposed biosynthetic pathway for haemanthamine suggests that a CYP71 family enzyme facilitates the methyl bridging, leading to the formation of vittatine/crinine. Subsequently, vittatine/crinine undergoes hydroxylation to produce 11-hydroxyvittatine, followed by *O*-methylation. These transformation steps are likely carried out by endogenous enzymes present in *N. benthamiana,* as has been reported in the reconstitution of the MIA pathway for strictosidine biosynthesis (Miettinen et al., 2014). Although the activity of endogenous enzymes in *N. benthamiana* may complicate the precise elucidation of the pathway, it offers a potential advantage by reducing the reliance on heterologous enzyme expression for biotechnological applications. However, the competition between these endogenous enzymes and the specific enzymes identified from *L. aestivum* needs to be verified. Future studies should focus on co-infiltrating the genes encoding *N*-methyltransferases, hydroxylases, and enzymes involved in oxygen or methyl bridging, alongside their functional characterization in heterologous hosts such as yeast, to provide deeper insight into these biosynthetic pathways.

2.6. Conclusion

In conclusion, our study elucidates the enzymatic steps involved in the biosynthesis of Amaryllidaceae alkaloids, demonstrating that four enzymes, NBS, NR, N4′OMT, and CYP96T, are sufficient to yield the three types of phenol coupling reaction in *N. benthamiana*, ultimately producing the potent antiviral and anticancer alkaloid, lycorine. Furthermore, our results highlight the substrate as well as product promiscuity of *La*NRII, *La*CYP96T1 and *La*CYP96T2. The investigation of the residues responsible for this promiscuity may pave the way towards understanding enzyme flexibility, developing novel biocatalysts and enhance our knowledge of evolutionary processes in protein function. Overall, we provide robust evidence for the synthesis of Amaryllidaceae alkaloids *in planta* and deliver new knowledge for metabolic engineering approaches to achieve sustainable production of SMs through synthetic biology. The elucidation

of the biosynthetic pathway of Amaryllidaceae alkaloids in *L. aestivum* represents a significant advancement in our understanding of plant specialized metabolism.

Funding

This research was financially supported by the Natural Sciences and Engineering Research Council of Canada (NSERC) award number RGPIN-2021-03218 to I.D-P. This work was also supported by the Canada Research Chair on plant specialized metabolism Award No CRC-2018-00137 to I.D-P. Thanks are extended to the Canadian taxpayers and to the Canadian government for supporting the Canada Research Chairs Program.

Acknowledgement:

We are grateful to Dr Bridget Milorey and Cyril Castel of NanoTember Technologies, Inc. for assistance with differential scanning fluorescence assay. We thank Patrick Lagüe from Université Laval for sharing his expertise on molecular docking. We thank Dr Bharat Bhusan Majhi for providing *LaNBS,* and *LaNRII* gene, Melodie B. Plourde for helping with confocal imaging, and Dr Fatma Meddeb for timely help in obtaining the lab materials along with and helpful discussions.

Authors Contribution:

Basanta Lamichhane: Conceptualization, Methodology, Investigation, Formal analysis, Validation, Visualization, Writing- Original draft, Reviewing and Editing; Sarah-Eve Gélinas: Methodology, Resources, and Editing, Natacha Merindol: Conceptualization, Methodology, Formal analysis, Project administration, Resources, Writing- Reviewing and Editing; Manoj Koirala: Methodology, Resources; Karen Cristine Goncalves dos Santos: Methodology, Resources; Hugo Germain: Conceptualization, Methodology, Resources, Co-supervision, Reviewing and Editing; Isabel Desgagné-Penix: Conceptualization, Methodology, Resources, Funding acquisition, Supervision, Writing- Reviewing and Editing.

Declaration of Interest:

The authors declare that there is no situation real, potential, or apparent conflict of interest.

2.7. Short legends for Supplementary Information

Figure 2.S1. Phylogenetic analysis, multiple sequence alignment and folding of *La*NBS

Figure 2.S2. Phylogenetic analysis, multiple sequence alignment and folding of *La*NRII

Figure 2.S3. Phylogenetic analysis, multiple sequence alignment and folding of *La*N4′OMT

Figure 2.S4. Phylogenetic analysis, multiple sequence alignment and folding of *La*CYP96T1 and *La*CYP96T2.

Figure 2.S5. Cellular localization of *La*N4'OMT and *La*CYP96T2.

Figure 2.S6. Western blot, SDS gel and RT-qPCR analysis illustrating the expression of fusion proteins of *La*CYP96T1 and *La*N4′OMT with EGFP along with *La*NBS, *La*NRII, *La*N4′OMT, *La*CYP96T1, *La*CYP96T2 in *N. benthamiana* leaf lysate.

Figure 2.S7. HPLC-MS/MS chromatograms of norbelladine and 4′-*O*-methylnorbelladine.

Figure 2.S8. Docked structures of candidates *La*CYP96T and *La*NRII.

Figure 2.S9. HPLC-MS/MS analysis of *N*-demethylnarwedine, produced upon transient expression of *LaCYP96T1* with 4′-*O*-methylnorbelladine as substrate, and *in vitro*.

Figure 2.S10. HPLC-MS/MS analysis of noroxomaritidine, produced upon transient expression of *LaCYP96T1* with 4′-*O*-methylnorbelladine, and *in vitro*.

Figure 2.S11. HPLC-MS/MS analysis of oxomaritinamine, produced upon transient expression of *LaCYP96T1* with 4′-*O*-methylnorbelladine as substrates in *N. benthamiana*.

Figure 2.S12. HPLC-MS/MS analysis of norpluviine produced upon transient co-expression of *LaCYP96T1 and LaNRII* with 4′-*O*-methylnorbelladine as substrates in *N. benthamiana*, and *in vitro.*

Figure 2.S13. HPLC-MS/MS chromatograms of the *ortho- para'* product lycorine, that was produced upon transient co-expression of *LaCYP96T1* and *LaNRII* with 4′-*O*-methylnorbelladine in *N. benthamiana.*

Figure 2.S14. HPLC-MS/MS chromatograms of the *para- para'* product normaritidine, that was produced upon transient co-expression of *LaCYP96T1 and LaNRII* with 4′-*O*-methylnorbelladine in *N. benthamiana.*

Figure 2.S15. The elucidated alkaloid biosynthesis pathway in *Leucojum aestivum* in this study.

Table 2.S1. The accession numbers of the sequences used for phylogenetic analysis for respective protein sequence used for phylogenetic analysis in Figures S1, S2, S3, and S4.

Table 2.S2. List of primers used in the experiments.

Table 2.S3. MRM transitions and instrumental parameters used on HPLC-MS/MS for *La*NBS, *La*NR and *La*OMT experiments.

Table 2.S4. MRM transitions and instrumental parameters used on HPLC-MS/MS for CYP experiments.

Table 2.S5. Instrumental parameters used in Product Ion mode on HPLC-MS/MS for CYP experiments.

Table 2.S6. Multiple Sequence Alignment Distance Matrix (Similarity in percent)

Table 2.S7. Active Site description and docking results of *La*NBS (tyramine and 3,4-DHBA), *La*NRII (norcraugsodine), *La*N4′OMT (norbelladine), and *La*CYP96T1 and T2 (4′-*O*-methylnorbelladine).

Table 2.S8. Differences in residues between SDRs

Table 2.S9. Differences in residues between *O*-methyltransferase enzymes of different substrate specificity.

Table 2.S10. Differences in residues between CYP enzymes with different product specificity/phenol coupling

Table 2.S11. Summary of *in vivo* enzymatic assay

2.8. References

Adasme, M.F., Linnemann, K.L., Bolz, S.N., Kaiser, F., Salentin, S., Haupt, V.J. and Schroeder, M. (2021) PLIP 2021: expanding the scope of the protein-ligand interaction profiler to DNA and RNA. *Nucleic Acids Res* **49**, W530-W534.

Bassard, J.E., Richert, L., Geerinck, J., Renault, H., Duval, F., Ullmann, P., Schmitt, M., Meyer, E., Mutterer, J., Boerjan, W., De Jaeger, G., Mely, Y., Goossens, A. and Werck-Reichhart, D. (2012) Protein-protein and protein-membrane associations in the lignin pathway. *Plant Cell* **24**, 4465-4482.

Belin, P., Le Du, M.H., Fielding, A., Lequin, O., Jacquet, M., Charbonnier, J.B., Lecoq, A., Thai, R., Courcon, M., Masson, C., Dugave, C., Genet, R., Pernodet, J.L. and Gondry, M. (2009) Identification and structural basis of the reaction catalyzed by CYP121, an essential cytochrome P450 in Mycobacterium tuberculosis. *Proc Natl Acad Sci U S A* **106**, 7426-7431.

Benach, J., Atrian, S.l., Gonzàlez-Duarte, R. and Ladenstein, R. (1999) The catalytic reaction and inhibition mechanism of Drosophila alcohol dehydrogenase: observation of an enzyme-bound NAD-ketone adduct at 1.4 Å resolution by X-ray crystallography. *Journal of molecular biology* **289**, 335-355.

Berkov, S., Pavlov, A., Georgiev, V., Bastida, J., Burrus, M., Ilieva, M. and Codina, C. (2009) Alkaloid synthesis and accumulation in Leucojum *aestivum in vitro* cultures. *Natural Product Communications* **4**, 1934578X0900400328.

Boccia, M., Grzech, D., Lopes, A.A., O'Connor, S.E. and Caputi, L. (2022) Directed Biosynthesis of New to Nature Alkaloids in a Heterologous *Nicotiana benthamiana* Expression Host. *Front Plant Sci* **13**, 919443.

Bonifacio, M.J., Archer, M., Rodrigues, M.L., Matias, P.M., Learmonth, D.A., Carrondo, M.A. and Soares-Da-Silva, P. (2002) Kinetics and crystal structure of catechol-*O*-methyltransferase complex with co-substrate and a novel inhibitor with potential therapeutic application. *Mol Pharmacol* **62**, 795-805.

Brock, A., Brandt, W. and Drager, B. (2008) The functional divergence of short-chain dehydrogenases involved in tropinone reduction. *Plant J* **54**, 388-401.

Burgstaller-Muehlbacher, S., Crotty, S.M., Schmidt, H.A., Reden, F., Drucks, T. and von Haeseler, A. (2023) ModelRevelator: Fast phylogenetic model estimation via deep learning. *Molecular Phylogenetics and Evolution* **188**, 107905.

Cahlikova, L., Breiterova, K. and Opletal, L. (2020) Chemistry and Biological Activity of Alkaloids from the Genus Lycoris (Amaryllidaceae). *Molecules* **25**, 4797.

Camacho, C., Coulouris, G., Avagyan, V., Ma, N., Papadopoulos, J., Bealer, K. and Madden, T.L. (2009) BLAST+: architecture and applications. *BMC Bioinformatics* **10**, 421.

Caputi, L., Franke, J., Farrow, S.C., Chung, K., Payne, R.M.E., Nguyen, T.D., Dang, T.T., Soares Teto Carqueijeiro, I., Koudounas, K., Duge de Bernonville, T., Ameyaw, B., Jones, D.M., Vieira, I.J.C., Courdavault, V. and O'Connor, S.E. (2018) Missing enzymes in the biosynthesis of the anticancer drug vinblastine in Madagascar periwinkle. *Science* **360**, 1235-1239.

Chen, S., Zhou, Y., Chen, Y. and Gu, J. (2018) fastp: an ultra-fast all-in-one FASTQ preprocessor. *Bioinformatics* **34**, i890.

Chen, Z., Jiang, J.C., Lin, Z.G., Lee, W.R., Baker, M.E. and Chang, S.H. (1993) Site-specific mutagenesis of Drosophila alcohol dehydrogenase: evidence for involvement of tyrosine-152 and lysine-156 in catalysis. *Biochemistry* **32**, 3342-3346.

Cui, W., Iwasa, K., Sugiura, M., Takeuchi, A., Tode, C., Nishiyama, Y., Moriyasu, M., Tokuda, H. and Takeda, K. (2007) Biotransformation of phenolic 1-benzyl-N-methyltetrahydroisoquinolines in plant cell cultures followed by LC/NMR, LC/MS, and LC/CD. *Journal of natural products* **70**, 1771-1778.

Desgagné-Penix, I. (2021) Biosynthesis of alkaloids in Amaryllidaceae plants: A review. *Phytochemistry Reviews* **20**, 409-431.

Dong, L., Miettinen, K., Goedbloed, M., Verstappen, F.W., Voster, A., Jongsma, M.A., Memelink, J., van der Krol, S. and Bouwmeester, H.J. (2013) Characterization of two geraniol synthases from Valeriana officinalis and Lippia dulcis: similar activity but difference in subcellular localization. *Metabolic engineering* **20**, 198-211.

Dudley, Q.M., Jo, S., Guerrero, D.A.S., Chhetry, M., Smedley, M.A., Harwood, W.A., Sherden, N.H., O'Connor, S.E., Caputi, L. and Patron, N.J. (2022) Reconstitution of monoterpene indole alkaloid biosynthesis in genome engineered *Nicotiana benthamiana*. *Commun Biol* **5**, 949.

Dumas, V.G., Defelipe, L.A., Petruk, A.A., Turjanski, A.G. and Marti, M.A. (2014) QM/MM study of the C-C coupling reaction mechanism of CYP121, an essential cytochrome p450 of Mycobacterium tuberculosis. *Proteins* **82**, 1004-1021.

Eddy, S.R. (2008) A probabilistic model of local sequence alignment that simplifies statistical significance estimation. *PLoS Computational Biology* **4**, e1000069.

Eddy, S.R. (2011) Accelerated profile HMM searches. *PLoS Computional Biology* **7**, e1002195.

El Tahchy, A., Boisbrun, M., Ptak, A., Dupire, F., Chrétien, F., Henry, M., Chapleur, Y. and Laurain-Mattar, D. (2010) New method for the study of Amaryllidaceae alkaloid biosynthesis using biotransformation of deuterium-labeled precursor in tissue cultures. *Acta Biochimica Polonica* **57**.

Filling, C., Berndt, K.D., Benach, J., Knapp, S., Prozorovski, T., Nordling, E., Ladenstein, R., Jornvall, H. and Oppermann, U. (2002) Critical residues for structure and catalysis in short-chain dehydrogenases/reductases. *J Biol Chem* **277**, 25677-25684.

Gani, O.A., Adekoya, O.A., Giurato, L., Spyrakis, F., Cozzini, P., Guccione, S., Winberg, J.O. and Sylte, I. (2008) Theoretical calculations of the catalytic triad in short-chain alcohol dehydrogenases/reductases. *Biophys J* **94**, 1412-1427.

Georgievaa, L., Berkov, S., Kondakova, V., Bastida, J., Viladomat, F., Atanassov, A. and Codina, C. (2007) Alkaloid variability in Leucojum *aestivum* from wild populations. *Zeitschrift für Naturforschung C* **62**, 627-635.

Girard, M.P., Karimzadegan, V., Heneault, M., Cloutier, F., Berube, G., Berthoux, L., Merindol, N. and Desgagne-Penix, I. (2022) Chemical Synthesis and Biological Activities of Amaryllidaceae Alkaloid Norbelladine Derivatives and Precursors. *Molecules* **27**, 5621.

Grabherr, M.G., Haas, B.J., Yassour, M., Levin, J.Z., Thompson, D.A., Amit, I., Adiconis, X., Fan, L., Raychowdhury, R., Zeng, Q., Chen, Z., Mauceli, E., Hacohen, N., Gnirke, A., Rhind, N., di Palma, F., Birren, B.W., Nusbaum, C., Lindblad-Toh, K., Friedman, N. and Regev, A. (2011) Full-length transcriptome assembly from RNA-Seq data without a reference genome. *Nature Biotechnology* **29**, 652.

Hansen, C.C., Nelson, D.R., Møller, B.L. and Werck-Reichhart, D. (2021) Plant cytochrome P450 plasticity and evolution. *Molecular Plant* **14**, 1244-1265.

Hnin, S.Y.Y., Nakashima, Y., Kodama, T. and Morita, H. (2024a) Structure-Based Catalytic Mechanism of Amaryllidaceae O-Methyltransferases. *ACS Catalysis* **14**, 11865-11880.

Hnin, S.Y.Y., Nakashima, Y. and Morita, H. (2024b) Substrate Flexibilities of Norbelladine Synthase and Noroxomaritidine/Norcraugsodine Reductase for Hydroxylated and/or Methoxylated Aldehydes. *Chemical and Pharmaceutical Bulletin* **72**, 507-511.

Hnin, S.Y.Y., Nakashima, Y. and Morita, H. (2024c) Substrate Flexibilities of Norbelladine Synthase and Noroxomaritidine/Norcraugsodine Reductase for Hydroxylated and/or Methoxylated Aldehydes. *Chem Pharm Bull (Tokyo)* **72**, 507-511.

Hoang, D.T., Chernomor, O., Von Haeseler, A., Minh, B.Q. and Vinh, L.S. (2018) UFBoot2: improving the ultrafast bootstrap approximation. *Molecular biology and evolution* **35**, 518-522.

Ilari, A., Franceschini, S., Bonamore, A., Arenghi, F., Botta, B., Macone, A., Pasquo, A., Bellucci, L. and Boffi, A. (2009) Structural basis of enzymatic (S)-norcoclaurine biosynthesis. *J Biol Chem* **284**, 897-904.

Irwin, J.J., Tang, K.G., Young, J., Dandarchuluun, C., Wong, B.R., Khurelbaatar, M., Moroz, Y.S., Mayfield, J. and Sayle, R.A. (2020) ZINC20-A Free Ultralarge-Scale Chemical Database for Ligand Discovery. *J Chem Inf Model* **60**, 6065-6073.

Iwasa, K. and Kim, C.W. (1997) Biotransformations of protoberberines in cell cultures of Dicentra spectablis. *Phytochemistry* **46**, 1359-1363.
Jayawardena, T.U., Merindol, N., Liyanage, N.S. and Desgagne-Penix, I. (2024) Unveiling Amaryllidaceae alkaloids: from biosynthesis to antiviral potential - a review. *Nat Prod Rep* **41**, 721-747.
Jornvall, H., Persson, B., Krook, M., Atrian, S., Gonzalez-Duarte, R., Jeffery, J. and Ghosh, D. (1995) Short-chain dehydrogenases/reductases (SDR). *Biochemistry* **34**, 6003-6013.
Kalyaanamoorthy, S., Minh, B.Q., Wong, T.K., Von Haeseler, A. and Jermiin, L.S. (2017) ModelFinder: fast model selection for accurate phylogenetic estimates. *Nature methods* **14**, 587-589.
Karimi, M., Depicker, A. and Hilson, P. (2007) Recombinational cloning with plant gateway vectors. *Plant Physiol* **145**, 1144-1154.
Kavanagh, K., Jörnvall, H., Persson, B. and Oppermann, U. (2008) Medium-and short-chain dehydrogenase/reductase gene and protein families: the SDR superfamily: functional and structural diversity within a family of metabolic and regulatory enzymes. *Cellular and Molecular Life Sciences* **65**, 3895-3906.
Kilgore, M.B., Augustin, M.M., May, G.D., Crow, J.A. and Kutchan, T.M. (2016a) CYP96T1 of Narcissus sp. aff. Pseudonarcissus catalyzes formation of the Para-Para'CC phenol couple in the Amaryllidaceae alkaloids. *Frontiers in plant science* **7**, 225.
Kilgore, M.B., Augustin, M.M., Starks, C.M., O'Neil-Johnson, M., May, G.D., Crow, J.A. and Kutchan, T.M. (2014) Cloning and characterization of a norbelladine 4′-*O*-methyltransferase involved in the biosynthesis of the Alzheimer's drug galanthamine in Narcissus sp. aff. pseudonarcissus. *PloS one* **9**, e103223.
Kilgore, M.B., Holland, C.K., Jez, J.M. and Kutchan, T.M. (2016) Identification of a Noroxomaritidine Reductase with Amaryllidaceae Alkaloid Biosynthesis Related Activities. *J Biol Chem* **291**, 16740-16752.
Kilgore, M.B., Holland, C.K., Jez, J.M. and Kutchan, T.M. (2016c) Identification of a noroxomaritidine reductase with Amaryllidaceae alkaloid biosynthesis related activities. *Journal of Biological Chemistry* **291**, 16740-16752.
Kilgore, M.B. and Kutchan, T.M. (2016b) The Amaryllidaceae alkaloids: biosynthesis and methods for enzyme discovery. *Phytochemistry reviews* **15**, 317-337.
Kohut, E., Ördögh, M., Jámbor-Benczúr, E. and Máthé, Á. (2007) Results with the establishment of *in vitro* culture of Leucojum *aestivum*. *International Journal of Horticultural Science* **13**, 67-71.
Koirala, M., Karimzadegan, V., Liyanage, N.S., Mérindol, N. and Desgagné-Penix, I. (2022) Biotechnological Approaches to Optimize the Production of Amaryllidaceae Alkaloids. *Biomolecules* **12**, 893.
Koirala, M., Merindol, N., Karimzadegan, V., Gelinas, S.E., Liyanage, N.S., Lamichhane, B., Tobon, M.C.G., Lague, P. and Desgagne-Penix, I. (2024) Kinetic and *in silico* structural characterization of norbelladine O-methyltransferase of Amaryllidaceae alkaloids biosynthesis. *J Biol Chem* **300**, 107649.
Krogh, A., Larsson, B., von Heijne, G. and Sonnhammer, E.L. (2001) Predicting transmembrane protein topology with a hidden Markov model: application to complete genomes. *Journal of Molecular Biology* **305**, 580.
Letunic, I. and Bork, P. (2021) Interactive Tree Of Life (iTOL) v5: an online tool for phylogenetic tree display and annotation. *Nucleic Acids Res* **49**, W293-W296.
Li, W., Qiao, C., Pang, J., Zhang, G. and Luo, Y. (2019) The versatile O-methyltransferase LrOMT catalyzes multiple O-methylation reactions in amaryllidaceae alkaloids biosynthesis. *International journal of biological macromolecules* **141**, 680-692.
Li, Y., Bai, Y., Fan, T.P., Zheng, X. and Cai, Y. (2022) Characterization of a putative tropinone reductase from Tarenaya hassleriana with a broad substrate specificity. *Biotechnol Appl Biochem* **69**, 2530-2539.

Liscombe, D.K., Louie, G.V. and Noel, J.P. (2012) Architectures, mechanisms and molecular evolution of natural product methyltransferases. *Nat Prod Rep* **29**, 1238-1250.
Liu, J., Han, L., Li, G., Zhang, A., Liu, X. and Zhao, M. (2023) Transcriptome and metabolome profiling of the medicinal plant Veratrum mengtzeanum reveal key components of the alkaloid biosynthesis. *Frontiers in Genetics* **14**, 1023433.
Liu, Z., Sun, B., Li, J., Xiang, Y., Wang, R., Jiang, X., Zhu, X., Xu, S. and Wang, R. (2024) Functional characterization of CYP96T1-like cytochrome P450 from Lycoris aurea catalyzing para-para' and para-ortho' oxidative coupling in Amaryllidaceae alkaloids biosynthesis. *Front Plant Sci* **15**, 1438102.
Liyanage, N.S., Awwad, F., Gonçalves dos Santos, K.C., Jayawardena, T.U., Mérindol, N. and Desgagné-Penix, I. (2024) Navigating Amaryllidaceae Alkaloids: Bridging Gaps and Charting Biosynthetic Territories – A Comprehensive Review. *Journal of experimental botany*.
Majhi, B.B., Gélinas, S.-E., Mérindol, N., Ricard, S. and Desgagné-Penix, I. (2023a) Characterization of norbelladine synthase and noroxomaritidine/norcraugsodine reductase reveals a novel catalytic route for the biosynthesis of Amaryllidaceae alkaloids including the Alzheimer's drug galanthamine. *Frontiers in Plant Science* **14**, 1231809.
Majhi, B.B., Gelinas, S.E., Merindol, N., Ricard, S. and Desgagne-Penix, I. (2023b) Characterization of norbelladine synthase and noroxomaritidine/norcraugsodine reductase reveals a novel catalytic route for the biosynthesis of Amaryllidaceae alkaloids including the Alzheimer's drug galanthamine. *Front Plant Sci* **14**, 1231809.
Mehta, N., Meng, Y., Zare, R., Kamenetsky-Goldstein, R. and Sattely, E. (2024) A developmental gradient reveals biosynthetic pathways to eukaryotic toxins in monocot geophytes. *Cell* **187**, 5620-5637 e5610.
Miettinen, K., Dong, L., Navrot, N., Schneider, T., Burlat, V., Pollier, J., Woittiez, L., van der Krol, S., Lugan, R., Ilc, T., Verpoorte, R., Oksman-Caldentey, K.M., Martinoia, E., Bouwmeester, H., Goossens, A., Memelink, J. and Werck-Reichhart, D. (2014) The seco-iridoid pathway from Catharanthus roseus. *Nat Commun* **5**, 3606.
Mirdita, M., Schütze, K., Moriwaki, Y., Heo, L., Ovchinnikov, S. and Steinegger, M. (2022) ColabFold: making protein folding accessible to all. *Nature methods* **19**, 679-682.
Nawrocki, E.P., Kolbe, D.L. and Eddy, S.R. (2009) Infernal 1.0: inference of RNA alignments. *Bioinformatics* **25**, 1337.
Nelson, B.K., Cai, X. and Nebenführ, A. (2007) A multicolored set of *in vivo* organelle markers for co-localization studies in Arabidopsis and other plants. *The Plant Journal* **51**, 1126-1136.
Nett, R.S., Lau, W. and Sattely, E.S. (2020) Discovery and engineering of colchicine alkaloid biosynthesis. *Nature* **584**, 148-153.
Okonechnikov, K., Golosova, O., Fursov, M. and team, U. (2012) Unipro UGENE: a unified bioinformatics toolkit. *Bioinformatics* **28**, 1166-1167.
Pavlov, A., Berkov, S., Courot, E., Gocheva, T., Tuneva, D., Pandova, B., Georgiev, M., Georgiev, V., Yanev, S. and Burrus, M. (2007) Galanthamine production by Leucojum *aestivum in vitro* systems. *Process Biochemistry* **42**, 734-739.
Paysan-Lafosse, T., Blum, M., Chuguransky, S., Grego, T., Pinto, B.L., Salazar, G.A., Bileschi, M.L., Bork, P., Bridge, A. and Colwell, L. (2023) InterPro in 2022. *Nucleic acids research* **51**, D418-D427.
Peng, W., Li, Z., Wang, S. and Wang, B. (2023) Unravelling the C-C and C-N coupling mechanism for the CYP96T1-catalyzed biosynthesis of Amaryllidaceae alkaloids. *Molecular Catalysis* **550**, 113609.
Porter, T.D. and Coon, M.J. (1991) Cytochrome P-450. Multiplicity of isoforms, substrates, and catalytic and regulatory mechanisms. *J Biol Chem* **266**, 13469-13472.
Qiao, F., He, Y., Zhang, Y., Jiang, X., Cong, H., Wang, Z., Sun, H., Xiao, Y., Zhao, Y. and Nick, P. (2023) Elucidation of the 1-phenethylisoquinoline pathway from an endemic conifer Cephalotaxus hainanensis. *Proceedings of the National Academy of Sciences* **120**, e2209339120.

Reed, J. and Osbourn, A. (2018) Engineering terpenoid production through transient expression in *Nicotiana benthamiana*. *Plant cell reports* **37**, 1431-1441.
Reinhardt, N., Fischer, J., Coppi, R., Blum, E., Brandt, W. and Drager, B. (2014) Substrate flexibility and reaction specificity of tropinone reductase-like short-chain dehydrogenases. *Bioorg Chem* **53**, 37-49.
Roth, S., Kilgore, M.B., Kutchan, T.M. and Muller, M. (2018) Exploiting the Catalytic Diversity of Short-Chain Dehydrogenases/Reductases: Versatile Enzymes from Plants with Extended Imine Substrate Scope. *Chembiochem* **19**, 1849-1852.
Samanani, N. and Facchini, P.J. (2002) Purification and characterization of norcoclaurine synthase: The first committed enzyme in benzylisoquinoline alkaloid biosynthesis in plants. *Journal of Biological Chemistry* **277**, 33878-33883.
Samanani, N., Liscombe, D.K. and Facchini, P.J. (2004) Molecular cloning and characterization of norcoclaurine synthase, an enzyme catalyzing the first committed step in benzylisoquinoline alkaloid biosynthesis. *The Plant Journal* **40**, 302-313.
Sievers, F., Wilm, A., Dineen, D., Gibson, T.J., Karplus, K., Li, W., Lopez, R., McWilliam, H., Remmert, M., Soding, J., Thompson, J.D. and Higgins, D.G. (2011) Fast, scalable generation of high-quality protein multiple sequence alignments using Clustal Omega. *Mol Syst Biol* **7**, 539.
Simao, F.A., Waterhouse, R.M., Ioannidis, P., Kriventseva, E.V. and Zdobnov, E.M. (2015) BUSCO: assessing genome assembly and annotation completeness with single-copy orthologs. *Bioinformatics* **31**, 3212.
Singh, A., Massicotte, M.-A., Garand, A., Tousignant, L., Ouellette, V., Bérubé, G. and Desgagné-Penix, I. (2018) Cloning and characterization of norbelladine synthase catalyzing the first committed reaction in Amaryllidaceae alkaloid biosynthesis. *BMC plant biology* **18**, 1-12.
Stanfield, J.K., Omura, K., Matsumoto, A., Kasai, C., Sugimoto, H., Shiro, Y., Watanabe, Y. and Shoji, O. (2020) Crystals in Minutes: Instant On-Site Microcrystallisation of Various Flavours of the CYP102A1 (P450BM3) Haem Domain. *Angewandte Chemie International Edition* **59**, 7611-7618.
Su, Y., Li, H.-P., Zhang, M., Ding, X.-W., Xu, J.-H., Chen, Q. and Zheng, G.-W. (2022a) Regioselectivity Inversion of an O-Methyltransferase via Semi-rational Mutagenesis Combined with Metal Ion Substitution. *ChemCatChem* **14**, e202200844.
Su, Y., Li, H.P., Zhang, M., Ding, X.W., Xu, J.H., Chen, Q. and Zheng, G.W. (2022b) Regioselectivity Inversion of an O-Methyltransferase via Semi-rational Mutagenesis Combined with Metal Ion Substitution. *ChemCatChem* **14**, e202200844.
Sun, B., Wang, P., Wang, R., Li, Y. and Xu, S. (2018) Molecular Cloning and Characterization of a meta/para-*O*-Methyltransferase from Lycoris aurea. *International journal of molecular sciences* **19**, 1911.
Takos, A.M. and Rook, F. (2013) Towards a molecular understanding of the biosynthesis of Amaryllidaceae alkaloids in support of their expanding medical use. *International journal of molecular sciences* **14**, 11713-11741.
Tousignant, L., Diaz-Garza, A.M., Majhi, B.B., Gélinas, S.-E., Singh, A. and Desgagne-Penix, I. (2022a) Transcriptome analysis of Leucojum *aestivum* and identification of genes involved in norbelladine biosynthesis. *Planta* **255**, 30.
Tousignant, L., Diaz-Garza, A.M., Majhi, B.B., Gelinas, S.E., Singh, A. and Desgagne-Penix, I. (2022b) Transcriptome analysis of Leucojum *aestivum* and identification of genes involved in norbelladine biosynthesis. *Planta* **255**, 30.
van Herpen, T.W., Cankar, K., Nogueira, M., Bosch, D., Bouwmeester, H.J. and Beekwilder, J. (2010) *Nicotiana benthamiana* as a production platform for artemisinin precursors. *PLoS One* **5**, e14222.
von Haeseler, A., Schmidt, H.A., Bui, M.Q. and Nguyen, L.T. (2014) IQ-TREE: A fast and effective stochastic algorithm for estimating maximum-likelihood phylogenies.
Waterhouse, A.M., Procter, J.B., Martin, D.M., Clamp, M. and Barton, G.J. (2009) Jalview Version 2--a multiple sequence alignment editor and analysis workbench. *Bioinformatics* **25**, 1189-1191.

Xu, J.J., Fang, X., Li, C.Y., Yang, L. and Chen, X.Y. (2020) General and specialized tyrosine metabolism pathways in plants. *aBIOTECH* **1**, 97-105.

2.9. Supplementary Figures

Elucidating the enzyme network driving Amaryllidaceae Alkaloids Biosynthesis in *Leucojum aestivum.*

Basanta Lamichhane[1], Sarah-Eve Gélinas[1], Natacha Merindol[1], Manoj Koirala[1], Karen Cristine Gonçalves dos Santos[1], Hugo Germain[1,2], Isabel Desgagné-Penix[1,2*]

[1]Department of Chemistry, Biochemistry and Physics, Université du Québec à Trois-Rivières, Trois-Rivières, QC, Canada

[2]Plant Biology Research Group, Trois-Rivières, Québec, Canada

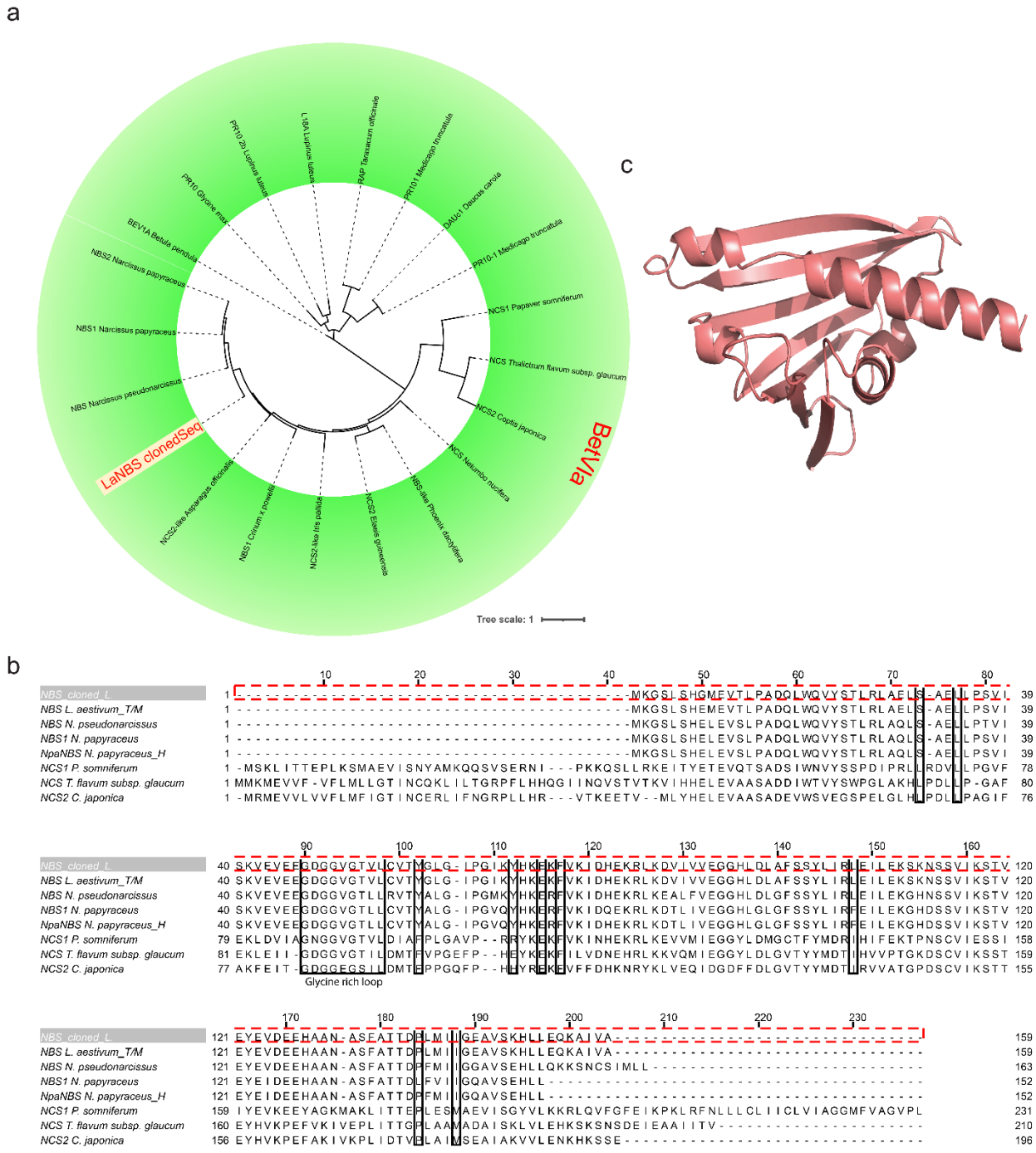


Figure 9. Phylogenetic analysis, multiple sequence alignment and folding of *La*NBS.

a Phylogenetic tree constructed using ModelRevelator software tool "Iqtree" with 1000 ultrafast bootstraps. Highlighted with red font is the transcript identified and used in the experiment. The accessions or sequences are listed in Table 2.S1. **b** Multiple sequence alignment was performed with 7 sequences. Boxes are the conserved major residues from the ligand binding and the catalytic site from different species **c** *La*NBS candidate folding predicted with Collabfold2 shown as cartoon.

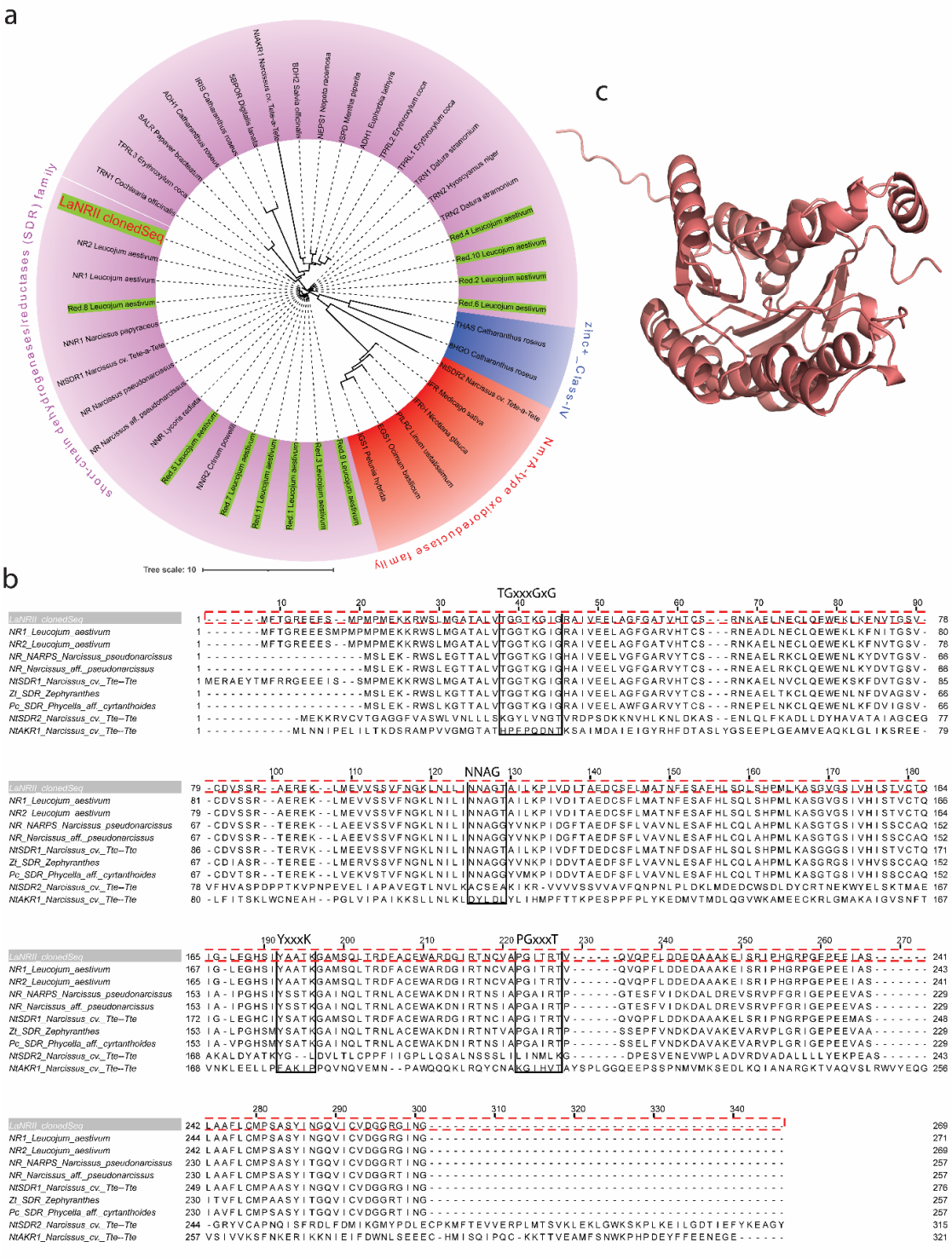


Figure 10. Phylogenetic analysis, multiple sequence alignment and folding of *La*NRII

a Phylogenetic tree constructed using ModelRevelator software tool "Iqtree" with 1000 ultrafast bootstraps. Green highlighted are the transcripts identified and with red font is the protein sequence used in the experiment. The accessions or sequences are listed in Table 2.S1. **b** Multiple sequence alignment was performed with 9 characterized sequences. Boxes are the conserved residues involved in ligand binding or catalysis. **c** *La*NRII candidate folding predicted with Collabfold2 shown as cartoon representation.

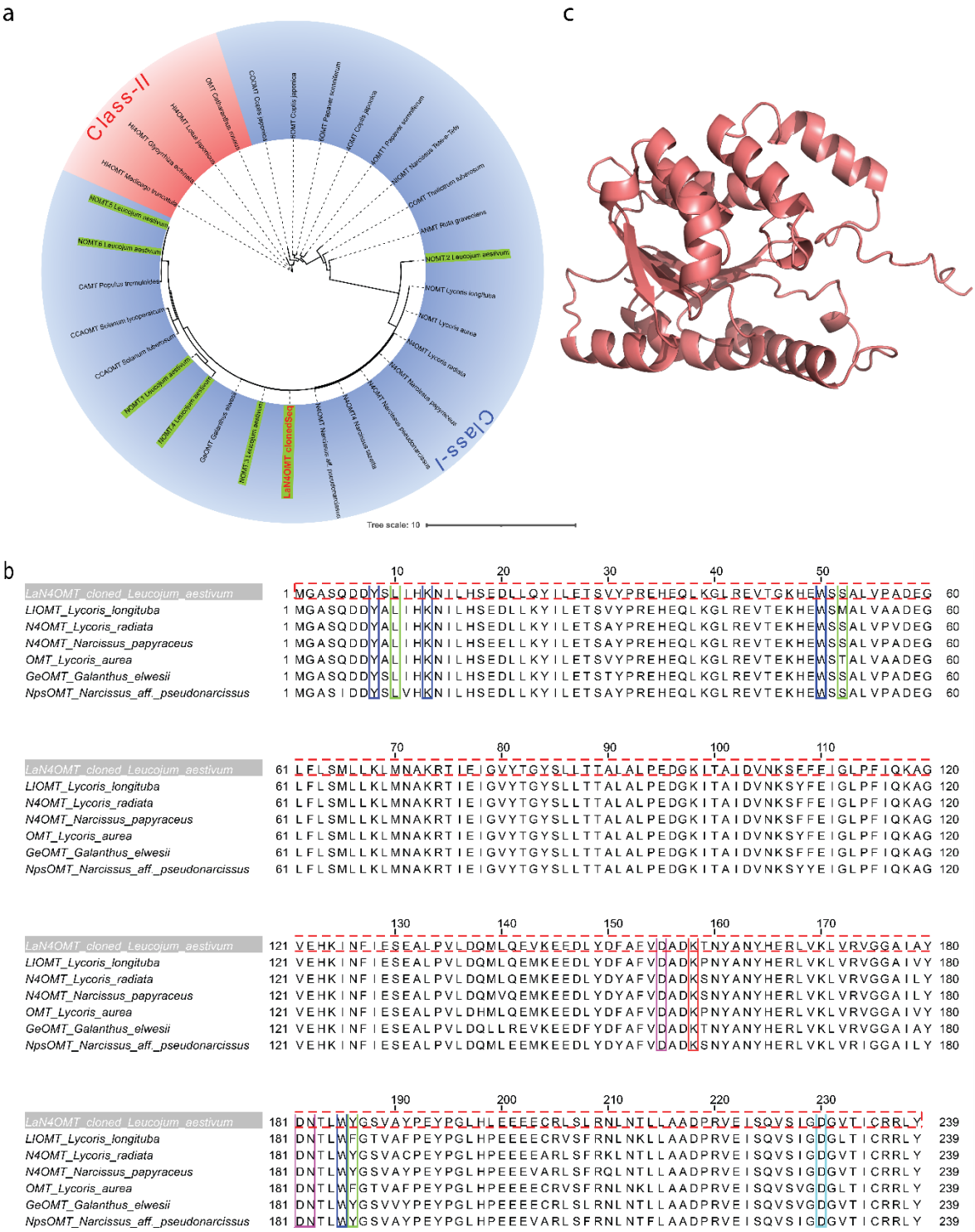


Figure 11. Phylogenetic analysis, multiple sequence alignment and folding of *La*N4´OMT.

a Phylogenetic tree constructed using ModelRevelator software tool "Iqtree" with 1000 ultrafast bootstraps. Green highlighted are the transcripts identified and with red font is the protein sequence used in the experiment. The accessions and sequences are listed in Table 2.S1. **b** Multiple sequence alignment was performed with 7 sequences. Boxes color code: red is catalytic residue K158; pink: three metal-binding residues, D155, D181, and N182, green: three Region A forming residues at 10, 52, and 186 positions, blue: substrate recognition residues, Y8, K13, W50, and W185. **c** *La*N4´OMT candidate folding was predicted with Collabfold2 and is shown as cartoon.

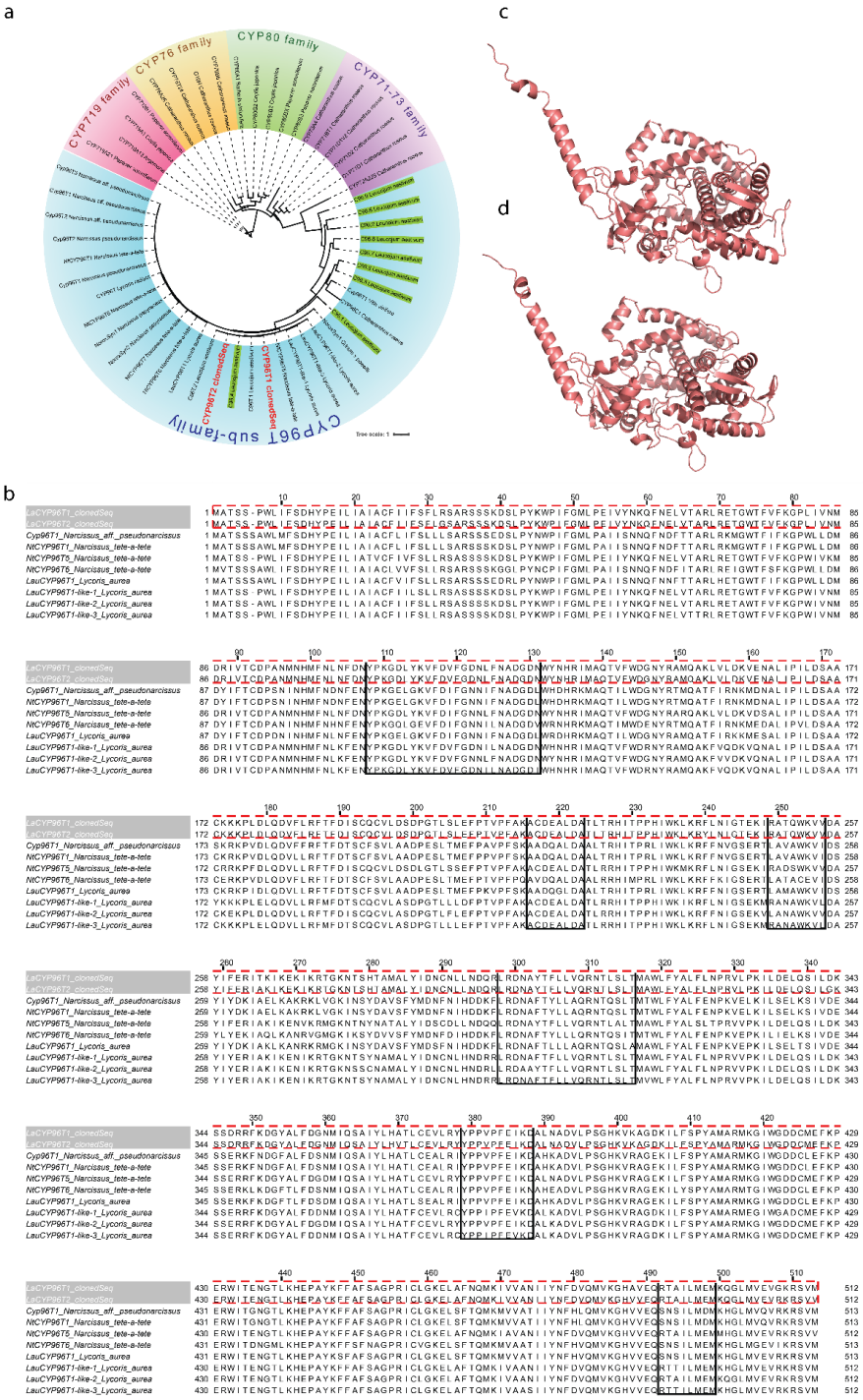


Figure 12. Phylogenetic analysis, multiple sequence alignment and folding of *La*CYP96T1 and *La*CYP96T2.

a Phylogenetic tree constructed using ModelRevelator software tool "Iqtree" with 1000 ultrafast bootstraps. Green highlighted are the transcripts identified from transcriptome database and red font is the protein sequence used in the experiment. Clustal W tool was used to align amino acid sequences. The accessions and sequences are listed in Table 2.S1. **b** Multiple sequence alignment was performed with 8 characterized sequences. Boxed are the conserved along with major residues of the catalytic site from different species. **c** *La*CYP96T1 candidate folding was predicted with Collabfold2 and is shown as cartoon. **d** *La*CYP96T2 candidate folding was predicted with Collabfold2 and is shown as cartoon.

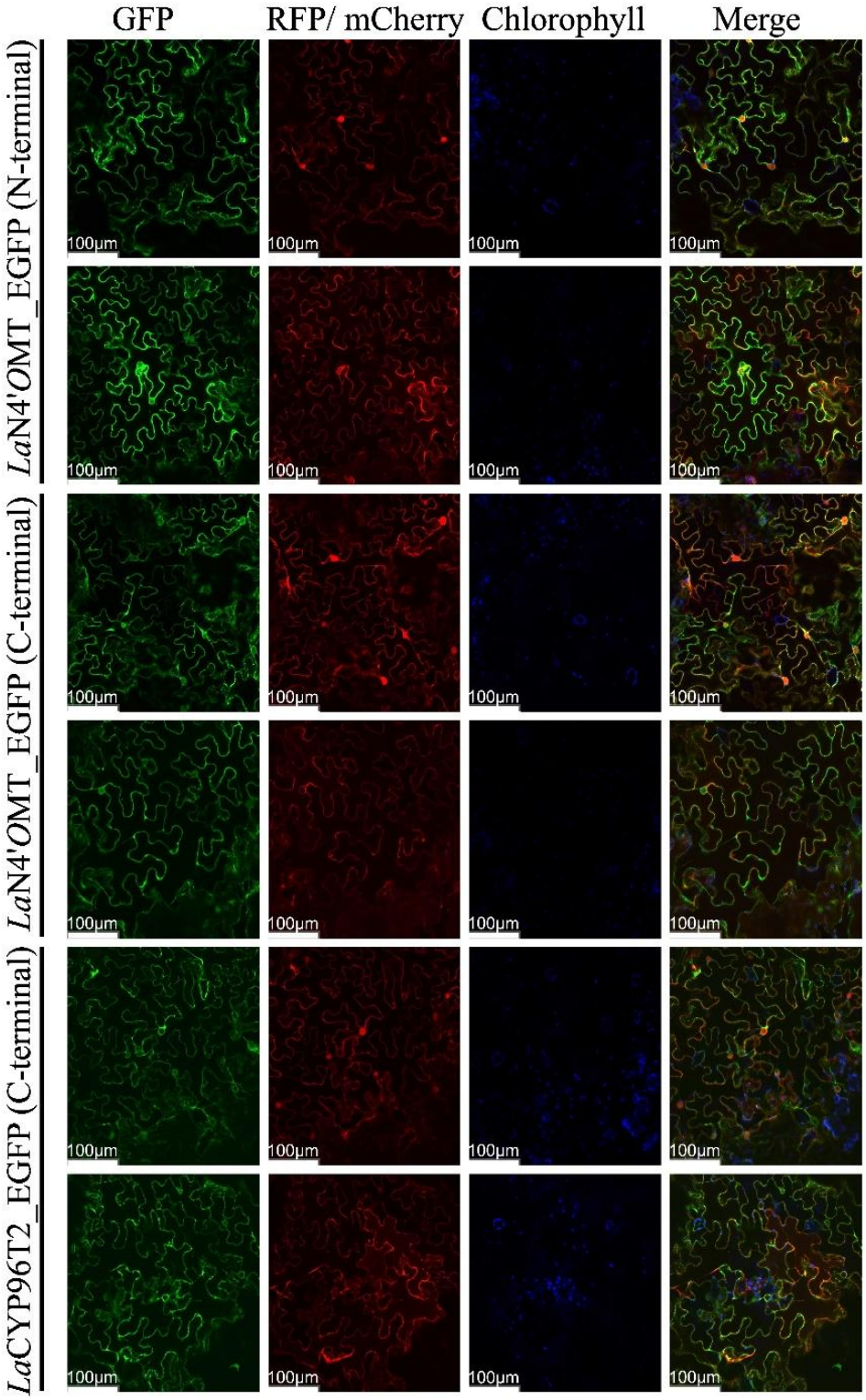


Figure 13. Cellular localization of *La*N4ˈOMT and *La*CYP96T2.

The indicated fusion proteins were co-expressed with the red fluorescent protein (RFP) or ER-mCherry in *N. benthamiana* leaves via *Agrobacterium tumefaciens*. Green fluorescent protein (fusion protein), Red florescence protein (RFP) or cherry red florescence protein (ER-mcherry), chlorophyll (blue), merged fluorescence images (Merge). Scale bar in the image is 100µm.

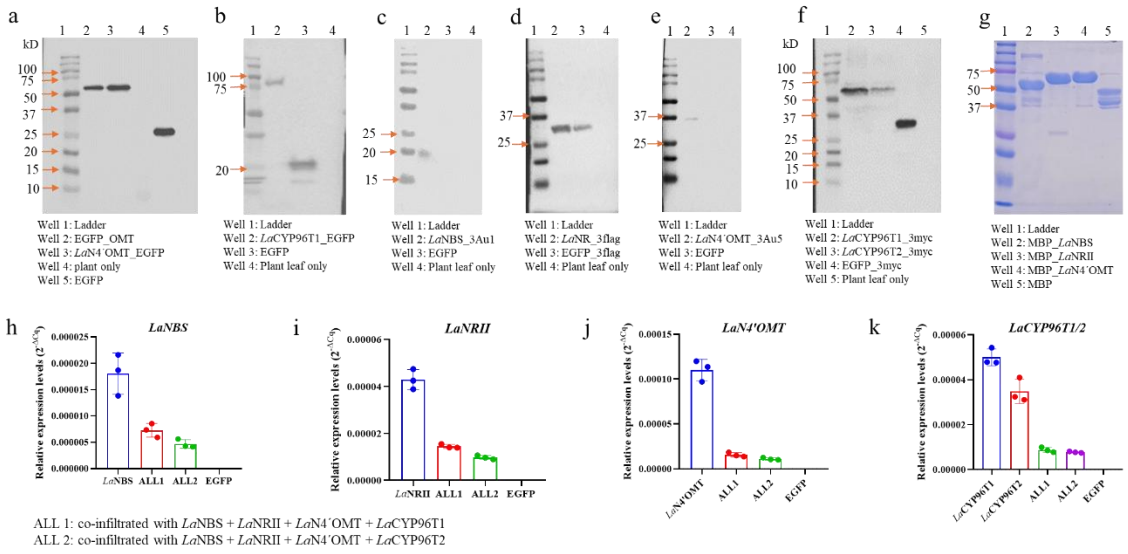


Figure 14. Western blot, SDS gel and RT-qPCR analysis

Upper panel. Western blot analysis illustrating the expression of fusion proteins of *La*CYP96T1 and *La*N4´*O*MT with EGFP along with *La*NBS, *La*NRII, *La*N4´*O*MT, *La*CYP96T1, *La*CYP96T2 in *N. benthamiana* leaf lysate and SDS gel for purified proteins. **a** N-terminal EGFP_*La*N4´*O*MT, C-terminal EGFP_*La*N4´*O*MT. **b** C-terminal EGFP_*La*CYP96T1. **c** *La*NBS. **d** *La*NRII. **e** *La*N4´*O*MT. **f** LaCYP96T1 and *La*CYP96T2. **g** SDS gel stained by Coomassie blue after running the purified MBP fusion proteins *La*NBS, *La*NRII, *La*N4´*O*MT and MBP alone respectively in each well.

Lower panel: Relative expression level of mRNA determined by RT-qPCR of each gene in RNA isolated from leaf samples infiltrated with gene or set of genes. RT-qPCR analysis of **h** *La*NBS **i** *La*NRII **j** *La*N4'OMT **k** *La*CYP96T1 and *La*CYP96T2. Histone3 specific primers were used as base for relative expression. Data are the means ± SE of three technical replicates of pooled biological triplicates.

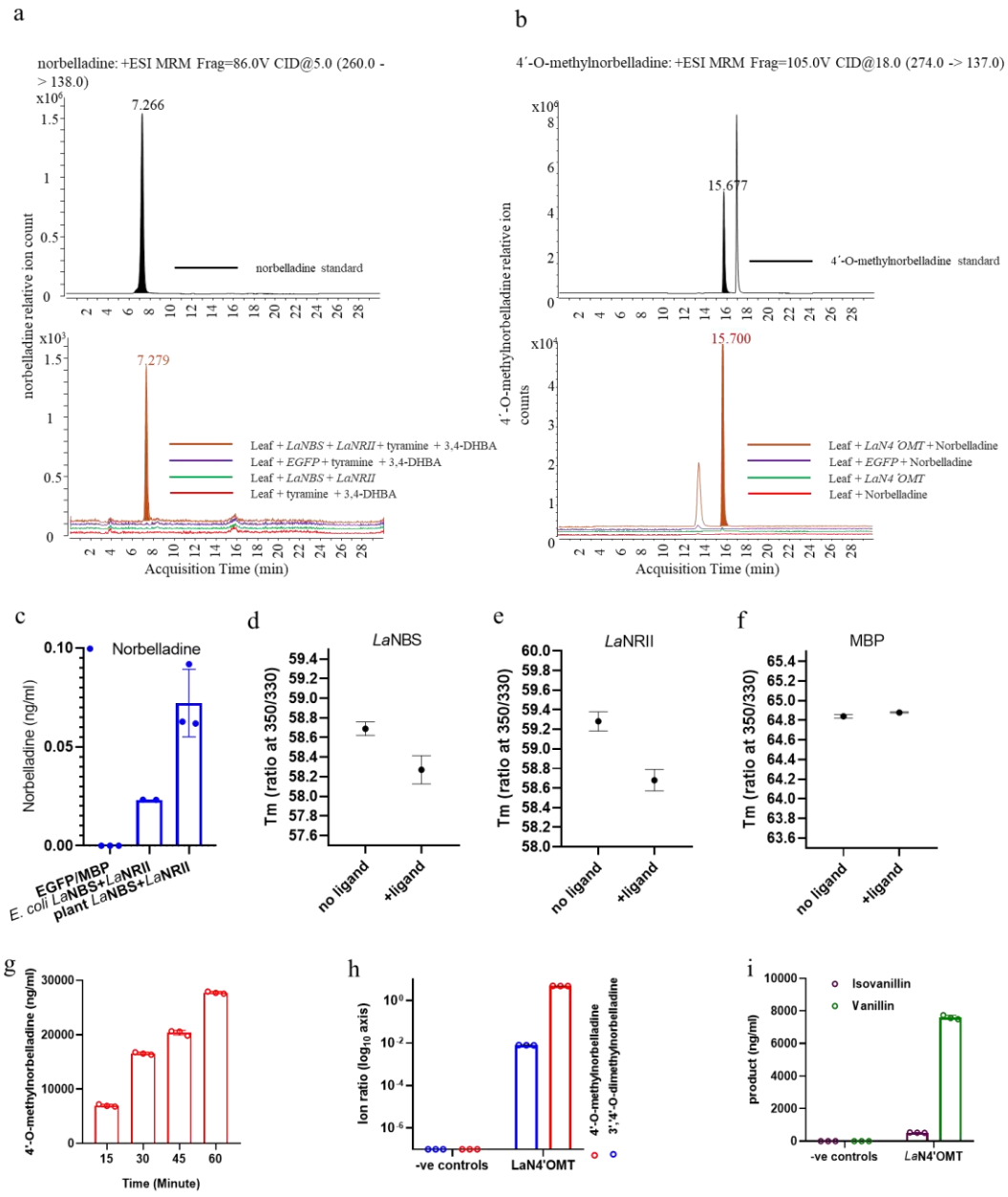


Figure 15. HPLC-MS/MS chromatograms of norbelladine and 4´-*O*-methylnorbelladineand *in vitro* detection.

a HPLC-MS/MS chromatograms of norbelladine produced upon transient co-expression of *LaNBS* and *LaNRII* with tyramine and 3,4-DHBA as substrates. The color of each chromatogram indicates either authentic reference standard of norbelladine (black), the *in vivo* assay (brown), or different negative controls (purple, green, red). **b** HPLC-MS/MS chromatograms of 4´-*O*-methylnorbelladine, produced upon transient expression of *LaN4´OMT* with norbelladine as substrate. The color of each chromatogram indicates either authentic reference standard of 4´-*O*-methylnorbelladine(black), the *in vivo* assay (brown), or different negative controls (purple, green, red). The identity of those products were confirmed by comparing this compound's retention time and other analytical parameters (Supplementary Table 2.S3) to the ones of norbelladine and 4´-*O*-methylnorbelladinestandard which were acquired in MRM analysis mode on the HPLC-MS/MS. **c** *In vitro* enzymatic assay of pure MBP tagged *La*NBS and MBP tagged *La*NRII produced in *E. coli* and crude *La*NBS and *La*NRII from *N. benthamiana* with tyramine and 3,4-DHBA as substrates, measuring the production of norbelladine. **d**, **e**, **f** Assessment of *La*NBS, *La*NRII and MBP protein thermal unfolding in presence of tyramine and 3,4-DHBA .Fluorescence monitored at both 330 and 350 nm using Prometheus Panta (NanoTemper Technologies). **g** Enzymatic assay of *La*N4'OMT with norbelladine as substrate and Mg^{2+}as metal ion, measuring the production of 4'-*O*-methylnorbelladine at different time interval. **h** Enzymatic assay of

*La*N4'OMT with norbelladine as substrate and Ni^{2+} as metal ion, detecting the production of 4'-*O*-methylnorbelladine and 3,4'-*O*-dimethylnorbelladine at 30 min. Y-axis is in log_{10} with base value 10^{-7} as zero for negative controls. **i** Enzymatic assay of *La*N4'OMT with 3,4-DHBA as substrate and Mg^{2+} as cation, measuring the production of vanillin and isovanillin at 30 minute. For all *in vitro* experiment, no substrate, no enzyme, boiled enzymes, purified MBP alone from *E. coli* were used as negative controls. All *in vitro* experiments were performed in triplicates and 1 ppm papaverine was used as internal standard after quenching.

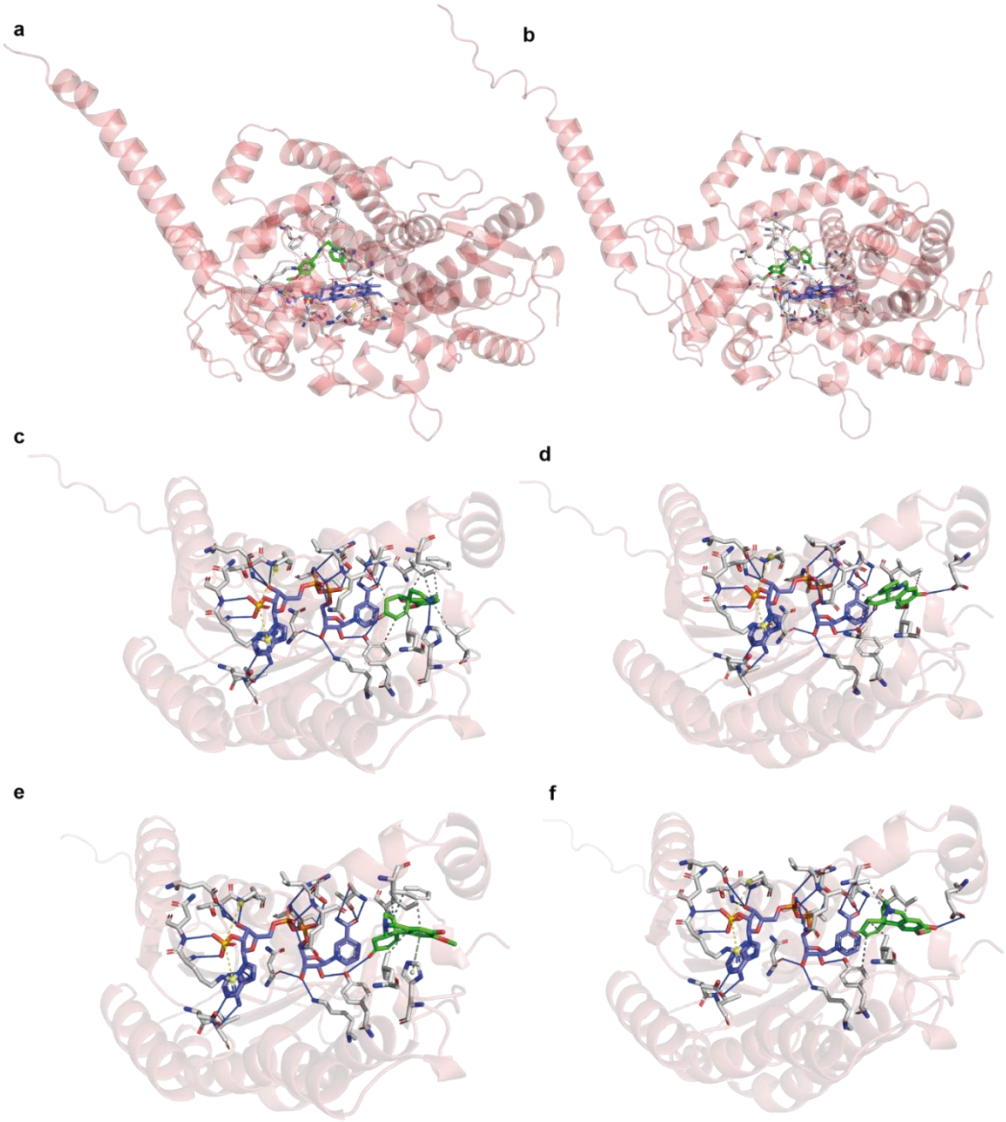


Figure 16 Docked structures of candidates *La*CYP96T and *La*NRII.

a Position of docked 4′-*O*-methylnorbelladinein the active site of *La*CYP96T1 **b** Position of docked 4′-*O*-methylnorbelladinein the active site of *La*CYP96T2. **c** Position of *N*-demethylnarwedine in the active site of *La*NRII. **d** Position of noroxopluviine in the active site of *La*NRII. **e** Position of noroxomaritidine to yield normaritidine in the active site of *La*NRII. **f** Position of noroxomaritidine to yield oxomaritinamine in the active site of *La*NRII.

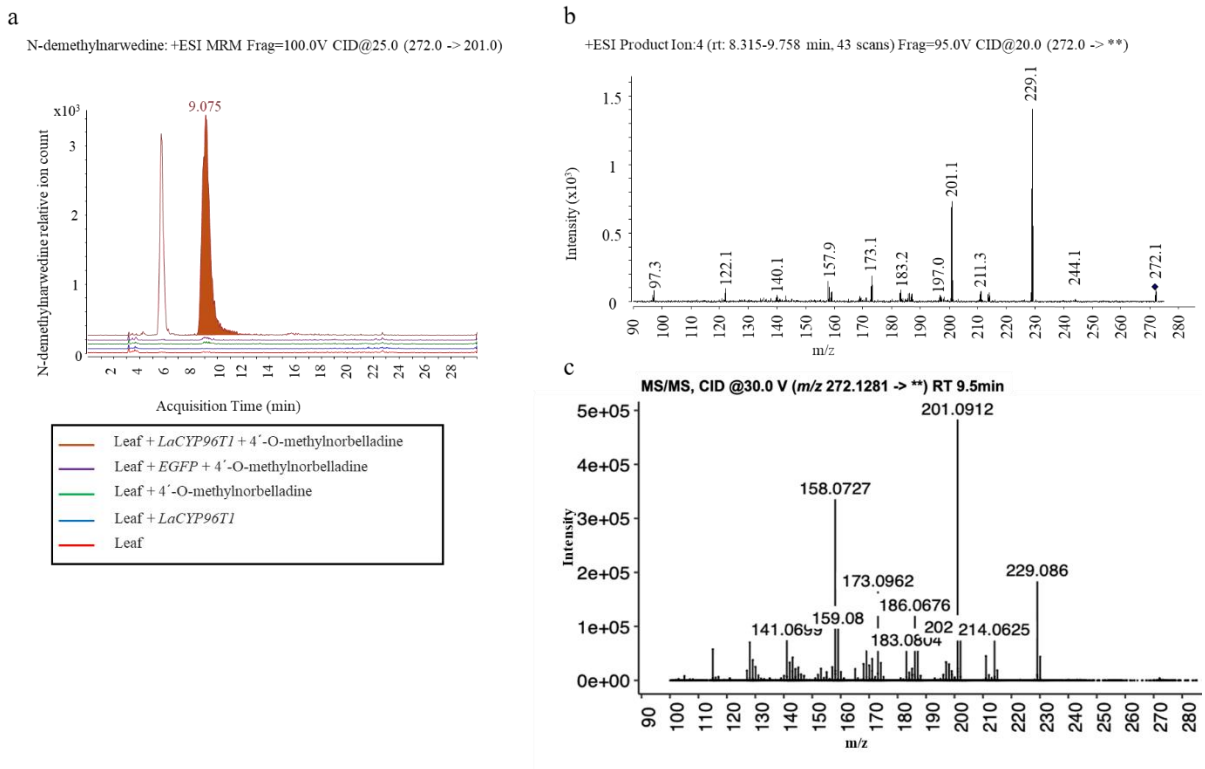


Figure 17. HPLC-MS/MS analysis of *N*-demethylnarwedine, produced upon transient expression of *LaCYP96T1* with 4´-*O*-methylnorbelladineas substrate.

a HPLC-MS/MS chromatograms and the color of each chromatogram indicates the *in vivo* assay (brown), along with different negative controls (purple, blue, green, red). **b** MS/MS fragmentation pattern of the *para- ortho'* product *N*-demethylnarwedine, that was produced upon transient expression of *LaCYP96T1* with 4´-*O*-methylnorbelladineas substrate in *N. benthamiana*. **c** Published fragmentation pattern of *N*-demethylnarwedine (Mehta et al., 2024). The identity of *N*-demethylnarwedine was confirmed by injecting these samples in MRM mode first (a), then in Product Ion mode to obtain the full collision-induced dissociation (CID) mass spectrum of this signal (b) and finally comparing it with previously published fragmentation pattern (c).

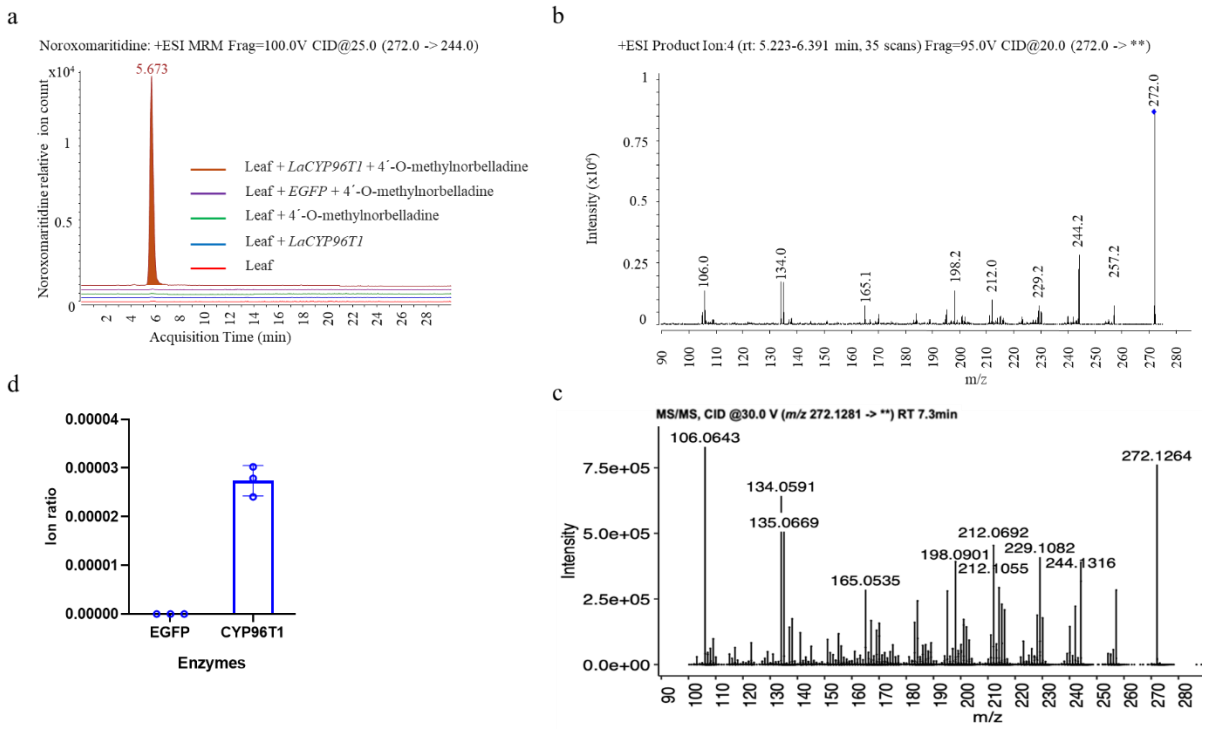


Figure 18. HPLC-MS/MS analysis of noroxomaritidine, produced upon transient expression of *LaCYP96T1* with 4´-*O*-methylnorbelladineand *in vitro*.

a HPLC-MS/MS chromatograms and the color of each chromatogram indicates the *in vivo* assay (brown), along with different negative controls (purple, blue, green, red). **b** MS/MS spectra of the *para- para'* product noroxomaritidine, that was produced upon transient expression of *LaCYP96T1* with 4´-*O*-methylnorbelladinein *N. benthamiana*. **c** Published fragmentation pattern of noroxomaritidine reactions (Mehta et al., 2024). **d** *In vitro* enzymatic assay of *La*CYP96T1 microsomes isolated from *N. benthamiana* with 4´-*O*-methylnorbelladineas substrate and measurement of production of noroxomaritidine. No enzyme, boiled microsomes, and microsomes with EGFP were used as negative controls and all showed zero product so, the representative EGFP is only shown in bar diagram. Data are the means ± SE of three biological triplicates and 1ppm papaverine used as internal standard after quenching. The identity of noroxomaritidine was confirmed by injecting these samples in MRM mode first (a), then in Product Ion mode to obtain the full collision-induced dissociation (CID) mass spectrum of this signal (b) and finally comparing it with previously published fragmentation pattern (c).

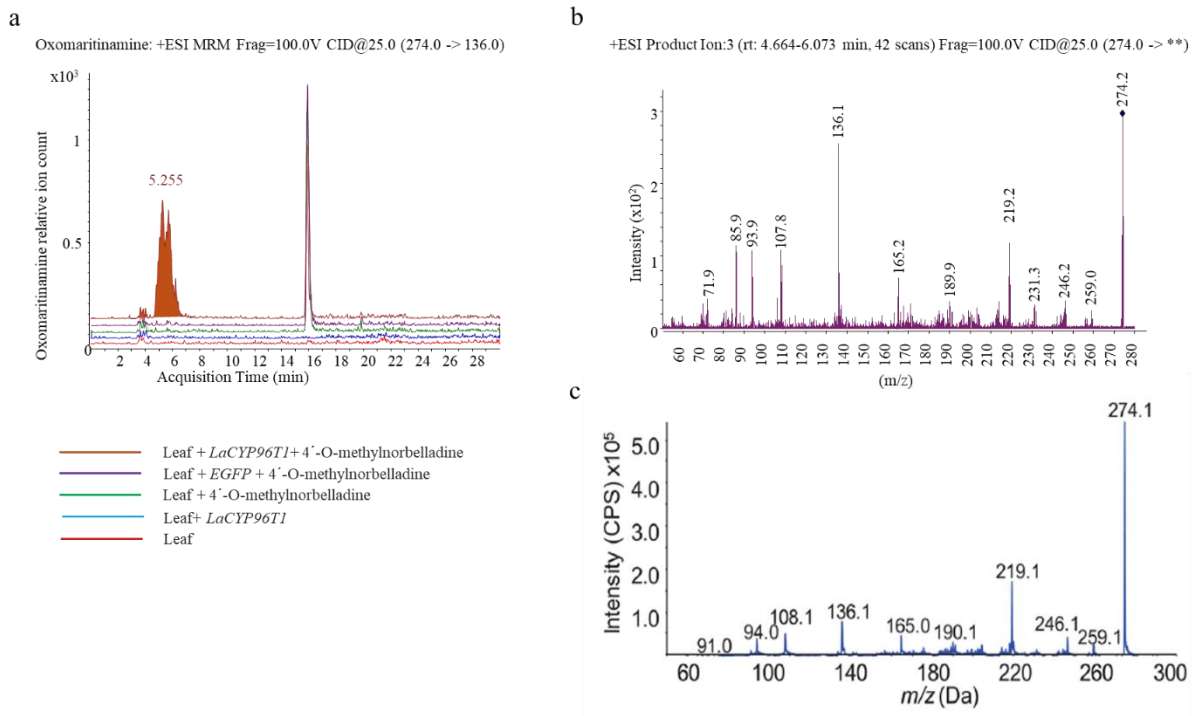


Figure 19. HPLC-MS/MS analysis of oxomaritinamine, produced upon transient expression of *LaCYP96T1* with 4´-*O*-methylnorbelladineas substrates.

a HPLC-MS/MS chromatograms and the color of each chromatogram indicates the *in vivo* assay (brown), along with different negative controls (purple, blue, green, red). **b** MS/MS spectra of the *para- para'* product oxomaritinamine, that was produced upon transient expression of *LaCYP96T1* with 4´-*O*-methylnorbelladinein *N. benthamiana*. **c** Published fragmentation pattern of oxomaritinamine (Kilgore et al., 2016). The identity of oxomaritinamine was confirmed by injecting these samples in MRM mode first (a), then in Product Ion mode to obtain the full collision-induced dissociation (CID) mass spectrum of this signal (b) and finally comparing it with previously published fragmentation pattern (c).

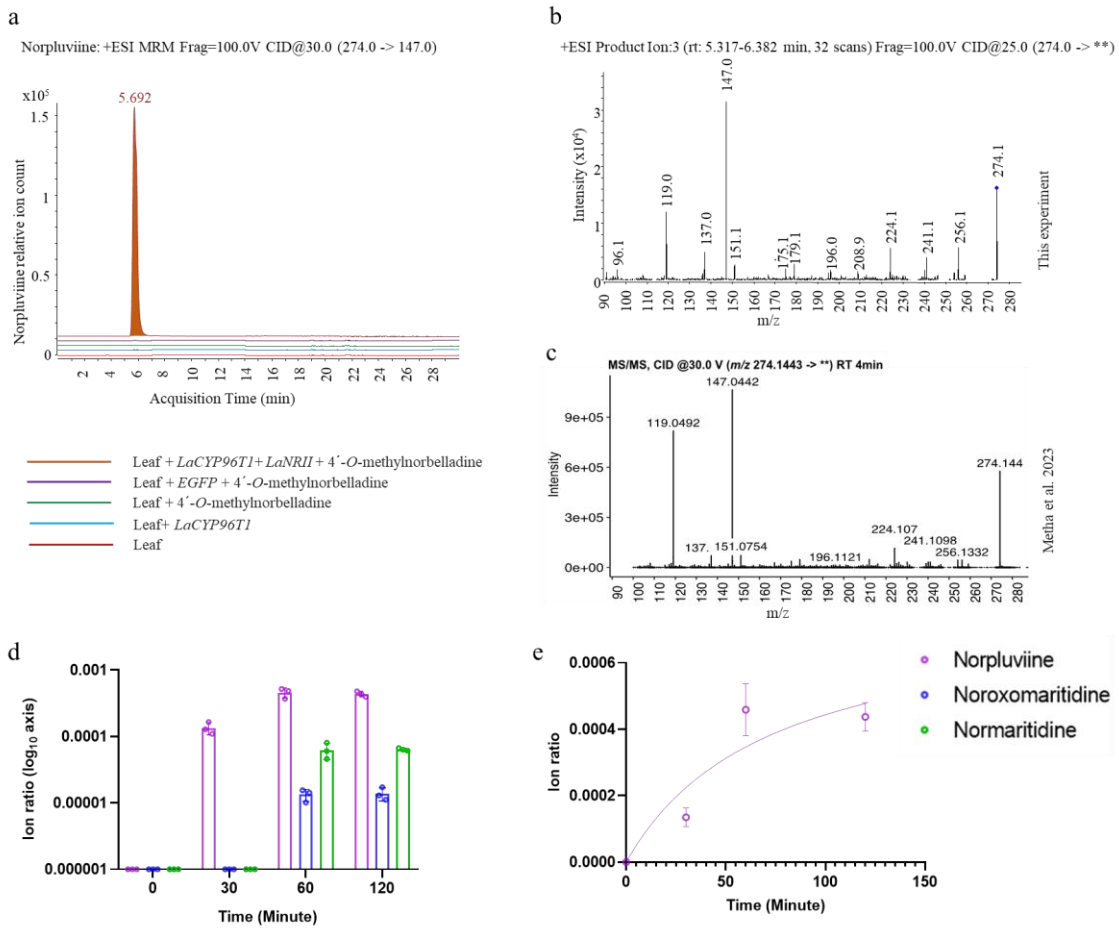


Figure 20. HPLC-MS/MS analysis of norpluviine produced upon transient co-expression of *LaCYP96T1 and LaNRII* with 4´-*O*-methylnorbelladineas substrates in *N. benthamiana* and *in vitro.*

a HPLC-MS/MS chromatograms and the color of each chromatogram indicates the *in vivo* assay (brown), along with different negative controls (purple, blue, green, red). **b** MS/MS spectra of the *ortho- para'* product norpluviine, that was produced upon transient expression of *LaCYP96T1* and *LaNRII* with 4´-*O*-methylnorbelladinein *N. benthamiana*. **c** Published fragmentation pattern of norpluviine (Mehta et al., 2024). **d** *In vitro* enzymatic assay of *La*CYP96T1 microsomes from *N. benthamiana* leaves in combination with MBP tagged *La*NRII from *E. coli* with 4´-*O*-methylnorbelladineas substrate and measuring the production of phenol coupled products at four time points. Y-axis is in $\log_{10}$ with base value 10^{-7} as zero for the zero minute. Purple, blue and green bar represents norpluviine, noroxomaritidine and normaritidine respectively. No enzyme, boiled enzymes, microsomes from EGFP infiltrated plant in combination with purified MBP alone from *E. coli* were used as negative controls and all showed zero product thus not shown in bar diagram. **e** nonlinear regression curve of norpluviine from d. The identity of norpluviine was confirmed by injecting these samples in MRM mode first (a), then in Product Ion mode to obtain the full collision-induced dissociation (CID) mass spectrum of this signal (b) and finally comparing it with previously published fragmentation pattern (c)(Mehta et al., 2024). Data are the means ± SE of three biological replicates and 1ppm papaverine used as internal standard after quenching.

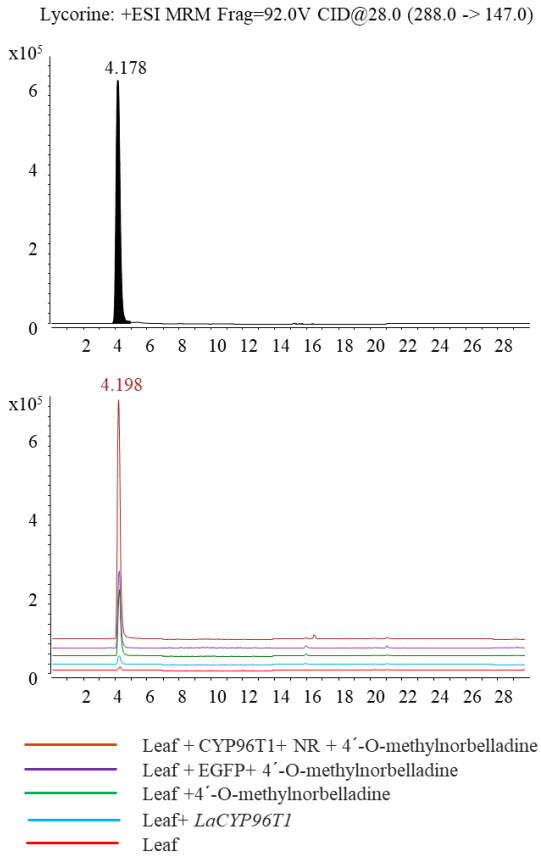


Figure 21. HPLC-MS/MS chromatograms of the *ortho- para'* product lycorine, that was produced upon transient co-expression of *LaCYP96T1* and *LaNRII* with 4´-*O*-methylnorbelladinein *N. benthamiana.*

The color of each chromatogram indicates the *in vivo* assay (brown), along with different negative controls (purple, blue, green, red). The identity of this product was confirmed by comparing this compound's retention time and other analytical parameters (Supplementary Table 2.S4) to the ones of lycorine standard which were acquired in MRM analysis mode on the HPLC-MS/MS.

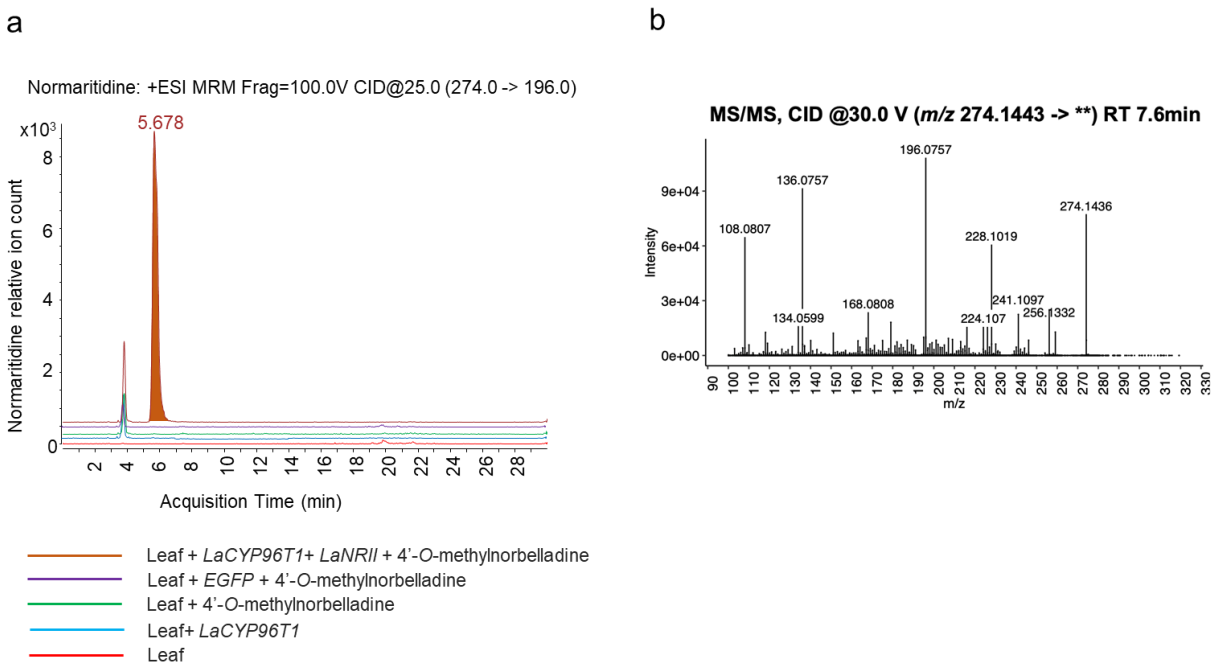


Figure 22. HPLC-MS/MS chromatograms of the *para- para'* product normaritidine, that was produced upon transient co-expression of *LaCYP96T1 and LaNRII* with 4´-*O*-methylnorbelladinein *N. benthamiana.*

a The color of each chromatogram indicates the *in vivo* assay (brown), along with different negative controls (purple, blue, green, red). **b** Published fragmentation pattern of normaritidine. The identity of this product was confirmed by MRM analysis based on three characteristic product ions (*i.e.* m/z 196, 228 and 256) published in literature (Mehta et al., 2024).

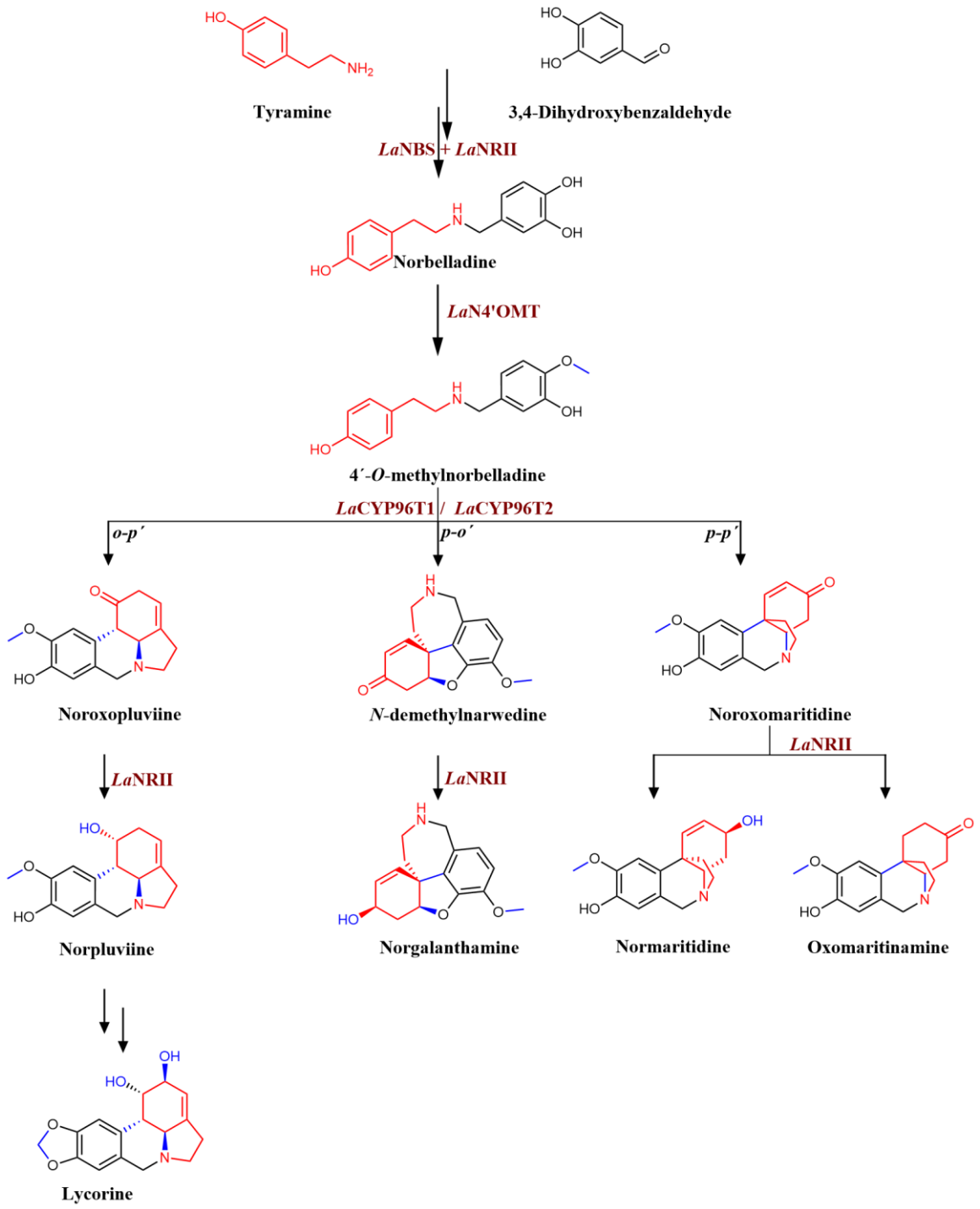


Figure 23. The elucidated alkaloid biosynthesis pathway in *Leucojum aestivum* in this study.

Red colored bonds are from tyramine, black bonds from 3,4-dihydroxybenzaldehyde, blue colored bond or the atoms, are formed by respective enzymes in brown color.

References

Kilgore, M.B., Holland, C.K., Jez, J.M. and Kutchan, T.M. (2016) Identification of a noroxomaritidine reductase with Amaryllidaceae alkaloid biosynthesis related activities. *Journal of Biological Chemistry* **291**, 16740-16752.

Mehta, N., Meng, Y., Zare, R., Kamenetsky-Goldstein, R. and Sattely, E. (2024) A developmental gradient reveals biosynthetic pathways to eukaryotic toxins in monocot geophytes. *Cell* **187**, 5620-5637 e5610.

2.10. Supplementary Tables

Table 2.S1. Active Site description and docking results of LaNBS (tyramine and 3,4-DHBA), LaNR (norcraugsodine), LaN4´*O*MT (norbelladine), and CYP96T1 and T2 (4´-*O*-methylnorbelladine).

	Active Site residues	**Ligand**	**Score**	**Interactions**		
				Hydrophobic	**H-bonds**	**Other**
***La*NBS**	Thr24, Leu25, Leu27, Ala28, Ser31, Val38, Ile39, Leu55, Val57, Tyr59, Ile63, Ile66, His69, Glu71, Phe73, Lys83, Val85, Val87, His92, Leu95, Tyr100, Ile102, Leu104, Val120, Ser133, Phe134, Ala135, Thr136, Thr137, Pro139, Leu140, Ile143	Tyramine	-5.1	Ile39, Pro139, Ile143	Tyr59, Glu71, Ile39	nd
		3,4-DHBA	-5.5	Val85, Leu104 (n=2), Leu140, I	Glu71, Lys83,	nd
***La*NR**	Thr29, Gly30, Gly31, Thr32, Lys33, Gly34, Ile35, Gly36, Cys53, Ser54, Arg55, Asn56, Glu59, Cys79, Asp80, Val81, Ser82, Asn108, Ala109, Gly110, Thr111, Ala112, Ile113, Leu114, Phe127, Thr131, Ile158, Ser159, Thr160, Val161, Cys162, Ile165, Leu167, His170, Tyr173, Lys177, Pro203, Gly204, Ile205, Thr206, Thr208, Val209, Gln210, Val211, Gln212, Pro213, Phe214, Glu224, Arg265	NADPH	-ud	n.d.	Thr32, Lys33, Ile35, Arg55 (n=2), Asn56, Glu59, Asp80, Val81, Asn108, Tyr173, Lys177, Thr206 (n=3), Thr208, Val209, Gln210 (n=2)	π cation: Arg55 Salt bridge: Lys33, Arg55
		Norcraugsodine to norbelladine	-6.29	Leu114, Val161, Val211, Phe214	Tyr173	nd
		N-demethylnarwedine o norgalanthamine	-6.6	Leu114, Leu167, Tyr173, Ile205 (n=2), Val211, Phe214	His170, Tyr173	n.d.
		Noroxopluviine to norpluvine	-6.3	Ala112, Leu114, Ile205, Gln210	Tyr173, Glu224	n.d.
		Noroxomaritidine to normaritidine	-6	Leu114, Ile205, Phe214 (n=2)	Tyr173	π cation: His170
		Noroxomaritidine to oxomaritinamine	-6	Leu114, Tyr173, Ile205, Val211	Glu224	n.d.
***La*N4´OMT**	SAM, Mg2+, Ser9, Leu10, Ile11, Lys13, Glu49, Trp50, Ser51, Ser52, Ala53, Asp155, Ala156, Asp157, Lys158, Asn182, Trp185, Tyr186, Gly196, Leu197, His198, Glu200, Glu201, Glu203, Cys204	SAM	-ud	Tyr81	Val55, Gly79 (n=2), Gly83, Tyr84, Asp103, Val104, Ala132, Asp157	*Salt bridge* Asp155
		Mg^{2+}	ud			*Metal complex* Ala153, Asp155,
		Norbelladine to 4´-*O*-methylnorbelladine	-8,8	Ile11, Trp185, Glu201	Ser52, Asp155, Lys158, Glu200	*Metal complex: Mg2+*

***La*CYP96T1**	Heme, Phe100, Lys109, Leu112, Phe116, Phe119, Leu123, Phe124, Trp131, Arg135, Phe142, Tyr147, Gln151, Val195, Leu220, Leu224, His227, Thr303, Phe304, Leu306, Val307, Gln308, Asn310, Thr311, Leu312, Leu375, Pro380, Val381, Phe383, Glu384, Ile385, Lys386, Phe408, Pro410, Phe448, Ala449, Phe450, Ser451, Arg455, Ile456, Cys457, Leu458, Gly459, Leu462, Ala463, Gln466, Ile494, Leu495	Heme		Leu123 (n=2), Phe142, Phe304, Val307, Leu312, Leu375, Phe450, Ala463	Trp131, Ser451	Salt bridge: Lys109, Arg135, Arg455, Metal complex with Fe Cys457, Heme (n=4), H_2O
		4′-*O*-methylnorbelladine to noroxopluviine, *N*-demethylnarwedine or noroxomaritidine	-10,4	Leu112, Phe116, Phe124, Leu224, Val307, Val381, Leu495	Lys109, Val307,	π cation: Phe116
***La*CYP96T2**	Heme, Phe100, Lys109, Leu112, Phe116, Phe119, Leu123, Phe124, Trp131, Leu220, Leu224, His227, Thr303, Leu306, Val307, Asn310, Thr311, Val381, Phe383, Glu384, Ile385, Lys386, Phe408, Phe448, Ser451, Arg455, Cys457, Ile494, Leu495	Heme		Leu123, Phe142 (n=2), Thr311, Leu375, Phe450, Ala463	Trp131, Ser451	Salt bridge: Arg135, Arg455, metal complex Cys457, Heme (n=4), H_2O
		4′-*O*-methylnorbelladine	-10,4	Phe116 (n=2), Phe124, Leu220, Val307, Leu495	Lys109	H_2O Val307

Table 24. The accession numbers of the sequences used for phylogenetic analysis for respective protein sequence.

For Supplementary Figure 2.1		**Sequence**
UniProtKB/ Swiss-Prot id	**phylogenetic tree**	
na	NBS *Leucojum aestivum*	MKGSLSHGMEVTLPADQLWQVYSTLRLAELSAELLPSVISKVEVEE GDGGVGTVLCVTYGLGIPGIKYHKEKFVKIDHEKRLKDVIVVEGG HLDLAFSSYLIRLEILEKSKNSSVIKSTVEYEVDEEHAANASFATTDP LMIIGEAVSKHLLEQKAIVA
P15494.2	BEV1A *Betula pendula*	
A2A1A1.2	NCS2 *Coptis japonica*	
E6YBW4.1	PR10 *Glycine max*	
Q43560.1	PR10-1 *Medicago sativa*	
P93333.1	PR101 *Medicago truncatula*	
A0A3G5BB24.1	NBS *Narcissus pseudonarcissus*	
Q4QTJ2.1	NCS1 *Papaver somniferum*	
Q67A25.1	NCS *Thalictrum flavum* subsp. *Glaucum*	
UIP35240.1	NBS2 *Narcissus papyraceus*	
UIP35239.1	NBS1 *Narcissus papyraceus*	
WGU11340.1	NBS1 *Crinum x powellii*	
XP_010911014.1	NCS2 *Elaeis guineensis*	
KAJ6818486.1	NCS2-like *Iris pallida*	

ANI26413.1	NCS *Nelumbo nucifera*	
O04298.1	DAUc1 *Daucus carota*	
P52778.1	L18A *Lupinus luteus*	
Q9LLQ2.1	PR10.2b *Lupinus luteus*	
O49065.1	RAP *Taraxacum officinale*	
XP_020261032.1	NCS2-like *Asparagus officinalis*	
XP_008800114.2	NBS-like *Phoenix dactylifera*	
For Supplementary Figure 2.2		
UniProtKB/ Swiss-Prot id	**phylogenetic tree**	
	LaNRII_clonedSeq	MFTGREEESMPMPMEKKRWSLMGATALVTGGTKGIGRAIVEELA GFGATVHTCSRNKAELNECLQEWEKLKFNVTGSVCDVSSRAEREK LMEVVSSVFNGKLNILINNAGTAILKPIVDITAEDCSFLMATNFESAF HLSQLSHPMLKASGVGSIVHISTVCTQIGLEGHSIYAATKGAMSQLT RDFACEWARDGIRTNCVAPGITRTVQVQPFLDDEDAAAKEISRIPH GRPGEPEEIASLAAFLCMPSASYINGQVICVDGGRGING
UIP35234.1	NR1_Leucojum_*aestivum*	MFTGREEESMPMPMPMEKKRWSLMGATALVTGGTKGIGRAIVEE LAGFGARVHTCSRNEADLNECLQEWEKLKFNITGSVCDVSSRAER EKLMEVVSSVFNGKLNILINNAGTAILKPIVDITAEDCSFLMATNFE SAFHLSQLSHPMLKASGVGSIVHISTVCTQIGLEGHSIYAATKGAMS QLTRDFACEWARDGIRTNCVAPGITRTVQVQPFLDDEDAAAKEISR IPHGRPGEPEEIASLAAFLCMPSASYINGQVICVDGGRGING
UIP35235.1	NR2_Leucojum_*aestivum*	MFTGREEESMPMPMEKKRWSLMGATALVTGGTKGIGRAIVEELA GFGATVHTCSRNKAELNECLQEWEKLKFNVTGSVCDVSSRAEREK LMEVVSSVFNGKLNILINNAGTAILKPIVDITAEDCSFLMATNFESAF HLSQLSHPMLKASGVGSIVHISTVCTQIGLEGHSIYAATKGAMSQLT RDFACEWARDGIRTNCVAPGITRTVQVQPFLDDEDAAAKEISRIPH GRPGEPEEIASLAAFLCMPSASYINGQVICVDGGRGING
	Red.1_Leucojum_*aestivum*	MEEYRWSLQGKTALVTGGTRGIGHAIVEELVKLGATVHICSEDGA DLDRCLKEWRVANIGVTGSICDVSSPSERAKLMDRVSSICNGKLDIF INNAGTMILKPTVDCTSKDYSSTMAINLEAAFHLSQLAHPLLKASG SSSIVFISSIAGTVVASPTVSIYAASKAALIQLAKNLACEWAKDGIRI NAIAPGAIRTRMYHQAIDTEKAEARFVTTVPLGRIGEPKEVASVAA FLCMPASSYVTGQVIGVDGGRSICRY
	Red.2_Leucojum_*aestivum*	MEGKENSRRTRWSLLGTTALVTGGTKGIGHAIVEELAGFGAIVYTC SRNETELNKCLQEWKDREFNVGGSVCDVSSRAEREELMEKVSSMF SGKLNILINNVATAVFKPATDYTTENYAFFMATNFESAFHLCQLAH PLLKVSSNGSIVNISSVAGIISFNNLSLYSATKGAMNQLTRNLACEW AKDNIRANCVAPGAIKTPLTQASPLSLKYENEGGRKQLIFYGQRAF SQSILSKIETESTMACRIHIGIQEIVDKQKYWKVWVDEEAVKREVSR YPLGRFGEPEEVASLVAFLCMPAAAYITGQIICTDGGRIING
	Red.3_Leucojum_*aestivum*	MEENRWSLQGRTALVTGGTRGIGHAIVEELVKLGVTVHTCSENEA DLSKCLKEWQDTQKGITGTVCDVSSPTEREKLMERVSSIFDGKLDIF INNAAKMPVKPVVEFTHDDFSTTMATNLEAAFHLSQLAHPLLKAS GSGSVVNISSILGTLAMPAPVSIYAASKAALIQLTKNLASEWAKDGI RANTIAPGTIRTRMFYQTANSEEAEAQFVRQIPLGRIGEPEELASAA TFLCMPAASYVTGQLISVDGGCSICRY
	Red.4_Leucojum_*aestivum*	MELSSSKRNTRWSLHGATALVTGGTRGIGHAIVEELAGFGVTVYT CARNEAELYVCLQKWKNLNFNVTGSICDVTSRAEREKLIENVSSIF NGKLNILVNNAGTGGNITILSCTAEEYSSTMATNFESAFHFCQLAHP LLMSSGMGSIVNISSICGIIHLHDGSIYSSSKGALNMLTKTLACEWA KDNIRTNSVAPGYIKTPSMQLLLDDEEASEVEVLRTPMGRFGEPEE VASLVVFLCMPAASYITGQIICPDGGRTVNG

	Red.5_Leucojum_*aestivum*	MSLEKRWSLKGTTALVTGGTKGIGRAIVEELAGFGARVYTCSRNQ AELDKCLQEWEDLKFDVTGSVCDVASRAEREKLVEKVSSVFNGKL NILINNAGGYVNKAIDDFTAEDFSFLMAVNLESAFHLCQLAHPMLK ASGTGSIVHISSCCAQIAIPGHTIYSATKGAINQLTRNLACEWAKDNI RTNSVAPGAIRTPAAESFVNDKDAVAKEVSRVPLGRIGEPDEVASL AAFLCMPSASYITGQVICVDGGRTING
	Red.6_Leucojum_*aestivum*	MDDNGATKSTPNSINKAGTRWTLNGTTALVTGGTKGIGRAIVEELS RFGATVYTCSRHEAELNRCLQEWQRLGFHVMGSVCDVSSRAAREE LMKAVSSAFNGKLNMLINNVGTVVEAATLEFTAEMYSFQMATNL EAAFHLSQLAHPLLKASEQQGNIIFISSIGGIIGLQGSSVYAASKGAIN QLTRALAWEWAKDNIRVNCVVPGFIKTPLIQDYVVSEEGAMEAAR IPLCRFGESEEVASLAVFLCLPAASYIMGQIICVDGGRVVSG
	Red.7_Leucojum_*aestivum*	MEGIEAKRSSVVTEENKWSLQGKTALVTGGSRGIGHAIVEELVGFG ARVHTCSNDEVELSTCLQEWEKLKFNVTGTFCDVSSRAEREELMK KVSSMFSGKLNILINNVGTGIVKPIVDFTAEDYSLLMATNLESAFHL SQLAHPMLRASGTGSVVNISSISGQIGVVGCCVYSATKGAMNQLTR DFACEWAKDGIRANCIAPGLVRTPRLEPFINDKDAMAREFSRIPLGR NGEPEEIASLAAFLCMPSASYITGQVICVDGGRIING
	Red.8_Leucojum_*aestivum*	MFTGREEESMPMPMPMEKKRWSLMGATALVTGGTKGIGRAIVEE LAGFGARVHTCSRNEADLNECLQEWEKLKFNITGSVCDVSSRAER EKLMEVVSSVFNGKLNILINNAGTAILKPIVDITAEDCSFLMATNFE SAFHLSQLSHPMLKASGVGSIVHISTVCTQIGLEGHSIYAATKGAMS QLTRDFACEWARDGIRTNCVAPGITRTVQVQPFLDDEDAAAKEISR IPHGRPGEPEEIASLAAFLCMPSASYINGQVICVDGGRGING
	Red.9_Leucojum_*aestivum*	MENAKISNSNKRWSLVGATALVTGGTSGIGHAIIEELVAFGATVHT CTENEAQLTECLQRWESLKFPITGSICDVSSPTEREKLIEKVSSLFNG KLDILINNAGRALVKPFLNVTAEDYSLIMETNLQSGLHLTQLAHPLL KASNAGSIVFISSIAGNIALKDLTMYSVSKGAMVQLTKSLACEWAK DSIRTNCIGPGVINTPFVRQLEEFKASEASRTPLGRNGEPEEVASLAV FLCLPAASYISGQTIYVDGARTVNG
	Red.10_Leucojum_*aestivum*	MEQVDNNRRMRWSLQGTTALVTGGTKGIGHAIIQELAGVGAVVY TCSRNETELNKCLQEWKNLGFSVVGSVCDVSSRAEREKLMESVSS MFNGKLNILINNAGTSMQKPLADYTAEDYSFVMATNFESPFHLCQL AHPLLKASGKGNIVNISAIGGIVAFVNLALYAATKGAMNQLTRNLA CEWAKDNIRTNCVAPGGIKTQMVQFILDDEEAVKSLLSRPPLGRFG EPEEVASLVAFLCMPAADYITGQIICSDGGWTVNG
	Red.11_Leucojum_*aestivum*	MEKRWSLMGTTALVTGGTKGIGHAIVEELAGFGVRVHTCSRNEAE LNKCLQEWEKLKFNVTGSVCDASSRAEREKLMEKVSSMFDGKLNI LINNVGLCLAKPVVDCTAEDYSLLMATNLESAFHLSQLAHPMLKA SGTGSIIHISSAMGIAAVPGLSIYATTKAAIRQLTKNLACEWAKDNIR TNCIAPGITRTPFVEPLLNDKDFMAEELSRIPLRRHGEPEETASVAAF LCMPAASYITGQVISVDGGRTISG
PP708076	NtSDR1_Narcissus_cv._Tête-à-Tête	
PP708077	NtSDR2_Narcissus_cv._Tête-à-Tête	
PP708064	NtAKR1_Narcissus_cv._Tête-à-Tête	
A7DY56.1	TRN1 *Cochlearia officinalis*	
A0A1A9TAK5.1	NR NARPS *Narcissus pseudonarcissus*	
P50162.1	TRN1 *Datura stramonium*	
P50163.1	TRN2 *Datura stramonium*	
A0A1C9II22.1	NR NARAP *Narcissus aff. pseudonarcissus*	
P50164	TRN2 *Hyoscyamus niger*	

H9BFQ0	TPRL1 *Erythroxylum coca*	
H9BFQ1	TPRL2 *Erythroxylum coca*	
H9BFQ2	TPRL3 *Erythroxylum coca*	
P52575.1	IFR *Medicago sativa*	
E6Y2X0.1	PILR2 *Linum usitatissimum*	
Q15GI3.1	IGS1 *Petunia hybrida*	
Q15GI4.1	EGS1 *Ocimum basilicum*	
B7UEU8.1	IFRH *Nicotianaglauca*	
Q6PQJ9.1	5BPOR *Digitalis lanata*	
AJO70763.1	ADH1 *Catharanthus roseus*	
A0A165U5V5.1	ADH1 *Euphorbia lathyris*	
A0A8F5XX49.1	BDH2 *Salvia officinalis*	
K7WDL7	IRIS *Catharanthus roseus*	
Q5C9I9	ISPD *Mentha piperita*	
A0A3Q8GL18	NEPS1 *Nepeta racemosa*	
A4UHT7	SALR *Papaver bracteatum*	
W8JWV8.1	8HGO *Catharanthus roseus*	
AKF02528.1	THAS *Catharanthus roseus*	
WGU11348.1	NNR2 *Crinum powellii*	
QFQ50502.1	NNR *Lycoris radiata*	
AXU39908.1	NNR1 *Narcissus papyraceus*	
For Supplementary Figure 2.3		
UniProtKB/ Swiss-Prot id/ PDB	**phylogenetic tree**	**Amino acid Sequence**
n/a	OMT_clonedSeq Leucojum *aestivum*	MGASQDDYSLIHKNILHSEDLLQYILETSVYPREHEQLKGLREVTG KHEWSSALVPADEGLFLSMLLKLMNAKRTIEIGVYTGYSLLTTALA LPEDGKITAIDVNKSFFEIGLPFIQKAGVEHKINFIESEALPVLDQML QEVKEEDLYDFAFVDADKTNYANYHERLVKLVRVGGAIAYDNTL WYGSVAYPEYPGLHLEEEECRLSLRNLNTLLAADPRVEISQVSIGD GVTICRRLY
n/a	NOMT.1_Leucojum *aestivum*	MDRYNEPPKNLLCSDALHDYILETNVYPREHEQLKKLREETVIKHP EALMGVPPEEGQLLSIMLKLMKAKKTMEIGVFTGYSLLATALALPE DAKITAIDIDRSAYEIGLPFIKEAGVAHKIDFIESPALPVIDKLLEEVK GEEDLFDFAFVDADKESYPKYHDRMAKLVKIGGVIAYDNTLWFGS IVTPNDPKLHPRIKEHVHNVIEFNKMLAKDSRFEISQVSIGDGVTICR RLC
n/a	NOMT.2_Leucojum *aestivum*	MLVQVLGAQRCIEVGVYTGYSSLAVALVLPESGRLVACERDARCL EIAKKYYDRAGVSHKVDIKHALAADTLRSLILNGESCSYDFAFVDA EKRMYDEYFELLLQLVRIGGLIVIDNVLWYGKVADPQVTDRKTTS LRNFNKKILEDERVSTSMVPIGDGMTICRKIRHMSRS

n/a	NOMT.3_Leucojum *aestivum*	MGASQDDYSLIHKNILHSEDLLKYILDTSVYPREHEQLKGLREVTG KHEWSSALVPADEGLFLSMLLKLMNAKRTIEIGVYTGYSLLTTALA LPEDGKIMAIDVNKSFFEIGLPFIQKAGVEHKINFIESEALPVLDQML QEVKEEDLYDFAFVDADKTNYANYHERLVKLVRVGGAIAYDNTL WYGSVAYPEYPGLHLEEEECRLSLRNLNTLLAADPRVEISQVSIGD GVTICRRLY
n/a	NOMT.4_Leucojum *aestivum*	MEAENFVDPPKILLRSEALHDYIIETNVYPREHEQLKKLREKTNLYE PEVLFSVPPEQGQLMSILLKVMKAKKTLEVGVFTGYSLLVTALAIP KDGKITAIDINRDAFEVGLPFMKEAGVAHKINFIESDALAALDKLVE EVNGEEDLFDFVFVDADKESYSKYHERVSKLVKIGGVIGYDNTLW YGSVVTPTDPTLHPEIKRVVYDVIAFNKKLANDLRFEISQIPVGDGF TICRRVY
n/a	NOMT.5_Leucojum *aestivum*	MTTSADEGQFLNMLLKLINAKNTMEIGVFTGYSLLATALALPEDG KILAMDVNRENYELGLPVIEKAGVAHKIDFREGPALPVLDQLLEDE KNHGSFDFIFVDADKDNYLNYHKRIIELVKIGGLIGYDNTLWNGSV VAPPDAPLRKYVRYYRDFVLELNMALAADPRIEICQLPVGDGITLC RRVK
n/a	NOMT.6_Leucojum *aestivum*	MKELRDITSKHPWNIMTTSADEGQFLNMLLKLINAKNTMEIGVFTG YSLLATALALPEDGKILAMDVNRENYELGLPVIEKAGVAHKIDFRE GPALPVLDQLLEDEKNHGSFDFIFVDADKDNYLNYHKRIIELVKIG GLIGYDNTLWNGSVVAPPDAPLRKYVRYYRDFVLELNMALAADP RIEICQLPVGDGITLCRRVK
8XDQ_A	OMT *Lycoris aurea*	MGASQDDYALIHKNILHSEDLLKYILETSVYPREHEQLKGLREVTE KHEWSTALVAADEGLFLSMLLKLMNAKRTIEIGVYTGYSLLTTAL ALPEDGKITAIDVNKSYFEIGLPFIQKAGVEHKINFIESEALPVLDHM LQEMKEEDLYDFAFVDADKPNYANYHERLVKLVRVGGAIVYDNT LWFGTVAFPEYPGLHPEEEECRVSFRNLNKLLAADPRVEISQVSVG DGLTICRRLY
n/a	GeOMT_Galanthus elwesii	MGASQDDYSLIHKNILHSEDLLKYILETSTYPREHEQLKGLREVTEK HEWSSALVPADEGLFLSMLLKLMNAKRTIEIGVYTGYSLLTTALAL PEDGKITAIDVNKSFFEIGLPFIQKAGVEHKINFIESEALPVLDQLLRE VKEEDFYDFAFVDADKTNYANYHERLVKLVRVGGAIAYDNTLWY GSVVYPEYPGLHPEEEECRLSLRNLNTLLAADPRVEISQVSVGDGV TICRRLY
Q29U70	I4OMT *Medicago truncatulata*	
A0A5P8H727	N4OMT *Lycoris radiata*	
A0A6B9TNK2	N4OMT *Lycoris longituba*	
A0A346TLF5	N4OMT *Narcissus papyraceus*	
A0A077EWA5	NOMT *Narcissus aff. pseudonarcissus*	
Q84KK4	I4OMT *Lotus japonicus*	
Q84KK6	I4OMT *Glycyrrhyza echinata*	
A0A2H5AIZ6	NOMT *Narcissus pseudonarcissus*	
Q6WUC1	6OMT *Papaver somniferum*	
Q9LEL5	4OMT *Coptis japonica*	
Q9LEL6	6OMT *Coptis japonica*	
A9X7L0	ANMT *Ruta graveolens*	
Q43095	CCoAOMT *Populus tremuloides*	
Q8H9A8	COMT *Coptis japonica*	
Q9XE91	COMT3 *Thalictrum tuberosum*	

Q7XB11	4OMT1 *Papaver somniferum*	
A0A346CM52	NOMT *Narcissus tazetta*	
Q6VCW3	F4'OM *Catharanthus roseus*	
K4CVP2	CCoAOMT *Solanum lycopersicum*	
L7TC72	CCoAOMT *Solanum tuberosum*	
PP708075	NtOMT *Narcissus Tête-à-Tête*	
For Supplementary Figure 2.4		
UniProtKB/ Swiss-Prot id	**phylogenetic tree**	
	LaCYP96T1_clonedSeq	MATSSPWLIFSDHYPEILIAIACFIIFSFLRSARSSSKDSLPYKWPIFG MLPEIVYNKQFNELVTARLRETGWTFVFKGPLIVNMDRIVTCDPAN MNHMFNLNFDNYPKGDLYKVFDVFGDNLFNADGDNWYNHRIMA QTVFWDGNYRAMQAKLVLDKVENALIPILDSAACKKKPLDLQDVF LRFTFDISCQCVLDSDPGTLSLEFPTVPFAKACDEALDATLTRHITPP HIWKLKRFLNIGTEKIRATQWKVVDAYIFERITKIKEKIKRTGKNTS HTAMALYIDNCNLLNDQRLRDNAYTFLLVQRNTLSLTMAWLFYA LFLNPRVLPKILDELQSILDKSSDRRFKDGYALFDGNMIQSAIYLHA TLCEVLRYYPPVPFEIKDALNADVLPSGHKVKAGDKILFSPYAMAR MKGIWGDDCMEFKPERWITENGTLKHEPAYKFFAFSAGPRICLGKE LAFNQMKIVVANIIYNFDVQMVKGHAVEQRTAILMEMKQGLMVE VGKRSVM
	LaCYP96T2_clonedSeq	MATSSPWLIFSDHYPEILIAIACFIIFSFLGSARSSSKDSLPYKWPIFG MLPEIVYNKQFNELVTARLRETGWTFVFKGPLIVNMDRIVTCDPAN MNHMFNLNFDNYPKGDLYKVFDVFGDNLFNADGDNWYNHRIMA QTVFWDGNYRAMQAKLVLDKVENALIPILDSAACKKKPLDLQDVF LRFTFDISCQCVLDSDPGTLSLEFPTVPFAKACDEALDATLTRHITPP HIWKLKRYLNIGTEKIRATQWKVVDAYIFERIAKIKEKIKRTGKNTS HTAMALYIDNCNLLNDQRLRDNAYTFLLVQRNTLSLTMAWLFYA LFLNPRVLPKILDELQSILGKSSDRRFKDGYALFDGNMIQSAIYLHV TLCEVLRYYPPVPFEIKDALNADVLPSGHKVKAGDKILFSPYAMAR MKGIWGDDCMEFKPERWITENGTLKHEPAYKFFAFSAGPRICLGKE LAFNQMKIVVANIIYNFDVQMVKGHVVEQRTAILMEMKQGLMVE VRKRSVV
	CYP96T1_Leucojum_aestivum	MATSSPWLIFSDHYPEILIAIACFIIFSFLRSARSSSKDSLPYKWPIFG MLPEIVYNKQFNELVTARLRETGWTFVFKGPLIVNMDRIVTCDPAN MNHMFNLNFDNYPKGDLYKVFDVFGDNLFNADGDNWYNHRIMA QTVFWDGNYRAMQAKLVLDKVENALIPILDSAACKKKPLDLQDVF LRFTFDISCQCVLDSDPGTLSLEFPTVPFAKACDEALDATLTRHITPP HIWKLKRFLNIGTEKIRATQWKVVDAYIFERITKIKEKIKRTGKNTS HTAMALYIDNCNLLNDQRLRDNAYTFLLVQRNTLSLTMAWLFYA LFLNPRVLPKILDELQSILDKSSDRRFKDGYALFDGNMIQSAIYLHA TLCEVLRYYPPVPFEIKDALNADVLPSGHKVKAGDKILFSPYAMAR MKGIWGDDCMEFKPERWITENGTLKHEPAYKFFAFSAGPRICLGKE

		LAFNQMKIVVANIIYNFDVQMVKGHAVEQRTAILMEMKQGLMVE VGKRSVM
	CYP96T2_Leucojum_aestivum	MATSSPWLIFSDHYPEILIAIACFIIFSFLGSARSSSKDSLPYKWPIFG MLPEIVYNKQFNELVTARLRETGWTFVFKGPLIVNMDRIVTCDPAN MNHMFNLNFDNYPKGDLYKVFDVFGDNLFNADGDNWYNHRIMA QTVFWDGNYRAMQAKLVLDKVENALIPILDSAACKKKPLDLQDVF LRFTFDISCQCVLDSDPGTLSLEFPTVPFAKACDEALDATLTRHITPP HIWKLKRYLNIGTEKIRATQWKVVDAYIFERIAKIKEKIKRTGKNTS HTAMALYIDNCNLLNDQRLRDNAYTFLLVQRNTLSLTMAWLFYA LFLNPRVLPKILDELQSILGKSSDRRFKDGYALFDGNMIQSAIYLHV TLCEVLRYYPPVPFEIKDALNADVLPSGHKVKAGDKILFSPYAMAR MKGIWGDDCMEFKPERWITENGTLKHEPAYKFFAFSAGPRICLGKE LAFNQMKIVVANIIYNFDVQMVKGHVVEQRTAILMEMKQGLMVE VRKRSVV
	C96.1_Leucojum_aestivum	MKGKTMTKKGPIDLLTPYMDLSMEDAGENSNIFQSTDKFLRDTLL TFLSAGKETTVNAIIWLLWLVTSNPDVEKKILKELREVRALWDPKK HSSLENEMTIFDAEELNSLIYLHAAVCESLRLYPPVTFNQKEAVKA DTLPSGHKVQPGMKVIYSLYSAGRMEAIWGEDCLDFKPERWITEK GTIRHEPSYKFIAFHSGPRACLGKSMAFTQVKVVAAAIIYNFNIHVV GDRVPEPKHSIITQMKNHLLVKLKKRNSSINGY
	C96.2_Leucojum_aestivum	METILESFQMKLAFAFFSLAVAFLGFAALLLFLRFRPWCNCHVCRS YLNSSWRDRFDNLSDWYAHLLRESPTQTVQVHVLNATITANPKNV EYMLKTNFDNFPKGKPFSSILGDLLGRGIFNVDGAAWRFQRKMAS LELGGVSVRSYAFSIASNEIQHRLFPLLDLVSDSGSVIDLQEIFRRFSF DTICKISFGLDPECLDLSLPSSDFAAAFDLASNLSAMRATSVTPIVW KLKRLLNWGSEKDLKTAIGVFNKLAEGVIKQKRKLGYASDQDLLS RFMASVDDDKYLRDIIGSFLLAGRDTVASALTTFFYLLSQNPNVVA KIREEIDQQHADGQMIGYEKLRSMSYVHAAIYESLRLYPPVQFDSK FCLEDDVLPDGTFVGRDSRVTYHPYAMGRMATIWGDDCEAYKPE RWLNQRGEFIPANAFRFPVFQGGPRTCLGKEISIVEMKTVAVSVLR DFDVDVVIGDDGAKGPKFKAALTASLSGGLKVTASRRQRGAC
	C96.3_Leucojum_aestivum	MATSFLFGFYQEIFMAIICFFCLFLCSKKHRKSTVPTNWPILGMFPA VLANLNHVHDWITEVLKEVGCTFKFHGPWFLGMDFLVTCDPANV NHVFNANFSNYPKGEEFLEIFDILGDGIFNVDGEPWKMQRKKAHG VISSTSFRAFVAKCTRDKVENGLVPLMSRLAEQEIVVDLQDVFLRL TFDMTCNLVFGVDPGCLSIEFPTIPFARAMDDAMEALFFRHVVPPQ CWKLMRRLRIGKERKLAAALRVIDEFVAQKIAKKREGKIYGEDLLT SYMEAKEQIDNKFLRDTAVNLMLAGRDTTGVALSWFFWLLAKNP EVKSKILGELQEKLHQNKMHPMVFDPEQIAKSVYLHASLCESLRLF PSVPFEHKASLQPETLPSGNQANSKEKILFSTYSMARVEGIWGKDC LEFNPERWISKQGSIKHEPSYKFLSFNCGPRTCLGKDIAFTQMKTVV AAVMCNFDVEMVEGHVVEPKPSIILHMKNGLLVGIKKKGQLNMIE KSD
	C96.4_Leucojum_aestivum	MATSSPWLIFSDHYPEILIAIACFIIFSFLGSARSSSKDSLPYKWPIFG MLPEIVYNKQFNELVTARLRETGWTFVFKGPLIVNMDRIVTCDPAN MNHMFNLNFDNYPKGDLYKVFDVFGDNLFNADGDNWYNHRIMA QTVFWDGNYRAMQAKLVLDKVENALIPILDSAACKKKPLDLQDVF LRFTFDISCQCVLDSDPGTLSLEFPTVPFAKACDEALDATLTRHITPP HIWKLKRYLNIGTEKIRATQWKVVDAYIFERITKIKEKIKRTGKNTS HTAMALYIDNCNLLNDQRLRDNAYTFLLVQRNTLSLTMAWLFYA LFLNPRVLPKILDELQSILGKSSDRRFKDGYALFDGNMIQSAIYLHA TLCEVLRYYPPVPFEIKDALNADVLPSGHKVKAGDKILFSPYAMAR MKGIWGDDCMEFKPERWITENGTLKHEPAYKFFAFSAGPRICLGKE

		LAFNQMKIVVANIIYNFDVQMVKGHVVEQRTAILMEMKQGLMVE VGKRSVM
	C96.5_Leucojum_aestivum	MDTSYFVSHLDIILAIACFVYLFLSYKNYRKKSIVPINWPIVGMLPG LLGNLHHLHDWGTMALKEAGGTIQFHAPWFVDMDIIATCDPANV NHVFNMNHSNYPKGEAFLEIFDILGDGIFNADDESWKVQRKKALG VISSPSFRAFVMRYSRNKVEDGLVPLLSQLADRGVVVDLQDLFLRL TFDMTCNLVFGVDPGSLTDGFPIIPFARAMDDAMVALFYRHAVPPT WWKLMRRLGIGWEKRLSVAAGVIDDFVAQNIAKKRKGKSNGADI LTCYIEGEESCNDKYIRDTTVNLMLAGRDTTGVALTWFFWLVATN PDVKTKILDELAEHDSRGKSYPVMFSHDAISRLVYLHAALCESLRL YPSVPFEHKEPLKSEVLPSGTKINAGAKLLFSTYSMARLEGVWGKD CYEFKPERWILEHGGIRHEPSYKFFSFNCGPRTCLGKDVAFTQMKT VAATMIYNFDVELVEGHVVEPKPSIILHLKNGLMVRFKRRARD
	C96.6_Leucojum_aestivum	MDPQSLLILISLCLLLGYFLFKKNKKHHEDTEPYPILGHLPQFLKNR HRIHDWIAELLACTQTNTVIFRRPGNIRGVITADPANVEHALKSNFD NFPKGPRFHSLLEDFLGDGIFNSDGHLWKVQRKTASFEFNTRSLRN FVVENVRKETETRLIPLLTKNSRSGQVIDIQDVLERYAFDNICKVAF NVDPACLADDDGLATSAFADAFRDAADLCAGRFRYAVPGFWKVK KLLNIGSERRLQESIAIVHNFAKEIIQSRLKEREISKPQSDDLLSRFITS KEYSEVFLRDIVISFILAGRETTSSALTWFFWLLSSRPDVQQKILAEI ASVRTRSGKTYGESFEFDELREMQYLHAAITESMRLYPPVPINMTF VEKDDVFPDGTQVKQGWFVWYHSYAMGRMEAVWGKECREFKP MRWIDGDGNFKPESPFKFLAFHAGPRMCLGKEMAYIQMKSIAACV LEKFALEVVEKKKMPEQMLSLTLRMRGGLAVRVRCRGDDDGTS
	C96.7_Leucojum_aestivum	MYVKLTWLFTGTDPGCLARGLPEVRFARAFEDATEATILRFITPTTI WHTCRFLNVGNERRLKRSLKAVDEFAYQVIRNRRKELELEGTKGK SDLLTVFMGMKDEDGKEYSEKFLRDICVNFILAGRDTSSVALAWFF WLLEKNRDVEEKIVEEVREIVKEREGDGGENNNSDVVFKPEEIKK MEYLHAALSEALRLYPSVPVDHKEVVDDEVFPDGTVLKGGTKIIYS IYSMGRMESIWGKDCREYKPERWLKDGRFMSESAYKFTAFNGGPR LCLGKDFAYYQMKYVASSILYCYHVKVVENHPVAPKLALTMYMK HGLKVTLEKRET
	C96.8_Leucojum_aestivum	MASLLQFVLHHYNFIDIAISLLILFISNSIITFFTSKRNPVMWPILGIAP AFVLHRSNIFDWITDATIHARGTFPFNGIKFGRLYGVVTINPKNIEYI LKTNFSNYPKGKYFHERFFDFLGDGIFNADDQVWKDQRRAATTEM HSSRFGKYSMETIRDLVHCKLLVLLDKIAEQNAVVDLQDLFLRFTF DNICSAAFGVDPGCLTVGLPQIAFAKAFEEATELTLFRFLVPPIVWK TMRTFNVGPEQKLKAAIQTVHEFAEKTVTDRRSDQFTDRSDLLSRL MAVDAEEGGPRFSDKFLQDFCISFILAGRDTSSVALAWFFWLLEQN PRVENCILEEISTIVGERSNTNIVFAVDELNRMEYLQASLSEALRLYP SVPIDFKQALKDDVFPDGTRVKKGARVIYLIYAMARAEGIWGKDC REFRPERWLKDGVFVSENQFKYVVFNAGPRLCIGKKFAYLQMKM VAASILMRYRVEVVKGQEVIPKLTTTLYMKNGLRVRLAPRETILKV
	C96.9_Leucojum_aestivum	MEIFTVSLLLISALSLLIVLKRYLNRKKRNYPPIAGTVFHQFLNLHRL QDLMTELSQRYRTFRMLTPVNNYIYVVDPVNVEYILKTNFANYGK GKYTHEIMEDLLGDGIFAVDAEKWRHQRKVASYEFSAKVLRDYSG AVFKHKATKLTEIVTEAARKIQKIDMQDLFMKSTLDSIFEVGFGVD LDTLSGSNREGRLFARAFDNSSAQTLRRFFDVFWKIKKFLNIGLEA KMKNDIKVIDDFVYKLIDMKNEQKSKQQHDFVKEDILSRFLIEREK DPEHMSEKYLRDIILNFVIAGKDTTAGTLSWFFYMLCKHPCVQEKV AQEVKQATNANENIHIKDFAATLTEEALNKMHYLHAALSETLRLY PAVPLDVKHCFSDDTLPDGFHVNKGDMINFQPYPMGRMKYLWGE DAETFRPERWLNENGVFVPESPFKFTAFQAGPRICLGKEFAYRQMK IFAATMLCFLKFKMWDEKKPVNYKSMLTLQIDGGLHLCALERSKY

	C96.10_Leucojum_aestivum	MENAKISNSNKRWSLVGATALVTGGTSGIGHAIIEELVAFGATVHT CTENEAQLTECLQRWESLKFPITGSICDVSSPTEREKLIEKVSSLFNG KLDILINNAGRALVKPFLNVTAEDYSLIMETNLQSGLHLTQLAHPLL KASNAGSIVFISSIAGNIALKDLTMYSVSKGAMVQLTKSLACEWAK DSIRTNCIGPGVINTPFVRQLEEFKASEASRTPLGRNGEPEEVASLAV FLCLPAASYISGQTIYVDGARTVNG
	LauCYP96T1_Lycoris_aurea	MATSSSAWLIFSDHYPEILIAIACFVIFSLLRSARSSSEDRLPYNWPIF GMLPAIISNNQFNNFTTARLHETGWTFIFKGPWLLDMDYIFTCDPD NINHMFNLNFENYPKGELGKVFDIFGNNIFNADGDLWRDHRKMAQ TILWDGNYRAMQATFIRKKMESALIPILDSAACKRKPIDLQDVLLRF TFDTSCFSVLAADPESLTMEFPKVPFSKAADQGLDAALTRHITPRLI WKLKRFFNIGSERTLAMAWKVIDSYIYDKIAKLKANRKRMGKINS YDAVSFYMDSFNIHDDKFLRDNAFTLLLAQRNTQSLAMAWLFYAL FENPKVEPKILSELTSIVDESSERKFKDGFTLFDSDMIQSAIYLHATL SEALRIYPPVPFEIKDAHKADVLPSGHKVRAGEKILFSPYAMARMK GIWGDDCLEFKPERWITENGTLKHEPAYKSFAFSAGPRICLGKELSF TQMKMVVATIIYNFHVQMVKGHVVEQSNSILMEMKHGLMVEVRK RSVM
	LauCYP96T1-like-1_Lycoris_aurea	MATSSPWLIFSDHYPEILIAIACFIILSLLRSASSSSKDSLPYKWPIFG MLPEIIYNKQFNELVTARLRETGWTFVFKGPWIVNMDRIVTCDPAN MNHMFNLKFENYPKGDLYKVFDVFGDNILNADGDNWHNHRIMA QTVFWDRNYRAMQAKFVQDKVQNALIPILDSAAYKKKPLELQDV LLRFMFDTSCQCVLASDPGTLLLDFPTVPFAKACDEALDATLRRHI TPPHIWKIKRFLNIGSEKMRANAWKVLDAYIYERIAKIKENIKRTGK NTSYNAMALYIDNCNLHNDRRLRDNAFTFLLVQRNTLSLTMAWLF YALFLNPRVVPKILDELQSILDKSSERRFKDGYALFDDNMIQSAIYL HATFCEVLRCYPPIPFEVKDALKADVLPSGHKVRAGDKILFSPYAM ARMEGIWGADCMEFKPERWITENGTLKHEPAYKFFAFSAGPRICLG KELAFTQMKIVAANIIYNFDVQMVKGHVVEQRTTILMEMKHGLM VEVRKRSVM
	LauCYP96T1-like-2_Lycoris_aurea	MATSSAWLIFSDHYPEILIAIACFIIFSLLRSASSSSKDSLPYKWPIFG MLPEIIYNKQFNELVTARLRETAWTFVFKGPWIVNMDRIVTCDPAN MNHMFNLKFENYPKGDLYKVFDVFGNNLFNADGDNWYNHRIMA QTVFWDGNYRAMQAKFVVDKVQNALIPILDSAACKEKPLDLQDV LLRFTFDISCQCVLASDPGTLFLEFPTVPFAKACDEALDATLRRHITP PHIWKLKRFFNIGSEKVLANAWKVVDAYIYERIAKIKENIKRTGKN SSCNAMALYIDNCNLHNDRLLRDAAYTFLLVQRNTLSLTMAWLFY ALFLNPRVVPKILDELQSILDKSSERRFKDGYALFDGDMIQSAIYLH ATFCEVLRYYPPVPFEIKDALKADVLPSGHKVRAGDKILFSPYAMA RMKGIWGDDCMEFKPERWITENGTLKHEPAYKFFAFSAGPRICLG KELAFTQMKIVAANIIYNFDVQMVKGHVVEQRTAILMEMKQGLM VEVRKRSVM
	LauCYP96T1-like-3_Lycoris_aurea	MATSSPWLIFSDHYPEILIAIACFIIFSLLRSASSSSKDSLPYKWPIFGM LPEIIYNKQFNELVTTRLRETGWTFVFKGPWIVNMDRIVTCDPANM NHMFNLKFENYPKGDLYKVFDVFGDNILNADGDIWHNHRIMAQT VFWDRNYRAMQAKFVQDKVQNALIPILDSAACKKKPLELQDVLLR FMFDTSCQCVLASDPGTLLLEFPTVPFAKACDEALDATLRRHITPPH IWKLKRFLNIGSEKMRANAWKVLDAYIYERIAKIKENIKRTGKNTS YNAMALYIDNCNLHNDRRLRDNAFTFLLVQRNTLSLTMVWLFYA LFLNPRVVPKILDELQSILDKSSERRFKDGYALFDDNMIQSAIYLHA TFCEVLRCYPPIPFEVKDALKADVLPSGHKVRAGDKILFSPYAMAR MKGIWGDDCMEFKPERWITENGTLKHEPAYKFFAFSAGPRICLGKE LAFTQMKIVAASIIYNFDVQMVKGHVVEQRTTILMEMKHGLMVEV RKRSVM

	NtCYP96T1_Narcissus_tete-a-tete	MATSSSAWLMFSDHYPEILIAIACFLIFSLLLSARSSSKDSLPYNWPIF GMLPAIISNNQFNDFTTARLRKMGWTFIFKGPWLLDMDYIFTCDPS NINHMFNDNFENYPKGELGKVFDIFGNNIFNADGDLWHDHRKMA QTILWDGNYRTMQATFIRNKMDNALIPILDSAACKRKPVDLQDVL LRFTFDTSCFSVLAADPESLTMEFPPVPFSKAADQALDAALTRHITP RLIWKLKRFFNVGSERTLAVAWKVIDSYIYDKIAELKAKRKLVGKI NSYDAVSFYMDNFNIHDDKFLRDNAFTYLLAQRNTQSLTMTWLFY ALFENPKVELKILSELKSIVDESSERKFNDGFALFDSNMIQSAIYLHA TLCEALRIYPPVPFEIKDAHKADVLPSGHKVRAGEKILFSPYAMAR MKGIWGDDCLEFKPERWITGNGTLKHEPAYKFFAFSAGPRICLGKE LSFTQMKMVVATIIYNFHLQMVKGHVVEQSNSILMDMKHGLMVQ VRKRSVM
	NtCYP96T5_Narcissus_tete-a-tete	MATSSPWLIFSDHYPEILIATVCFIVFSLLRSASSSSKDSLPYKWPIFG MLPEIIYNKQFNELVTARLRETGWTFVFKGPWIVKMDRIVTCDPAN MNHMFNLNFDNYPKGDLYKVFDIFGNNLFNADGDNWYNHRIMA QTVFWDGNYRARQAKLVLDKVDSALIPILDSAACRRKPFDLQDVL LRFTFDISCQCVLDSDLGTLSSEFPTVPFAKACDEALDATLRRHITPP HIWKMKRFLNIGSEKIRADSWKVVDAYIFERIAKIKENVKRMGKNT NYNATALYIDSCDLLNDQQLRDNAYTFLLVQRNTLALTMAWLFY ALSLTPRVVPKILDELQSILDKSSERRFKDGYALFDGDMIQSAIYLH ATLCEVLRYYPPVPFEIKDALNADVLPSGHKVRAGEKILFSPYAMA RMKGIWGDDCMEFKPERWITENGTLKHEPAYKFFAFSAGPRICLG KELAFNQMKIAVANIIYNFDVQMVKGHVVEQRTAILMEMMHGLM VEVRKRSVV
	NtCYP96T6_Narcissus_tete-a-tete	MVTSSSAWLIFSDHYREILIAIACLVVFSLLRSARSSSKGGLPYNCPI FGMLPAIISNNQFNDFITARLREIGWTFSFKGPWLLDMDYIFTCDPA NINHMFNHNFENYPKGQLGEVFDIFGNNILNADGDVWRNHRKMA QTIMWDENYRTMQATFIRNKMEDALIPVLDSAACERKPVDLQDVF LRFTFDTSCFSVLAADPESLTMEFPTVPFPQAVDQALDAALRRHIMP RLIWKLKRFFKIGSERTLATACEVIDSYLYEKIAQLKANRVGMGKI KSYDVVSFYMDNFDIHDDKFLRDNAFTYLLLQRNTQSITMTWLFY ALFENPKVEPKILIELKSIVDESSERKLKDGFTLFDSNMIQSAIYLHA TLCEALRIYPPVPFEIKNAHEADVLPSGHKVRAGEKILYSPYAMAR MTGIWGDDCLEFKPERWITDNGMLKHEPAYKFFSFNAGPRICVGK ELSFTQMKMVAATIIYNFHVQMVKGHVVEQSNSILMEMKHGLMG EVIKRSVM
	NtCYP96T7_Narcissus_tete-a-tete	MATSSSAWLIFSDHYTEILIAIACFLIFSLLRSARSSSQGSLPYDWPIF GMLPALISNNQFNDFITALLGKTGWTFVFKGPWLLDMDYIFTCDPS NINHLFDDNFENYPKGHRAKVFDIFGDSIFNADGDLWRDHRKMAQ TIFWDGNYRTMQAAFIRDKMDNALIPILDSAACKRKPVLDLQDVLL RFTFDTSCFSVLAADPESLSMEFPDVPFSNAADRALDESLARQITPP VIWKLKRFLGIGSERELAMAWKAIDSYIYDKIAEIKARRKLAGKVN SYDAVSSYMDTFNIHDDKFLRDSALTILLVQRNTQSLAMSWLFYAL FENPKLEQKILSELKSIADGSSERKSNDGFTLFDGNMIQSAIYLHATL CEAMRMYPPIPFEVRDAQKADVLPSGHKVRAGEKILFSPFAMARM KGIWGDDCLEFKPERWIAGNGTLKHEPAYKFFAFSAGPRICVGKEL AFTQMKMVVATIVYNFHLQMAKGHVVEHRNTILNHMKHGLMVE VTKRSAI
	NtCYP96T8_Narcissus_tete-a-tete	MATSSAAWLIFSDHYPEILIAIACLLIFSLLLSARSLSEGGLPYNWPIF GMLPAIISNSQFNDFITARLRKTGWTFIFKGPWLLDMDYIFTCDPSNI NHMFNDNFENYPKGELGKVLDIFGNNIFNADGDLWHDHRKMAQSI LWDGNYRAMQATFIRNKMDNALIPILDSAACKRRPVDLQDVLLRF TFDTSCFSVLAADPESLAMEFPAVPFSRAADQALDAALTRHITPRVI WKLKRFFNVGSERTLATAWKVIDSYIYDKIAELKAKRKLAGKINSY DAVSFYMDSFDIHDDKFLRDNAFTYLLAQRNTQSLTMTWLFYALF ENPRVELKILSELKSIVDESSERKSKDGFTLFGSNMIQSATYLHAAL CEALRMYPPVPFEIKDAHKADVLPSGHKVRAGEKILFSPYAMARM KGIWGDDCLEFKPERWITGNGTLKHEPAYKFFAFSAGPRICLGKEL SFTQMKMVVATIIYNFHVQMVKGHVVEQNNSILMDMKHGLMAEV RKRSVM
B1NF19.1	CYP719A13 *Argemone mexicana*	

P47195.1	CYP80A1 *Berberis stolonifera*	
A8CDR5.1	CYP80G2 *Coptis japonica*	
Q948Y1	CYP719A1 *Coptis japonica*	
Q9FXW4.1	CYP80B2 *Coptis japonica*	
B1NF18.1	CYP719B1 *Papaver somniferum*	
Q9SP06.1	CYP80B3 *Papaver somniferum*	
I3QBP4.1	CYP719A21 *Papaver somniferum*	
I3V6B1.1	CYP80BX *Papaver somniferum*	
Q8VWZ7.1	CYP76B6 *Catharanthus roseus*	
P48522.1	CYP73A4 *Catharanthus roseus*	
Q05001.1	CPR *Catharanthus roseus*	
I1TEM1.1	CYP71D1V2 *Catharanthus roseus*	
W8JCE8.1	CYP71BT1 *Catharanthus roseus*	
W8JIT4.1	CYP71D2 *Catharanthus roseus*	
W8JMV1.1	CYP76T24 *Catharanthus roseus*	
W8JWW3.1	CYP72A225 *Catharanthus roseus*	
W8JIS5.1	CYP76A26 *Catharanthus roseus*	
Q8VWZ7.1	G10H *Catharanthus roseus*	
I1TEM1.1	CYP71D1 *Catharanthus roseus*	
Q9XFZ0	CYP96C1 *Catharanthus roseus*	
A0A140IL90.1	CYP96T1 *Narcissus aff. pseudonarcissus*	
A0A140IL91.1	CYP96T2 *Narcissus aff. pseudonarcissus*	
A0A140IL92.1	CYP96T3 *Narcissus aff. pseudonarcissus*	
A0A2H5AIZ9.1	CYP96T2 *Narcissus pseudonarcissus*	
A0A2H5AJ00.1	CYP96T1 *Narcissus pseudonarcissus*	
RVW55154.1	CYP96T1 *Vitis vinifera*	
QFQ50505.1	CYP96T *Lycoris radiata*	
WGU11344.1	NoroxSyn1 *Crinum x powellii*	
AXU39906.1	NoroxSyn1 *Narcissus papyraceus*	
AXU39907.1	NoroxSyn2 *Narcissus papyraceus*	

Table 2.S3. List of primers used in the experiment.

Gene	Primers	Purpose	Sequence (5'-3')
LaNBS	Forward	*In vivo* assay	GGGGACAAGTTTGTACAAAAAAGCAGGCTATGAAGGGAAGTCTCTCCCAT
LaNBS_x3Au1	Reverse		GGGGACCACTTTGTACAAGAAAGCTGGGTCTAGATATACCTGTAAGTATCGATATACCTGTAAGTATCGATATACCTGTAAGTATCCGCTACAATAGCTTTTTGCTCCAAGAG
LaNR II	Forward		GGGGACAAGTTTGTACAAAAAAGCAGGCTATGTTTACAGGAAGAGAAGAGGAATCAATGCCAATGCCAATGGAGAAGAAGAGATGGTCTC
LaNR-II_x3flag	Reverse		GGGGACCACTTTGTACAAGAAAGCTGGGTCTACTTATCGTCGTCATCCTTATAGTCCTTATCGTCGTCATCCTTATAGTCCTTGTCGTCATCGTCTTTGTAGTCACCGTTTATGCCCCGTCCTCC
LaN4'OMT	Forward		GGGGACAAGTTTGTACAAAAAAGCAGGCTATGGGTGCTAGCCAAGAT
LaN4'OMT_x3Au5	Reverse		GGGGACCACTTTGTACAAGAAAGCTGGGTCTACAAGTAGAAGTCCGTTTTCAAGTAGAAGTCCGTTTTCAAGTAGAAGTCCGTATAAAGACGTCGACAAATAGTCACT
LaCYP96T1	Forward		GGGGACAAGTTTGTACAAAAAAGCAGGCTATGGCCACTTCTTCTCCAT
LaCYP96T1_x3myc	Reverse		GGGGACCACTTTGTACAAGAAAGCTGGGTCTACAGATCCTCCTCAGATATTAATTTTTGCTCCAAATCCTCCTCAGAGATGAGTTTTTGTTCCAGATCCTCTTCTGAGATGAGTTTTTGTTCCATGACTGATCTCTTTCCAACC
LaCYP96T2	Forward		GGGGACAAGTTTGTACAAAAAAGCAGGCTATGGCCACTTCTTCTCCAT
LaCYP96T2_x3myc	Reverse		GGGGACCACTTTGTACAAGAAAGCTGGGTCTACAGATCCTCCTCAGATATTAATTTTTGCTCCAAATCCTCCTCAGAGATGAGTTTTTGTTCCAGATCCTCTTCTGAGATGAGTTTTTGTTCCACGACTGATCTCTTTCTAACC
EGFP	Forward		GGGGACAAGTTTGTACAAAAAAGCAGGCTATGGTGAGCAAGGGCGAGGAGCTGTTCACC
EGFP_x3myc	Reverse		GGGGACCACTTTGTACAAGAAAGCTGGGTCTACAGATCCTCCTCAGATATTAATTTTTGCTCCAAATCCTCCTCAGAGATGAGTTTTTGTTCCAGATCCTCTTCTGAGATGAGTTTTTGTTCCTTGTACAGCTCGTCCATGC
EGFP_x3flag	Reverse		GGGGACCACTTTGTACAAGAAAGCTGGGTCTACTTATCGTCGTCATCCTTATAGTCCTTATCGTCGTCATCCTTATAGTCCTTGTCGTCATCGTCTTTGTAGTCCTTGTACAGCTCGTCCATGC

LaN4'OMT for N terminal fusion	Forward	Localization study	GGGGACAAGTTTGTACAAAAAAGCAGGCTTCATGGGTGCTAGCCAAGAT
LaN4'OMT for N terminal fusion	Reverse		GGGGACCACTTTGTACAAGAAAGCTGGGTCTAATAAAGACGTCGACAAATAGTCACT

LaN4'OMT for C terminal fusion	Forward		GGGGACAAGTTTGTACAAAAAAGCAGGCTATGGGTGCTAGCCAAGAT
LaN4'OMT for C terminal fusion	Reverse		GGGGACCACTTTGTACAAGAAAGCTGGGTCATAAAGACGTCGACAAATAGTCACT
LaCYP96T2 for C terminal fusion	Forward		GGGGACAAGTTTGTACAAAAAAGCAGGCTATGGCCACTTCTTCTCCAT
LaCYP96T2 for C terminal fusion	Reverse		GGGGACCACTTTGTACAAGAAAGCTGGGTCCACGACTGATCTCTTTCTAACC

*LaNBS*_BamHI.F	Forward	*In vitro* assay	AACG**GGATCC**ATGAAGGGAAGTCTCTCCCATGAG
*LaNBS*_HindIII.R	Reverse		ACGC**AAGCTT**CTACGCTACAATAGCTTTTTGCTCC
*LaNR II*_BamHI.F	Forward		AACG**GGATCC**ATGTTTACAGGAAGAGAAGAGGAATCAATGC
*LaNR II*_HindIII.R	Reverse		ACGC**AAGCTT**TCAACCGTTTATGCCCCGTCCTC
*LaN4'OMT*_BamHI.F	Forward		ATTC**GGATCC**ATGGGTGCTAGCCAAGATGATTATT
*LaN4'OMT*_HindIII.R	Reverse		TGCC**AAGCTT**TCAATAAAGACGTCGACAAATAG

qLaNBS	Forward	qRT-PCR	AGGAAGCATTTGCTGCATGT
qLaNBS	Reverse		GAGGGAGGGCACTTGG
qLaNRII	Forward		GCCGATTCGAAATTGGTGGC
qLaNRII	Reverse		AACAATGCAGGGACAGCCAT
qLaN4'OMT	Forward		GGGATATCTCGACACGGGGA
qLaN4'OMT	Reverse		CCACGAGCGATTAGTGAAGC
qLaCyp96T1/2	Forward		CCG AGG ATC TGT TTA GGG AAA G
qLaCyp96T1/2	Reverse		GTC CCT TCA CCA TCT GAA CAT
qHistone3	Forward		ACAAGCCTTTGGAAGGGCAG
qHistone3	Reverse		GGAGTGAAGAAGCCCCACC

Table 2.S4. MRM transitions and instrumental parameters used on HPLC-MS/MS for NBS, NR and OMT experiments.

Compound name	**Retention time (min)**	**Precursor (m/z)**	**Product (m/z)**	**Fragmentor (V)**	**Collision energy (V)**	**Polarity (ESI +/-)**
3,4-dihydroxybenzaldehyde	15.602	137	119	114	20	Negative
			108		26	
			92		26	
3'-*O*-methylnorbelladine	16.988	274	**137**	105	18	Positive
			121		15	

			109		40	
4'-*O*-methylnorbelladine	15.808	274	**137**	105	18	Positive
			122		40	
			94		40	
3',4'-*O*-dimethylnorbelladine	16.824	288	**151**	100	10	Positive
			135		40	
			107		40	
Norbelladine	7.281	260	**138**	86	5	Positive
			123		20	
			121		17	
Papaverine	18.302	340	324	165	40	Positive
			202		27	
			171		40	
Tyramine	3.482	138	121	81	5	Positive
			91		20	
			77		20	

Notes: Quantifier ion for each compound is **bold** and qualifier ions are not.

Identification criteria used:

Retention time window (tolerance on RT): 10%

Signals with signal-to-noise ratio ≤ 3 were not considered in the analysis.

Qualifier ratio tolerance: uncertainty of 20% (relative)

Number of qualifiers used (MRM transitions monitored per compound): 3

ISTD used: Papaverine

This Table should fit on one page. The columns are too small and the words are splitted. Please fix this.

Table 2.S5. MRM transitions and instrumental parameters used on HPLC-MS/MS for CYP experiments

Compound name	Retention time (min)	Precursor (m/z)	Product (m/z)	Fragmentor (V)	Collision energy (V)	Polarity (ESI +/-)
3,4-dihydroxybenzaldehyde	15.641	137	119	114	20	Negative
			108		26	
			92		26	
3'-*O*-methylnorbelladine	17.001	274	**137**	105	18	Positive
			121		15	
			109		40	
	16.033	288	**137**	70	14	Positive

4'-*O*, *N*-dimethylnorbelladine			122		40	
			94		40	
4'-*O*-methylnorbelladine	15.823	274	**137**	105	18	Positive
			122		40	
			94		40	
11-hydroxyvittatine	4.773	288	226	105	26	Positive
			196		34	
			153		40	
3',4'-*O*-dimethylnorbelladine	16.838	288	**151**	100	10	Positive
			135		40	
			107		40	
Galanthamine	5.327	288	270	120	14	Positive
			225		18	
			213		22	
Haemanthamine	14.82	302	211	105	22	Positive
			196		34	
			181		30	
Lycorine	4.123	288	270	92	20	Positive
			177		20	
			147		28	
			119		40	
Narwedine	10.654	286	**229**	95	25	Positive
			225		18	
			201		26	
N-demethylnarwedine	N/A	272	229	100	25	Positive
			201		25	
			158		25	
Norbelladine	7.296	260	**138**	86	5	Positive
			123		20	
			121		17	
Norgalanthamine	4.466	274	231	115	14	Positive
			213		18	
			198		40	
Normaritidine	N/A	274	256	100	25	Positive
			228		25	
			196		25	
Noroxomaritidine	N/A	272	244	100	25	Positive
			229		25	
			212		25	
Norpluviine	N/A	274	224	100	25	Positive
			147		25	
			119		25	
Oxomaritinamine	N/A	274	**219**	100	25	Positive

			165		25	
			136		25	
*Papaver*ine	18.311	340	324	165	40	Positive
			202		27	
			171		40	
Tyramine	3.491	138	121	81	5	Positive
			91		20	
			77		20	
Vittatine and/or crinine	12.169	272	226	105	26	Positive
			196		34	
			136		26	

Notes:

Quantifier ion for each compound is **bold** and qualifier ions are not.

N/A: not applicable (*i.e.* reference standard not available)

Table 2.S6. Instrumental parameters used in Product Ion mode on HPLC-MS/MS for CYP experiments

Precursor	Start mass	End mass	Fragmentor	Collision energy
(m/z)	(m/z)	(m/z)	(V)	(V)
272	50	275	100	25
274	50	280	100	25

Table 2.S7. Multiple Sequence Alignment Distance Matrix (Similarity in percent) without removing gaps

Table 2.S7. a (For *La*NBS)

	*La*NBS cloned Seq	NBS *L._aestivum* (T/M)	NBS *Narcissus pseudonarcissus*	NBS *Narcissus papyraceus*	NpaNBS_Narcissus papyraceus (H)	NCS1 *Papaver somniferum*	NCS *Thalictrum flavum* subsp. *glaucum*	NCS 2 *Coptis japonica*
*La*NBS clonedSeq	100%	100%	87%	86%	88%	31%	36%	38%
NBS *L._aestivum* (T/M)	100%	100%	88%	87%	88%	32%	36%	39%
NBS *Narcissus pseudonarcissus*	87%	88%	100%	89%	90%	30%	35%	37%
NBS *Narcissus papyraceus*	86%	87%	89%	100%	99%	27%	34%	36%
NpaNBS_Narcissus	88%	88%	90%	99%	100%	28%	34%	37%

papyraceus (H)								
NCS1 *Papaver somniferum*	31%	32%	30%	27%	28%	100%	37%	31%
NCS *Thalictrum flavum* subsp. *glaucum*	36%	36%	35%	34%	34%	37%	100%	64%
NCS2 *Coptis japonica*	38%	39%	37%	36%	37%	31%	64%	100%

Table 2.S7. b (For LaNRII)

	LaNRII_clonedSeq	NR2 *Leucojum aestivum*	NR1 *Leucojum aestivum*	NtSDR1 *Narcissus cv. Tête-à-Tête*	NR_NARPS *Narcissus pseudonarcissus*	NpsNR *Narcissus* aff. *pseudonarcissus*	Pc_SDR *Phycella* aff. *cyrtanthoides*	Zt_SDR *Zephyranthes treatiae*	NtAKR1_*Narcissus cv. Tête-à-Tête*	NtSDR2_*Narcissus cv. Tête-à-Tête*
LaNRII_clonedSeq	100 %	100 %	98%	90%	77%	77%	77%	76%	15%	13%
NR2 *Leucojum aestivum*	100 %	100 %	98%	90%	77%	77%	77%	76%	15%	13%
NR1 *Leucojum aestivum*	98%	98%	100 %	90%	77%	77%	76%	75%	16%	14%
NtSDR1 *Narcissus cv. Tête-à-Tête*	90%	90%	90%	100 %	76%	76%	75%	74%	13%	11%
NR_NARPS *Narcissus pseudonarcissus*	77%	77%	77%	76%	100%	100%	91%	90%	15%	15%
NpsNR *Narcissus* aff. *pseudonarcissus*	77%	77%	77%	76%	100%	100%	91%	90%	15%	15%
Pc_SDR *Phycella* aff.	77%	77%	76%	75%	91%	91%	100%	93%	16%	15%

cyrtantho ides										
Zt_SDR *Zephyran thes treatiae*	76%	76%	75%	74%	90%	90%	93%	100%	16%	16%
NtAKR1 _*Narciss us cv. Tête-à-Tête*	15%	15%	16%	13%	15%	15%	16%	16%	100%	12%
NtSDR2_ *Narcissus cv. Tête-à-Tête*	13%	13%	14%	11%	15%	15%	15%	16%	12%	100%

Table 2.S7. c (For *La*N4'OMT)

	*La*N4'OMT clonedSeq	*Ge*OMT *Galanthus elwesii*	N4OMT *Lycoris radiata*	N4OMT *Narcissus papyraceus*	OMT *Lycoris aurea*	LIOMT *Lycoris longituba*	*Np*N4OMT *Narcissus* aff. *pseudonarcissus*	*Nt*OMT1 *Narcissus cv. Tête-à-Tête*
*La*N4'OMT clonedSeq	100%	98%	96%	96%	95%	95%	95%	13%
*Ge*OMT *Galanthus elwesii*	98%	100%	96%	95%	95%	94%	95%	13%
N4OMT *Lycoris radiata*	96%	96%	100%	98%	95%	95%	97%	14%
N4OMT *Narcissus papyraceus*	96%	95%	98%	100%	95%	94%	97%	14%
OMT *Lycoris aurea*	95%	95%	95%	95%	100%	98%	94%	14%
LIOMT *Lycoris longituba*	95%	94%	95%	94%	98%	100%	93%	13%
*Np*N4OMT *Narcissus* aff. *pseudonarcissus*	95%	95%	97%	97%	94%	93%	100%	14%
*Nt*OMT1 *Narcissus cv. Tête-à-Tête*	13%	13%	14%	14%	14%	13%	14%	100%

Table 2.S7. d (For LaCYP96T1 and LaCYP96T2)										
	*La*CYP96T1 clonedSeq	*La*CYP96T2 clonedSeq	*Nt*CYP96T5 *Narcissus cv. Tête-à-Tête*	*Lau*CYP96T1-like-2 *Lycoris aurea*	*Lau*CYP96T1-like-3 *Lycoris aurea*	*Lau*CYP96T1-like-1 *Lycoris aurea*	*Lau*CYP96T1 *Lycoris aurea*	Cyp96T1 *Narcissus* aff. *pseudonarcissus*	NtCYP96T1 *Narcissus cv. Tête-à-Tête*	NtCYP96T6 *Narcissus cv. Tête-à-Tête*
*La*CYP96T1 clonedSeq	100%	98%	90%	92%	90%	89%	74%	73%	73%	69%
*La*CYP96T2 clonedSeq	98%	100%	90%	91%	89%	89%	73%	72%	73%	68%
*Nt*CYP96T5 *Narcissus cv. Tête-à-Tête*	90%	90%	100%	90%	88%	87%	74%	71%	72%	69%
*Lau*CYP96T1-like-2 *Lycoris aurea*	92%	91%	90%	100%	94%	93%	77%	75%	75%	72%
*Lau*CYP96T1-like-3 *Lycoris aurea*	90%	89%	88%	94%	100%	98%	76%	74%	75%	72%
*Lau*CYP96T1-like-1 *Lycoris aurea*	89%	89%	87%	93%	98%	100%	75%	73%	74%	71%
*Lau*CYP96T1 *Lycoris aurea*	74%	73%	74%	77%	76%	75%	100%	92%	92%	86%
Cyp96T1 *Narcissus* aff. *pseudonarcissus*	73%	72%	71%	75%	74%	73%	92%	100%	99%	86%
NtCYP96T1	73%	73%	72%	75%	75%	74%	92%	99%	100%	86%

Narcissus cv. Tête-à-Tête										
NtCYP96T6 *Narcissus cv. Tête-à-Tête*	69%	68%	69%	72%	72%	71%	86%	86%	86%	100%

Table 2.S8. Differences in residues between SDRs

	Amaryllidaceae																		
aminoacid position	*La*NRII clonedSeq	NtSDR1 *Narcissus cv. Tête-à-Tête*	NNR1 *Narcissus papyraceus*	NR *Narcissus* aff. *pseudonarcissus*	NR *Narcissus pseudonarcissus*	NNR *Lycoris radiata*	NtSDR2 *Narcissus cv. Tête-à-Tête*	NtAKR1 *Narcissus cv. Tête-à-Tête*	Pc_SDR_*Phycella* aff. *cyrtanthoides*	Zt_SDR_*Zephyranthes treatiae*	Ao_SDR_*Asparagus officinalis*	Pb_SDR_*Pinus banksiana*	TRN1_*Cochlearia officinalis*	M77_SDR *Methylobacterium sp.*	M77_SDR_opt_mutant *Methylobacterium sp.*	Bs_GDH *Bacillus subtilis*	Bs_GDH_op_mutant *Bacillus subtilis*	3β/17β-hydroxysteroid [illegible]	3β/17β-hydroxysteroid dehydrogenase_*Comamonas testosteroni* mutant
29	T	T	T	T	T	T	K	H	T	T	T	T	T	T	T	T	T	T	T
30	G	G	G	G	G	S	G	P	G	G	G	G	G	G	G	G	G	V	V
31	G	G	G	G	G	G	Y	F	G	G	G	G	G	A	A	A	A	V	V
32	T	T	T	T	T	T	L	P	T	T	T	T	S	S	S	A	A	A	A
33	K	K	K	K	K	K	V	Q	K	K	K	K	K	K	K	S	S	S	S
34	G	G	G	G	G	G	N	D	G	G	G	G	G	G	G	G	G	G	G
35	I	I	I	I	I	I	G	N	I	I	I	I	I	I	I	L	L	V	V
36	G	G	G	G	G	G	T	T	G	G	G	G	G	G	G	G	G	G	G
53	C	C	C	C	C	C	K	T	C	C	C	C	C	Y	Y	Y	Y	D	D
54	S	S	S	S	S	S	A	A	S	S	S	A	A	A	A	Y	Y	I	I
55	R	R	R	R	R	R	E	G	R	R	R	R	R	S	S	S	S	N	N
56	N	N	N	N	N	N	N	S	N	N	N	T	D	S	S	N	N	A	A
59	E	E	E	E	E	E	L	P	E	E	E	D	Q	G	G	D	D	Q	Q
79	C	C	C	C	C	C	F	L	C	C	C	C	C	G	G	G	G	H	H

80	D	D	D	D	D	D	H	F	D	D	D	D	D	D	D	D	D	D	D	D
81	V	V	V	V	V	V	V	I	V	I	V	L	V	V	V	V	V	V	V	V
82	S	S	S	S	S	S	A	T	T	A	S	S	S	T	T	T	T	S	S	S
108	N	N	N	N	N	N	C	Y	N	N	N	N	N	N	N	N	N	N	N	N
109	A	A	A	A	A	A	S	L	A	A	A	V	A	S	S	A	A	A	A	A
110	G	G	G	G	G	A	E	D	G	G	G	G	G	G	G	G	G	G	G	G
111	T	T	T	G	G	S	A	L	G	G	T	T	T	V	V	L	L	I	I	I
112	A	A	A	Y	Y	T	K	Y	Y	Y	F	N	C	Y	Y	E	Y	L	L	L
113	I	I	I	V	V	L	I	L	V	V	I	M	I	A	A	N	N	L	L	L
114	L	L	L	N	N	Y	K	I	M	N	T	R	T	F	N	P	N	P	P	P
127	F	F	F	F	F	F	K	F	F	F	F	F	F	Q	Q	K	K	R	R	R
131	T	T	T	V	V	A	E	K	V	V	T	T	T	V	V	T	T	I	I	I
132	N	N	N	N	N	N	N	N	N	N	N	N	N	N	N	N	N	N	N111L	N111L
158	I	I	I	I	I	I	A	A	I	V	I	I	I	I	I	M	M	M	M	M
159	S	S	S	S	S	S	L	I	S	S	S	S	S	S	S	S	S	A	A	A
160	T	T	T	S	S	S	D	G	S	S	S	S	S	S	S	S	S	S	S138A	S138A
161	V	V	V	C	C	A	Y	V	C	C	I	V	V	A	C	V	C	V	V	V
162	C	C	C	C	C	C	A	S	C	C	A	A	A	I	C	H	C	S	S	S
165	I	I	I	I	I	I	Y	T	I	I	V	V	V	I	I	I	I	L	L	L
167	L	L	L	I	I	I	L	N	V	L	L	I	V	M	M	W	W	I	I	I
170	H	H	H	H	H	H	L	E	H	H	L	G	G	S	H	F	H	Y	Y	Y
173	Y	Y	Y	Y	Y	Y	C	L	Y	Y	Y	Y	Y	Y	Y	Y	Y	Y	Y151F	Y151F
177	K	K	K	K	K	K	I	K	K	K	K	K	K	K	K	K	K	K	K	K
203	P	P	P	P	P	P	V	K	P	P	P	P	P	P	P	P	P	P	P	P
204	G	G	G	G	G	G	E	G	G	G	G	W	G	G	G	G	G	D	D	D
205	I	I	I	A	A	A	N	I	A	A	G	Y	F	Y	Y	A	A	G	G	G

206	T	T	T	I	I	I	E	H	I	I	I	T	I	V	V	I	I	I	I
208	T	T	T	T	T	T	W	T	T	T	T	T	T	T	T	T	T	T	T
209	V	V	V	P	P	P	P	A	P	P	P	S	P	E	E	P	P	P	P
210	Q	Q	Q	G	G	G	A	Q	S	S	M	L	L	T	T	I	I	M	M
211	V	V	V	T	T	T	D	E	S	S	V	V	A	Q	Q	N	S	M	M
212	Q	Q	Q	E	E	E	V	E	E	E	Q	E	S	S	S	A	A	Q	Q
213	P	P	P	S	S	S	R	P	L	P	P	K	N	A	A	E	E	A	A
214	F	F	F	F	F	F	D	S	F	F	L	L	Y	G	G	K	K	S	S
224	E	E	E	E	E	E	E	D	E	E	I	I	V	L	L	V	V	V	V
265	R	R	R	R	R	R	R	L	R	R	F	M	F	V	V	M	M	I	I

Table 2.S9. Differences in residues between O-methyltransferase enzymes of different substrate specificity.

Position	3'- and 4'-*O*-methy-lation of norbelladine	only 4'-*O*-methylation of norbelladine	4'-*O*-methylation and dimethylation of norbelladine	3,4-DHBA or caffeic acid 3 or 4-*O*-methylation
9	A/S	S	A	A/S
20	D	D	E	E/D
30	V	A/T	A	A/T/V
108	Y	Y/F	F	Y/F
140	L	V/L	V	V/L
141	Q	E/R	Q	Q/E/R
148	F	L/F	L	L/F
151	F	Y/F	Y	Y/F
179	V/I	L/A	L	L/A/V/I
186	F	Y	Y	F/Y
188	T	S	S	T/S
191	F	Y	Y	F/Y
203	E	V/E	V	V/E
204	C	A/C	A	A/C
206	V	L	L	V/L
210	N	N	Q	Q/N
213	K	T	T	K/T
228	V/T	I/V	I	I/V/T
232	L	V	V	V/L

Table 2.S10. Differences in residues between CYP enzymes with different product specificity/phenolcoupling

	Cloned candidates		Haementhamine Pathway						Galanthamine Pathway					Lycorine Pathway
			para-para'						*para-ortho'*					*ortho-para'*
Position	LaCYP96T1	LaCYP96T2	NARAPCYP96T1	NtCYP96T1	LauCYP96T1-like2	LauCYP96T1-like2_mutated	LauCYP96T1-like3	LauCYP96T1-like3_mutated	NtCYP96T6	LauCYP96T1-like1	LauCYP96T1-like3	LauCYP96T1-like3 mutated	NtCYP96T5	
123	**L**	**L**	I	I	I	**L**	**L>I**	I	**L>I**	I	I	I	I	**L**
124	**F**	**F**	F	F	F	**F**	**F>L**	L	**F>L**	L	L	L	L>F/W	**F**
142	**F**	**F**	L	L	L	**F**	F	F	F	M	F	F	F	**F**
304	**F**	**F**	Y	Y	L	**F**	F	F	F	Y	F	F	F	**F**
307	**V**	**V**	A	A	A	**V**	V	V	V	L	V	V	V	**V**
312	**L**	**L**	Q	Q	Q	**L**	L	L	L	Q	L	L	L	**L**
381	**V**	**V**	V	V	V	**V**	V	I	V	V	I	I	I	**V**
385	**I**	**I**	I	I	I	**I**	I	V	I	I	V	V	V	**I**
449	**A**	**A**	A	A	A	**A**	A	A	A	S	A	A	A	**A**
451	**S**	**S**	S	S	S	**S**	S	S	S	N	S	S	S	**S**
463	**A**	**A**	S	S	S	**A**	A	A	A	S	A	A	A	**A**

Table 2.S11. Summary of *in vivo* enzymatic assay

Samples	Product										
	Norbelladine	4'-*O*-methylnorbelladine	*N*-demethylnarwedine	Norgalanthamine	Noroxomaritidine	Oxomaritinamine	Narmaritidine	Vittatine and/or crinine	Haemanthamine	Norpluviine	Lycorine
Leaf	---	---	---	---	---	---	---	---	---	---	---
EGFP	---	---	---	---	---	---	---	---	---	---	---
LaNBS+LaNRII	***	---	---	---	---	---	---	---	---	---	---
LaNBS+LaNRII+LaN4'OMT	***	***	---	---	---	---	---	---	---	---	---
LaNBS+LaNRII+LaN4'OMT+LaCYP96T1	***	***	-**	-**	***	---	***	** *	** *	***	***
LaNBS+LaNRII+LaN4'OMT+LaCYP96T2	***	***	-*-	** *	***	---	***	---	---	***	***

Feeding tyramine and 3,4-dihydroxybenzaldehyde each experiment was performed in triplicates and respective product detected/or not by HPLC-MS/MS is represented by three consecutive signs for each experiment in product column. Small dash line in black color represents no signal detected for the compound. Green asterisk sign * represents detection and identification of the compound by Multiple Reaction Monitoring (MRM) or using theoritical MRM transitions found in the

literature for corresponding compound. Orange * is signal detected but the identification of the compound is not fully confirmed by HPLC-MS/MS (e.g., weak signal presents through background noise, S/N ratio near of 3, or qualifier ion ratios not exactly the same as standard).

Chapter III

Chapter III contains a study that presents

"**A Golgi-Localized *N*-Methyltransferase and Reversible Aldo–Keto Reductases Coordinate Dual Terminal Routes in Galanthamine Biosynthesis"**

The manuscript was submitted on Nov 11, 2025, and is accepted for publication on 24th April 2026 in "The Plant Journal".

This chapter discusses the establishment of the ultimate AAs core pathway leading to galanthamine.

Contributions: Basanta Lamichhane carried out bioinformatics, candidate gene identification, pathway construction, *in vivo* and *in vitro* enzymatic assay, enzyme characterization, LC-MS and writing the manuscript draft, revision and finalization. Archana Niraula helped in cloning and colony PCR of the genes in bacterial expression vector. Sarah-Eve Gélinas performed the metabolite analysis using LC-MS/MS. Simon performed GC-MS and substrate synthesis. Natacha Merindol finalized molecular docking and revised the draft. Hugo Germain co-supervised and revised the draft. Isabel Desgagné-Penix supervised the project, provided funding and material for the project, and assisted with the writing and revising the paper.

A Golgi-Localized N-Methyltransferase and Reversible Aldo–Keto Reductases Coordinate Dual Terminal Routes in Galanthamine Biosynthesis

Basanta Lamichhane[1], Archana Niraula[1], Natacha Merindol[1], Sarah-Eve Gélinas[1], Patrick Lagüe[2], Simon Ricard[1,3], Hugo Germain[1,3], Isabel Desgagné-Penix[1,3*]

[1]Department of Biochemistry, Chemistry, Physics and Forensic Science, Université du Québec à Trois-Rivières, Trois-Rivières, Québec, Canada

[2]Department of Biochemistry, Microbiology and Bioinformatics, Université Laval, Québec, Québec, Canada

[3]Plant Biology Research Group, Trois-Rivières, Québec, Canada

BL: Basanta.Lamichhane@uqtr.ca

AN: Archana.Niraula@uqtr.ca

NM: Natacha.Merindol@uqtr.ca

SEG: Sarah-Eve.Gelinas@uqtr.ca

SR: Simon.Ricard@uqtr.ca

PL: patrick.lague@bcm.ulaval.ca

HG: Hugo.Germain@uqtr.ca

IDP: Isabel.Desgagne-Penix@uqtr.ca

*Corresponding author's email address: Isabel.Desgagne-Penix@uqtr.ca

3.1. SUMMARY

Galanthamine, a therapeutic Amaryllidaceae alkaloid produced exclusively by species within the *Amaryllidoideae* subfamily, is a key treatment for early-stage symptoms of Alzheimer's disease. Elucidating its biosynthetic pathway is essential for strategies aimed at enhancing production through metabolic engineering. Galanthamine derives from the metabolic precursor 4′-*O*-methylnorbelladine, which undergoes cytochrome P450-mediated para-ortho' C-C phenol coupling to yield nornarwedine. Two competing terminal routes have been proposed: (i) reduction of nornarwedine to norgalanthamine, followed by *N*-methylation, or (ii) *N*-methylation of nornarwedine to narwedine prior to reduction. Here, we identify three aldo-keto reductase (AKR) candidates (*La*AKR1, *La*AKR2, and *La*AKR3) and three *N*-methyltransferase (NMT) candidates from *Leucojum aestivum*: *La*NMT, homologous to coclaurine N-methyltransferase-like (NMT-like), and two γ-tocopherol methyltransferases (TMT) homologs, *La*TMT1 and *La*TMT2. Subcellular localization studies revealed distinct compartmentalization, with *La*NMT targeted to the ER-cytosol, *La*TMT1 to plastids, and *La*TMT2 to the Golgi apparatus. *In vitro, La*TMT2 methylated both nornarwedine and norgalanthamine, with a kinetic preference for nornarwedine. *La*TMT1 methylated γ-tocopherol to α tocopherol (vitamin E). All three AKRs catalyzed reversible interconversions between nornarwedine and norgalanthamine, and between narwedine and galanthamine, with *La*AKR3 favoring the reduction reaction whereas *La*AKR1 the oxidation reaction. These findings identify *La*TMT2 and *La*AKRs as key branch-enabling enzymes, reconcile long-standing models of galanthamine biosynthesis, and provide a strategic target for metabolic engineering strategies to enhance galanthamine production.

Keywords: Amaryllidaceae alkaloids**,** Alzheimer's disease treatment, specialized metabolism, *Leucojum aestivum*, oxidoreductase, heterologous expression, enzyme kinetics

Significant statement:

We identify *La*TMT2, a Golgi-localized methyltransferase from *Leucojum aestivum*, as the key enzyme reconciling two competing models of galanthamine biosynthesis — an FDA-approved anti-Alzheimer's drug — supported by reversible aldo-keto reductases that fine-tune metabolic flux. These findings unlock new targets for metabolic engineering of this clinically vital compound.

3.2. Introduction

Amaryllidaceae alkaloids (AAs) are specialized isoquinoline-derived metabolites produced predominantly within the Amaryllidoideae subfamily (Desgagné-Penix, 2021). AAs exhibit diverse biological activities (Cimmino et al., 2017), including antitumor, antiviral, antibacterial, antifungal, antimalarial, analgesic, acetylcholinesterase inhibitory, and cytotoxic effects (Jayawardena et al., 2024; Ka et al., 2021; Paiva et al., 2023; Sokhna et al., 2024; Tallini et al., 2024). Among AAs, galanthamine is of particular importance as an FDA-approved therapeutic used for symptomatic management of early-stage Alzheimer's disease. Like other alkaloids, the structural and pharmacological diversity of AAs is shaped by tailoring enzymes such as methyltransferases (MTs), which modulate a molecule's stereo-electronic profile, encourage or inhibit specific conformations, enhance steric bulk, increase overall hydrophobicity, and invert the polarity of an electronegative moiety (Wessjohann et al., 2014). Despite galanthamine's importance, the enzymatic steps responsible for efficient terminal *N*-methylation and reduction remain ambiguous (Liyanage et al., 2025; Mehta et al., 2024), highlighting key outstanding questions in AA biosynthesis.

Aldo-keto reductases (AKRs) are a large protein superfamily of NAD(P)H-dependent oxidoreductases that catalyze the reduction of various carbonyl substrates into their corresponding primary and secondary alcohols (Jez et al., 1997a). The superfamily is organized into 16 families and subfamilies based on amino acid sequence identity: a family is defined by less than 40% identity, while a subfamily shares greater than 60% identity(Jez et al., 1997b; Penning, 2015). In plants, AKRs are predominantly members of the AKR4 family and function as metabolically versatile enzymes that participate in diverse biochemical pathways and stress responses, serving as key catalysts in specialized metabolism, including the biosynthesis of pharmaceutically important alkaloids (de Sousa et al., 2025; Unterlinner et al., 1999). Structurally, AKRs are primarily 34–37 kDa monomeric soluble proteins with a highly conserved $(\alpha/\beta)_8$-barrel (triose-phosphate isomerase) motif, and a catalytic tetrad, typically consisting of aspartate, tyrosine, lysine, and histidine (Kratzer et al., 2006; Penning, 2015).

Plant MTs are classified based on the atom they methylate (*e.g.,* O, N, C, or S), and typically use *S*-adenosyl-L-methionine (SAM) as a methyl donor (Liscombe et al., 2012). Structural studies of

benzylisoquinoline alkaloids (BIA) *N*-MTs provide mechanistic insight into substrate activation and specificity. Coclaurine *N*-MT (CNMT) from *Coptis japonica* and pavine *N*-MT (PNMT) from *Thalictrum flavum* are canonical SAM-dependent enzymes that share a Rossmann-fold SAM-binding domain and an α-helical substrate-binding region. Both utilize conserved acidic and histidine residues, specifically the E204/E207/H208 triad in CNMT and the E205/H206 dyad in PNMT, for general base catalysis (Bennett et al., 2018; Torres et al., 2016), reflecting convergent strategies for substrate activation and specificity across structurally homologous *N*-MTs.

Within plant specialized metabolism pathways, AKRs and MTs are particularly prominent, catalyzing essential transformations in diverse alkaloid pathways, including tropane, monoterpenoid indole, purine, isoquinoline, and benzylisoquinoline alkaloids. In *Papaver somniferum,* the BIA pathway, which shares L-tyrosine as a common precursor with AA, leading to morphinan, protoberberine, and benzophenanthridine alkaloids, relies on enzymes such as coclaurine *N*-MT (CNMT) (Choi et al., 2002), reticuline *N*-MT (Morris and Facchini, 2016), tetrahydroprotoberberine *N*-MT (Liscombe and Facchini, 2007), 1,2-dehydroreticuline reductase, and codeinone reductase (Carr et al., 2021). Similar orthologs and functional homologs have been reported across *Ranunculales*, including *Papaver bracteatum, Glaucium flavum, T. flavum, C. japonica, C. chinensis, C. teeta,* and *Eschscholzia californica* (Morris and Facchini, 2019). In monoterpenoid indole alkaloids (MIA), *N*-MTs evolved from γ-tocopherol MTs (TMTs) catalyze the methylation of intermediates, while AKRs such as perakine reductase from *Rauvolfia serpentina* contribute to redox transformations essential for the formation of alkaloids, including ajmaline and ervincine (Bennett et al., 2018; Torres et al., 2016). In *Catharanthus roseus*, Cr2270, a homolog of the TMT family from *Arabidopsis thaliana,* exhibits high specificity for *N*-methylation of substrates in the vindoline pathway (Liscombe et al., 2010), and AKR cathenamine reductase converts intermediates like cathenamine to ajmalicine (Hasnain, 2010).

The terminal architecture of AA biosynthesis remains incompletely resolved, including the role of AKRs in shaping redox flux at the branch-point intermediate nornarwedine. Following cytochrome P450–mediated *para–ortho′* phenol coupling of 4′-*O*-methylnorbelladine, nornarwedine occupies a central metabolic node subject to reduction (Figure 3.1). In our previous study, we detected norgalanthamine in some of the replicates in the *in vivo* system upon agroinfiltration of *CYP96T* and *norcraugsodine/noroxomaritidine short-chain*

dehydrogenase/reductase (Lamichhane et al., 2025) (Figure 3.1), whereas AKRs in *Narcissus* and *Lycoris* have been shown to catalyze the reduction of narwedine (Mehta et al., 2024; Xiang et al., 2025). Consequently, the contribution of AKRs to terminal pathway directionality remains unresolved. Similarly, the type of *N*-MTs involved in the AA biosynthesis remains unclear, particularly regarding the final *N*-methylation step leading to galanthamine, for which recent studies reached divergent conclusions (Liyanage et al., 2025; Mehta et al., 2024). Two alternative routes have been proposed: (i) reduction to norgalanthamine by an undidentified reductase, followed by *N*-methylation to yield galanthamine, (ii) *N*-methylation of nornarwedine to narwedine followed by reduction by AKR to galanthamine (Figure 3.1). Critically, direct enzymatic evidence for *N*-methylation of nornarwedine *in planta* is lacking, leaving the order of the terminal reactions unresolved. While our previous work supported the first route by identifying a CNMT-like enzyme capable of converting norgalanthamine to galanthamine (Liyanage et al., 2025), Mehta *et al.* reported evidence for a TMT acting prior to reduction (Mehta et al., 2024).

To clarify the enzymology underlying the final steps of galanthamine biosynthesis, we systematically compared CNMT-like and TMT along with AKRs and NR candidate enzymes from *Leucojum aestivum* using nornarwedine, narwedine, and norgalanthamine as substrates (Figure 3.1). By combining subcellular localization, *in vitro* biochemical assays, and transient expression in *Nicotiana benthamiana*, we identified a Golgi-localized TMT homolog that performs both proposed terminal *N*-methylation reactions. These methylation events are dynamically interconnected by reversible AKR-mediated redox interconversions, thereby reconciling competing terminal pathway models. These findings resolve galanthamine biosynthesis and provide a strategic enzymatic target for metabolic engineering efforts aimed at enhancing galanthamine production.

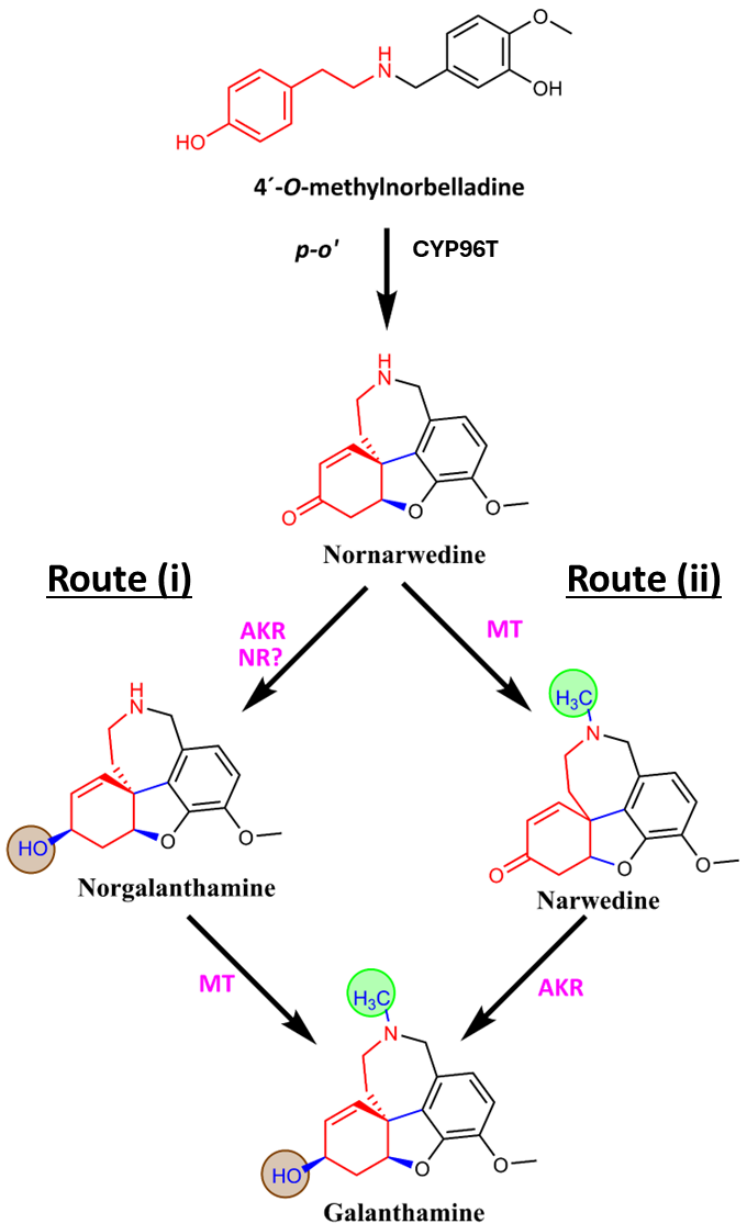


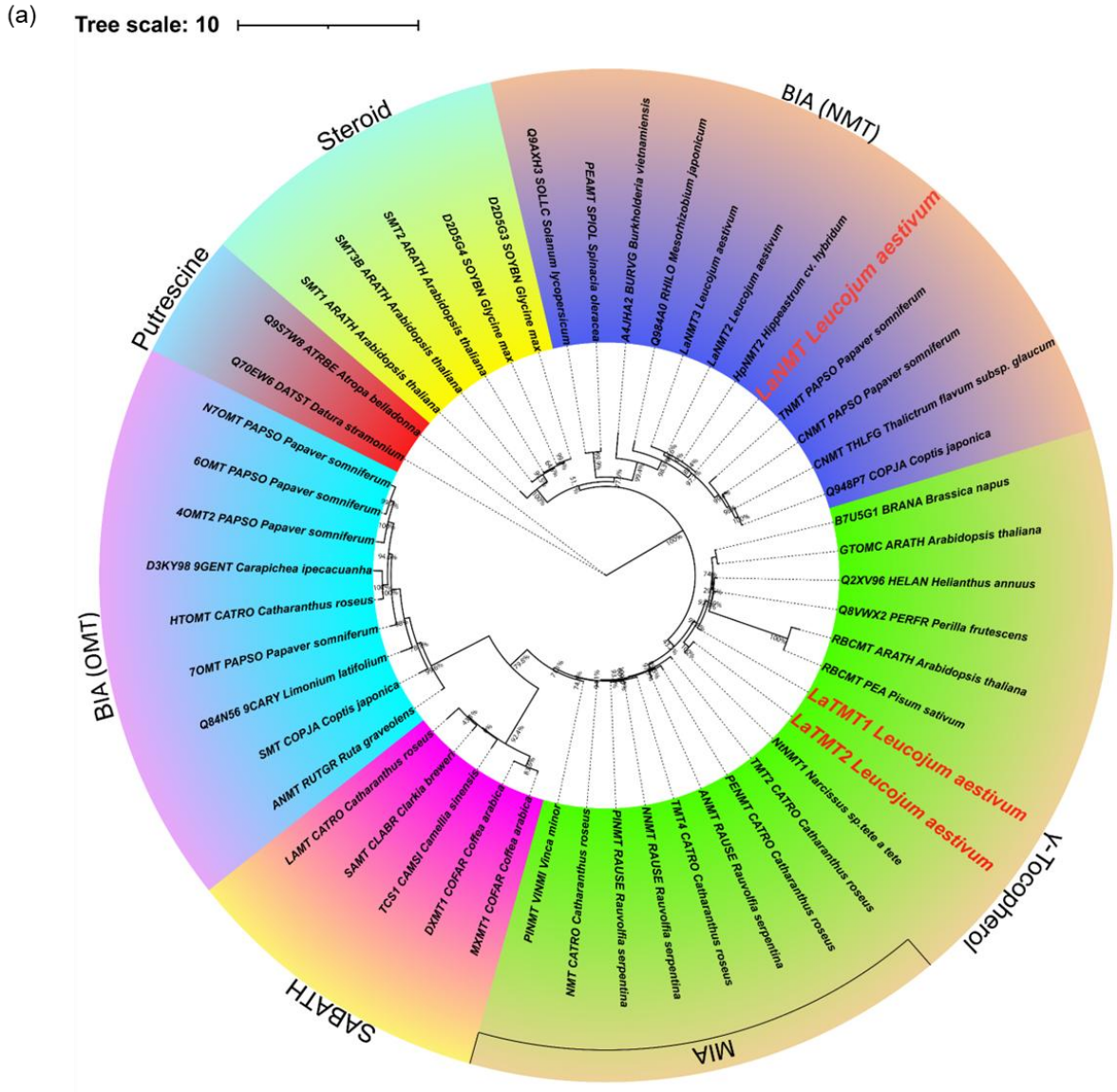
Figure 25. Proposed galanthamine biosynthetic pathway from 4'-*O*-methylnorbelladine.
From the cytochrome P450 (CYP) superfamily, the CYP96 family specifically members of the CYP96T subfamily have been reported to catalyze the *para-ortho'* (*p-o'*) oxidative phenol coupling of 4′-*O*-methylnorbelladine to yield nornarwedine. From there, two competing routes have been proposed: Route (i) with the reduction of nornarwedine to norgalanthamine followed by *N*-methylation, and Route (ii) with the *N*-methylation of nornarwedine to narwedine prior to reduction. Methyltransferase (MT) in pink that performs methylation in green circle and aldo-keto reductase (AKR) in pink that performs reduction as mentioned in brown circle, are the enzymes of this study. Structure in red and black is the backbone from tyramine and 3,4-dihydroxybenzaldehyde, respectively, and blue is newly formed bonds on action of enzymes. Other abbreviations: Noroxomaritidine/norcraugsodine reductase (NR).

3.3. Results

3.3.1. Identification and phylogeny of *N*-methyltransferase candidates

To identify enzymes responsible for the terminal *N*-methylation steps in galanthamine biosynthesis, we mined the *Leucojum aestivum* transcriptome using three TMT reference sequences: *Arabidopsis thaliana* (Uniprot Q9ZSK1), *Catharanthus roseus* Cr2270 (vindoline *N*-methyltransferase; Uniprot W5U2K2), and Cr7756 (picrinine *N*-methyltransferase; Uniprot A0A8X8M501). This search yielded 26, 28, and 29 candidate transcripts per query, respectively. Among them, two *TMT-like* transcripts with the highest sequence similarity with baits were selected for further analysis, together with the previously characterized CNMT-like *La*NMT (Liyanage et al., 2025). Phylogenetic reconstruction using ClustalW alignments within a previously established NMT framework (Liscombe et al., 2010) placed *La*TMT1 and *La*TMT2 in the TMT clade, while *La*NMT clustered with BIA-related CNMTs (Figure 3.2a, Table 3.S1). Notably, *La*TMT2 subclustered with a previously proposed *N*-methylating TMT candidate (*Nt*NMT1) from *Narcissus* cv. Tête-à-Tête (Liscombe et al., 2010; Mehta et al., 2024). *La*TMT2 shares 44% and 16% sequence similarity with *La*TMT1 and *La*NMT, respectively, but exhibits 82% similarity with *Nt*NMT1 (Table 3.S2), supporting its identification as a homolog of *Nt*NMT1. Likewise, *La*TMT1 displays 71% and 61% similarity to canonical vitamin E–synthesizing methyltransferases from *Canna indica* and *Arabidopsis thaliana*, respectively (Table 3.S2). Coding sequences of *LaTMT1*, *LaTMT2*, and *LaNMT* were 1044, 876, and 1065 bp, encoding 348, 292, and 355 amino acids, respectively. Conserved domain analyses (InterProScan, the NCBI Conserved Domain Database, and ScanProsite/ExPASy) confirmed their assignment to the SAM-dependent methyltransferase superfamily. Multiple sequence alignment revealed that all three candidates retained the canonical Rossmann-fold motifs II, III, and IV, and conserved catalytic residues Glu204, Glu207, and His208 (Figure 3.2b). AlphaFold3 structural predictions further revealed that *La*TMT1 and *La*TMT2 were structurally similar (Root mean square deviation (RMSD) = 1.273 Å), while *La*NMT diverged more substantially (RMSD = 3.485 and 3.067 Å, respectively). The N-terminal regions were especially divergent between *La*TMTs and *La*NMT. As expected, *La*NMT superposed well with *C. japonica* CNMT (RMSD = 0.498 Å), while *La*TMT1 and *La*TMT2 were more distant (RMSD = 2.839Å; 2.895 Å, respectively) (Figure 3.S1). The folding of SAM and ligand binding pockets was, however, similar, following the class I

methyltransferase α/β Rossmann-fold, with an active site composed mainly of α-helices, and four of the seven conserved β-sheets pointing towards SAM (Figure 3.S1). The catalytic residues Glu204, Glu207, and His208, as well as the active-site Tyr81 (Tyr72 for *La*TMT1, Tyr17 for *La*TMT2), were oriented towards the superposed CNMT substrate nitrogen. Overall, the predicted structures highlighted divergence in the N-terminal region among the candidate MT enzymes, together with pocket compatible with isoquinoline-like alkaloids as substrates for SAM-dependent *N*-methylation. Despite the lack of prior mechanistic studies on plant TMTs, the conservation of the sequence and conformation of the putative catalytic residues' Glu-Glu-His motif in NMTs suggests a possible shared mechanism.



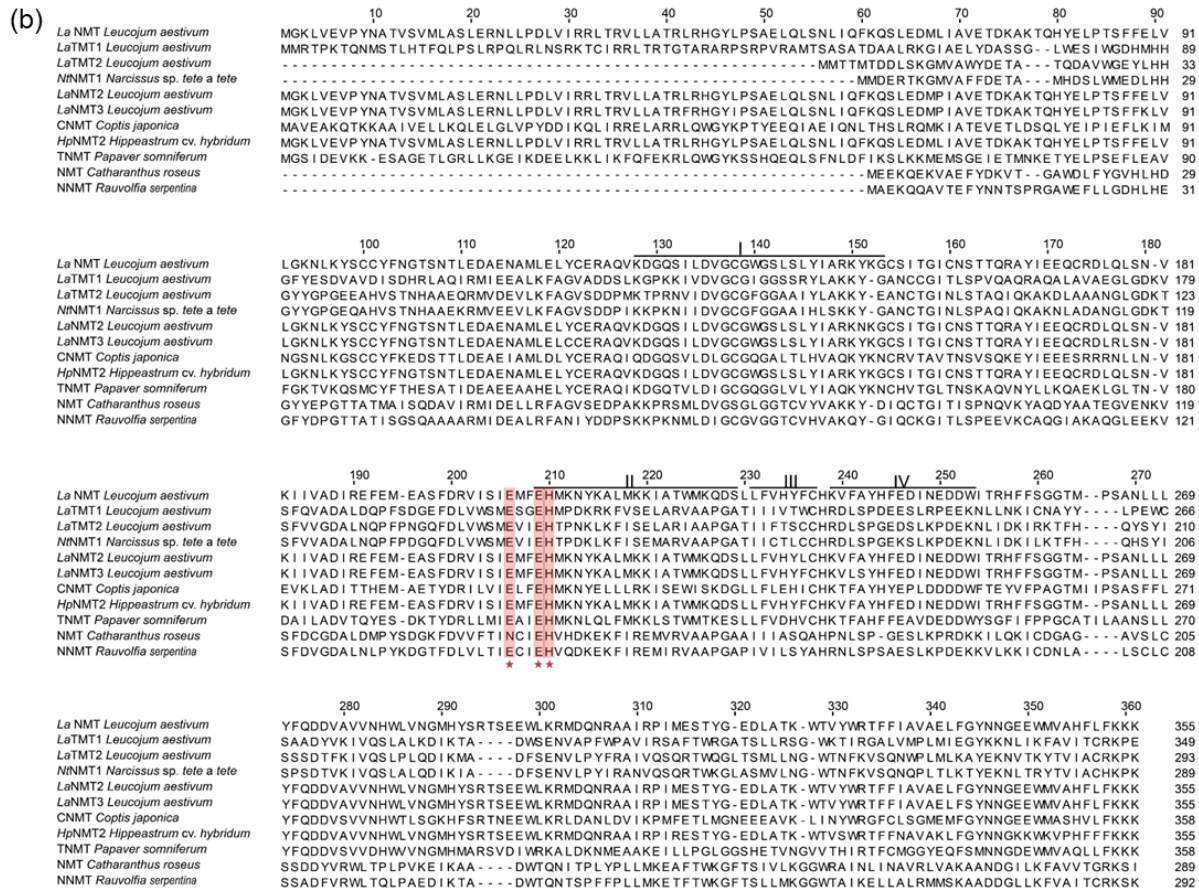


Figure 26. Phylogenetic analysis and sequence alignment of *N*-methyltransferase candidates in Amaryllidaceae alkaloid biosynthesis.

(a) The Phylogenetic tree was constructed using the Maximum Likelihood method with 1000 bootstraps. This analysis involved 50 amino acid sequences. Evolutionary analyses were conducted in IQ-Tree and viewed in ITOL software. The transcripts highlighted in bold red font are those included in the present study. The accessions or sequences are listed in Table 3.S1. BIA and MIA stand for benzylisoquinoline alkaloids and monoterpene indole alkaloids. (b) Multiple sequence alignments of 11 sequences, including the first three candidates selected in this study. I, II, III, and IV are the SAM binding sites from different species, and the star represents the residues of the catalytic triad for substrate binding.

3.3.2. Identification and phylogeny of aldo-keto reductase candidates

Using *Narcissus* cv. Tête-à-Tête *NtAKR1* as bait (Mehta et al., 2024), four sequences with more than 75% sequence identity with the bait were identified in our transcriptome database. The two longest sequences were selected and named *La*AKR1 and *La*AKR2. While amplifying from cDNA, a third sequence, *LaAKR3,* with 8 amino acid differences relative to *AKR2*, was identified (Figure 3.S2). Sequences of *LaAKR1*, *LaAKR2*, and *LaAKR3* were 963, 975, and 975 bp, respectively, encoding proteins with approximate molecular weights of 36.27, 37.09, and 36.97

kDa, respectively. The NCBI Conserved Domain Database confirmed their assignment as NAD(P)H-dependent AKR4A and 4B family. Phylogenetic analysis by maximum likelihood using 1000 bootstraps revealed class 4B as a distinct clade, grouping enzymes from plants that produce specialized metabolites (Figure 3.S3a, Table 3.S3). Multiple sequence alignment with crystallized and previously characterized AKR sequences of *Papaver somniferum* and *Zea mays* confirmed the presence of the conserved catalytic tetrad Asp50, Tyr55, Lys84, and His117 in the candidates (Figure 3.S3b). *La*AKR3 shares 86% and 98% sequence similarity with *La*AKR1 and *La*AKR2, respectively, and 92% and 81% similarity with the characterized AKRs from *Lycoris aurea* (Xiang et al., 2025) and *Narcissus* cv. Tête-à-Tête (Mehta et al., 2024), respectively (Table 3.S4). The AlphaFold3 structural predictions of AKR candidates superposed with the reference crystal structure *Ec*AKR from *Echinochloa colona* (PDB:7F7L) (Li et al., 2022) revealed that *La*AKR1 was more similar to 7F7L (RMSD=0.669 Å) than were *La*AKR2 and *La*AKR3, deviating by 2.422 Å and 2.387 Å from the reference, respectively, with a longer and more exposed C-terminal α-helix for *La*AKR2 (Figure 3.S4a). Nonetheless, superimposition confirmed the similarity between the structures (Figure 3.S4a), with NADPH and the catalytic tetrad clearly superimposed, in a configuration consistent with aldo-keto substrate reduction (Figure 3.S4b).

3.3.3. Leaf-specific AA biosynthesis and relative expression of candidate genes in *L. aestivum*

To assess the biosynthetic capacity of *L. aestivum* leaves, targeted LC-MS/MS metabolite profiling detected *N*-methylated alkaloids lycoramine and galanthamine, along with AA intermediates, including tyramine, phenylalanine, haemanthamine, norgalanthamine, dopamine, vittatine (or crinine), 4'-*O*-methylnorbelladine, L-tyrosine, 3,4-dihydroxybenzoic acid, 4-hydroxybenzoic acid, and norbelladine (Figure 3.S5). Notably, several metabolites predicted in the pathway, including 3,4-dihydroxybenzaldehyde, 3′,4′-*O*-dimethylnorbelladine, 3′-*O*-methylnorbelladine, 9-*O*-demethylhomolycorine, and tazettine, previously reported (Ptak et al., 2020; Szlávik et al., 2004) in the genus, were not detected in any replicate of this organ. A broader absence was noted for additional biosynthetically or structurally related phenolic intermediates such as caffeic acid, *p*-coumaric acid, ferulic acid, isoferulic acid, vanillin, and levodopa, suggesting either abundance below detection limits, tissue-specific biosynthesis, or pathway divergence. 11-Hydroxyvittatine, lycorine, and sanguinine were detected at low signal intensity in all samples; however,

confirmation was not possible due to insufficient spectral quality. Untargeted metabolite screening was also performed using GC-MS, resulting in the detection of four previously unreported masses (m/z 207, 420, 476, and 490) in the nonpolar fraction (Figure 3.S6a- g). A complete list of both detected and undetected metabolites is provided in Table 3.S5 along with the documented metabolites in either leaves or shoots cultures or bulbs of *L. aestivum* (Table 3.S6). Altogether, these results confirmed that leaves are active tissues for galanthamine and precursors accumulation and provided a metabolic context for enzyme function.

To determine whether the metabolite accumulation observed in leaves is supported by transcriptional regulation of pathway genes, we analyzed the tissue-specific expression of candidate genes encoding enzymes involved in galanthamine biosynthesis in *L. aestivum* organs using RT–qPCR (Figure 3.3). Distinct expression patterns were observed across bulb, leaf, and flower tissues. Genes associated with the early step of the galanthamine pathway, like *LaCYP96T2, LaOMT* and *LaNR,* showed higher transcript abundance in bulbs (for example, the mean relative expression of *La*CYP96T2 in bulb is 0.5040 vs 0.1932 in leaf, $^{**}p < 0.0078$). In contrast, several downstream tailoring enzymes exhibited elevated expressions in leaves, including *LaTMT1*, *LaTMT2*, *LaNMT*, *LaAKR2*, and *LaAKR3* ($^{*}p < 0.0232$ and $^{**}p < 0.0082$). In combination with the expression patterns, the metabolite profiling results support the leaf tissue as a site of late-stage galanthamine biosynthesis, where reductive and methylation reactions are transcriptionally enriched.

To further examine whether the transcriptional and metabolite profiles observed in leaves correspond to the occurrence of active enzymatic conversions, crude protein extracts from *L. aestivum* leaves were subjected to *in vitro* assays following extensive dialysis to remove endogenous metabolites and cofactors. When norgalanthamine was supplied as substrate in the presence of SAM, the dialyzed crude extract catalyzed the *N*-methylation to form galanthamine (Figure 3.S7a). When nornarwedine was used as a substrate in the presence of SAM and NADPH, the crude extract catalyzed *N*-methylation, and/or reduction to form narwedine, norgalanthamine, and galanthamine, indicating that these reactions are catalyzed by enzymes present in the leaf-extract (Figure 3.S7b). Together with tissue-specific transcripts accumulation and metabolite profiling data, these results provide functional evidence that *L. aestivum* leaf tissue harbors the enzymatic machinery required to support late-stage galanthamine biosynthesis.

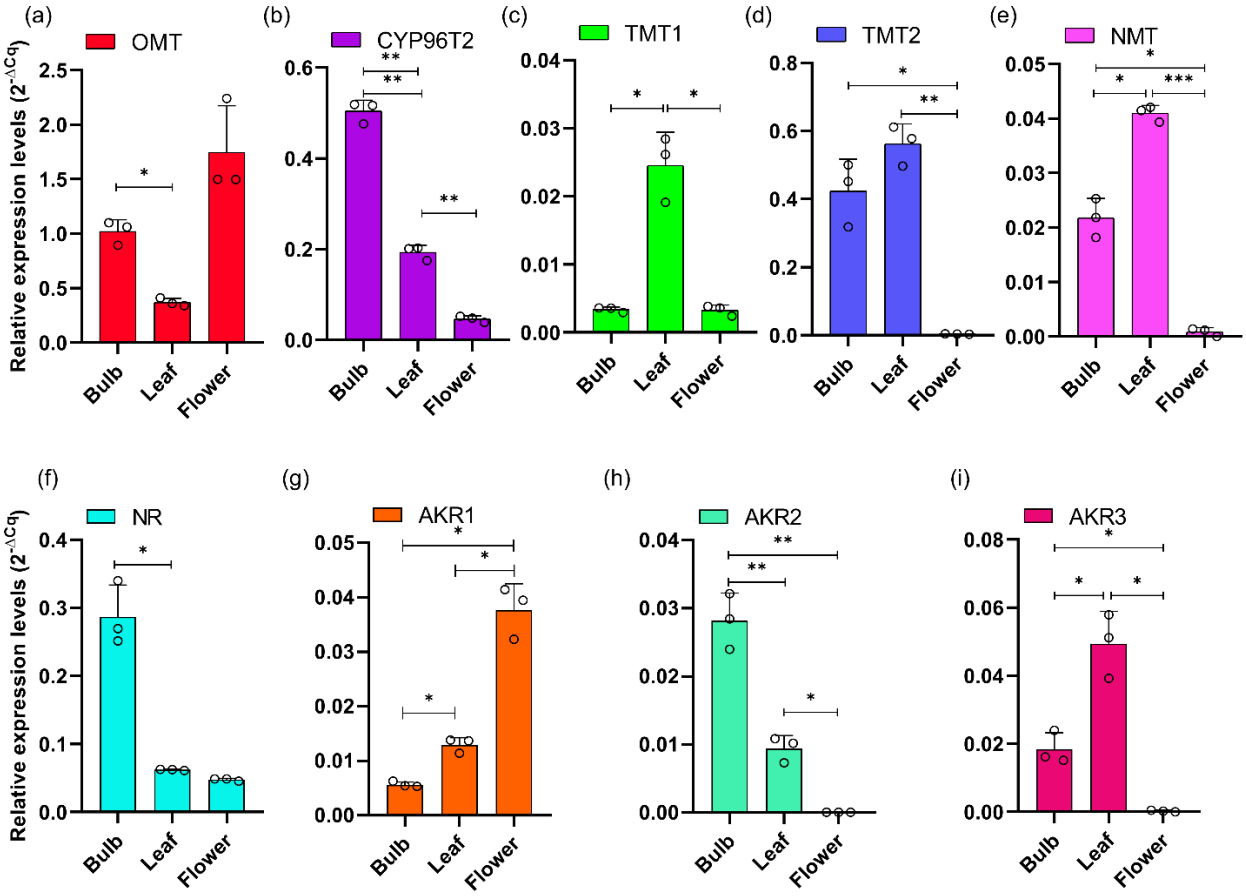


Figure 27. Tissue-specific expression analysis of genes encoding enzymes involved in galanthamine biosynthesis in *Leucojum aestivum*.

Relative transcript abundance of candidate pathway genes was determined by RT–qPCR using RNA isolated from bulb, leaf, and flower tissues of *L. aestivum*. Expression profiles are shown for **(a)** *La*N4ˈOMT **(b)** *La*CYP96T2 **(c)** *La*TMT1 **(d)** *La*TMT2 **(e)** *La*NMT **(f)** *La*NR **(g)** *La*AKR1 **(h)** *La*AKR2 **(i)** *La*AKR3. Expression levels were normalized against *Histone3* as the internal reference gene. Data represent mean ± SE of three technical replicates derived from pooled biological triplicates.

3.3.4. *La*TMT1, *La*TMT2, and *La*NMT localize in distinct compartments

Signal peptide prediction using TargetP-2.0 indicated a high likelihood of chloroplast transit peptide for *La*TMT1 (score: 0.8761), whereas *La*TMT2 and *La*NMT were predicted as "other" with organelle-targeting signals (scores: 0.9986 and 0.9979, respectively) with the remaining likelihood out of 1 was extremely low for subcellular destinations (Table 3.S7). To experimentally

determine their subcellular localization, *La*NMT, *La*TMT1 and *La*TMT2 coding sequences were cloned into the pB7FWG2 expression vector to generate C-terminal EGFP fusion constructs.

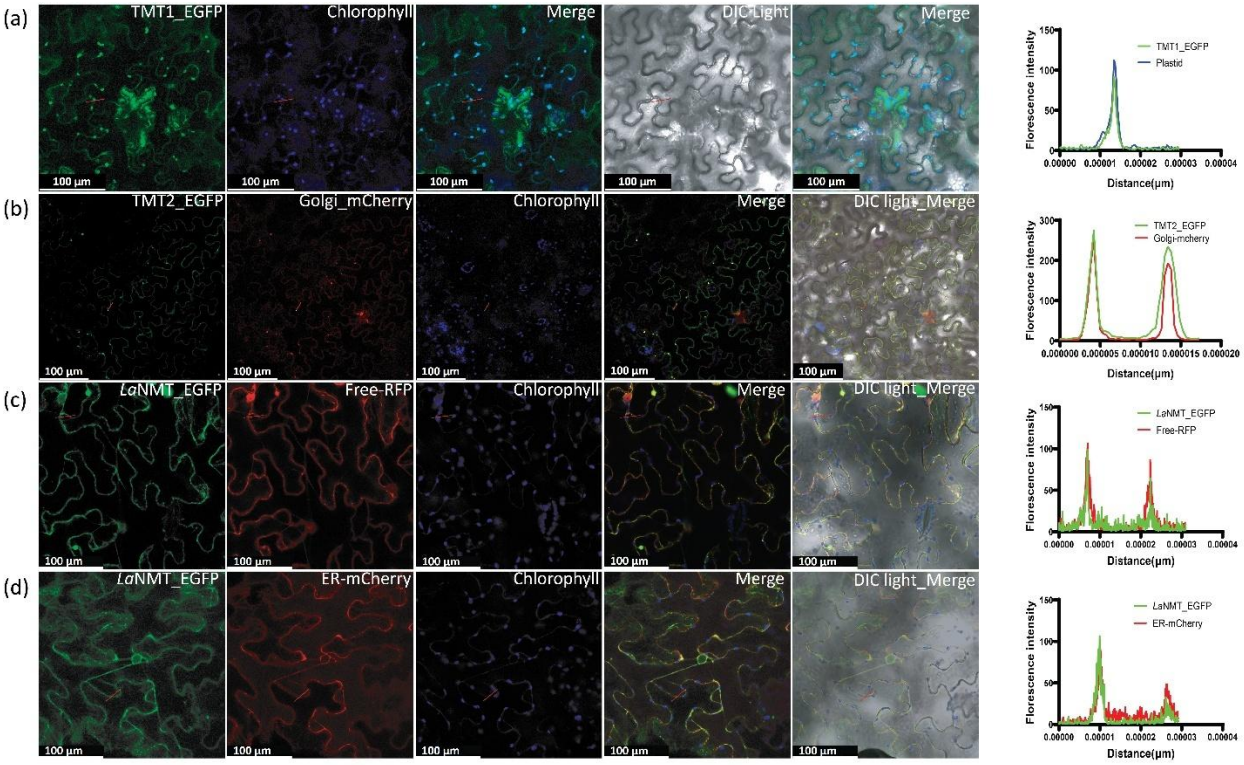


Figure 28. Subcellular localization of *La*TMT1, *La*TMT2 and *La*NMT proteins in *Nicotiana benthamiana*.
(a) Panel showing C-terminal-EGFP-fusion *La*TMT1 with chlorophyll autofluorescence. (b) panel showing co-agroinfiltrated C-terminal-EGFP-fusion-*La*TMT2 with Golgi-mcherry marker. (c) Panel showing co-agroinfiltrated C-terminal-EGFP-fusion-*La*NMT with free RFP marker. (d) Panel showing co-agroinfiltrated C-terminal-EGFP-fusion-*La*NMT with ER-mCherry. The histogram of the right in each panel shows the fluorescence intensity profile of respective panel. Scale bars resemble 100 µm. Image processed in Adobe illustrator software.

These constructs were transiently co-expressed in *Nicotiana benthamiana* leaves alongside organelle-specific fluorescent markers(Nelson et al., 2007): free RFP (nucleus; cytosol), ER-rk *CD3-959* (endoplasmic reticulum- mCherry), and G-rk *CD3-967* (Golgi bodies-mCherry). Confocal laser scanning microscopy was performed 48 hours post-infiltration to assess the subcellular distribution of the fusion proteins. Distinct localization patterns were observed for each candidate. The *La*TMT1-EGFP fusion protein displayed a punctate and reticulated fluorescence pattern consistent with chloroplast localization, showing clear overlap with the intrinsic chlorophyll autofluorescence (Figure 3.4a). In contrast, *La*TMT2-EGFP signal co-localized with Golgi-mCherry, indicating Golgi targeting (Figure 3.4b). As previously reported, *La*NMT-EGFP exhibited a dispersed fluorescence signal throughout the cytosol and a partial overlap with ER-mCherry (Figure 3. 4c & 3.4d). This differential compartmentalization suggests distinct functional niches, potentially minimizing cross-reactions while supporting pathway efficiency in distinct metabolic landscape inside the cell.

3.3.5. Docking supports promiscuous biosynthetic machinery from *N*-methylation to carbonyl reduction

To investigate the catalytic potential of the candidates, we performed molecular docking. SAM was positioned in the binding pocket based on superimposition with the *Cj*CNMT crystal structure (PDB: 6GKV). Substrate-binding poses were analyzed for both norgalanthamine and nornarwedine, the two hypothesized intermediates in galanthamine biosynthesis. The two very similar ligands shared comparable docking scores, positioning, and interaction patterns, reflecting a common binding mode across the tested enzymes. All three enzymes yielded docking scores ranging from -6.3 to -6.8 kcal/mol (Table 3.1, Figure 3.5). *La*TMT2 showed the shortest substrate-SAM distances (3.2 Å) and the most favorable S–C:N–C dihedral angles (149.1° and 159.5° for norgalanthamine and nornarwedine, respectively), consistent with a catalytically competent SN2 geometry. *La*TMT1 showed distances at the upper limit (3.4-3.5 Å) but favorable angles (164–175°). In contrast, *La*NMT showed comparable distances (3.3 Å) but dihedral angles far from the optimal 180° (-85.9° and -72.7°), suggesting suboptimal catalytic geometry toward both substrates despite productive binding. In *La*NMT, norgalanthamine binding was stabilized by a conserved hydrophobic core involving Phe234 and Phe257, as well as hydrogen bonds with Tyr98, Glu204, and His208. Notably, Glu204 and Tyr98 formed a direct bond with the substrate amine. Interactions with His208 and Glu204 were lost upon docking nornarwedine. *La*TMT1 featured hydrophobic contacts from Leu71, Trp83, and Tyr260, with Tyr72 and Glu206 forming hydrogen bonds with the substrate nitrogen. For *La*TMT2, norgalanthamine's hydrophobic interacting residues included Trp27, Leu31, and Phe204. Tyr17, His33, and His151 contributed polar contacts, with Tyr17 and His151 directly interacting with the substrate amine. Nornarwedine was stabilized by two additional hydrophobic bonds with Trp16 and Glu147. Tyr17 interaction with the amine was conserved. These results support the catalytic potential of *La*NMT for norgalanthamine, as docking led to interactions with the catalytic Glu204 and His208 (Figure 3.5). *La*TMT1 could accommodate both substrates, although the distance between the amine and SAM was the highest among the three candidates (Table 3.1). *La*TMT2 exhibited the most compact and enclosed binding cavity with a favorable substrate-SAM geometry. The ability of all three enzymes to stably bind both norgalanthamine and nornarwedine *in silico* suggests functional promiscuity.

Table 3. 3. *L. aestivum N*-MT candidates' interactions with docked norgalanthamine and nornarwedine.

Substrate (Ligand	Enzyme	Score (kCal/mol)	Distance C-N (Å)	S-C:N-C dihedral	Interactions	
					Hydrophobic	H-bonds
Norgalanthamine	*La*NMT	-6.3	3.3	-85.9°	Glu207, Phe234, Phe257 (n=3)	Glu204 (N), Tyr98 (N), His208
	*La*TMT1	-6.8	3.5	164°	Tyr260, Trp83, Leu71	Tyr72 (N), Glu206 (N), Tyr260
	*La*TMT2	-6.7	3.2	149.1°	Trp27, Leu31, Phe204	Tyr17 (N), His33, His151 (N)
Nornarwedine	*La*NMT	-6.3	3.3	-72.7°	Glu207, Phe234, Phe257 (n=3), Phe337	Tyr98 (N)
	*La*TMT1	-6.6	3.4	175°	Leu71, Trp83, Tyr260 (n=2)	Tyr72 (N), Glu206 (N)
	*La*TMT2	-6.5	3.2	159.5°	Trp16, Trp27, Leu31, Glu147, Phe204	Tyr17 (N), His33

The binding score is expressed in (kCal/mol). The distance between the substrate and methyl donor was measured between the amine of norgalanthamine or nornarwedine and the carbon of the methyl group of SAM. The S–C:N–C dihedral angle was measured between the SAM sulfur, the methyl carbon, the substrate nitrogen, and the adjacent carbon, as an indicator of SN2 catalytic competence.

Extending the docking analysis to reductase candidates revealed a similar pattern of promiscuity. The predicted ligand positions were consistent with the reduction of the C=O bond for narwedine and nornarwedine inside *La*AKR1, 2 and 3 (Figure 3.S8a-c), although an alternative reduction of the endocyclic C=C bond cannot be excluded. Ligands interacted with catalytic Tyr54 in all cases via both H-bonds and hydrophobic interactions, suggesting a key role in the reaction. H-bonds between C=O and Tyr54 were detected for both substrates in *La*AKR2 and *La*AKR3; in *La*AKR1, NADPH engaged preferentially with nornarwedine, and His117 formed a hydrogen bond specifically with narwedine, an interaction absent in *La*AKR2 and *La*AKR3 (Table 3.S8, Figure 3.S8). To further assess the geometry of hydride transfer, distances between the C4 atom of the NADPH nicotinamide ring and the acceptor carbons were measured (Table 3.S8). C4–C(carbonyl) distances ranged from 3.4 to 3.6 Å across isoforms, while C4–C(olefinic) distances ranged from 3.2 to 3.7 Å, with *La*AKR3 showing the shortest distance for narwedine (3.2 Å). Asp49 contributed to NADPH stabilization via salt bridges with Lys261/262 and Arg267/268 in all isoforms, consistent with its established role in cofactor binding.

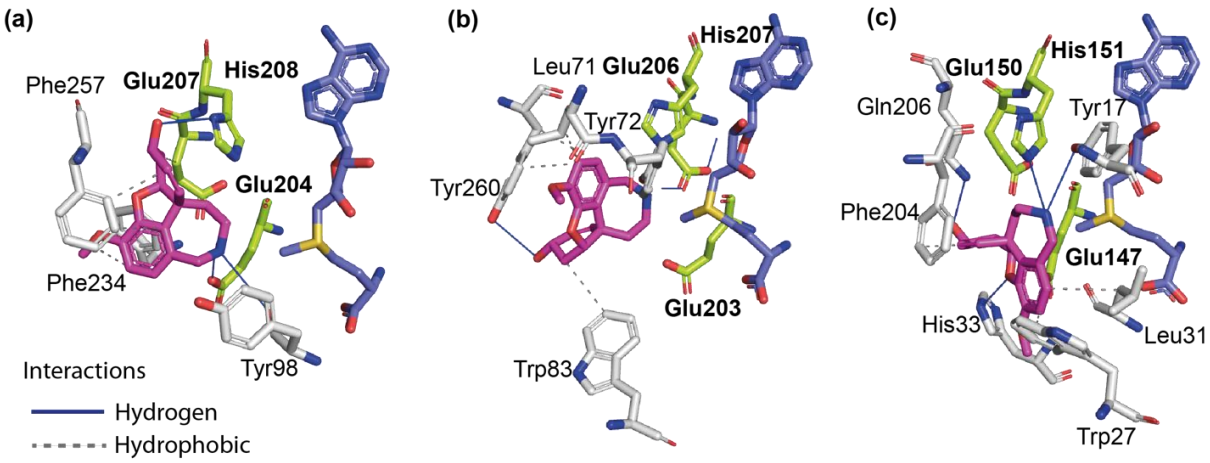


Figure 29. Docking poses and active site interactions of norgalanthamine within the predicted structures of *N*-methyltransferase candidates.
(a) *La*NMT, (b) *La*TMT1, and (c) *La*TMT2. In all panels, the ligand norgalanthamine is shown as pink sticks, SAM as purple sticks, and interacting residues are represented as grey sticks. Putative catalytic residues corresponding to the conserved triad are shown as lime sticks. Hydrophobic interactions are depicted as dashed grey lines, and hydrogen bonds as solid blue lines. The orientation is preserved across panels to enable comparison of ligand positioning and interaction networks within the active sites.

3.3.6. *La*TMT2 exhibits superior catalytic activity *in vitro* and *in vivo*

To evaluate the enzymatic activity of *La*NMT, *La*TMT1, and *La*TMT2, we conducted both *in vitro* and *in vivo* assays using nornarwedine and norgalanthamine as substrates. Maltose binding protein (MBP) and EGFP tags served as negative controls, and papaverine was included as an internal standard for LC-MS/MS analysis. In the *in vitro* assays, all proteins were expressed as N-terminal MBP fusion constructs. *La*TMT1 (~82 kDa) was found to be insoluble. To overcome this, the predicted signal peptide was removed, yielding a truncated version (Δ*La*TMT1) that could be purified as a soluble protein. SDS-PAGE confirmed expected band sizes of ~75 kDa (Δ*La*TMT1), ~76 kDa (*La*TMT2), and ~84 kDa (*La*NMT) (Figure 3.S9a). When using nornarwedine as a substrate for enzymatic assays, LC-MS/MS analysis showed that crude *La*TMT1 and purified Δ*La*TMT1, along with *La*NMT, exhibited detectable activity above control MBP background, though not statistically significant (*La*TMT1 0.0022 ± 0.0016; Δ*La*TMT1= 0.0225 ±0.0025; *La*NMT = 0.0203 ± 0.0026, respectively). By contrast, *La*TMT2 catalyzed the formation of narwedine with a 17-fold increase over MBP background and a 9-fold increase over *La*NMT ($p <$ 0.0001, Figure 3.6a), indicating higher activity. Similarly, using norgalanthamine as a substrate, galanthamine production was detectable in reactions with Δ*La*TMT1 and *La*NMT, but *La*TMT2

showed the highest catalytic efficiency, producing ~6-fold more galanthamine than the other enzymes ($p < 0.0001$, Figure 3.6b).

We further proceed to fully characterize the *La*TMT2 enzyme by testing its activity on norgalanthamine and nornarwedine at various enzyme concentrations, temperatures, incubation times, buffer pH, and substrate concentrations. At 30 °C to 35 °C, the enzyme activity for both substrates was optimal with an incubation time of at least 3 hours, reaching a plateau at pH 7.5 (Figure 3.S10a-f). Enzyme kinetic characterization of *La*TMT2 was performed with norgalanthamine and nornarwedine as substrates under optimized *in vitro* conditions. Michaelis–Menten analysis revealed comparable substrate affinities, with Km values of 353.2 ± 28.5 μM for norgalanthamine and 332.2 ± 28.7 μM for nornarwedine. The corresponding maximal velocities (Vmax) were 4.5 and 5.5 $nmol \cdot min^{-1} \cdot \mu g^{-1}$, respectively. Turnover numbers (kcat) were 0.225 ± 0.008 s^{-1} for norgalanthamine and 0.284 ± 0.010 s^{-1} for nornarwedine (Table 3.2, Figure 3.6c). We also examined the enzyme's substrate preference in mixed-substrate assays, in which both substrates were supplied at either similar concentrations or one at half-concentration in a single-pot reaction incubated 3 hours in 30 °C with buffer at pH 7.5. The amount of product formed indicated a preference for nornarwedine over norgalanthamine of more than 1.5 % (Figure 3.6d).

To confirm these findings *in planta*, the three candidates were transiently expressed in *N. benthamiana*. Immunoblotting confirmed expression of EGFP-3HA (~30.1 kDa), *La*TMT2-3HA (~35.7 kDa), *La*TMT1-3HA (~41.9 kDa), and *La*NMT-3HA (~44.6 kDa) (Figure 3.S9b). Δ*La*TMT1 was omitted in the *in vivo* assay, as it was not necessary to purify the proteins afterwards. *La*NMT produced galanthamine *in vivo*, but was unable to methylate nornarwedine, whereas *La*TMT*1* catalyzed *N*-methylation of nornarwedine, but not its reduced counterpart. In agreement with the *in vitro* results, *La*TMT*2* expression led to the highest accumulation of narwedine, with 50-fold and 120-fold increases over *La*TMT1 and *La*NMT, respectively ($p < 0.0001$, Figure 3.6e). When infiltrated with norgalanthamine, *La*TMT2 yielded at least a 6-fold higher galanthamine accumulation than all other enzymes ($p < 0.0001$, Figure 3.6f), confirming its superior activity across both substrates and systems. Taken together, these results establish *La*TMT2 as a robust, substrate-promiscuous *N*-methyltransferase, outperforming both *La*TMT1 and *La*NMT *in vitro* and *in planta* settings. Its consistent activity toward two structurally related intermediates highlights its potential as a key enzyme in galanthamine biosynthesis.

Table 3. 2.Michaelis-Menten enzyme kinetic parameters for *La*TMT2 with respect to nornarwedine and norgalanthamine.

Substrate	Km (µM)	Vmax (nmol. min^{-1}. μg^{-1})	Kcat (s^{-1})	Kcat/Km (M. s^{-1})
nornarwedine	332.2 ± 28.7	5.68	0.284 ± 0.010	$8.55x10^2$
norgalanthamine	353.2 ± 28.5	4.50	0.225 ± 0.007	$6.37\ x10^2$

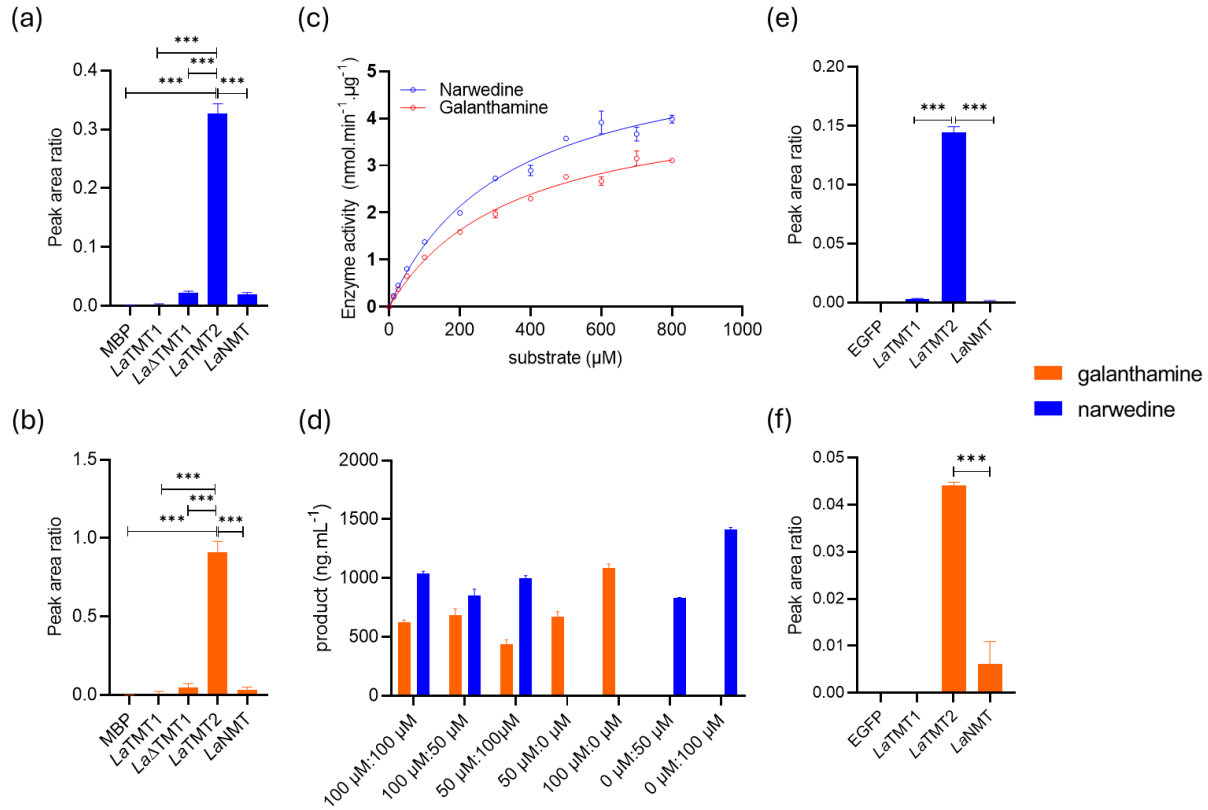


Figure 30. *In vitro* and *in vivo* enzymatic assay by candidate N-methyltransferases.
(a) *In vitro* enzymatic assay using nornarwedine as substrate. (b) *In vitro* enzymatic assay using norgalanthamine as substrate. (c) *In vitro* enzyme activity of *La*TMT2 using norgalanthamine and nornarwedine as substrate. (d) Catalytic conversion of substrates norgalanthamine: nornarwedine by *La*TMT2 in a single pot reaction at various ratios. (e) *In vivo* enzymatic assay using nornarwedine as substrate. (f) *In vivo* enzymatic assay using norgalanthamine as substrate.

3.3.7. *La*TMT1 is a putative classical tocopherol methyltransferase

To further investigate *La*TMT1, *in vitro* enzymatic assays were performed to evaluate the catalytic activity using γ-tocopherol as substrate in the presence of SAM as the methyl donor (Figure

3.S11a). Docking suggested that γ- tocopherol fit in the active site of *La*TMT1 in a bent conformation comparable to that of 1R5L(Min et al., 2003), an α-tocopherol transferase from *Homo sapiens* (Figure 3.S11b; Table 3.S9). The full-length enzyme, expressed as an *N*-terminal MBP fusion, was largely insoluble, consistent with the presence of a predicted *N*-terminal chloroplast-targeting signal peptide. To obtain soluble protein suitable for biochemical analysis, we generated a truncated construct lacking this signal (Δ*La*TMT1), which yielded a readily purifiable enzyme. Enzymatic assays were performed using crude extract/inclusion bodies containing full-length *La*TMT1 (c.*LaTMT*1), purified Δ*La*TMT1, and MBP alone together with other negative controls, boiled enzyme and no enzyme with substrate. Reaction mixtures were analyzed by LC–MS/MS using MRM mode demonstrated that ΔLaTMT1 produced significantly higher α-tocopherol (~17 µg/mL) compared to crude c.*La*TMT1 (~6 µg/mL) whereas the MBP negative control did not show any product (Figure 3.S11c) confirming enzyme-dependent product formation. To further verify product identity, the reaction mixture was analyzed on LC-MS/MS in product ion mode and the resulting fragmentation spectrum displayed matching fragmentation profile as that of authentic α-tocopherol (Figure 3.S11 d, e). These results confirm *La*TMT1 as a functional γ-tocopherol methyltransferase, functionally distinct from the alkaloid *N*-methyltransferase.

3.3.8. *La*AKR isoforms catalyze reversible redox interconversion

To assess AKR candidates' ability to catalyze the reductive tailoring steps of the galanthamine biosynthetic pathway, we measured enzyme activities using purified recombinant proteins under *in vitro* conditions. Reductive assays conducted in the presence of NADPH confirmed that all three *La*AKR isoforms catalyze the reduction of nornarwedine to norgalanthamine and narwedine to galanthamine. However, substantial differences in catalytic efficiency were observed. *La*AKR3 exhibited the highest specific activity, producing ~90 ng/mL norgalanthamine from nornarwedine and ~144 ng/mL galanthamine from narwedine per µg of enzyme ($p < 0.0001$; Figure 3.7 a, c). *La*AKR2 displayed intermediate activity, whereas *La*AKR1 catalyzed comparatively lower reductive conversion. In contrast, *La*NRII demonstrated negligible reductive activity of nornarwedine to norgalanthamine; in one of three biological replicates, yielding 1.8 ng/mL per µg enzyme, not significantly different from negative controls ($p < 0.0001$; Figure 3.7a), indicating that *La*NRII does not substantially contribute to this reductive step.

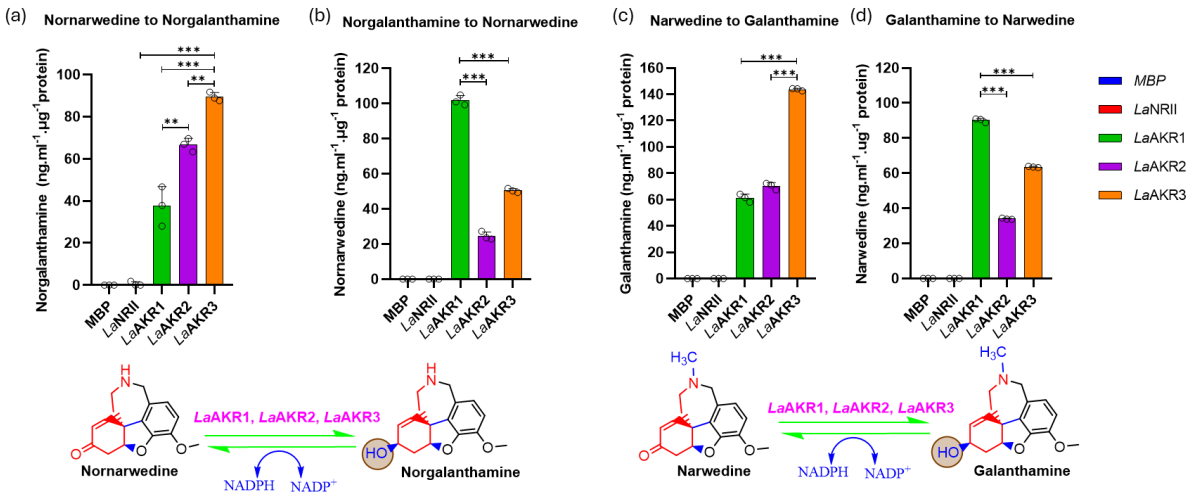


Figure 31. Reductive and oxidative activities of AKR enzymes in late stage of galanthamine pathway.
Bar graphs show LC–MS/MS–quantified product formation from *in vitro* assays using purified MBP (-ve control), *La*NRII, *La*AKR1, *La*AKR2 and *La*AKR3. Metabolite levels are normalized to total protein used (ng mL^{-1} μg^{-1} protein) and presented as mean ± SD (n = 3 independent assays) after subtracting the background. Statistical significance was determined by one-way ANOVA with Tukey's multiple-comparison test (* * **P** < 0.001; * * * **P** < 0.0001). Below the bar diagram is a schematic representation of NADPH/$NADP^+$-dependent reversible reductions catalyzed by *La*AKR isoforms showing interconversion between nornarwedine and norgalanthamine (left) along with narwedine and galanthamine (right).

When reactions were conducted under oxidative conditions ($NADP^+$), the three AKR isoforms exhibited distinct directional preferences. *La*AKR1 showed the highest oxidative activity, catalyzing the reverse conversion of norgalanthamine to nornarwedine and galanthamine to narwedine with significantly greater efficiency than *La*AKR2 and *La*AKR3 ($p < 0.0001$; Figure 3.7b, d). In contrast, *La*AKR3 showed a clear bias toward the pathway's reductive direction. To further investigate potential alternative products generated during AKR-mediated reductions, we performed comprehensive metabolite profiling of both *in vivo* and *in vitro* reactions using LC–MS/MS operated in positive electrospray ionization mode with a scan range of *m/z* 100–400. In reactions supplied with nornarwedine, an additional ion corresponding to *m/z* 274 $[M+H]^+$ was consistently detected at a retention time of ~14 min in assays containing *La*AKR enzymes, clearly distinct from the authentic norgalanthamine peak at ~8.5 min (Figure 3.S12a, b). Product-ion fragmentation analysis of *m/z* 274 $[M+H]^+$ revealed a spectrum closely resembling that of nornarwedine, suggesting preservation of the core alkaloid scaffold (Figure 3.S13a, b). Based on the observed mass shift and fragmentation pattern, this metabolite likely represents a reduced derivative arising from C2–C3 bond reduction, tentatively corresponding to dihydronornarwedine or norlycoraminone (Figure 3.8). In addition, *La*AKR1 produced a second *m/z* 274 species eluting

at 16.72 min whose fragmentation profile closely matched that of norgalanthamine, consistent with formation of the stereoisomer epi-norgalanthamine (Figure 3.8; Figure 3.S12a, 3.S13c, 3.S13d).

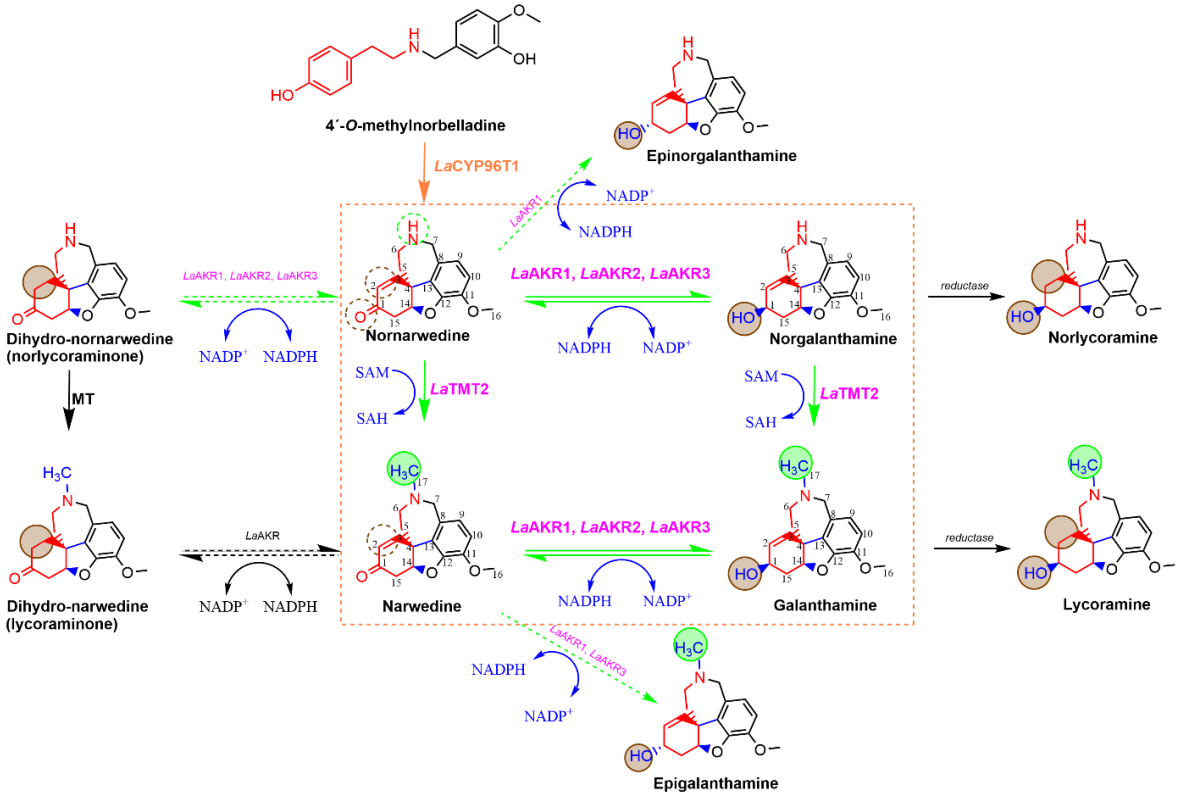


Figure 32. Identified biosynthetic pathway leading to galanthamine.
Solid green arrows denote biosynthetic steps elucidated and experimentally validated in this study using authentic standards, whereas dashed green arrows indicate reactions supported by biochemical evidence but awaiting confirmation with purified reference compounds. Enzymes shown in bold pink represent functionally characterized proteins, while pink subscript annotations indicate candidate enzymes whose activities require further validation with authentic standards. Orange arrows and labels correspond to previously characterized enzymatic steps. Black arrows annotated by enzyme class represent hypothetical transformations that remain uncharacterized. Green dotted circles mark methylation sites and brown circles indicate reduction sites, with filled circles representing the corresponding post-enzymatic products. Reactions enclosed within the orange box highlight pathway steps experimentally confirmed in the present study. MT, methyltransferase; SAM, *S*-adenosylmethionine; NADPH, nicotinamide adenine dinucleotide phosphate.

Similarly, when narwedine was used as substrate, LC–MS/MS analysis detected an additional ion at *m/z* 288 $[M+H]^+$ eluting at ~17 min (Figure 3.S14) in reactions catalyzed by *La*AKR1 and *La*AKR3, in addition to the canonical galanthamine peak at ~11 min. Product ion fragmentation of this later-eluting metabolite closely mirrored that of galanthamine, supporting its assignment as the stereoisomer epi-galanthamine (Figure 3.S15). These findings indicate that AKR-catalyzed reductions generate not only the canonical pathway intermediate, but also alternative reduced and

stereoisomeric derivatives, highlighting previously unrecognized catalytic plasticity in the late stages of galanthamine biosynthesis.

To assess *in vivo* relevance of *La*AKR1-3 activity, we used *Agrobacterium*-mediated transient expression in *N. benthamiana*. LC-MS/MS metabolite profiling confirmed that all three enzymes catalyzed the interconversion of the pathway intermediates nornarwedine/norgalanthamine and narwedine/galanthamine *in planta*, although with markedly different efficiencies. Among the tested isoforms, *La*AKR3 consistently displayed the highest activity, yielding at least two-fold greater accumulation of both norgalanthamine and galanthamine compared with *La*AKR1 and *La*AKR2 ($p < 0.001$, Figure 3.S16a, b). *La*AKR3 was then co-expressed with the *N*-methyltransferase *La*TMT2, followed by infiltration of nornarwedine as substrate. This combination resulted in the accumulation of both norgalanthamine and narwedine, together with downstream formation of galanthamine reaching 0.078 ng/mg fresh weight in *N. benthamiana* leaves (Figure 3.S16 c), demonstrating that *La*AKR3 efficiently supports reductive flux and operates compatibly with downstream methylation steps.

These results reveal functional divergence among the AKR isoforms: *La*AKR1 preferentially catalyzes the ‘’reverse’’ oxidative reactions, while *La*AKR3 is the predominant NADPH-dependent reductase responsible for the formation of norgalanthamine and galanthamine. Together with *La*TMT2, these AKRs coordinate the final reduction and methylation steps that define flux through the galanthamine pathway.

3.4. Discussion

Prior to this study, the enzymatic basis for the terminal steps of galanthamine biosynthesis remained unresolved: while a CNMT-like enzyme was shown to N-methylate norgalanthamine to galanthamine (Liyanage et al., 2025), and a TMT-like enzyme was implicated in the N-methylation of nornarwedine (Mehta et al., 2024), neither the relative contribution nor the substrate scope of these enzymes had been fully established, and the role of AKRs in governing reductive flux and pathway directionality at this terminal node remained largely uncharacterized (Mehta et al., 2024; Xiang et al., 2025). To resolve this ambiguity, we exploited the biosynthetic activity of *L. aestivum* leaves and identified *La*TMT2 as a Golgi-localized *N*-methyltransferase acting on both nornarwedine and norgalanthamine, and three AKR isoforms mediating reversible

redox interconversions at the final stage of the pathway, thereby providing enzyme-level resolution of both competing biosynthetic models.

Phylogenetic analysis placed *La*TMT2 within the clade of TMT homologs known to catalyze N-methylation in specialized metabolism (Koudounas et al., 2022; Levac et al., 2016; Liscombe et al., 2010; Mehta et al., 2024), clustering near the TMT from *Narcissus* cv. Tête-à-Tête previously implicated in narwedine methylation *in vivo* (Mehta et al., 2024), while *La*TMT1 grouped with canonical plastid-localized γ-TMTs involved in tocopherol biosynthesis, and *La*NMT with BIA-associated CNMTs. Similarly, the three *La*AKR isoforms cluster within the AKR4A/4B subfamilies alongside codeinone reductase from *P. somniferum* and AKRs from *Lycoris aurea* (Desgagné-Penix and Facchini, 2012; Liscombe and Facchini, 2007), consistent with a conserved role in reductive tailoring steps in alkaloid pathways (Gavidia et al., 2002; Unterlinner et al., 1999). Together, these relationships point to the independent recruitment of MT and AKR scaffolds from both primary and specialized metabolism to serve terminal biosynthetic functions in AA pathways.

The choice of leaf tissue as the primary system for candidate characterization is supported by converging lines of evidence. In agreement with previous reports, metabolite profiling confirmed the accumulation of galanthamine and late-stage intermediates, including norgalanthamine, in leaves, consistent with active late-stage biosynthesis in this organ. Moreover, four previously unreported masses detected by GC-MS expand the known chemical diversity of *L. aestivum* and represent potential targets for future structural characterization and bioactivity assessment. Preferential transcript accumulation of *La*TMT2, *La*AKR2, and *La*AKR3 in leaves relative to bulbs further indicates that the terminal methylation and reduction steps are transcriptionally enriched in this tissue. Crucially, dialyzed crude leaf extracts retained the capacity to convert nornarwedine to narwedine, norgalanthamine, and galanthamine in the presence of SAM and NADPH, providing direct enzymatic evidence that the required catalytic machinery is active in leaves. Together, these observations establish leaves as an active site of terminal galanthamine biosynthesis in *L. aestivum,* consistently with previous studies (Berkov et al., 2011; Karimzadegan et al., 2024).

Despite the lack of prior mechanistic studies on plant TMTs, conservation of the GluxxGluHis catalytic motif, characteristic of CNMTs (Bennett et al., 2018), in both *La*TMT1 and *La*TMT2 suggests that γ-TMTs may have been functionally repurposed for alkaloid *N*-methylation in *L.*

aestivum. Molecular docking provided a structural basis for the differences in enzymatic activity observed among the three MT candidates. *La*TMT2 showed both the shortest substrate-SAM distances and the most favorable S–C:N–C dihedral angles for both substrates, supporting its superior activity. *La*TMT1 showed acceptable dihedral angles (164–175°) but distances at the upper limit for methyl transfer (3.4–3.5 Å), consistent with its detectable but lower activity toward alkaloid substrates. *La*NMT, despite comparable distances, showed dihedral angles far from the optimal 180° (-73° to -86°), suggesting that productive substrate binding does not translate into optimal catalytic geometry, which may account for its reduced efficiency relative to *La*TMT2. *La*NMT interactions with Glu204 and His208 in the presence of norgalanthamine remain consistent with its CNMT-like identity (Liyanage et al., 2025). Among the AKR candidates, variation within the C-terminal loop regions of the conserved $(\alpha/\beta)_8$-barrel (Simpson et al., 2009) likely underlies the distinct substrate preferences and directional biases observed among *La*AKR1, *La*AKR2, and *La*AKR3 (Jez et al., 1997a). The predicted binding poses positioned the carbonyl group of both nornarwedine and narwedine in proximity to the catalytic Tyr54 and the NADPH nicotinamide ring, consistent with hydride transfer to the C=O bond, while Asp49 contributed to cofactor stabilization. Together with the RT-qPCR, these results provided a structural and transcriptional basis for prioritizing *La*TMT2 and the three *La*AKRs for full biochemical characterization.

The distinct subcellular compartmentalization of the three MT candidates reflects their divergent functions. *La*TMT1 localizes to plastids, consistent with its role in tocopherol biosynthesis (Muñoz and Munné-Bosch, 2019; Zbierzak et al., 2010), while *La*NMT distributes between the cytosol and ER, in line with the cytosolic localization reported for alkaloid NMTs in *P. somniferum* and *Coffea arabica* (Hagel and Facchini, 2012; Kodama et al., 2008). The Golgi localization of *La*TMT2 is more unusual and biologically significant. Several SAM-dependent MTs have been identified in the Golgi, where they access cytosol-imported SAM to methylate substrates destined for trafficking (Guirimand et al., 2011a; Guirimand et al., 2011b; Hugueney et al., 2009). Within the AA pathway, early steps occur in the nucleo-cytosolic compartment (Majhi et al., 2023), *O*-methylation is cytosolic, and oxidative coupling by CYP96T2 takes place at the ER (Lamichhane et al., 2025), placing *La*TMT2-mediated *N*-methylation at the Golgi as the terminal biosynthetic step, in a compartment consistent with subsequent product sequestration or vacuolar trafficking. Future work should establish whether *La*TMT2 resides in the cis-, medial-, or trans-Golgi, and

whether alkaloids are subsequently trafficked to the vacuole via vesicular transport. This extends the known subcellular architecture of the AA pathway and positions the Golgi as an unanticipated site of late-stage alkaloid tailoring in *L. aestivum*.

*La*TMT2 showed markedly higher activity than *La*TMT1, Δ*La*TMT1, and *La*NMT toward both nornarwedine and norgalanthamine, consistent with the proposed catalysis reported for an 80%-similar TMT from *Narcissus* cv. Tête-à-Tête (Mehta et al., 2024), whose substrate scope had not been verified until now. The comparable Km values for both substrates indicate that *La*TMT2 binds nornarwedine and norgalanthamine with similar affinity, while the higher Kcat for nornarwedine demonstrates that substrate discrimination occurs at the catalytic step rather than during binding. This kinetic profile supports a model in which *La*TMT2 can serve both terminal routes but preferentially drives *N*-methylation prior to reduction. The *in planta* activity in *N. benthamiana*, with accumulation of both narwedine and galanthamine upon co-expression with *La*AKR3, confirmed this catalytic function in a cellular context and demonstrated that *La*TMT2 and the AKRs operate compatibly within the same biosynthetic system.

The biochemical characterization of *La*TMT1 confirmed its identity as a canonical γ-tocopherol methyltransferase. Detection of α-tocopherol in the presence of SAM and γ-tocopherol aligns with the established role of plastid-localized TMTs in vitamin E biosynthesis (Bergmüller et al., 2003; Shintani and DellaPenna, 1998; Tavva et al., 2007) and is consistent with its phylogenetic placement and plastid localization. Taken together, *La*TMT1 appears to function in primary metabolism rather than in AA biosynthesis, narrowing the functionally relevant MT candidates to *La*TMT2 and *La*NMT. While *La*NMT retains activity toward norgalanthamine *in vitro* and *in vivo*, its markedly lower efficiency relative to *La*TMT2 and its ER/cytosolic localization suggest it may represent an accessory route, potentially active in a different tissue or developmental context, rather than the primary methylating enzyme at the terminal step.

All three *La*AKR isoforms catalyzed reversible interconversions between nornarwedine/norgalanthamine and narwedine/galanthamine, indicating that the terminal redox steps operate bidirectionally rather than as a strictly committed sequence. Within this system, *La*AKR3 functions as the predominant reductive isoform driving forward flux toward galanthamine, while *La*AKR1 preferentially catalyzes the ‘reverse’ oxidative reactions. Docking analysis provided partial structural insight into this divergence. While C4(NADPH)–C(carbonyle)

distances were comparable across isoforms (3.4–3.6 Å), LaAKR3 showed the shortest C4–C(olefinique) distance for narwedine (3.2 Å), consistent with its superior reductive activity toward this substrate. In contrast, *La*AKR1 showed less favorable geometry for both reduction modes, coherent with its oxidative bias. The engagement of His117 with narwedine specifically in *La*AKR1, absent in *La*AKR2 and *La*AKR3, may further contribute to its distinct directional preference. One additional structural basis for this functional divergence may be the substitution of methionine by leucine at position 119, analogous to residue substitutions in codeinone reductase COR1.3 that alter activity and product selectivity (Carr et al., 2021). The detection of norlycoraminone — consistent with C2–C3 bond reduction — alongside epi-galanthamine points to catalytic plasticity within the *La*AKR family, suggesting these enzymes may contribute to structural diversification of AAs beyond galanthamine, and that their reversible activity plays a broader role in shaping pathway flux than previously recognized (Dastmalchi et al., 2018).

These findings provide enzyme-level support for the dual biosynthetic routes to galanthamine suggested by earlier isotope-labeling studies (Eichhorn et al., 1998). The dual activity of *La*TMT2 toward both nornarwedine and norgalanthamine, combined with the reversible redox activity of the *La*AKR isoforms, suggests that the two routes are not competing alternatives but rather dynamically interconnected branches whose relative contributions may shift depending on substrate availability and redox state.

3.5. Conclusion

This study resolves the long-standing ambiguity in the terminal steps of galanthamine biosynthesis by identifying *La*TMT2 as a Golgi-localized *N*-methyltransferase acting on both nornarwedine and norgalanthamine, and by establishing that three AKR isoforms mediate reversible redox interconversions that dynamically modulate flux through the final stage of the pathway. Together, these enzymes reconcile competing biosynthetic models and reveal an unanticipated level of enzymatic flexibility at the terminal node of galanthamine formation. The Golgi localization of *La*TMT2 further redefines the subcellular architecture of AA biosynthesis in *L. aestivum*. From a broader perspective, the substrate promiscuity of *La*TMT2 and the tunable directionality of *La*AKRs provide a rational enzymatic basis for metabolic engineering strategies aimed at

enhancing galanthamine production and exploring the structural diversity of Amaryllidaceae alkaloids.

3.6. Materials and methods

3.6.1. Identification of candidates and phylogenetic analysis and Multiple Sequence Alignment

To find putative gamma tocopherol-like NMT, γ-TMT from *Arabidopsis thaliana* and Cr2270 from *Catharanthus roseus*, and CNMT from *P. somniferum* were used as bait to pull the candidate transcripts from the *Leucojum aestivum* transcriptome database. For Aldo-keto reductase, sequence from *Narcissus* species was used as bait (Mehta et al., 2024). Sequences were aligned by ClustalW. Phylogenetic analysis was done using IQ-TREE with sequences of MTS obtained from UniProt SwissProt or the NCBI database along with published sequences by Liscombe et al. (Liscombe et al., 2012; Liscombe et al., 2010; Tamura et al., 2021). For AKRs, sequences were taken from database and published sequences. The phylogenetic tree was inferred using the Maximum Likelihood method with the JTT matrix-based model. As part of the heuristic search, initial tree topologies were generated automatically using the Neighbor-Joining and BioNJ algorithms, and the best-scoring topology based on log-likelihood was selected for ML optimization. The tree was drawn to scale with branch lengths representing substitutions per site, and visualized using iTOL v6 (Jones et al., 1992; Letunic and Bork, 2021).

3.6.2. Molecular modelling of *La*NMT, *La*TMT1, *La*TMT2, *La*AKR1, *La*AKR2, and *La*AKR3.

The established models of CNMT bound to *N*- (6GKZ, 6GKV) and *S*-adenosyl-L-homocysteine from *C. japonica* were used as reference structures (Bennett et al., 2018). Folding prediction of *La*NMT, *LaTMT1,* and *LaTMT2* candidates was performed using AlphaFold Server Beta powered by AlphaFold3 (Abramson et al., 2024). Receptor preparation and docking were completed using MOE 2024.0601 software with the AMBER: EHT10 force field (Chemical Computing Group). *Cj*NMT was used as a reference to position the methyl donor SAM in the active site of the candidate following superimposition. The docking site was predicted using *Site Finder* tools. Ligands (norgalanthamine, nornarwedine) isomeric SMILES codes retrieved from PubChem were submitted to the ZINC20 database to obtain 3D charge data files (Irwin et al., 2020). Two protomers predicted at pH = 8.0 were included as possible ligands. *Triangle matcher* was used as a placement method for 200 poses generated with tethered *induced fit* refinement. Ten docking

poses for each protomer were compared with the crystalized protein-ligand complex. Coding sequences of *La*TMT1 and *La*AKR candidates were also submitted to Boltz2 using default parameters with appropriate cofactor (SAM and NADPH retrieved from PUBCHEM, respectively) for structure prediction and docking with γ-tocopherol (TMT), and with narwedine and nornarwedine (AKRs) (neurosnap.ai; (Passaro et al., 2025)) . The pose with the best docking score, consistent with the catalyzed reaction compared to reference crystal structures, was selected. PLIP was used to detect the interactions between ligands and receptor residues (Adasme et al., 2021). Visualization and figure preparation were performed using Pymol 2.3.4 (Schrödinger, CA, USA).

3.6.3. RNA extraction and cDNA synthesis

RNA was isolated from 80 mg of snap-frozen *Leucojum aestivum* leaves using the RNeasy® Plant Mini Kit (Qiagen, Mississauga, Canada) according to the manufacturer's protocol. DNAse treatment was performed using Turbo-DNAse according to the standard protocol from the supplier (Invitrogen, TURBO DNA-*free* Kit). cDNA synthesis was carried out using the M-MLV reverse transcriptase Kit (Thermo Fisher Scientific, Canada) according to the manufacturer's protocol, employing both random hexamers and oligo(dT). The resulting cDNA was stored at –80°C.

3.6.4. PCR amplification of key candidate genes and RT-qPCR gene expression analysis.

Coding sequences of *LaNMT*, *LaTMT1*, *LaTMT2* from *L. aestivum* were amplified using primers with attB1 and attB2 overhang along with a 3HA tag in the C-terminal and 3Flag for *La*AKR1, *La*AKR2 and *La*AKR3 (Table 3.S10) for *in vivo* enzymatic assays in *N. benthamiana*. For the *in vitro* enzymatic assay, coding sequences were amplified using gene-specific primers with restriction sites overhangs compatible with pMAL-c2x multiple cloning site i.e. EcoRI and SalI for *La*TMT1, EcoRI and XbaI for *La*TMT2 as well as *La*NMT. For *La*AKR1, *La*AKR2 and *La*AKR3, the restriction sites were embedded after attB1 and stop codon. PCR amplifications were performed using PrimeStar GXL premix (TaKaRa Bio) in a T100 Thermal Cycler (Bio-Rad). Amplifications were verified by running 2 µL of PCR product on a 0.9% agarose gel, with images

captured using the Bio-Rad ChemiDoc Imaging System. PCR clean-up and gel purification were carried out following the manufacturer's instructions using the GeneAid PCR & Gel Kit.

Gene expression analysis was performed using reverse transcription quantitative PCR (RT-qPCR). Total RNA was extracted from approximately 150 mg of snap-frozen plant tissue using a TRIzol-based protocol. Briefly, samples were homogenized in 500 µL of TRIzol reagent by vortexing, followed by the addition of 200 µL chloroform. After vigorous mixing and incubation on ice for 3 min, the samples were centrifuged at 12,000 × g for 10 min at 4 °C to separate the phases. The aqueous phase containing RNA was carefully transferred to a fresh tube containing 35 µL of 5 M NaCl and 400 µL isopropanol, mixed thoroughly, and incubated at −20 °C for 10 min to precipitate RNA. Following centrifugation at 12,000 × g for 10 min at 4 °C, the resulting RNA pellet was retained while the supernatant was discarded. The pellet was washed twice with 1 mL of 75% ethanol, centrifuged at 7,500 × g at 4 °C, and then air-dried for approximately 10 min. Residual genomic DNA was removed by treatment with TURBO DNase according to the manufacturer's instructions (Invitrogen TURBO DNA-free Kit). RT-qPCR reactions were carried out using the Luna® Universal One-Step RT-qPCR Kit (New England Biolabs) following the supplier's protocol. Gene expression levels were normalized to the reference gene *Histone3* using threshold cycle (Ct) values. Relative transcript abundance was calculated using the comparative ΔΔCt method based on the mean Ct values obtained from technical triplicates of pooled biological triplicates. Data analysis and visualization were performed using GraphPad Prism.

3.6.5. Cloning and *Agrobacterium* transformation for *in vivo* characterization

PCR-amplified fragments were cloned using the Gateway cloning system according to the manufacturer's instructions (Thermo Fisher Scientific). In this process, the attP-flanked pDONR221 vector, which contains a kanamycin resistance gene, was used in a BP recombination reaction to produce attL-flanked entry clones with attB-flanked sequences for *LaNMT*, *LaTMT1*, *LaTMT2* and *EGFP*. These entry clones were then transformed into *E. coli* DH5α chemically competent cells, which were cultured on LB agar plates containing 50 µg/mL kanamycin. Positive clones were identified via colony PCR, followed by plasmid extraction using the Presto Mini Plasmid Kit (Geneaid), according to the manufacturer's protocol. The integrity of each positive entry clone was confirmed by Sanger sequencing (Genome Quebec). After verification, selected plasmids were used in an LR recombination reaction, conducted overnight with LR clonase enzyme, to facilitate the recombination between the attL-flanked entry clone and attR-flanked destination vector (pK7WG2). The resulting LR reaction products were transformed into *E. coli*

DH5α cells and selected on LB agar plates containing 50 µg/mL spectinomycin. Positive clones were confirmed through colony PCR using Taq polymerase (Taq'Ozyme, France) and, from positive clones, plasmids were extracted using 10 mL LB broth cultures supplemented with spectinomycin. The confirmed expression clones were then transformed into *Agrobacterium tumefaciens* strain GV3101 by electroporation. For the localization, constructs of *LaNMT*, *LaTMT1* and *LaTMT2* cloned were in pB7FWG2 expression vectors to have C-terminal fusion EGFP protein and were co-transformed with free RFP or ER-mCherry (ER-rk *CD3-959*), or Golgi-mCherry (G-rk *CD3-967*) plasmids into *Agrobacterium tumefaciens* strain GV3101(Nelson et al., 2007). After 48 hours of incubation on LB plates at 28°C, the presence of the insert was re-confirmed via colony PCR like before.

3.6.6. Confocal image acquisition

Laser scanning confocal microscopy was performed using a Leica TCS SP8 system (Leica Microsystems) equipped with a HC PL APO CS2 40×/1.30 oil immersion objective. Fluorescence signals were examined in sequential mode from agroinfiltrated leaf discs. GFP and chlorophyll were excited at 488 nm, while RFP/mCherry was excited at 561 nm. Emission was recorded at 520–540 nm for GFP, 580–620 nm for RFP/mCherry, and 680–700 nm for chlorophyll autofluorescence. Subcellular localization was assessed in three independent experiments, and image processing was carried out using LAS AF Lite software (v.4.0.0.11706).

3.6.7. Cloning, transformation, and protein purification for *in vitro* characterization

PCR-amplified fragments were cloned using the restriction digestion/ligation cloning system according to the manufacturer's instructions (NEB). The PCR fragments and pMAL-c2X plasmids were double digested with restriction enzymes and ligated by T4 DNA ligase. Transformation and plasmid amplification/purification was performed like before using 100 µg/mL ampicillin in growth media. Plasmids were transformed into *E. coli* Rossetta cells on LB agar plates containing 100 µg/mL ampicillin and chloramphenicol (34 µg/mL). Positive clones were confirmed through colony PCR, and single colony of *E. coli* Rosetta (BL21) harboring the gene of interest were further grown in 5 mL LB broth cultures (seed culture), supplemented with ampicillin and

chloramphenicol overnight. After 14 hours, 1 mL of seed culture was transferred in 300 mL LB broth supplemented with antibiotics. As the OD_{600} reached 0.5, 0.25 mM isopropyl-β-D-thiogalactopyranoside, 50 µM zinc chloride, and 50 µM magnesium chloride were added, and the cultures were incubated overnight at 18°C with 210 rpm in a shaking incubator. Cells were harvested and protein extraction and purification was performed (Lamichhane et al., 2025). Finally, the pure, concentrated, and desalted proteins were obtained using amicon ultra centrifugal filters (Merk, Millipore) and aliquoted in individual tubes and preserved at –80°C.

3.6.8. *In vitro* enzymatic assay

Recombinant MTs proteins were expressed as N-terminal maltose-binding protein (MBP) fusion constructs and purified using affinity chromatography as detailed by New England Biolabs, Inc. For *La*TMT1, which remained insoluble, crude protein extracts were used directly at a final concentration of 20 µM. All enzymatic reactions were performed in a total volume of 100 µL under the following standardized conditions: 100 mM sodium phosphate buffer (pH 7.5), 2 mM SAM as the methyl donor, 100 µM of substrate, and 5 µM of purified enzyme. Initially reactions were incubated at 35°C for 2 hours and 30 minutes. Following incubation, reactions were quenched by adding an equal volume of mobile phase acidified to pH 2. Papaverine was added as an internal standard to make final 1 ppm in the reaction mix from a stock of 200 ppm. Samples were centrifuged at 10,000 rpm for 15 minutes to remove precipitated proteins, and the resulting supernatants were subjected to downstream metabolite analysis by LC-MS/MS. To comprehensively characterize the *La*TMT2 enzyme, we performed enzyme kinetics under systematically varied conditions. Serial dilutions of *La*TMT2 (5–0.156 µM, two-fold dilutions) were assayed at 1, 3, and 5 hours to determine optimal enzyme concentration and reaction duration. Temperature dependence was evaluated over a gradient of 20, 30, 40, and 50°C for 1–5 hours. Using the optimal enzyme concentration, reaction time, and temperature, the effect of pH on enzymatic activity was assessed across five buffer conditions (pH 5.0, 5.5, 6.5, 7.5, 8.5, and 9.5). In all assays, S-adenosylmethionine (SAM, 2 mM) served as the methyl donor, and the substrate concentration was maintained at 50 µM. Finally, under the identified optimal conditions (enzyme concentration, reaction time, temperature, and pH), substrate saturation experiments were performed to determine the Michaelis–Menten kinetic parameters, Km and kcat. Similarly, for AKRs 1 mM NADPH in 100 mM sodium phosphate buffer (pH 7.5) with 100 µM of substrate and

2µl of enzyme was used and incubated for 2 hours prior to quenching. Final yield was normalized based on enzyme concentration used.

For the *in vitro* enzymatic study using total protein extracts from *L. aestivum* leaves, crude protein extracts were prepared from cryopreserved *L. aestivum* leaf tissues. Approximately 400 mg of frozen tissue was finely ground and resuspended in 4 mL protein extraction (PE) buffer containing 100 mM Tris–HCl (pH 7.5), 1 mM phenylmethylsulfonyl fluoride (PMSF), 10 % glycerol, 10 mM β-mercaptoethanol, and 2% polyvinylpyrrolidone (PVP). The homogenate was lysed by sonication at 40% amplitude for 8 min using cycles of 15 s pulse followed by 30 s cooling intervals.

To remove endogenous metabolites and small cofactors, the crude lysate was dialyzed using 'Spectra/Por 3' dialysis membranes against 40 mL PE buffer at 4 °C with gentle shaking. The dialysis buffer was replaced every 2 h for four cycles. The dialyzed extract was subsequently clarified by centrifugation at 4,000 × g for 20 min, and the supernatant protein was collected for enzymatic assays following protein quantification. *In vitro* enzyme reactions were performed using 400 µg protein in 100 mM sodium phosphate buffer (pH 7.5) containing 100 µM substrate. Reactions were supplemented with 2 mM SAM for methyltransferase assays or together with 2 mM NADPH for methyltransferase followed by reductase assays. Reaction mixtures were incubated at 30 °C for 4 h prior to quenching with mobile phase and run in LC-MS/MS analysis. Authentic standards were used in all the experiments for standardization as well as quantification, however while quantification was not essential, peak area ratio was calculated dividing the peak area of observed metabolite with the peak area of internal standard i.e. papaverine to represent relative abundance. Minor background contributions were accounted for in all analyses. Specifically, narwedine, synthesized from galanthamine, and nornarwedine, derived from narwedine, carryover was subtracted from experimental measurements as background. A similar background elimination was applied to the norgalanthamine standard (MedChemExpress; 96.6% purity), which contained trace galanthamine contamination.

3.6.9. Transient expression of candidate genes in *N. benthamiana* (*in vivo* assay)

Individual *Agrobacterium tumefaciens* GV3101 colonies carrying the desired gene constructs (*LaNMT*, *LaTMT1*, *LaTMT2*, *LaAKR1, LaAKR2, LaAKR3* and *EGFP*) were grown in LB broth containing 50 µg/mL spectinomycin, 50 µg/mL rifampicin, and 30 µg/mL gentamicin, and

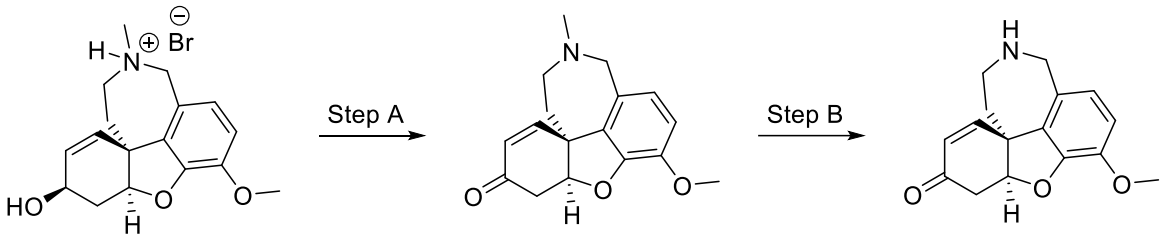
incubated at 28°C for 18-20 hours. Culture was centrifuged at 3000 rpm, the pellet was washed in *Agrobacterium* induction buffer (10 mM MES, pH 5.6, 10 mM $MgCl_2$, and 150 µM acetosyringone) and following incubation for 2 hours at room temperature. 3-4 weeks old *N. benthamiana* plants, grown in a controlled environment chamber at 22°C with a 16-hour /8-hour dark cycle, were used. The leaves were infiltrated with *Agrobacterium* suspensions adjusted to an optical density at 600 nm (OD_{600}) of 0.6 units, using a needleless syringe to infiltrate the suspensions to the abaxial side of the leaves. Three leaves from three independently infiltrated plants were used as a triplicate to test the hypothesis. Initially, the *Agrobacterium* suspensions containing the gene constructs were infiltrated into the leaves and incubated for 48 hours, followed by a second infiltration step with 100 µM substrates. After 24 hours, leaves were harvested, snap-frozen, and stored at –80°C for further analysis.

3.6.10. Western blotting

The frozen samples were ground into a fine powder using a mortar and pestle under liquid nitrogen. The expression of the agroinfiltrated genes in *N. benthamiana* leaves was verified by western blot. For this, 100 mg of tissue was resuspended in 0.5 mL of lysis buffer (100 mM Tris-HCl, pH 7.5, 1 mM phenylmethylsulfonyl fluoride, 10% glycerol, 10 mM β-mercaptoethanol, and 2% polyvinylpolypyrrolidone) and incubated on ice for 30 minutes with gentle inversion. The extracts were then centrifuged at 12,000 g for 30 minutes at 4°C to pellet the debris, and the supernatants were collected. Protein samples were run in an SDS gel with 6% stacking and 10% resolving phase. A specific primary antibody was used to verify protein expression on PVDF membranes after semi-dry transfer, followed by blocking with 5% milk for 2 hours at room temperature. A rabbit anti-HA or anti-flag monoclonal primary antibody raised in rabbit (Cell Signaling) was used overnight at 4°C. Host-specific secondary antibodies conjugated with horseradish peroxidase (HRP), specifically the Immun-Star goat anti-rabbit HRP conjugate from Bio-Rad, were utilized, and the membrane was illuminated with ECL reagent to detect the bands on the membrane.

3.6.11. Substrates and standards preparation

Narwedine and nornarwedine were synthesized from galanthamine hydrobromide in two steps via a protocol adapted from reported procedures(Hirnschall et al., 2002; Kogure et al., 2011).



Scheme 1: Chemical synthesis of narwedine and nornarwedine

Step A. Galanthamine hydrobromide (200.9 mg, 0.546 mmol) and potassium carbonate (150.7 mg, 1.090 mmol) were added to dry dichloromethane (10 mL), then stirred at room temperature for 1.5 hour. The mixture was filtered over glass wool to remove the remaining solid and the latter was rinsed with dry dichloromethane (3 x 5 mL). The combined dichloromethane solution (25 mL) was brought to 0°C before adding manganese (IV) oxide (94.2 mg, 1.084 mmol), then stirred at 0°C for 5 minutes. The mixture was then stirred at room temperature for 50 hours before adding a second portion of manganese (IV) oxide (47.2 mg, 0.543 mmol). The mixture was stirred at room temperature again for 20 hours before adding a third portion of manganese (IV) oxide (47.7 mg, 0.549 mmol). The solution was finally stirred at room temperature for 30 hours. The reaction mixture was then passed through Celite, rinsed with dichloromethane, and the filtrate was evaporated under reduced pressure to afford narwedine (26.1mg, 17%) without further purification. Spectroscopic data (GCMS, ^{1}H-NMR and ^{13}C-NMR) matched those reported in the literature (Hirnschall et al., 2002; Kogure et al., 2011).

Step B. Narwedine (21.0 mg, 0.0736 mmol) and *meta*-chloroperoxybenzoic acid (14.5 mg, 0.0840 mmol) were added to dry dichloromethane (2 mL), then stirred at room temperature for 3.5 hours to form narwedine *N*-oxide *in situ*. To the latter crude solution of narwedine *N*-oxide was added a solution of ferrous sulfate heptahydrate (12.7 mg, 0.0457 mmol) in methanol (1 mL), and the mixture was stirred at room temperature for 30 minutes. A solution of disodium hydrogen phosphate (15.6 mg, 0.110 mmol) in water (1 mL) was added to the reaction, and the mixture was stirred at room temperature for 10 minutes. The precipitate was collected by filtration, then washed with dichloromethane. The pH of the biphasic mixture was adjusted to > 8.5 with concentrated ammonium hydroxide (5 drops) under vigorous stirring. The resulting phases were then separated, and the aqueous phase was extracted with dichloromethane (2 x 10 mL). The combined organic layers were washed with 0.25 M NaOH (15 mL), and brine (15 mL), then dried with sodium

sulfate, filtered by gravity, and concentrated under reduced pressure. The crude residue was purified by flash chromatography (SiO_2) with 10% methanol in chloroform as eluent to afford nornarwedine (8.3 mg, 42%). Spectroscopic data (GCMS, ^{1}H-NMR and ^{13}C-NMR) matched those reported in the literature (Hirnschall et al., 2002; Kogure et al., 2011).

3.6.12. Sample preparation for metabolite analysis.

Metabolites were extracted from the crushed snap-frozen samples using a methanol-water extraction solvent (80:2, v/v) at a consistent ratio of 20 µL/mg of the sample. Before extraction, an internal standard of papaverine was added at a concentration of 2 ppm. The samples were then placed on a shaker at 200 rpm overnight, followed by heating at 65°C for 20 minutes with the lids closed. After centrifugation at 10,000 rpm for 10 minutes, the supernatants were collected and dried using a rotary evaporator. The dried extracts were reconstituted in the mobile phase, consisting of Milli-Q water and methanol (both containing 0.1% formic acid) at a 90:10 ratio by concentrating 20 times of initial extraction volume. The reconstituted samples were vortexed, filtered through a 0.2 µm PTFE filter, and subsequently analyzed by HPLC-MS/MS.

3.6.13. Metabolite screening in *Leucojum aestivum* leaf

Leucojum aestivum bulbs purchased from The Seed Company (Canada) were grown indoor in the laboratory plant room. Untargeted metabolite analysis of *L. aestivum* leaves was performed by GC-MS, while targeted metabolite analysis was performed by LC-MS/MS. Cryopreserved macerated leaves (100 mg) were extracted with 2000 µL of solvent (80:20 methanol:water), heated at 60°C for 20 minutes, followed by 20 minutes of vortexing. The extract was centrifuged, and the supernatant was collected in another tube. For the remaining biomass, the non-polar solvent hexane was used for further extraction with an equal volume as before. The supernatant of the extracts collected in new tubes was evaporated under vacuum in a rotary evaporator for the polar fraction and under a stream of nitrogen for the non-polar fraction. The dried sample was reconstituted with mobile phase for LC-MS/MS and in 100% methanol for GCMS analysis (Baeshen et al., 2023).

3.6.14. Instrumentation and chromatographic conditions

LC-MS/MS:

High-performance liquid chromatography (HPLC) coupled with tandem mass spectrometry (MS/MS) (Agilent Technologies, Santa Clara, California, USA) system equipped with an Agilent Jet Stream ionization source, a binary pump, an autosampler and a column compartment were used for the analysis. Compounds separation was achieved using a Kinetex EVO C18 column (150 × 4.6 mm, 5 µm, 100 Å; Phenomenex, Torrance, USA). Five microliters of each sample were injected onto the column that was set at 30°C. A gradient method made of (A) formic acid 0.1% v/v in water and (B) formic acid 0.1% v/v in methanol with a flow rate of 0.4 mL/min was used to achieve chromatographic separation. The HPLC elution program is described as follows: 0 min, 10% B; 10.0 min, 10% B; 20.0 min, 100% B; 25.0 min, 100% B; 26.0 min, 10% B. The total run time was 30 min per sample to allow the reconditioning of the column prior to the next injection. The parameters used in the MS/MS source were set as follows: gas flow rate 10 $L \cdot min^{-1}$, gas temperature 300°C, nebulizer 45 psi, sheath gas flow 11 $L \cdot min^{-1}$, sheath gas temperature 300°C, capillary voltage 4000 V in ESI^+ and 3500 V in ESI^- and nozzle voltage 500 V. Agilent MassHunter Data Acquisition (version 1.2) software was used to control the HPLC-MS/MS. MassHunter Qualitative Analysis (version 10.0) and MassHunter Quantitative QQQ Analysis (version 10.0) softwares were used for data processing. Compound identifications were made using authentic reference standards or by using collision-induced dissociation (CID) mass spectra published in literature (Kilgore et al., 2016a; Kilgore et al., 2016b; Mehta et al., 2023) in the case where reference standards were not available. MRM transitions and instrument parameters used for identifications in *in vivo* experiments are included in Table 3.S11. Instrument parameters used in MRM mode for metabolite screening in *L. aestivum* leaves and in SIM mode for in-vitro assays are presented in Tables 3.S12 and 3.S13, respectively. Instrument parameters used in Product Ion mode to obtain the full CID mass spectra of signals detected in SIM mode are presented in Table 3.S14.

GC-MS:

For GC-MS analysis, samples were injected into the GC-MS (Agilent Technologies 6890N GC coupled with 5973N inert MSD) in electron ionization mode at 70 eV. The temperature ramp used is described as follows: temperature was set at 100°C for 2 min, followed by 100–180°C at

15°C·min^{-1}, 180–300°C at 5°C·min^{-1}, and a 10 min hold at 300°C. Injector and detector temperatures were set at 250°C and 280°C, respectively, and the flow rate of carrier gas (He) was 1 mL·min^{-1}. A split ratio of 1:10 was applied, and the injection volume was 1 µL.

3.6.15. Statistical analysis

All statistical analyses were performed using GraphPad Prism 8 (GraphPad Software, San Diego, CA). Data are presented as mean ± standard deviation (SD) from at least three independent biological replicates unless otherwise stated. Comparisons between groups were evaluated using two-way analysis of variance (ANOVA), followed by Tukey's multiple comparisons test to determine statistical significance between group means. A *p*-value of less than 0.05 was considered statistically significant.

Funding

This research was financially supported by the Canada Research Chair on plant specialized metabolism Award No CRC-2023-00353 to I.D-P. Thanks are extended to the Canadian taxpayers and to the Canadian government for supporting the Canada Research Chairs Program.

Acknowledgement

We thank Priya Gatti and Melodie B. Plourde for helping with confocal imaging and Arthur Renault for assistance with experiments during his research internship. We also thank Nuwan Sameera Liyanage for insightful discussion for substrate synthesis required for experiment and Karen Cristine Gonçalves dos Santos for support in editing the manuscript.

Authors Contribution

Basanta Lamichhane: Conceptualization, Methodology, Investigation, Formal analysis, Validation, Visualization, Writing- Original draft, Reviewing and Editing; Archana Niraula: Methodology, Investigation, Resources, and Editing; Natacha Merindol: Conceptualization, Methodology, Formal analysis, Project administration, Resources, Reviewing and Editing; Sarah-Eve Gélinas: Methodology, Resources, and Editing; Patrick Lagüe: Review of docking analysis; Simon Ricard: Substrate synthesis, Reviewing and Editing; Hugo Germain: Conceptualization, Methodology, Resources, Co-supervision, Reviewing and Editing; Isabel Desgagné-Penix:

Conceptualization, Methodology, Resources, Funding acquisition, Supervision, Reviewing and Editing.

Declaration of Interest

The authors declare that there is no situation real, potential, or apparent conflict of interest.

3.7. References

Abramson, J., Adler, J., Dunger, J., Evans, R., Green, T., Pritzel, A., Ronneberger, O., Willmore, L., Ballard, A.J., Bambrick, J., Bodenstein, S.W., Evans, D.A., Hung, C.C., O'Neill, M., Reiman, D., Tunyasuvunakool, K., Wu, Z., Zemgulyte, A., Arvaniti, E., Beattie, C., Bertolli, O., Bridgland, A., Cherepanov, A., Congreve, M., Cowen-Rivers, A.I., Cowie, A., Figurnov, M., Fuchs, F.B., Gladman, H., Jain, R., Khan, Y.A., Low, C.M.R., Perlin, K., Potapenko, A., Savy, P., Singh, S., Stecula, A., Thillaisundaram, A., Tong, C., Yakneen, S., Zhong, E.D., Zielinski, M., Zidek, A., Bapst, V., Kohli, P., Jaderberg, M., Hassabis, D. and Jumper, J.M. (2024) Accurate structure prediction of biomolecular interactions with AlphaFold 3. *Nature* **630**, 493-500.

Adasme, M.F., Linnemann, K.L., Bolz, S.N., Kaiser, F., Salentin, S., Haupt, V.J. and Schroeder, M. (2021) PLIP 2021: expanding the scope of the protein–ligand interaction profiler to DNA and RNA. *Nucleic Acids Research* **49**, W530-W534.

Baeshen, N.A., Almulaiky, Y.Q., Afifi, M., Al-Farga, A., Ali, H.A., Baeshen, N.N., Abomughaid, M.M., Abdelazim, A.M. and Baeshen, M.N. (2023) GC-MS analysis of bioactive compounds extracted from plant Rhazya stricta using various solvents. *Plants* **12**, 960.

Bennett, M.R., Thompson, M.L., Shepherd, S.A., Dunstan, M.S., Herbert, A.J., Smith, D.R.M., Cronin, V.A., Menon, B.R.K., Levy, C. and Micklefield, J. (2018) Structure and Biocatalytic Scope of Coclaurine N-Methyltransferase. *Angew Chem Int Ed Engl* **57**, 10600-10604.

Bergmüller, E., Porfirova, S. and Dörmann, P. (2003) Characterization of an Arabidopsis mutant deficient in γ-tocopherol methyltransferase. *Plant Molecular Biology* **52**, 1181-1190.

Berkov, S., Bastida, J., Viladomat, F. and Codina, C. (2011) Development and validation of a GC–MS method for rapid determination of galanthamine in Leucojum *aestivum* and Narcissus ssp.: A metabolomic approach. *Talanta* **83**, 1455-1465.

Carr, S.C., Torres, M.A., Morris, J.S., Facchini, P.J. and Ng, K.K. (2021) Structural studies of codeinone reductase reveal novel insights into aldo-keto reductase function in benzylisoquinoline alkaloid biosynthesis. *Journal of Biological Chemistry* **297**, 101211.

Choi, K.-B., Morishige, T., Shitan, N., Yazaki, K. and Sato, F. (2002) Molecular cloning and characterization of coclaurinen-methyltransferase from cultured cells of Coptis japonica. *Journal of Biological Chemistry* **277**, 830-835.

Cimmino, A., Masi, M., Evidente, M., Superchi, S. and Evidente, A. (2017) Amaryllidaceae alkaloids: Absolute configuration and biological activity. *Chirality* **29**, 486-499.

Dastmalchi, M., Chang, L., Torres, M.A., Ng, K.K. and Facchini, P.J. (2018) Codeinone reductase isoforms with differential stability, efficiency and product selectivity in opium poppy. *The Plant Journal* **95**, 631-647.

de Sousa, S.M., de Giuseppe, P.O., Murakami, M.T., Guan, J.-C., Saunders, J.W., Kiyota, E., Santos, M.L., Schmelz, E.A., Yunes, J.A. and Koch, K.E. (2025) Functional genomics and structural insights into maize aldo-keto reductase-4 family: Stress metabolism and substrate specificity in embryos. *Journal of Biological Chemistry* **301**, 110404.

Desgagné-Penix, I. (2021) Biosynthesis of alkaloids in Amaryllidaceae plants: A review. *Phytochemistry Reviews* **20**, 409-431.

Desgagné-Penix, I. and Facchini, P.J. (2012) Systematic silencing of benzylisoquinoline alkaloid biosynthetic genes reveals the major route to papaverine in opium poppy. *The Plant Journal* **72**, 331-344.

Eichhorn, J., Takada, T., Kita, Y. and Zenk, M.H. (1998) Biosynthesis of the Amaryllidaceae alkaloid galanthamine. *Phytochemistry* **49**, 1037-1047.

Gavidia, I., Pérez-Bermúdez, P. and Seitz, H.U. (2002) Cloning and expression of two novel aldo-keto reductases from Digitalis purpurea leaves. *European Journal of Biochemistry* **269**, 2842-2850.

Guirimand, G., Guihur, A., Ginis, O., Poutrain, P., Héricourt, F., Oudin, A., Lanoue, A., St-Pierre, B., Burlat, V. and Courdavault, V. (2011a) The subcellular organization of strictosidine biosynthesis in Catharanthus roseus epidermis highlights several trans-tonoplast translocations of intermediate metabolites. *The FEBS journal* **278**, 749-763.

Guirimand, G., Guihur, A., Poutrain, P., Héricourt, F., Mahroug, S., St-Pierre, B., Burlat, V. and Courdavault, V. (2011b) Spatial organization of the vindoline biosynthetic pathway in Catharanthus roseus. *Journal of plant physiology* **168**, 549-557.

Hagel, J.M. and Facchini, P.J. (2012) Subcellular localization of sanguinarine biosynthetic enzymes in cultured opium poppy cells. *In vitro Cellular & Developmental Biology-Plant* **48**, 233-240.

Hasnain, G. (2010) *The ORCA-ome as a key to understanding alkaloid biosynthesis in Catharanthus roseus*:PhD Thesis, Leiden University, The Netherlands.

Hirnschall, M., Froehlich, J., Jordis, U. and Mereiter, K. (2002) Seco-isopowellaminone: A new heterocycle from nornarwedine. *Journal of heterocyclic chemistry* **39**, 1265-1270.

Hugueney, P., Provenzano, S., Verries, C., Ferrandino, A., Meudec, E., Batelli, G., Merdinoglu, D., Cheynier, V., Schubert, A. and Ageorges, A. (2009) A novel cation-dependent O-methyltransferase involved in anthocyanin methylation in grapevine. *Plant physiology* **150**, 2057-2070.

Irwin, J.J., Tang, K.G., Young, J., Dandarchuluun, C., Wong, B.R., Khurelbaatar, M., Moroz, Y.S., Mayfield, J. and Sayle, R.A. (2020) ZINC20-A Free Ultralarge-Scale Chemical Database for Ligand Discovery. *J Chem Inf Model* **60**, 6065-6073.

Jayawardena, T.U., Merindol, N., Liyanage, N.S. and Desgagné-Penix, I. (2024) Unveiling Amaryllidaceae alkaloids: from biosynthesis to antiviral potential–a review. *Natural Product Reports*.

Jez, J.M., Bennett, M.J., Schlegel, B.P., Lewis, M. and Penning, T.M. (1997a) Comparative anatomy of the aldo–keto reductase superfamily. *Biochemical Journal* **326**, 625-636.

Jez, J.M., Flynn, T.G. and Penning, T.M. (1997b) A new nomenclature for the aldo-keto reductase superfamily. *Biochemical pharmacology* **54**, 639-647.

Jones, D.T., Taylor, W.R. and Thornton, J.M. (1992) The rapid generation of mutation data matrices from protein sequences. *Bioinformatics* **8**, 275-282.

Ka, S., Merindol, N., Sow, A.A., Singh, A., Landelouci, K., Plourde, M.B., Pépin, G., Masi, M., Di Lecce, R. and Evidente, A. (2021) Amaryllidaceae alkaloid cherylline inhibits the replication of dengue and Zika viruses. *Antimicrobial Agents and Chemotherapy* **65**, 10.1128/aac. 00398-00321.

Karimzadegan, V., Koirala, M., Sobhanverdi, S., Merindol, N., Majhi, B.B., Gélinas, S.-E., Timokhin, V.I., Ralph, J., Dastmalchi, M. and Desgagné-Penix, I. (2024) Characterization of cinnamate 4-hydroxylase (CYP73A) and p-coumaroyl 3′-hydroxylase (CYP98A) from Leucojum *aestivum*, a source of Amaryllidaceae alkaloids. *Plant Physiology and Biochemistry* **210**, 108612.

Kilgore, M.B., Augustin, M.M., May, G.D., Crow, J.A. and Kutchan, T.M. (2016a) CYP96T1 of Narcissus sp. aff. Pseudonarcissus catalyzes formation of the Para-Para'CC phenol couple in the Amaryllidaceae alkaloids. *Frontiers in plant science* **7**, 225.

Kilgore, M.B., Holland, C.K., Jez, J.M. and Kutchan, T.M. (2016b) Identification of a noroxomaritidine reductase with Amaryllidaceae alkaloid biosynthesis related activities. *Journal of Biological Chemistry* **291**, 16740-16752.

Kodama, Y., Shinya, T. and Sano, H. (2008) Dimerization of N-methyltransferases involved in caffeine biosynthesis. *Biochimie* **90**, 547-551.

Kogure, N., Katsuta, N., Kitajima, M. and Takayama, H. (2011) Two new alkaloids from Crinum asiaticum var. sinicum. *Chemical and Pharmaceutical Bulletin* **59**, 1545-1548.

Koudounas, K., Guirimand, G., Hoyos, L.F.R., Carqueijeiro, I., Cruz, P.L., Stander, E., Kulagina, N., Perrin, J., Oudin, A. and Besseau, S. (2022) Tonoplast and peroxisome targeting of γ-tocopherol N-methyltransferase homologs involved in the synthesis of monoterpene indole alkaloids. *Plant and Cell Physiology* **63**, 200-216.

Kratzer, R., Wilson, D.K. and Nidetzky, B. (2006) Catalytic mechanism and substrate selectivity of aldo-keto reductases: insights from structure-function studies of Candida tenuis xylose reductase. *IUBMB life* **58**, 499-507.
Lamichhane, B., Gélinas, S.E., Merindol, N., Koirala, M., Dos Santos, K.C.G., Germain, H. and Desgagné-Penix, I. (2025) Elucidating the enzyme network driving Amaryllidaceae alkaloids biosynthesis in Leucojum *aestivum*. *Plant Biotechnology Journal*.
Letunic, I. and Bork, P. (2021) Interactive Tree Of Life (iTOL) v5: an online tool for phylogenetic tree display and annotation. *Nucleic acids research* **49**, W293-W296.
Levac, D., Cázares, P., Yu, F. and De Luca, V. (2016) A picrinine N-methyltransferase belongs to a new family of γ-tocopherol-like methyltransferases found in medicinal plants that make biologically active monoterpenoid indole alkaloids. *Plant Physiology* **170**, 1935-1944.
Li, H., Yang, Y., Hu, Y., Chen, C.C., Huang, J.W., Min, J., Dai, L. and Guo, R.T. (2022) Structural analysis and engineering of aldo-keto reductase from glyphosate-resistant Echinochloa colona. *J Hazard Mater* **436**, 129191.
Liscombe, D.K. and Facchini, P.J. (2007) Molecular cloning and characterization of tetrahydroprotoberberine cis-N-methyltransferase, an enzyme involved in alkaloid biosynthesis in opium poppy. *Journal of Biological Chemistry* **282**, 14741-14751.
Liscombe, D.K., Louie, G.V. and Noel, J.P. (2012) Architectures, mechanisms and molecular evolution of natural product methyltransferases. *Natural product reports* **29**, 1238-1250.
Liscombe, D.K., Usera, A.R. and O'Connor, S.E. (2010) Homolog of tocopherol C methyltransferases catalyzes N methylation in anticancer alkaloid biosynthesis. *Proceedings of the National Academy of Sciences* **107**, 18793-18798.
Liyanage, N.S., Lamichhane, B., Fantino, E., Mérindol, N., Gélinas, S.-E., Tobón, M.C.G. and Desgagné-Penix, I. (2025) Coclaurine N-methyltransferase-like enzymes drive the final biosynthetic reaction of the anti-Alzheimer's drug galanthamine in Amaryllidaceae. *Plant Physiology and Biochemistry*, 110067.
Majhi, B.B., Gélinas, S.-E., Mérindol, N., Ricard, S. and Desgagné-Penix, I. (2023) Characterization of norbelladine synthase and noroxomaritidine/norcraugsodine reductase reveals a novel catalytic route for the biosynthesis of Amaryllidaceae alkaloids including the Alzheimer's drug galanthamine. *Frontiers in Plant Science* **14**, 1231809.
Mehta, N., Meng, Y., Zare, R., Kamenetsky-Goldstein, R. and Sattely, E. (2023) A developmental gradient reveals biosynthetic pathways to eukaryotic toxins in monocot geophytes. *bioRxiv*.
Mehta, N., Meng, Y., Zare, R., Kamenetsky-Goldstein, R. and Sattely, E. (2024) A developmental gradient reveals biosynthetic pathways to eukaryotic toxins in monocot geophytes. *Cell* **187**, 5620-5637. e5610.
Min, K.C., Kovall, R.A. and Hendrickson, W.A. (2003) Crystal structure of human alpha-tocopherol transfer protein bound to its ligand: implications for ataxia with vitamin E deficiency. *Proc Natl Acad Sci U S A* **100**, 14713-14718.
Morris, J.S. and Facchini, P.J. (2016) Isolation and characterization of reticuline N-methyltransferase involved in biosynthesis of the aporphine alkaloid magnoflorine in opium poppy. *Journal of Biological Chemistry* **291**, 23416-23427.
Morris, J.S. and Facchini, P.J. (2019) Molecular Origins of Functional Diversity in Benzylisoquinoline Alkaloid Methyltransferases. *Frontiers in Plant Science* **10**.
Muñoz, P. and Munné-Bosch, S. (2019) Vitamin E in plants: biosynthesis, transport, and function. *Trends in plant science* **24**, 1040-1051.
Nelson, B.K., Cai, X. and Nebenführ, A. (2007) A multicolored set of *in vivo* organelle markers for co-localization studies in Arabidopsis and other plants. *The Plant Journal* **51**, 1126-1136.
Paiva, M., Nascimento, G., Damasceno, I., Santos, T. and Silveira, D. (2023) Pharmacological and toxicological effects of Amaryllidaceae. *Brazilian Journal of Biology* **83**, e277092.

Passaro, S., Corso, G., Wohlwend, J., Reveiz, M., Thaler, S., Somnath, V.R., Getz, N., Portnoi, T., Roy, J., Stark, H., Kwabi-Addo, D., Beaini, D., Jaakkola, T. and Barzilay, R. (2025) Boltz-2: Towards Accurate and Efficient Binding Affinity Prediction. *bioRxiv*.

Penning, T.M. (2015) The aldo-keto reductases (AKRs): Overview. *Chemico-biological interactions* **234**, 236-246.

Ptak, A., Morańska, E., Skrzypek, E., Warchoł, M., Spina, R., Laurain-Mattar, D. and Simlat, M. (2020) Carbohydrates stimulated Amaryllidaceae alkaloids biosynthesis in Leucojum *aestivum* L. plants cultured in RITA® bioreactor. *PeerJ* **8**, e8688.

Shintani, D. and DellaPenna, D. (1998) Elevating the vitamin E content of plants through metabolic engineering. *Science* **282**, 2098-2100.

Simpson, P.J., Tantitadapitak, C., Reed, A.M., Mather, O.C., Bunce, C.M., White, S.A. and Ride, J.P. (2009) Characterization of two novel aldo–keto reductases from Arabidopsis: expression patterns, broad substrate specificity, and an open active-site structure suggest a role in toxicant metabolism following stress. *Journal of molecular biology* **392**, 465-480.

Sokhna, S., Mérindol, N., Presset, M., Seck, I., Girard, M.-P., Ka, S., Ndoye, S.F., Ba, A.L., Samb, I. and Berthoux, L. (2024) Potential of several triazene derivatives against DENGUE viruses. *Bioorganic & Medicinal Chemistry Letters* **101**, 129646.

Szlávik, L., Gyuris, Á., Minárovits, J., Forgo, P., Molnár, J. and Hohmann, J. (2004) Alkaloids from Leucojum vernum and antiretroviral activity of Amaryllidaceae alkaloids. *Planta medica* **70**, 871-873.

Tallini, L.R., das Neves, G.M., Vendruscolo, M.H., Rezende-Teixeira, P., Borges, W., Bastida, J., Costa-Lotufo, L.V., Eifler-Lima, V.L. and Zuanazzi, J.A.S. (2024) Antitumoral activity of different Amaryllidaceae alkaloids: *In vitro* and *in silico* assays. *Journal of Ethnopharmacology* **329**, 118154.

Tamura, K., Stecher, G. and Kumar, S. (2021) MEGA11: molecular evolutionary genetics analysis version 11. *Molecular biology and evolution* **38**, 3022-3027.

Tavva, V.S., Kim, Y.-H., Kagan, I.A., Dinkins, R.D., Kim, K.-H. and Collins, G.B. (2007) Increased α-tocopherol content in soybean seed overexpressing the Perilla frutescens γ-tocopherol methyltransferase gene. *Plant Cell Reports* **26**, 61-70.

Torres, M.A., Hoffarth, E., Eugenio, L., Savtchouk, J., Chen, X., Morris, J.S., Facchini, P.J. and Ng, K.K.-S. (2016) Structural and functional studies of pavine N-methyltransferase from Thalictrum flavum reveal novel insights into substrate recognition and catalytic mechanism. *Journal of Biological Chemistry* **291**, 23403-23415.

Unterlinner, B., Lenz, R. and Kutchan, T.M. (1999) Molecular cloning and functional expression of codeinone reductase: the penultimate enzyme in morphine biosynthesis in the opium poppy Papaver somniferum. *The Plant Journal* **18**, 465-475.

Wessjohann, L., Dippe, M., Tengg, M. and Gruber-Khadjawi, M. (2014) Methyltransferases in biocatalysis. *Cascade biocatalysis: integrating stereoselective and environmentally friendly reactions*, 393-426.

Xiang, Y., Jiang, X., Li, J., Sun, B., Liu, Z., Li, D., Wu, M., Wang, R. and Xu, S. (2025) Functional characterization of aldo-keto reductase genes from Lycoris aurea that participate in galantamine biosynthesis. *Plant Science*, 112869.

Zbierzak, A.M., Kanwischer, M., Wille, C., Vidi, P.-A., Giavalisco, P., Lohmann, A., Briesen, I., Porfirova, S., Bréhélin, C. and Kessler, F. (2010) Intersection of the tocopherol and plastoquinol metabolic pathways at the plastoglobule. *Biochemical Journal* **425**, 389-399.

3.8. Supplementary Tables

Branch-Enabling N-Methyltransferase in Golgi Reconciles Divergent Models of Galanthamine Biosynthesis

Basanta Lamichhane[1], Archana Niraula[1], Natacha Merindol[1], Sarah-Eve Gélinas[1], Patrick Lagüe[2], Simon Ricard[1], Hugo Germain[1,3], Isabel Desgagné-Penix[1,3*]

[1]Department of Biochemistry, Chemistry, Physics and Forensic Science, Université du Québec à Trois-Rivières, Trois-Rivières, Québec, Canada

[2]Department of Biochemistry, Microbiology and Bioinformatics, Université Laval, Québec, Québec, Canada

[3]Plant Biology Research Group, Trois-Rivières, Québec, Canada

BL: Basanta.Lamichhane@uqtr.ca

AN: Archana.Niraula@uqtr.ca

NM: Natacha.Merindol@uqtr.ca

SEG: Sarah-Eve.Gelinas@uqtr.ca

SR: Simon.Ricard@uqtr.ca

PL: patrick.lague@bcm.ulaval.ca

HG: Hugo.Germain@uqtr.ca

IDP: Isabel.Desgagne-Penix@uqtr.ca

*Corresponding author's email address: Isabel.Desgagne-Penix@uqtr.ca

Table 1.S1. List of sequences used for phylogenetic analysis of MTs.

Q9S7W8_ATRBE_Atropa_belladonna

MEVNHNNGSTTKIILKNGSICNGDVNGNSHTHKKIENKLVECTNSIKPGWFSEFSALWPGEAFSLKIEKLL
FQGKSDYQDVMLFESATYGKVLTLDGAIQHTENGGFPYTEMIVHLPLGSIPSPKKVLIIGGGIGFTLFEVS
RYPTIDTIDIVEIDDVVVDVSRKYFPYLAAGFDDPRVTLIIGDGAAFVKAAQPGYYDAIIVDSSDPIGPAKD
LFERPFFEAVAKALRPGGVVCTQAESIWLHMHLIKQIIANCRQVFKGSVNYAWTTVPTYPTGVIGYMLC
STEGPEVNFKNPVNSIDKDTSHVKSKGPLKFYNSDIHKAAFILPSFARDLVEF

CNMT_PAPSO_Papaver_somniferum

MQLKAKEELLRNMELGLIPDQEIRQLIRVELEKRLQWGYKETHEEQLSQLLDLVHSLKGMKMATEMEN
LDLKLYEAPMEFLKIQHGSNMKQSAGYYTDESTTLDEAEIAMLDLYMERAQIKDGQSVLDLGCGLGAV
ALFGANKFKKCQFTGVTSSVEQKDYIEGKCKELKLTNVKVLLADITTYETEERFDRIFAVELIEHMKNYQ
LLLKKISEWMKDDGLLFVEHVCHKTLAYHYEPVDAEDWYTNYIFPAGTLTLSSASMLLYFQDDVSVVN
QWTLSGKHYSRSHEEWLKNMDKNIVEFKEIMRSITKTEKEAIKLLNFWRIFCMCGAELFGYKNGEEWM
LTHLLFKKK

D3KY98_9GENT_Carapichea_ipecacuanha

METVESSSSAELLRAQTHFSRQVFSFQNFAALKCALQLGIPDAIKQHGKPMNLSELTSALPINPSKAPCIH
RLMRLLVNAGYFAQENECFALTSLGRLLLKDDPLHIRALVLSEFHTALVMPWFALSEWFKNDDVAPFA
TAHGKSFWDYTSCDPELRNVFDGAMACDSHLIAKALVTEFKYLFEGLKSLVDVGGGNGTLARSIAKAF
TNLKCTVCDLPEAVANEQGDGNLDFVAGDMFDRVPSADAILLKSILHDWSDENCVKILKNCKRAISGKD
KGGKVIVIDGVVELQKKAGNDDPGLDNMDMQMLVLFNSKERNEKEWAKLFSDAGFSDYGIVRTFGW
WCIMELSP

Q70EW6_DATST_Datura_stramonium

MEVLSSTHTNGSSLLKNGVITMNGHHNGNSDHRNGGTTVHENGRKLLGNSNSIKPGWFSEFSALWPGE
AFSLKIEKLLFQGKSDYQDVMLFESATYGKVLTLDGAIQHTENGGFPYTEMIVHLPLGSIPNPKKVLIIGG
GIGFTLFEVLRYPTVEKIDIVEIDDVVVDVSRKFFPYLAANFNDPRVTLVLGDGAAFVKAAQAGYYDAII
VDSSDPIGPAKDLFERPFFEAVAKALRPGGVVCTQAESIWLHMHIIKQIIANCRQVFKGSVNYAWTTVPT
YPTGVIGYMLCSTEGPEVDFKNPVNPIDKDETHANSKLGPLKFYNTDIHKAAFILPSFARSMIES

A4JHA2_BURVG_Burkholderia_vietnamiensis

MFWEKKLAQWADEVRTKANLPARLVLWNGEQLDFGTFSAPQVTLKVNSASALPLLLEPSLDNLGEAY
VKGKIDIEGRLSDIINISYSLARSTVTSASKLARVRRYFNHTKSTDKKAIQYHYDVSNEFYKLWLDENMV
YSCAYFENGDEDLATAQIKKIDHILTKIQLEPGQRLLDIGCGWGALVLRAAQKFGATCLGVTLSQNQFDL
ATARVKAAGLEDKIEIRLQDYREIDGQFDRITSVGMFEHVGRKNLPLYFSRVRELLVDDGIAMNHGITST
DAESGETALGGGEFIDRYVFPDGELPHISLALEAAQRGGLEAVDIESLRRHYARTLEIWTENFEANAEQA
RGLVDDEKFRIWRVYLAGCAYAFEHDDVSIFQIVCRKAGRSAKTLPWSRRYMYEHALPR

N7OMT_PAPSO_Papaver_somniferum

MEVVSQIDQENQAIIWKQIYGFSESLLLKCAVQCEIAETIHNHGTPMSILELAAKLPIDQPVNIDRLYRVM
RYLVHQKLFNKEVISTLNGGTVQVTEKYWLAPPAKYLIRGSQQSMVPSVLGIIDEDMFAPWHILKDSLT
GECNIFETALGKSISVYMSENPEMNQISNGAMAFDSGLVTSHLVNECKSVFGDEIKTLVDVGGGTGTAL
RAISKAFPNIKCTLFDLPHVIADSPEIPTITKVSGDMFKSIPSADAIFMKNILHDWNDDECIQILKRCKDVVS
AGGKLIMVEMVLDEDSFHPYSKLRLTSDIDMMVNNGGKERTEKEWEKLFDAAGFASCKFTQMSVGFA
AQSIIEVY

PEAMT_SPIOL_Spinacia_oleracea

MAASAMGVLQEREVFKKYWIEHSVDLTVEAMMLDSQASDLDKVERPEVLSMLPPYEGKSVLELGAGI
GRFTGELAEKASQVIALDFIESVIKKNESINGHYKNVKFMCADVTSPSLNISPNSVDIIFSNWLLMYLSDEE
VERLVERMLKWLKPGGYIFFRESCFHQSGDHKRKSNPTHYREPRFYTKIFKECHMQDDSGNSYELSLIGC
KCIGAYVKSKKNQNQISWLWQKVDSEDDKGFQRFLDSSQYKFNSILRYERVFGPGYVSTGGLETTKEFV
SKLDLKPGQKVLDVGCGIGGGDFYMAENYDVEVVGIDLSINMISFALERSIGLKCAVEFEVADCTKKDY
PENSFDVIYSRDTILHIQDKPALFRSFHKWLKPGGKVLISDYCKSAGTPSAEFAAYIRQRGYDLHDVKAY
GKMLKDAGFVEVIAENRTDQFIQVLQKELDALEQEKDDFIDDFSEEDYNDIVDGWKAKLVRTTEGEQQ
WGLFIAKKM

4OMT2_PAPSO_Papaver_somniferum

MGSLDAKPAAATQEVSIKDQAQLWNIIYGFADSLVLRCAVEIGIADIIKNNDGAITLAQLAAKLPITNVSS
DYLYRMVRYLVHLNIIEQETCNGGVEKVYSLKPVGTLLLRDAERSMVPMILGMTQKDFMVSWHFMKE
GLGNGSTTAFEKGMGMDIWKYLEGNPDQSQLFNEGMAGETRLLTKTLIEDCRDTFQGLDSLVDIGGGN
GTTIKAIYEAFPHIKCTLYDLPHVVANSHDLPNIEKVPGDMFKSVPSAQAILLKLILHDWTDEECVNILKK
CKEAIPKETGKVIIVDVALEEESNHELTKTRLILDIDMLVNTGGRERTADDWENLLKRAGFRSHKIRPIRA
IQSVIEAFP

GTOMC_ARATH_Arabidopsis_thaliana

MKATLAAPSSLTSLPYRTNSSFGSKSSLLFRSPSSSSSVSMTTTRGNVAVAAAATSTEALRKGIAEFYNET
SGLWEEIWGDHMHHGFYDPDSSVQLSDSGHKEAQIRMIEESLRFAGVTDEEEEKKIKKVVDVGCGIGGS
SRYLASKFGAECIGITLSPVQAKRANDLAAAQSLAHKASFQVADALDQPFEDGKFDLVWSMESGEHMP
DKAKFVKELVRVAAPGGRIIIVTWCHRNLSAGEEALQPWEQNILDKICKTFYLPAWCSTDDYVNLLQSH
SLQDIKCADWSENVAPFWPAVIRTALTWKGLVSLLRSGMKSIKGALTMPLMIEGYKKGVIKFGIITCQKP
L

HTOMT_CATRO_Catharanthus_roseus

MDVQSEEFRGAQAQIWSQSCSFITSASLKCAVKLGIPDTIDNHGKPITLSELTNALVPPVHPSKAPFIYRL
MRVLAKNGFCSEEQLDGETEPLYSLTPSSRILLKKEPLNLRGIVLTMADPVQLKAWESLSDWYQNEDDS
STAFETAHGKNFWGYSSEHMEHAEFFNEAMASDSQLISKLLIGEYKFLFEGLASLVDIGGGTGTIAKAIA
KNFPQLKCTVFDLPHVVANLESKENVEFVAGDMFEKIPSANAIFLKWILHDWNDEDCVKILKSCKKAIP
AKGGKVIIIDMVMYSDKKDDHLVKTQTSMDMAMLVNFAAKERCEKEWAFLFKEAGFSDYKIYPKLDF
TRSLIEVYP

P93628_MAIZE_Zea_mays

MALAVRTPRFQPRPASISAPTTPASTSLAAGNARPRPCAGAAVRASPFTEATSSSRYRRDAWSYAADGSS
NSASPSSAAAAAAGRRDDEIALQLPELRRLLDVLRASRGRGAEEGGGPGEVALVGTGPGDPELLTLKAV
RAIEAADLVLYDRLVSNDVLDLVGEGARLLYVGKTAGYHSRTQEEIHELLLSFAEAGANVVRLKGGDPL
VFGRGGEEMDFLQQQGIKVEVIPGITSASGIAAELGIPLTHRGVATSVRFLTGHSRNGGTDPLYVAGNAA
DPDTTLVVYMGLSTLPSLAPKLMKHGLPPDTPAVAVERGTTPQQRTVFASLKDLVDEVKSADLVSPTLII
IGKVVSLSPFWVESSEHDALKVQSSYANEADDNRFSWFLVTGQYLRNARSQIWEHRFDLVYTETSQEA
WILNGGW

B7U5G1_BRANA_Brassica_napus

PSLLLQSQRPSSALMTTTASRGSVAVTAAATSSAEALREGIAEFYNETSGLWEEIWGDHMHHGFYDPDS
SVQLSDSGHREAQIRMIEESLRFAGVTEEEKKIKRVVDVGCGIGGSSRYIASKFGAECIGITLSPVQAKRA
NDLATAQSLSHKVSFQVADALDQPFEDGIFDLVWSMESGEHMPDKAKFVKELVRVTAPGGRIIIVTWCH
RNLSQGEESLQPWEQNLLDRICKTFYLPAWCSTSDYVELLQSLSLQDIKCADWSENVAPFWPAVIRTALT
WKGLVSLLRSGM

Q84N56_9CARY_Limonium_latifolium

MANHSSAAAMVVDETSEARNNARLKIIELANLISVPMSLTAIVRLKVPEAIWSNGSNTPVSAAEILSRLPD
APATADAENLQRLLRVLTSFGVFSEHLDTTSSSSSSTSERRYCLTEVGQTLVSFDESCPSHGAYVLQHHQ
ETLLKAWPFLHTAILDASTEPFARVNGEPAYQYYGKNDELNKNMQYAMSGVSVPYMKALLGSGYDGF
EGVKTLVDVGGSSGDCLRMIINKYKDIPKAINFDLPEVVAKAPKIPGITHVGGNMFESVPSGDAIFVKWV
LTCFTDEEVITLMRNCNKALPVGGKLICSEPTLPENSDESHRTRALLVADIFIMTTYRAKGKHRTEEEYRQ
LGLLAGFPKFRVIHVDYFFPVVEFQK

D2D5G3_SOYBN_Glycine_max

MDPLSLFCTGALLAGGLYWFVCVLGPAEQKGKRATDLSGGSISAEKVQDNYKQYWSFFRRPKEIETAD
KVPDFVDTFYNLVTDIYEWGWGQSFHFSPSIPGKSHRDATRLHEEMAVDLIEAKPGNRILDVGCGVGGP
MRAIAAHSRANVVGITINEYQVNRARMHNKKAGLESLCEVVCGNFLKMPFPDNSFDGAYSIEATCHAP
KLEEVYAEIFRVLKPGALYVSYEWVTTDKYRGDDPEHVEVIQGIERGDALPGLRNYTDIAETARKVGFA
VVKERDLAKPPAQPWWSRLKMGRIAYWRNHIVVTVLAALGIAPKGTVDVHEMLFKTADYLTRGGDSG
IFSPMHMILCRKPHDKDDHN

6OMT_PAPSO_Papaver_somniferum

METVSKIDQQNQAKIWKQIYGFAESLVLKCAVQLEIAETLHNNVKPMSLSELASKLPVAQPVNEDRLFRI
MRYLVHMELFKIDATTQKYSLAPPAKYLLRGWEKSMVDSILCINDKDFLAPWHHLGDGLTGNCDAFEK
ALGKSIWVYMSVNPEKNQLFNAAMACDTRLVTSALANECKSIFSDGISTLVDVGGGTGTAVKAISKAFP
DIKCTIYDLPHVIADSPEIPNITKISGDMFKSIPSADAIFMKCILHDWNDDECIQILKRCKEALPKGGKVIIV
DVVIDMDSTHPYAKIRLTLDLDMMLNTGGKERTKEEWKTLFDAAGFASHKVTQISAVQSVIEAYPY

D2D5G4_SOYBN_Glycine_max

MDSLSLFCTGALLAGGLYWFVCVLGPAEQKGKRATDLSGGSISAEKVQDNYKQYWSFFRRPKEIETAD
KVPDFVDTFYNLVTDIYEWGWGQSFHFSPSIPGKSHREATRLHEEMAVDLIEAKPGNKILDVGCGVGGP
MRAIAAHSRANVVGITINEYQVNRARMHNKKAGLDSLCEGVCGNFLKMPFVDNSFDGAYSIEATCHAP
KLEEVYAEIFRVLKPGALYVSYEWVTTDKYSGDDPEHVEVIQGIERGDALPGLRSYAEIAETARKVGFA
VVKERDLAKPPALPWWSRLKMGRIAYWRNHIVVTVLAALGIAPKGTVDVHEMLFKTADYLTRGGDSGI
FSPMHMILCRKPHDKDEQNSG

TCS1_CAMSI_Camellia_sinensis

MELATAGKVNEVLFMNRGEGESSYAQNSSFTQQVASMAQPALENAVETLFSRDFHLQALNAADLGCA
AGPNTFAVISTIKRMMEKKCRELNCQTLELQVYLNDLFGNDFNTLFKGLSSEVIGNKCEEVPCYVMGVP
GSFHGRLFPRNSLHLVHSSYSVHWLTQAPKGLTSREGLALNKGKIYISKTSPPVVREAYLSQFHEDFTMF
LNARSQEVVPNGCMVLILRGRQCSDPSDMQSCFTWELLAMAIAELVSQGLIDEDKLDTFNIPSYFASLEE
VKDIVERDGSFTIDHIEGFDLDSVEMQENDKWVRGEKFTKVVRAFTEPIISNQFGPEIMDKLYDKFTHIVV
SDLEAKLPKTTSIILVLSKIDG

SMT_COPJA_Coptis_japonica

MCTSLSELKCPVFSTKRKLLLEFALRTSVDMAAQEGVNYLSGLGLSRLICLPMALRAAIELNVFEIISQAG
PDAQLSPSDIVAKIPTKNPSAAISLDRILRMLGASSILSVSTTKSGRVYGLNEESRCLVASEDKVSVVPMLL
FTSDKAVVESFYNIKDVVLEEGVIPFDRTHGMDFFQYAGKEERVNKSFNQAMGAGSTIAFDEVFKVYKG
FDNLKELVDVGGGIGTSLSNIVAKHPHIRGINFELPHVIGDAPDYPGVEHVPGDMFEGVPNAQNILLKWV
LHDWDDDRSIKILKNCWKALPENGTVIVIEFVLPQVLGNNAESFNALTPDLLMMALNPGGKERTTIEFDG
LAKAAGFAETKFFPISQGLHVMEFHKINC

DXMT1_COFAR_Coffea_arabica

MELQEVLHMNGGEGDTSYAKNSFYNLFLIRVKPILEQCIQELLRANLPNINKCIKVADLGCASGPNTLLT
VRDIVQSIDKVGQEKKNELERPTIQIFLNDLFQNDFNSVFKSLPSFYRKLEKENGCKIGSCLIGAMPGSFY
GRLFPEESMHFLHSCYCLHWLSQVPSGLVTELGISANKGCIYSSKASRPPIQKAYLDQFTKDFTTFLRIHS
EELISRGRMLLTWICKEDEFENPNSIDLLEMSINDLVIEGHLEEEKLDSFNVPIYAPSTEEVKCIVEEEGSFE
ILYLETFKVPYDAGFSIDDDYQGRSHSPVSCDEHARAAHVASVVRSIFEPIVASHFGEAILPDLSHRIAKN
AAKVLRSGKGFYDSVIISLAKKPEKADM

TNMT_PAPSO_Papaver_somniferum

MGSIDEVKKESAGETLGRLLKGEIKDEELKKLIKFQFEKRLQWGYKSSHQEQLSFNLDFIKSLKKMEMSG
EIETMNKETYELPSEFLEAVFGKTVKQSMCYFTHESATIDEAEEAAHELYCERAQIKDGQTVLDIGCGQG
GLVLYIAQKYKNCHVTGLTNSKAQVNYLLKQAEKLGLTNVDAILADVTQYESDKTYDRLLMIEAIEHM
KNLQLFMKKLSTWMTKESLLFVDHVCHKTFAHFFEAVDEDDWYSGFIFPPGCATILAANSLLYFQDDVS
VVDHWVVNGMHMARSVDIWRKALDKNMEAAKEILLPGLGGSHETVNGVVTHIRTFCMGGYEQFSMN
NGDEWMVAQLLFKKK

Q948P7_COPJA_Coptis_japonica

MAVEAKQTKKAAIVELLKQLELGLVPYDDIKQLIRRELARRLQWGYKPTYEEQIAEIQNLTHSLRQMKI
ATEVETLDSQLYEIPIEFLKIMNGSNLKGSCCYFKEDSTTLDEAEIAMLDLYCERAQIQDGQSVLDLGCG
QGALTLHVAQKYKNCRVTAVTNSVSQKEYIEEESRRRNLLNVEVKLADITTHEMAETYDRILVIELFEH
MKNYELLLRKISEWISKDGLLFLEHICHKTFAYHYEPLDDDDWFTEYVFPAGTMIIPSASFFLYFQDDVS
VVNHWTLSGKHFSRTNEEWLKRLDANLDVIKPMFETLMGNEEEAVKLINYWRGFCLSGMEMFGYNNG
EEWMASHVLFKKK

*CNMT_THLFG_Thalictrum_flavum*_subsp._*glaucum*

MAVEGKQVAPKKAIIVELLKKLELGLVPDDEIKKLIRIQLGRRLQWGCKSTYEEQIAQLVNLTHSLRQMK
IATEVETLDDQMYEVPIDFLKIMNGSNLKGSCCYFKNDSTTLDEAEIAMLELYCERAQIKDGHSVLDLGC
GQGALTLYVAQKYKNSRVTAVTNSVSQKEFIEEESRKRNLSNVEVLLADITTHKMPDTYDRILVVELFE
HMKNYELLLRKIKEWMAKDGLLFVEHICHKTFAYHYEPIDEDDWFTEYVFPAGTMIIPSASFFLYFQDD
VSVVNHWTLSGKHFSRTNEEWLKRLDANVELIKPMFVTITGQCRQEAMKLINYWRGFCLSGMEMFGY
NNGEEWMASHVLFKKK

SMT3B_ARATH_Arabidopsis_thaliana

MDSVALYCTAGLIAGAVYWFICVLGPAERKGKRASDLSGGSISAEKVKDNYNQYWSFFRKPKEIESAEK
VPDFVDTFYNLVTDIYEWGWGQSFHFSPHVPGKSDKDATRIHEEMAVDLIKVKPGQKILDAGCGVGGP
MRAIAAHSKAQVTGITINEYQVQRAKLHNKKAGLDSLCNVVCGNFLKMPFDENTFDGAYSIEATCHAP
KLEEVYSEIFRVMKPGSLFVSYEWVTTEKYRDDDEEHKDVIQGIERGDALPGLRSYADIAVTAKKVGFE

VVKEKDLAKPPSKPWWNRLKMGRIAYWRNHVVVVILSAIGVAPKGTVDVHKMLFKTADYLTRGGETG
IFSPMHMILCRKPEKASE

Q9AXH3_SOLLC_Solanum_lycopersicum

MAAASGQEREVQKSYWIEHTAELTVEAMMLDSKAADLDKEERPEVLSLLPPYEGKTVLELGAGIGRFT
GELAQKAGQLIALDFIEGAIKKNENINGHYKNVKFMCADVTSPNLIFSPESVDLIFSNWLLMYLSDEEVK
ALVERMVIWLKVGGHIFFRESCFHQSGDHKRKNNPTHYRDPSFYTKVFRECHVNAGDGKSFELSLAGC
KCIGAYVKNKKNQNQICWTWQKVTSKDDMEFQRFLDTVQYKCSGILRYERVFGQGFVSTGGLETTKEF
VAMLDLQRGQKVLDVGCGIGGGNFYMAEKYDVHVVGIDLSINMISFALERAIGLKCAVEFEVADCTKK
TYPDCTFDVIYSRDTILHIQDKPALFRSFYKWLRPGGKVLISDYCKRAGPASKEFEGYIKQRGYDLHDVE
AYGQMLRDAGFHEVVAEDRTEQFIKVLQKELDTVEKERESFIHEFSEQDYNEIVGGWKSKLIRSSSGEQR
WGLFIAKKK

UPM1_ARATH_Arabidopsis_thaliana

MALVQRIPISSSSIRNWQQARTNLTPICCLHYNTASSSSSPFTEKHSVERYQRDQWLYKAVEPTPPSTPSPS
PFEDEVFVRENDIASQLPELKKLLAVLKEKRVKGCKGGDCGPGDVYLVGTGPGDPELLTLKAVRVIQSA
DLLLYDRLVSNDVLELVAPDARLLYVGKTAGYHSRTQEEIHELLLNFAEAGATVVRLKGGDPLVFGRG
GEEMDFLQQQGIRVQVIPGITAASGIAAELGIPLTHRGVATSVRFLTGHSRKGGTDPLFVAENAADPDTT
LVVYMGLGTLPSLAQKLMDHGLPSDTPAVAVERGTTPLQRTVFAELKDFATEIQSAGLVSPTLIIIGKVV
ELSPLWPHCTKESSCLVETR

LAMT_CATRO_Catharanthus_roseus

MVATIDSIEMPALPTAVEAHPMKGGDDSHSYSQNSCYQKGVIDAAKAVIVEAVNEKLDLENNPIFDPIKP
FRIADFGCSTGPNTFHAMQNIVESVETKYKSLQKTPEFHVFFNDHVNNDFNVLFRSLPPNREFFAAGVPG
SFYTRVFPKNSIHFAHCSYALHWLSKVPKEIQDKNSLAYNKGRIHYTGTEKHVVKAYFGQFQRDFEGFL
KARAQEIVVGGLMVIQIPGLPSGEVLFSRTGAGLLHFLLGTSLMELVNKGIINEESVDSFNLPQYHPSVED
LEMVIEMNDCFTIERVGTLPHPMKNLPFDVQRTSLQVRAIMECILTEHFGENILDPLFEIYTKNLQENFHV
FDKEIRKDADLYLVLKRKGN

Q8VWX2_PERFR_Perilla_frutescens

MAEAVTPGICTTGWRRGGVHAPTYNISIKPATALLVGCTTKTKSITSFSTDSLRTRGRARRPTMSLNAAA
AEMETEMETLRKGIAEFYDESSGVWENIWGDHMHHGFYEPAADVSISDHRAAQIRMIEESLRFASFSPIT
TTEKPKNIVDVGCGIGGSSRYLARKYGAKLSRAITLSSPVQAQRAQQLADAQGLNGKVSFEVADALNQP
FPEGKFDLVWSMESGEHMPDKKKFVNELVRVAAPGGRIIIVTWCHRDLSPSEESLRQEEKDLLNKICSAY
YLPAWCSTADYVKLLDSLSMEDIKSADWSDHVAPFWPAVIKSALTWKGITSLLRSGWKTIRGAMVMPL
MIEGYKKGVIKFAIITCRKPAS

7OMT_PAPSO_Papaver_somniferum

MDTAEERLKGQAEIWEHMFAFVDSMALKCAVELGIPDIINSHGRPVTISEIVDSLKTNTPSSSPNIDYLTRI
MRLLVHKRLFTSELHQESNQLLYNLTRSSKWLLKDSKFNLSPLVLWETNPILLKPWQYLGKCAQEKSSP
FERAHGCEIWDLALADPKFNNFLNGAMQCSTTTIINEMLLEYKDGFSGIAGSLVDVGGGTGSIIAEIVKA
HPHIQGINFDLPHVVATAAEFPGVKHVGGDMFVDIPEADAVIMKWILHDWSDEDCTIILKNCYRAIRKK
KNGKVIIVDCVLRPDGNDLFDKMGLIFDVLMMAHTTAGKERTEAEWKILLNNAGFPRYNVIRTPAFPCII
EAFPE

ANMT_RUTGR_Ruta_graveolens

MGSLSESHTQYKHGVEVEEDEEESYSRAMQLSMAIVLPMATQSAIQLGVFEIIAKAPGGRLSASEIATILQ
AQNPKAPVMLDRMLRLLVSHRVLDCSVSGPAGERLYGLTSVSKYFVPDQDGASLGNFMALPLDKVFM
ESWMGVKGAVMEGGIPFNRVHGMHIFEYASSNSKFSDTYHRAMFNHSTIALKRILEHYKGFENVTKLV
DVGGGLGVTLSMIASKYPHIQAINFDLPHVVQDAASYPGVEHVGGNMFESVPEGDAILMKWILHCWDD
EQCLRILKNCYKATPENGKVIVMNSVVPETPEVSSSARETSLLDVLLMTRDGGGRERTQKEFTELAIGAG
FKGINFACCVCNLHIMEFFK

Q2XV96_HELAN_Helianthus_annuus

MATTAVGVSATPMTEKLTAADDDQQQQKLKKGIAEFYDESSGMWENIWGEHMHHGYYNSDDVVELS
DHRSAQIRMIEQALTFASVSDDPEKKPKTIVDVGCGIGGSSRYLARKYGAECHGITLSPVQAERANALAA
AQGLADKVSFQVADALNQPFSDGKFDLVWSMESGEHMPDKLKFVSELTRVAAPGATIIIVTWCHRDLN
PGEKSLRPEEEKILNKICSSFYLPAWCSTADYVKLLESLSLQDIKSADWSGNVAPFWPAVIKTALSWKGIT
SLLRSGWKSIRGAMVMPLMIEGFKKDVIKFSIITCKKPE

SMT1_ARATH_Arabidopsis_thaliana

MDLASNLGGKIDKSDVLTAVEKYEQYHVFHGGNEEERKANYTDMVNKYYDLATSFYEYGWGESFHFA
QRWKGESLRESIKRHEHFLALQLGIQPGQKVLDVGCGIGGPLREIARFSNSVVTGLNNNEYQITRGKELN
RLAGVDKTCNFVKADFMKMPFPENSFDAVYAIEATCHAPDAYGCYKEIYRVLKPGQCFAAYEWCMTD
AFDPDNAEHQKIKGEIEIGDGLPDIRLTTKCLEALKQAGFEVIWEKDLAKDSPVPWYLPLDKNHFSLSSFR
LTAVGRFITKNMVKILEYIRLAPQGSQRVSNFLEQAAEGLVDGGRREIFTPMYFFLARKPE

Q984A0_RHILO_Mesorhizobium_japonicum

MADYSIAEHAQAANEQHYELPPEFFGLTLGPNRKYSCCLYPKGNESLAEAEIAALEQTVEHAGLGDGQS
ILELGCGWGSLTLYMAKRFPAARIVAMSNSTPQRLHIEAEAAARGLRNVEVITADMNGFEPRERFDRIVS
VEMFEHMSNWRDLLARIRSWLEPEGRLFVHVFSHRHSPYRFDHRDDADWIARHFFTGGIMPSHGLIGHF
ADCFAIERDWRWNGMHYARTAQQWLSRFDDNYKRIGEILAEVYGRDAALWRRRWRLFHMATEGLFG
HDQGREWGVSHYLLRPAW

SMT2_ARATH_Arabidopsis_thaliana

MDSLTLFFTGALVAVGIYWFLCVLGPAERKGKRAVDLSGGSISAEKVQDNYKQYWSFFRRPKEIETAEK
VPDFVDTFYNLVTDIYEWGWGQSFHFSPSIPGKSHKDATRLHEEMAVDLIQVKPGQKILDVGCGVGGPM
RAIASHSRANVVGITINEYQVNRARLHNKKAGLDALCEVVCGNFLQMPFDDNSFDGAYSIEATCHAPKL
EEVYAEIYRVLKPGSMYVSYEWVTTEKFKAEDDEHVEVIQGIERGDALPGLRAYVDIAETAKKVGFEIV
KEKDLASPPAEPWWTRLKMGRLAYWRNHIVVQILSAVGVAPKGTVDVHEMLFKTADYLTRGGETGIFS
PMHMILCRKPESPEESS

MXMT1_COFAR_Coffea_arabica

MELQEVLHMNEGEGDTSYAKNASYNLALAKVKPFLEQCIRELLRANLPNINKCIKVADLGCASGPNTLL
TVRDIVQSIDKVGQEEKNELERPTIQIFLNDLFQNDFNSVFKLLPSFYRKLEKENGRKIGSCLISAMPGSFY
GRLFPEESMHFLHSCYSVHWLSQVPSGLVIELGIGANKGSIYSSKGCRPPVQKAYLDQFTKDFTTFLRIHS
KELFSRGRMLLTCICKVDEFDEPNPLDLLDMAINDLIVEGLLEEEKLDSFNIPFFTPSAEEVKCIVEEEGSC
EILYLETFKAHYDAAFSIDDDYPVRSHEQIKAEYVASLIRSVYEPILASHFGEAIMPDLFHRLAKHAAKVL
HMGKGCYNNLIISLAKKPEKSDV

SAMT_CLABR_Clarkia_breweri

MDVRQVLHMKGGAGENSYAMNSFIQRQVISITKPITEAAITALYSGDTVTTRLAIADLGCSSGPNALFAV
TELIKTVEELRKKMGRENSPEYQIFLNDLPGNDFNAIFRSLPIENDVDGVCFINGVPGSFYGRLFPRNTLHF
IHSSYSLMWLSQVPIGIESNKGNIYMANTCPQSVLNAYYKQFQEDHALFLRCRAQEVVPGGRMVLTILG
RRSEDRASTECCLIWQLLAMALNQMVSEGLIEEEKMDKFNIPQYTPSPTEVEAEILKEGSFLIDHIEASEIY
WSSCTKDGDGGGSVEEEGYNVARCMRAVAEPLLLDHFGEAIIEDVFHRYKLLIIERMSKEKTKFINVIVS
LIRKSD

PINMT_RAUSE_Rauvolfia_serpentina

MAEKQQAVAEFYDNSTGAWEVFFGDHLHDGFYDPGTTATIAGSRAAVVRMIDEALRFANISDDPAKKP
KTMLDVGCGIGGTCLHVAKKYGIQCKGITISSEQVKCAQGFAEEQGLEKKVSFDVGDALDMPYKDGTF
DLVFTIQCIEHIQDKEKFIREMVRVAAPGAPIVIVSYAHRNLSPSEGSLKPEEKKVLKKICDNIVLSWVCSS
ADYVRWLTPLPVEDIKAADWTQNITPFYPLLMKEAFTWKGFTSLLMKGGWSAIKVVLAVRMMAKAAD
DGVLKFVAVTCRKSK

PINMT_VINMI_Vinca_minor

MYTCSIIIYILTFWQLSKIKKQVAAAEKQVMTVTEKQEAVAEFYDKSTDAWEVFFGEHLHDGFYEPGTT
ATIPGSKVAVVRMIDELLRFAGISDDPEKKPKTMLDVGCGLGGTCLHVAKKYDIKCTGITISPEQVKCAQ
DLAATQGLESKVSFDVGDALDMPYKDGTFDLVFTIQCIEHIQDKEKFIREMVRVAAPGAPVVIAGYAAR
NLSPSEESLKPEEKMVLEKICDHIVLSWLCSTGDYVKWLTPLPVQDIKVWDLTQNITPFYPLCIKEAFTW
KSFTSLLKMGGWSAIKVVFAVKMMAMAAEEGLLKFAAVTCRKSK

RBCMT_PEA_Pisum_sativum

MATIFSGGSVSPFLFHTNKGTSFTPKAPILHLKRSFSAKSVASVGTEPSLSPAVQTFWKWLQEEGVITAKT
PVKASVVTEGLGLVALKDISRNDVILQVPKRLWINPDAVAASEIGRVCSELKPWLSVILFLIRERSREDSV
WKHYFGILPQETDSTIYWSEEELQELQGSQLLKTTVSVKEYVKNECLKLEQEIILPNKRLFPDPVTLDDFF
WAFGILRSRAFSRLRNENLVVVPMADLINHSAGVTTEDHAYEVKGAAGLFSWDYLFSLKSPLSVKAGE
QVYIQYDLNKSNAELALDYGFIEPNENRHAYTLTLEISESDPFFDDKLDVAESNGFAQTAYFDIFYNRTLP
PGLLPYLRLVALGGTDAFLLESLFRDTIWGHLELSVSRDNEELLCKAVREACKSALAGYHTTIEQDRELK
EGNLDSRLAIAVGIREGEKMVLQQIDGIFEQKELELDQLEYYQERRLKDLGLCGENGDILGDLGKFF

RBCMT_ARATH_Arabidopsis_thaliana

MSASVAVVSGFLRIPSIQKSQNPSFLFSRPKKSLVRPISASSSELPENVRNFWKWLRDQGVVSGKSVAEPA
VVPEGLGLVARRDIGRNEVVLEIPKRLWINPETVTASKIGPLCGGLKPWVSVALFLIREKYEEESSWRVY
LDMLPQSTDSTVFWSEEELAELKGTQLLSTTLGVKEYVENEFLKLEQEILLPNKDLFSSRITLDDFIWAFGI
LKSRAFSRLRGQNLVLIPLADLINHNPAIKTEDYAYEIKGAGLFSRDLLFSLKSPVYVKAGEQVYIQYDLN
KSNAELALDYGFVESNPKRNSYTLTIEIPESDPFFGDKLDIAESNKMGETGYFDIVDGQTLPAGMLQYLR
LVALGGPDAFLLESIFNNTIWGHLELPVSRTNEELICRVVRDACKSALSGFDTTIEEDEKLLDKGKLEPRL
EMALKIRIGEKRVLQQIDQIFKDRELELDILEYYQERRLKDLGLVGEQGDIIFWETK

TMT4_CATRO_Catharanthus_roseus

MAEKQQAVAEFYDNSTGAWEVFFGDHLHDGFYDPGTTATIPASRAAVVRMIDEALRFANVSTDPAKKP
RNMLDVGCGIGGTCLYVAKKYDIQCTGITISPEQVKCAQGFAAAQGLENKATFDCGDALNMPYKDGTF
DVVFTIQCIEHIQDKEKFIREMVRVAAPGAAIVIVSYGHRNLSPGEESLKPEEKKTLKKICDNIVLSWLCSS
ADYVRWLTPLPVQDIKTADWTQNIQPFYPLLFKEAFTWRGFTSLLMKGGWSAIKVVLAVKVMAKAAD
DGLLKFMAVTCKKSK

NMT_CATRO_Catharanthus_roseus

MEEKQEKVAEFYDKVTGAWDLFYGVHLHDGYYEPGTTATMAISQDAVIRMIDELLRFAGVSEDPAKKP
RSMLDVGSGLGGTCVYVAKKYDIQCTGITISPNQVKYAQDYAATEGVENKVSFDCGDALDMPYSDGKF
DVVFTINCIEHVHDKEKFIREMVRVAAPGAAIIIASQAHPNLSPGESLKPRDKKILQKICDGAGAVSLCSS
DDYVRWLTPLPVKEIKAADWTQNITPLYPLLMKEAFTWKGFTSIVLKGGWRAINLINAVRLVAKAAND
GILKFAVVTGRKSI

TMT2_CATRO_Catharanthus_roseus

MAAVVEKQEAVAEFYDNSTGAWEELFGEHLHDGYYEPGTTATIPAHRAAVVRMIDEALRFAGVSTDDP
AKKPRNLLDVGCGLGGTCLYLAKKYDIKCTGITISPEQVKCAEDLAAAQGLENKVSFDVGDALDMPYQ
DGEFDVVFTLQCIDHVQDKEKFIREMVRVGSPGAAIVVITYTHRDLSPTEQSLKPHEIKTLKKICDNIVLSS
ISSTHDYVNWMTSLSLKDIKTADWTQNIIPFYPLLFKVSFSMKGFISLLMKGGWSAIKVVLAVKMMSKAI
DDGLLYYTAVSGRKPN

NMT1_ARATH_Arabidopsis_thaliana

MADNNSPPGSVEQKADQIVEANPLVKDDTSLETIVRRFQDSMSEAKTHKFWETQPVGQFKDIGDTSLPE
GPIEPATPLSEVKQEPYNLPSVYEWTTCDMNSDDMCSEVYNLLKNNYVEDDENMFRFNYSKEFLRWAL
RPPGYYQSWHIGVRAKTSKKLVAFISGVPARIRVRDEVVKMAEINFLCVHKKLRSKRLAPVMIKEVTRR
VHLENIWQAAYTAGVILPTPITTCQYWHRSLNPKKLIDVGFSRLGARMTMSRTIKLYKLPDAPITPGFRK
MEPRDVPAVTRLLRNYLSQFGVATDFDENDVEHWLLPREDVVDSYLVESPETHDVTDFCSFYTLPSTIL
GNPNYTTLKAAYSYYNVATQTSFLQLMNDALIVSKQKGFDVFNALDVMHNESFLKELKFGPGDGQLHY
YLYNYRLKSALKPAELGLVLL

ANMT_RAUSE_Rauvolfia_serpentina

MAENQEALAEFYDKGVGVWDNLSREHMHFGYYAPGATATIGGHRASLVRLIDEALCFAEFPDDPEKKP
RNMLDVGCGIGGTCLHVAKKYDIQCKGINISPEQVKIAQGLAAAQGLESKVSFDVGDALDMPYPDGAF
DLVLSIHCIEHLQDKEKFIREMVRVAASGATIIILSHVHRDLSPSEQSLKPQEERVLRKIGSSVQAWFCPLS
NYVSLLAPLPVEVIKIADWSRNIDPSSRLMLKVAFSVKGIVSNLMKGVQGWTAIKNVLPMKLLHKALHD
GLVKFVVLTCRKSN

NNMT_RAUSE_Rauvolfia_serpentina

MAEKQQAVTEFYNNTSPRGAWEFLLGDHLHEGFYDPGTTATISGSQAAAARMIDEALRFANIYDDPSKK
PKNMLDIGCGVGGTCVHVAKQYGIQCKGITLSPEEVKCAQGIAKAQGLEEKVSFDVGDALNLPYKDGT
FDLVLTIECIEHVQDKEKFIREMIRVAAPGAPIVILSYAHRNLSPSAESLKPDEKKVLKKICDNLALSCLCS
SADFVRWLTQLPAEDIKTADWTQNTSPFFPLLMKETFTWKGFTSLLMKGGWTAIKELLALRMMSKAAD
DGLLKFVAITCRKSK

PENMT_CATRO_Catharanthus_roseus

MASMGEKEAVAELYDKVTSNGILEELFGEHLHDGYYEVGTVATISAHRVAVVRIIDEALRFADVFTDDQ
AKKPRNILDVGCGKGGTCVHMARKYDIQCTGISISPDEIQCAKHLAASQGLENKVSFDVGDALNMRYSD
GSFELIFVIQCIEHIQDKEKFIREIVRVAAPGAQIVIISTACRNLSPSEKSLKPKEEKTLKKICNYLHLSGFCS
LSDYSNWLTPLPIEDMKIADWTQNAAPFYTLLLREAFSIKGFISLLMNGGWTAVKVILGMKTIHEAIEND
LLKIVAVTFRKTK

NtNMT1_Narcissus_sp. tete_a_tete

MMDERTKGMVAFFDETAMHDSLWMEDLHHGYYGPGEQAHVSTNHAAEKRMVEEVLKFAGVSDDPIK
KPKNIIDVGCGFGGAAIHLSKKYGANCTGINLSPAQIQKAKNLADANGLGDKTSFVVADALNQPFPDGQ

FDLVWSMEVIEHTPDKLKFISEMARVAAPGATIICTLCCHRDLSPGEKSLKPDEKNLIDKILKTFHQHSYIS
PSDTVKIVQSLALQDIKIADFSENVLPYIRANVQSQRTWKGLASMVLNGWTNFKVSQNQPLTLKTYEKN
LTRYTVIACHKPK

LaTMT1_Leucojum_aestivum

MMRTPKTQNMSTLHTFQLPSLRPQLRLNSRKTCIRRLTRTGTARARPSRPVRAMTSASATDAALRKGIA
ELYDASSGLWESIWGDHMHHGFYESDVAVDISDHRLAQIRMIEEALKFAGVADDSLKGPKKIVDVGCGI
GGSSRYLAKKYGANCCGITLSPVQAQRAQALAVAEGLGDKVSFQVADALDQPFSDGEFDLVWSMESGE
HMPDKRKFVSELARVAAPGATIIIVTWCHRDLSPDEESLRPEEKNLLNKICNAYYLPEWCSAADYVKIVQ
SLALKDIKTADWSENVAPFWPAVIRSAFTWRGATSLLRSGWKTIRGALVMPLMIEGYKKNLIKFAVITC
RKPE

LaTMT2_Leucojum_aestivum

MMTTMTDDLSKGMVAWYDETATQDAVWGEYLHHGYYGPGEEAHVSTNHAAEQRMVDEVLKFAGVS
DDPMKTPRNVIDVGCGFGGAAIYLAKKYEANCTGINLSTAQIQKAKDLAAANGLGDKTSFVVGDALNQ
PFPNGQFDLVWSMEVIEHTPNKLKFISELARIAAPGATIIFTSCCHRDLSPGEDSLKPDEKNLIDKIRKTFH
QYSYISSSDTFKIVQSLPLQDIKMADFSENVLPYFRAIVQSQRTWQGLTSMLLNGWTNFKVSQNWPLML
KAYEKNVTKYTVIACRKPK

LaNMT_Leucojum_aestivum

MGKLVEVPYNATVSVMLASLERNLLPDLVIRRLTRVLLATRLRHGYLPSAELQLSNLIQFKQSLEDMLIA
VETDKAKTQHYELPTSFFELVLGKNLKYSCCYFNGTSNTLEDAENAMLELYCERAQVKDGQSILDVGC
GWGSLSLYIARKYKGCSITGICNSTTQRAYIEEQCRDLQLSNVKIIVADIREFEMEASFDRVISIEMFEHMK
NYKALMKKIATWMKQDSLLFVHYFCHKVFAYHFEDINEDDWITRHFFSGGTMPSANLLLYFQDDVAV
VNHWLVNGMHYSRTSEEWLKRMDQNRAAIRPIMESTYGEDLATKWTVYWRTFFIAVAELFGYNNGEE
WMVAHFLFKKK

LaNMT2_Leucojum_aestivum

MGKLVEVPYNATVSVMLASLERNLLPDLVIRRLTRVLLATRLRHGYLPSAELQLSNLIQFKQSLEDMPIA
VETDKAKTQHYELPTSFFELVLGKNLKYSCCYFNGTSNTLEDAENAMLELYCERAQVKDGQSILDVGC
GWGSLSLYIARKNKGCSITGICNSTTQRAYIEEQCRDLQLSNVKIIVADIREFEMEASFDRVISIEMFEHMK
NYKALMKKIATWMKQDSLLFVHYLCHKVFAYHFEDINEDDWITRHFFSGGTMPSANLLLYFQDDVAV
VNHWLVNGMHYSRTSEEWLKRMDQNRAAIRPIMESTYGEDLATKWTVYWRTFFIAVAELFGYNNGEE
WMVAHFLFKKK

LaNMT3_Leucojum_aestivum

MGKLVEVPYNATVSVMLASLERNLLPDLVIRRLTRVLLATRFRHGYIPSAELQLSNLIQFKQSLEDMPIA
VETDKAKTQHYELPTSFFKLVLGKNLKYSCCYFNGTSNTLEDAENAMLELCCERAQVKDGQSILDVGC
GWGSLSLYIARKYKGCSITGICNSTTQRAYIEEQCRDLRLSNVKIIVADIREFEMEASFDRVISIEMFEHMK
NYKALMKKIATWMKQDSLLFVHYFCHKVLSYHFEDINEDDWITRHFFSGGTMPSANLLLYFQDDVAVV
NHWLVNGMHYSRTSEEWLKRMDQNRAAIRPIMESTYGEDLATKWTVYWRTFFIAVAELFSYNNGEEW
MVAHFLFKKK

HpNMT2_Hippeastrum_cv._hybridum

MGKLVEVPYNATVSVMLASLERNLLPDLVIRRLTRVLLATRLRHGYLPSAELQLSNLIQFKQSLEDMLIA
VETDKAKTQHYELPTSFFELVLGKNLKYSCCYFNGTSNTLEDAENAMLELYCERAQVKDGQSILDVGC
GWGSLSLYIARKYKGCSITGICNSTTQRAYIEEQCRDLQLSNVKIIVADIREFEMEASFDRVISIEMFEHMK
NYKALMKKIATWMKQDSLLFVHYFCHKVFAYHFEDINEDDWITRHFFSGGTMPSANLLLYFQDDVAV
VNHWLVNGMHYSRTSEEWLKRMDQNRAAIRPIRESTYGEDLATKWTVSWRTFFNAVAKLFGYNNGK
KWKVPHFFFKKK

Table 2.S2. Multiple Sequence Alignment Distance Matrix with similarity in percentage for selected methyltransferases.

	LaTMT2_Leucojum_aestivum	*NtNMT1_Narcissus_sp._tete_a_tete*	*LaTMT1_Leucojum_aestivum*	*GTOMC_Arabidopsis_thaliana*	*GTOMC_Canna_indica*	*TMT3_Catharanthus roseus*	*CNMT_PAPSO_Papaver_somniferum*	*LaNMT_Leucojum_aestivum*
LaTMT2_Leucojum_aestivum	100%	81%	53%	47%	53%	50%	18%	19%
NtNMT1_Narcissus_sp._tete_a_tete	82%	100%	54%	47%	52%	49%	17%	19%
LaTMT1_Leucojum_aestivum	44%	44%	100%	61%	72%	66%	17%	18%
GTOMC_Arabidopsis_thaliana	40%	39%	61%	100%	61%	62%	18%	17%
GTOMC_Canna_indica	44%	43%	71%	61%	100%	67%	18%	19%
TMT3_Catharanthus roseus	39%	39%	62%	58%	63%	100%	15%	17%
CNMT_Papaver_somniferum	15%	14%	17%	17%	18%	16%	100%	49%
LaNMT_Leucojum_aestivum	16%	16%	17%	17%	19%	18%	48%	100%

Table 3.S3. List of sequences used for phylogenetic analysis of AKRs.

> AKR2A1_P28475.1_*Malus domestica*
MSTVTLSSGYEMPVIGLGLWRLEKDELKEVILNAIKIGYRHFDCAAHYKSEADVGEALAEAFK
TGLVKREELFITTKIWNSDHGHVVEACKNSLEKLQIDYLDLYLVHYPMPTKHNAIGKTASLLG
EDKVLDIDVTISLQQTWEGMEKTVSLGLVRSIGLSNYELFLTRDCLAYSKIKPAVSQFETHPYF
QRDSLVKFCMKHGVLPTAHTPLGGAAANKDMFGSVSPLDDPVLNDVAKKYGKSVAQICLRW
GIQRKTAVIPKSSKIQRLKENLEVLEFQLSDEDMQLIYSIDRKYRTSLPSKTWGLDVYA
>AKR2A2_AAB97617.1_*Apium graveolens*
MAITLNSGFKMPVLGLGVWRMDRNEIKNLLLSAINLGYRHFDCAADYKNELEVGEAFKEAFD
TDLVKREDLFITTKLWNSDHGHVIEACKNSLKKLQLEYLDLYLIHFPMASKHSGIGTTRSILDD
EGVWEVDATISLEATWHEMEKLVEMGLVRSIGISNYDVYLTRDILSYSKIKPAVNQIETHPYFQ
RDSLIKFCQKYGIAITAHTPLGGALANTERFGSVSCLDDPVLKKLSDKHNKSPAQIVLRWGVQ
RNTIVIPKSSKTKRLEENINIFDFELSKEDMELIKTMERNQRSNTPAKAWGIDVYA
>AKR2A3_QLF98851.1_*Oryza sativa*
SSRLRFQRGGGAEQRRGMAAAQGSGVPAALALSSGHTMPSVGLGVWRMDSPAIRDLIHSALR
IGYRHFDCAADYQNEAEVGDALAEAFQTGLVKREDLFITTKLWNSDHGHVVEACKDSLKKLR
LDYLDLYLIHFPVATRHTGVGTTASALGDDGVLDIDTTISLETTWHAMEDLVSMGLVRSIGISN
YDIFLTRDCLAYAKIKPAVNQIETHPYFQRDCLVKFCQKHGILVTAHTPLGGSTANTEWFGSVS
CLDDPVIKSLAEKYGKTPAQLVLRWGLQRNTVVIPKTSKEERLQENFAVFDFAISDEDMEKMR
SIDRKYRTNQP
>AKR4A1_P26690.1_*Glycine max*

MAAAIEIPTIVFPNSSAQQRMPVVGMGSAPDFTCKKDTKEAIIEAVKQGYRHFDTAAAYGSEQ
ALGEALKEAIHLGLVSRQDLFVTSKLWVTENHPHLVLPALRKSLKTLQLEYLDLYLIHWPLSS
QPGKFSFPIEVEDLLPFDVKGVWESMEECQKLGLTKAIGVSNFSVKKLQNLLSVATIRPVVDQ
VEMNLAWQQKKLREFCKENGIIVTAFSPLRK-
GASRGPNEVMENDVLKEIAEAHGKSIAQVSLRWLYEQGVTFVPKSYDKERMNQNLHIFDWAL
TEQDHHKISQISQSRLISGPTKPQLADLWDDQI

>AKR4A2_Q40333_*Medicago sativa*

MGSVEIPTKVLTNTSSQLKMPVVGMGSAPDFTCKKDTKDAIIEAIKQGYRHFDTAAAYGSEQA
LGEALKEAIELGLVTRDELFVTSKLWVTENHPHLVIPALQKSLKTLQLDYLDLYLIHWPLSSQP
GKFTFPIDVADLLPFDVKGVWESMEESLKLGLTKAIGVSNFSVKKLENLLSVATVLPAVNQVE
MNLAWQQKKLREFCNAHGIVLTAFSPLRKGASRGPNEVMENDMLKEIADAHGKSVAQISLR
WLYEQGVTFVPKSYDKERMNQNLRIFDWSLTKEDHEKIDQIKQNRLIPGPTKPGLNDLYDD

>AKR4A3_BAA12084.1_*Glycyrrhiza echinate*

MAAAAAAAIEIPTKVLPNSTCELRVPVIGMGSAPDFTCKKDTKEAIIEAIKQGYRHFDTAAAYG
SETALGEALKEARDLGLVTREELFVTSKLWVTENHPHLVIPALRKSLETLQLEYLDLYLIHWPL
SSQPGKFSFPIQVEDLLPFDVKGVWESMEECLKLGLTKAIGVSNFSVKKLQNLLSVATIRPAVN
QVEMNLAWQQKKLREFCTANGIVLTAFSPLRKGASRGPNEVMENDMLKGIAEAHGKSIAQVS
LRWLYEQGVTFVAKSYDKERMNQNLQIFDWELTTEDHQKIDQIKQNRLIPGPTKPQLNDLWD
DEL

>AKR4A4_BAA13113.1_*Glycyrrhiza glabra*

MAAAAIEIPTKVLPNSTCELRVPVIGMGSAPDFTCKKDTKEAIIEAIKQGYRHFDTAAAYGSET
ALGEALKEARDLGLVTREDLFVTSKLWVTENHPHLVVPALRKSLETLQLEYLDLYLIHWPLSS
QPGKFSFPIQAEDLLPFDVKGVWESMEESLKLGLTKAIGVSNFSVKKLQNLLSVATIRPAVNQV
EMNLAWQQKKLREFCNANGIVLTAFSPLRKGASRGPNEVMENDMLKGIAEAHGKSIAQVSLR
WLYEQGVTFVAKSYDKERMNQNLQIFDWELTTEDHQKIDQIKQNRLIPGPTKPQLNDLWDDE
I

>AKR4B1_CAA11226.1_*Sesbania rostrata*

MAEKKIPEVLLNSGHKMPVIGMGTSVESRPSNDVLASIFVDAIQVGYRHFDSASVYGTEEAIG
MAVSKAIEQGLIKSRDEVFITSKPWNTDAHHDLIVPALKTTLKKLGMEYVDLYLIHWPVRLRH
DLENPVIFSKEDLLPFDIEGTWKAMEECYRLGLAKSIGICNYGTKKLTKLLEIATIPPAVNQVEM
NPSWQQGNLREFCKQKGIHVSAWSPLGAYKIFWGSGAVMENQILQDIATAKGKTIAQVALRW
VYQQGSSAMAKSFNKERMKQNLEIFDFELSEEELEKIKQIPQRRQYTGDMWLSENGSCKTLEE
LWDGDV

>AKR4B2_AAF13739.1_*Papaver somniferum*

MESNGVPMITLSSGIRMPALGMGTAETMVKGTEREKLAFLKAIEVGYRHFDTAAAYQSEECL
GEAIAEALQLGLIKSRDELFITSKLWCADAHADLVLPALQNSLRNLKLEYLDLYLIHHPVSLKP
GKFVNEIPKDHILPMDYKSVWAAMEECQTLGFTRAIGVSNFSCKKLQELMAAAKIPPVVNQV
EMSPTLHQKNLREYCKANNIMITAHSVLGAIGAPWGSNAVMDSKVLHQIAVARGKSVAQVS
MRWVYQQGASLVVKSFNEGRMKENLKIFDWELTAEDMEKISEIPQSRTSSAAFLLSPTGPFKT
EEEFWDEKD

>AKR4B3_AAF13736.1_*Papaver somniferum*

MESNGVPMITLSSGIRMPALGMGTAETMVKGTEREKLAFLKAIEVGYRHFDTAAAYQTEECL
GEAIAEALQLGLIKSRDELFITSKLWCADAHADLVLPALQNSLRNLKLDYLDLYLIHHPVSLKP
GKFVNEIPKDHILPMDYKSVWAAMEECQTLGFTRAIGVCNFSCKRLQELMETANSPPVVNQV
EMSPTLHQKNLREYCKANNIMITAHSVLGAVGAAWGTNAVMHSKVLHQIAVARGKSVAQVS
MRWVYQQGASLVVKSFNEARMKENLKIFDWELTAEDMEKISEIPQSRTSSAAFLLSPTGPFKT
EEEFWDEKD

>AKR4B4_AAB97005.1_*Fragaria ananassa*

MAKVPSVTLSSCGDDIQTMPVIGMGTSSYPRADPETAKAAILEAIRAGYRHFDTAAAYGSEKD
LGEAIAEALRLQLIKSRDELFITTKLWASFAEKDLVLPSIKASLSNLQVEYIDMYIIHWPFKLGK

EVRTMPVERDLVQPLDIKSVWEAMEECKKLGLARGIGVSNFTSSMLEELLSFAEIPPAVNQLE
MNPAWQLKKLRDFCKAKGIHVTAYSPLGAARTKWGDDRVLGSDIIEEIAQAKGKSTAQISLR
WVYEQGVSIVTKSYNKERMRQNLDIFDFCLTEEELEKMSHLPQRKGVTFASILGPHDIVLEVD
EEL

>AKR4B5_BAF03164.1_*Zea mays*
MSATGRAPCGLPRVGLGTAVQGPRPDPVRAAVLRAIQLGYRHFDTAAHYATEAPIGEAAAEA
VRTGLVASREDLFVTSKVWCADAHRDRVLPALRRTLSNLQMEYVDLYMVHWPVTMKAGRF
TAPFTPEDFEPFDMRAVWEAMEECHRLGLAKAIGVCNFSCKKLETLLSFATIPPVVNQVEINPV
WQQRKLREFCRAKGIQLCAYSPLGAKGTHWGSDSVMDSGVLHEIAKSKGKTVAQVCLRWVY
EQGDCLIVKSFDEGRMKENLDIVDWELSEEERQRISKIPQRKINQGRRYVSEHGPYKSFEELWA
GEI

>AKR4B6_BAF03161.1_*Oryza sativa*
MSDGGAGAKGAGFGMPRVGMGTAVQGPRPEPIRRAVLKAIEAGYRHFDTAAHYETEAPIGEA
AAEAVRSGAIASRADPFITSKLWCSDAHRDRVLPALRQTLWNLQMEYVDLYLVHWPVSMKP
GRYKAPFTADDFVPFDMRAVWEAMEECHRLGLAKAIGVCNFSCKKLDTLLSFATIPPAVNQV
EVNPVWQQRKLRELCREKGVQICAYSPLGASGTHWGSDSVMASAVLRDIAQSKGKTVAQVC
LRWVYEQGDCLIVKSFDEARMRENLDIVGWELTEEERQRIAGIPQRKINRALRFVSDHGPYKS
LDDLWDGEI

>AKR4B7_BAF03162.1_*Hordeum vulgare*
MGAGDRTVAGMPRIGMGTAVQGPKPDPIRRAVLRAIEIGYRHFDTAAHYETEAPIGEAAAEA
VRSGAVASRDDLFITSKLWCSDAHGDRVVPALRHTLRNLQMEYVDLYLVHWPVSMKPGRFK
APFTAEDFVPFDMRAVWEAMEECHRLGLAKAIGVANFSCKKLDTLLSFATIPPTVNQVEVNPV
WQQRKLREFCRGKGIQLCAYSPLGAKGTHWGSDAVMDAGVLQDIAASRGKSVAQVCLRWV
YEQGDCLIVKSFDEARMRENLDVDGWELTEEERRRIAEIPQRKINLGKRYVSDHGPYKSLEEL
WDGEI

>AKR4B8_BAF03163.1_*Triticum aestivum*
MGAGDRTAAGMPRIGMGTAVQGPKPDPIRRAVLRAIEVGYRHFDTAAHYETEAPIGEAAAEA
VRSGAVASRDDLFITSKLWCSDAHRDRVVPALRQTLRNLQMEYVDLYLVHWPVSMKPGRFK
APFTADDFVPFDMRAVWEAMEECHRLGLAKAIGVANFSCKKLDTLLSFATIPPTVNQVEVNP
VWQQRKLREFCRGKGIQLCAYSPLGAKGTHRGSDAVMDAGVLQEIAASRGKSVAQVCLRWV
YEQGDCLIVKSFDEARMRENLDVDGWELTEEERRRIAEIPQRKINLGKRYVSEHGPYKSLEEL
WDGEI

>AKR4B10_ADK94763.1_*Erythroxylum coca*
MERQVPRVLLNSGHEMPVIGFGTAIDPLPEPEQLVSAILHAIEVGYRHFDTASAYMTEEPVGRA
ISEAMKRGLIKGREELFVTSKLWCADAHRDLIIPALKETLKRLGLDYLDLYLIHFPVRLKKEAV
SLEHEIDDFRFEDHELLPFDIKGTWEAMEECSRLGLTKSIGVSNYGTVKISQLLQHATIPPAVNQ
VEMNVAWQQKKLREFCSKKGIHVTAWSPLAGIGAFWGSTVVIESKTLKEIAAAKGKSVAQVA
LRWIQDQGASCIVKSMNKDRMKQNLEIFGWKLSDEDGRKIEQIKQSRLYPAKLFINENSPYPSL
EALWDGDL

>AKR4C1_P23901.1_*Hordeum vulgare*
MASAKATMGQGEQDHFVLKSGHAMPAVGLGTWRAGSDTAHSVRTAITEAGYRHVDTAAEY
GVEKEVGKGLKAAMEAGIDRKDLFVTSKIWCTNLAPERVRPALENTLKDLQLDYIDLYHIHW
PFRLKDGAHMPPEAGEVLEFDMEGVWKEMENLVKDGLVKDIGVCNYTVTKLNRLLRSAKIPP
AVCQMEMHPGWKNDKIFEACKKHGIHVTAYSPLGSSEKNLAHDPVVEKVANKLNKTPGQVL
IKWALQRGTSVIPKSSKDERIKENIQVFGWEIPEEDFKVLCSIKDEKRVLTGEELFVNKTHGPYR
SAADVWDHEN

>AKR4C2_AAA21751.1_*Bromus inermis*
MASAKAMMGQERQDHFVLKSGHAIPAVGLGTWRAGSDTAHSVQTAITEAGYRHVDTAAEY
GVEKEVGKGLKAAMEAGIDRKDLFVTSKLWCTDLVPDRVRPALEKTLKDLQLDYLDLYLIH
WPFRLKDGAHKPPEAGEVLEFDMEGVWKEMENLVKDGLVKDIGVCNYTVTKLNRLLQSAKI

APAVCQMEMHPGWKNDKILEACKKHGIHATAYSPLCSSEKNLAHDPVVEKVANKLNKTPGQ
VLIKWALQRGTIVIPKSSKDERIKENIQVFGWEIPEEDFQVLCSIKDEKRVLTGEELFVNKTHGP
YKSASEVWDNEN

>AKR4C3_Q43320_*Avena fatua*
MASAKAMGQGEQDRFVLKSGHAIPAVGLGTWRAGSDTAHSVQTAITEAGYRHVDTAAQYGI
EKEVDKGLKAAMEAGIDRKDLFVTSKIWRTNLAPERARPALENTLKDLQLDYIDLYLIHWPFR
LKDGAHQPPEAGEVLEFDMEGVWKEMEKLVKDGLVKDIDVCNFTVTKLNRLLRSANIPPAVC
QMEMHPGWKNDKIFEACKKHGIHVTAYSPLGSSEKNLVHDPVVEKVANKLNKTPGQVLIKW
ALQRGTSVIPKSSKDERIKENIQAFGWEIPEDDFQVLCSIKDEKRVLTGEELFVNKTHGPYKSAS
EVWDHEN

>AKR4C4_AAD22264.1_*Xerophyta viscosa*
MAHAPCFADAKTQSFKLLSGHSIPAVGLGTWKSGDKAGNAVYTAITEGGYRHIDTAAQYGVH
EEVGNALQSALKAGINRKALFVTSKVWCEDLSPERVRPALKNTLEELQLDYLDLYLIHWPIHL
KKGAHMPPEAGEVLEFDIGGVWREMEKLVKVGLVRDIGISNFTVKKLEKLLNFAEIKPSVCQ
MEMHPGWRKHKMFEICRKYGIHTTAYSPLGSSERDLLSDPTVLKIANKLNKSPGQLLVRWAV
QRGTSVIPKSTNPERIKENIQVFGWEIPAEDFQILSSLSEQKRVLDGEDLFVNKTHGPFRSAAEL
WDGEV

>AKR4C5_CAC32834.1_*Digitalis purpurea*
MAEEIRFFKLNTGAKIPSVGLGTWQSSPGDAAQAVEVAIKCGYRHIDGARLYENEKEIGVVLK
KLFDDGVVKREDLFITSKLWSTDHAPEDVPVALDKTLEDLQLDYIDLYLIHWPVRLKKGSVGL
DPENFIPTDIPGTWKAMEALYDSGKARAIGVSNFTLKKLSDLLDVARIPPAVNQVGCHPSCAQ
TKLRAFCKSKGVHLSGYSPLGSPGTPWVKHDVLENPILVDVAEKLGKTPAQVAIRWGLQMGH
SVLPKSVHESRIKENIDVFSWCIPDDLFAKFSEIEQVSPGKPEFPVHPEISQYKTVEEMWDGGI

>AKR4C6_CAC32835.1_*Digitalis purpurea*
MAEEIRFFELNTGAKIPSVGLGTWQSSPGDAAQAVEVAIKCGYRHIDGARLYENEKEIGVVLK
KLFDDGVVKREDLFITSKLWSTDHAPEDVPVALDKTLEDLQLDYIDLYLIHWPVRLKKGSVGL
DPENFVPTDIPGTWKAMEALYDSGKARAIGVSNFTLKKLSDLLDVARIPPAVNQVGCHPSCAQ
TKLRAFCKSKGIHLSGYSPLGSPGTPWVKHDVLENPILVDVAEKLGKTPAQVALRWGLQMGH
SVLPKSVHESRIKENIDVFSWCIPDVLFAKFSEIEQVSPGKPEFPVHPEISQYKTVEEMWDGGI

>AKR4C7_ABF61890.1_*Zea mays*
MARHFVLNTGAKIPSVGLGTWQSDPGVVGNAVYAAVKAGYRHIDCARVYGNEKEIGLALKK
LFEEGVVKREDLFITSKLWNDHHAPEDVPEALNDSLNDLQLEYLDLYLIHWPFRVKKGTNTSP
ENFVTPDFPATWGAMEKLYDAGKARAIGVSNFSSKKLGDLLAVARVPPAVDQVECHPGWQQ
TKLHSFCQSTGVHLTAYSPLGSPGTTWMNGNVLKEPIIISIAEKLGKTSAQVALRWNIQMGHSV
LPKSTNEERIKQNLDVYDWSIPDDLLAKFSEIKQARLLRGNFIVNPESVYKTHEELWDGEL

>AKR4C8_ABH07514.1_*Arabidopsis thaliana*
MAAPIRFFELNTGAKLPCVGLGTYAMVATAIEQAIKIGYRHIDCASIYGNEKEIGGVLKKLIGD
GFVKREELFITSKLWSNDHLPEDVPKALEKTLQDLQIDYVDLYLIHWPASLKKESLMPTPEML
TKPDITSTWKAMEALYDSGKARAIGVSNFSSKKLTDLLNVARVTPAVNQVECHPVWQQQGL
HELCKSKGVHLSGYSPLGSQSKGEVRLKVLQNPIVTEVAEKLGKTTAQVALRWGLQTGHSVL
PKSSSGARLKENLDVFDWSIPEDLFTKFSNIPQEKFCRATEFAHETHGFYKTIEELWDGEI

>AKR4C9_ABH07515.1_*Arabidopsis thaliana*
MANAITFFKLNTGAKFPSVGLGTWQASPGLVGDAVAAAVKIGYRHIDCAQIYGNEKEIGAVL
KKLFEDRVVKREDLFITSKLWCTDHDPQDVPEALNRTLKDLQLEYVDLYLIHWPARIKKGSVG
IKPENLLPVDIPSTWKAMEALYDSGKARAIGVSNFSTKKLADLLELARVPPAVNQVECHPSWR
QTKLQEFCKSKGVHLSAYSPLGSPGTTWLKSDVLKNPILNMVAEKLGKSPAQVALRWGLQM
GHSVLPKSTNEGRIKENFNVFDWSIPDYMFAKFAEIEQARLVTGSFLVHETLSPYKSIEELWDG
EI

>AKR4C10_ABH07516.1_*Arabidopsis thaliana*

MAEEIRFFELNTGAKIPSVGLGTWQADPGLVGNAVDAAVKIGYRHIDCAQIYGNEKEIGLVLK
KLFDGGVVKREEMFITSKLWCTYHDPQEVPEALNRTLQDLQLDYVDLYLIHWPVSLKKGSTG
FKPENILPTDIPSTWKAMESLFDSGKARAIGVSNFSSKKLADLLVVARVPPAVNQVECHPSWQ
QNVLRDFCKSKGVHLSGYSPLGSPGTTWLTSDVLKNPILGGVAEKLGKTPAQVALRWGLQM
GQSVLPKSTHEDRIKQNFDVFNWSIPEDMLSKFSEIGQGRLVRGMSFVHETSPYKSLEELWDG
EI

>AKR4C11_ABH07517.1_Arabidopsis thaliana
MADEIGFFQLNTGAKIPSVGLGTWQAAPGVVGDAVAAAVKIGYQHIDCASRYGNEIEIGKVLK
KLFDDGVVKREKLFITSKIWLTDLDPPDVQDALNRTLQDLQLDYVDLYLMHWPVRLKKGTV
DFKPENIMPIDIPSTWKAMEALVDSGKARAIGVSNFSTKKLSDLVEAARVPPAVNQVECHPSW
QQHKLHEFCKSKGIHLSGYSPLGSPGTTWVKADVLKSPVIEMIAKEIGKSPAQTALRWGLQMG
HSILPKSTNEGRIRENFDVLGWSIPKEMFDKFSKIEQARLVQGTSFVHETLSPYKTLEELWDGEI

>AKR4C12_ABL61257.1_*Aloe arborescens*
MAKFFTLNTGAKIPSIGLGTWRAEPGVVENAVTAAIKAGYRHIDCAAMYGNEKEIGFSLKKLL
EDAVVKREDLFITSKLWLTEQAREDVPLALAKTLEELQLDYIDLYLIHWPFRLKKGTTLSADN
LIPSDIPSTWSAMEKLFYSGKSRAIGVSNFSSKKLEDLLAVALVPPAVNQVECHPVWQQKQLR
SVCESKGVHLSAYSPLGSPGTKRIDVLAHPVIVEAAEKLGKTPAQVALRWGLQMGQSMLPKS
TNESRIKANLDIFDWSIPEDMFAKFAEIEQVRLIRGNFVKPDGLYKSEEEVWDGEI

>AKR4C13_ADU32868.1_*Zea mays*
MASAQAVGQGERGHFVLKSGHTIPAVGLGTWRAGSDTAHSVRTAIAEAGYRHVDTAAQYGV
EKEVGRGLKAAMEGGINRKDLFVTSKLWCTELAPDRVRPALEKTLKDLQLDYLDLYLIHWPF
RLKDGAHMPPEAGEVLEFDMEGVWREMEGLVKDGLVKDIGVCNYTVAKLNRLMRSANVPP
AVCQMEMHPGWKNDRIFEACKKHGIHVTAYSPLGSSEKNLAHDPLVEKVANKLDKTPGQVL
LRWALQRGTSVIPKSTRDERIKENIQVFGWEIPEEDFRALCGIKDEKRVLTGEELFVNKTHGPY
KSATEVWDHED

>AKR4C14_ACS92968.1_*Oryza sativa*
MAKHLVLNTGAKIPSVGLGTWQSDPGVVGNAVYAAVKAGYRHIDCASAYNNEKEVGLALK
KLFEEGVVKREDLFITSKLWCDHHAPEDVPEALDATLNDLQLEYLDLYLIHWPFRTKKGSSIG
KPESYLPPDIPSTWAAMEKLYDSGKSRAIGVSNFSSKKLGDLLAAARVPPAVDQVECHPGWQ
QMKLHNFCQSTGIHLSAYSPLGSPGSTFMNGNVLKEPIIISIAEKLGKTPAQVALRWNIQMGHS
VLPKSVSEERIKQNLDVYDWSIPEDLLAKFSEIKQVRLLRGNFIVNPQSVYKTHEELWDGEI

>AKR4C15_ALN39070.1_*Oryza sativa*
MARCFVLNTGAKIPSVGLGTWQAEPGVVGNAVYAAVKAGYRHIDCAQAYFNEKEIGVALKK
VFDEGIVKREDIFITSKLWCTNHAPEDVPVALDSTLQDLQTDYVDLYLIHWPVRMKKGAGFG
GQNVLPTDIPATWAAMEKLHDSGKARAIGVSNFSSKKLEDLLAVARVPPAVDQVECHPVWQ
QTKLRKFCTSKGIHLSAYSPLGSPGTASVKAVGNVLAHPVVVSTAEKLGKTPAQVALRWGIQ
MGHSVLPKSTHEERIKENIDVYDWSIPEDLFIKLSEIEQMKLIRGEFWTHPEGVYKSIEELWDGE
I

>AKR4C16_QFG75509.1_*Echinochloa colona*
MARHFVLNTGAKIPSVGLGTWQSDPGVVGDAVYAAVKAGYRHIDCARVYGNEKEIGLALKK
LFEEGVVKREDLFITSKLWNDHHAPEDVPEALNESLKDLQLDYLDLYLIHWPFRVKKGTNTSP
ENFITPDIPATWGAMEKLYDAGKARAIGVSNFSSKKLGDLLAVARVPPAVDQVECHPGWQQT
KLHNFCQSTGVHLSAYSPLGSPGTTWMNGNVLKEPVIISIAEKLGKTPAQVALRWNIQMGHSV
LPKSTNEERIKQNLDVYDWSIPDDLLAKFSEIKQARLLRGNFIVNPQSVYKTHEELWDGEL

>AKR5C17_QFG75510.1_*Echinochloa colona*
MARHFVLNTGAKIPSVGLGTWQSDPGVVGDAVYTAVKAGYRHIDCAKVYGNEKEIGLALKK
LFEEGVVKREDLFITSKLWNDRHAPEDVPEALNESLTDLQLDYLDLYLIHWPFRVKKGTNTSP
ENFITPDIPATWGAMEKCYDAGKARAIGVSNFSSKKLGDLLAVARVHPAVDQVECHPGWQQT
KLHNFCQSTGVHLTAYSPLGSPGTTWMNGNVLKEPVIISIAEKLGKTPAQVALRWNIQMGHSV
LPKSTNEERIKQNLDVYDWSIPDDLLAKFSEIKQARLLRGNFIVNPQSVYKTHEELWDGEL

>AKR6C1_AAA87294.1_*Arabidopsis thaliana*
MQYKNLGKSGLKVSTLSFGAWVTFGNQLDVKEAKSILQCCRDHGVNFFDNAEVYANGRAEE
IMGQAIRELGWRRSDIVISTKIFWGGPGPNDKGLSRKHIVEGTKASLKRLDMDYVDVLYCHRP
DASTPIEEAVRAMNYVIDKGWAFYWGISEWSAQQITEAWGAADRLDLVGPIVEQPEYNMFAR
HKVETEFLPLYTNHGIGLTTWSPLASGVLTGKYNKGAIPSDSRFALENYKNLANRSLVDDVLR
KVSGLKPIAGELGVTLAQLAIAWCASNPNVSSVITGATRGSQIQENMKAVDVIPLLTPIVLDKIE
QVIQSKPKRPESYR

>AKR6C2_CAA12646.1_*Egeria densa*
MQYKNLGRSGLRVSQLSYGSWVSFGNQVDVKEAKALLQCCRDHGVNFFDNAEVYANGRAE
EIMGQAFRELGWKRSDLVVSTKIFWGGPGPNDKGLSRKHVVEGLRASLKRLDMDYVDIVYC
HRPDASTPIEETVRAMNHVIDRGWAFYWGTSEWSSQQITEPWAAAENLDLVGPIVEQPEYNLL
SRHKVEAEYLPLYEKYGIGLTTWSPLASGVLTGKYTKGNIPADSRFALENYKNLASRTLVDDI
LRKVNGLKPIAAELGVPLAQLAIAWCASNPHVSSVITGATKESQIIENMKAIDVIPLLTPEVLEKI
EAVVQSKPKRPESYR

>AKR13D1_AAX11684.1_*Rauvolfia serpentina*
MPRVKLGTQGLEVSKLGFGCMGLSGDYNDALPEEQGIAVIKEAFNCGITFFDTSDIYGENGSN
EELLGKALKQLPREKIQVGTKFGIHEIGFSGVKAKGTPDYVRSCCEASLKRLDVDYIDLFYIHRI
DTTVPIEITMGELKKLVEEGKIKYVGLSEASPDTIRRAHAVHPVTALQIEYSLWTRDIEDEIVPL
CRQLGIGIVPYSPIGRGLFAGKAIKESLPENSVLTSHPRFVGENLEKNKQIYYRIEALSQKHGCTP
VQLALAWVLHQGEDVVPIPGTTKIKNLHNNVGALKVKLTKEDLKEISDAVPLDEVAGESIHEV
IAVTNWKFANTPPLK

>AKR13D2_A08G1908_*Gossypium hirsutum*
MAIQIPRVKLGSQGFEVSKLGFGCMGLSDHYGSVSDEVGIAIIKHAFERGITHFDTAELYGPKT
NEILVGKALKHLPREKVQLATKFGVESMGAGGPVINGTPEFVRSSLEASLQRLDVDYIDLYYII
RVDTNTPIEDTMEELKKLVEEGKIKYIGISEASPETIRRAHAVHPLTAVQIEWSLWTRDVEEEIIP
LCRELGIGIVPYSPLGRGFFAGKAKGDISSFLGMFPRFQGENLEKNRILYSKVEKLAEKYGCTP
AQLALSWVLHQGDDVAPIPGTTKIKNLDSNIDSVKVKLTKEDLKEISDVIPIHEVSGGSYPDAL
KKYSWQYGNTPPKKST

>NtAKR_PP708064_*Narcissus* cv. *Tête*-à-*Tête*
MLNNIPELILTKDSRAMPVVGMGTATHPFPQDNTKSAIMDAIEIGYRHFDTASLYGSEEPLGEA
MVEAQKLGLIKSREELFITSKLWCNEAHPGLVIPAIKKSLLNLKLDYLDLYLIHMPFTTKPESPP
FPLYKEDMVTMDLQGVWKAMEECKRLGMAKAIGVSNFTVNKLEELLPFAKIPPQVNQVEMN
PAWQQQKLRQYCNAKGIHVTAYSPLGGQEEPSSPNMVMKSEDLKQIANARGKTVAQVSLRW
VYEQGVSIVVKSFNKERIKKNIEIFDWNLSEEECHMISQIPQCKKTTVEAMFSNWKPHPDEYFF
EENEGE

>LauAKR1_*Lycoris aurea*
MSNIPELILTKESRAMPVVGMGTAAYPFAPENTESAIINAIEIGYRHFDTASLYGSEEPLGKAVV
EAQKLGFIKSREELFITSKLWCNEAYPDLVIPAIKKSLRNLKMEYLDLYLIHMPFSTKPDSSPPV
PVNGEDIVAMDMEGVWKAMEECQRLGMAKAIGVSNFTVKKLEELLSVANIPPQVNQVEMNP
TWQQKKLREYCNVKGIHVTAYSPLGGQDTLISPNMVVKSEVLKEIANARGKTLAQVSLRWVY
EQGVSIVVKSFNKERIKKNIEIFDWNLSEDECHRISQIPQYKRVTVETLVSNWKPRPDEFFSEEN
EDE

>LauAKR2_*Lycoris aurea*
MSNIPELILTKDSRAMPVVGMGTAAYPLAPENTESAIINAIEIGYRHFDTASLYGSEEPLGKAIV
EAQKLGFIKSREELFITTKLWCNEAHPDLVIPAIKKSLRNLKMDYLDLYLIHLPFSTIPESPPFPL
YEEDIVAMDMQGVWKAMEECKRLGMAKAIGVSNFTVKKLEELLPIAKIPPQVNQVEMNPTW
QQKKLRQYCNAKGIHVTAYSPLGGQEAPISTNMVTKSEVLKQIANARGKTVAQVSLRWAYEQ
GVSMVVKSFNKERMKANIEIFDWNLSEEECCMISQIPQCKRYTMETIISNWKSHTDDEHFFVEE
ENRDNEF

>AKR1_*Leucojum aestivum*
MLSIPEVILTKDSRAMPVVGMGTAAFPFAPENTELAIINAIEIGYRHFDTASLYCSEEPLGKAVV
EAQKLGFIKSREELFITSKLWCNEAHPDLVIPAIKKSLRNLKMEYLDLYLIHMPFSTKWDSSPPI
PVNGKDIVAMDMEGVWKAMEECQRLGMAKAIGVSNFTIKKLEELLSVANIPPQVNQVEMNP
TWQQKKLREYCNVKGIHVTAYSPLGGQDALVSPNMVVKSEVLKEIANARGKTVAQVSLRWI
YEQGVSVVVKSFNKERIKNNIEIFDWNLSEEECYQISQIPQRKRVTVETVVSNSKPHPDEFFFEE
NGEE

>AKR2_*Leucojum aestivum*
MLSIPEVILTKESRAMPVVGMGTAAFPFAPENTELAIINAIEIGYRHFDTASLYCSEEPLGKAVV
EAQKLGFIKSREELFITSKLWCNEAHPDLVIPAIKKSLRNLKMEYLDLYLIHLPFSTKPGSPPFPL
YEEDIAAMDMQGVWKAMEECKRLGMAKAIGVSNFTVKKLEELLPIVKMPPQVNQVEMNPT
WQQKKLMQYCNAKGIHVTAYSPLGGQEAPIFPNMVTKSEILKEIANARGKTVAQVSLRWVYE
QGVSMVVKSFNKERMKANIEIFNWNLSEEECRMISQIPQCKRWTMETMISNWKSHTDDEHFF
VEEVNRDNEL

>AKR3_*Leucojum aestivum*
MLSIPEVILTKDSRAMPVVGMGTAAFPFAPENTELAIINAIEIGYRHFDTASLYCSEEPLGKAVV
EAQKLGFIESREELFITSKLWCNEAHPDLVIPAIKKSLRNLKMEYLDLYLIHLPFSTKPGSPPFPL
YEEDIAAMDMQGVWKAMEECKRLGMAKAIGVSNFTVKKLEELLPIAKMPPQVNQVEMNPT
WQQKKLMQYCNAKGIHVTAYSPLGGQEAPIFPNMVAKSEVLKEIANARGKTVAQISLRWVYE
QGVSMVVKSFNKERMKANIEIFDWNLSEEECRMISQIPQCKRHTMETMISNWKSHTDDEHFFV
EEVNRDNEL

Table 4.S4. Multiple Sequence Alignment Distance Matrix with similarity in percentage for selected aldo-keto reductases.

	AKR3_Leucojum_aestivum	*AKR2_Leucojum_aestivum*	*AKR1_Leucojum_aestivum*	*LauAKR2_Lycoris_aurea*	*NtAKR_Narcissus_cv._Tete-Tete*	*AKR4B4_Fragaria_ananassa*	*AKR4B3_Papaver_somniferum*	*AKR4B2_Papaver_somniferum*
AKR3_Leucojum_aestivum	100%	98%	85%	92%	80%	52%	51%	53%
AKR2_Leucojum_aestivum	98%	100%	84%	91%	79%	51%	51%	53%
AKR1_Leucojum_aestivum	86%	85%	100%	83%	79%	53%	52%	54%
LauAKR2_Lycoris_aurea	92%	91%	82%	100%	82%	53%	52%	53%
NtAKR_Narcissus_cv._Tete-Tete	81%	80%	79%	83%	100%	52%	51%	53%
AKR4B4_Fragaria_ananassa	53%	52%	53%	54%	53%	100%	51%	52%
AKR4B3_Papaver_somniferum	52%	52%	52%	53%	51%	50%	100%	96%
AKR4B2_Papaver_somniferum	54%	54%	54%	54%	53%	52%	96%	100%

Table 5.S5. Targeted compounds detected and identified using Multiple Reaction Monitoring (MRM) mode on HPLC-MS/MS

Compound name	[M-H]- (m/z)	[M+H]+ (m/z)	RT (min)	Sample I.D					
				1	2	3	4	5	6
11-hydroxyvittatine		288	4.440	X	X	X			
3,4-dihydroxybenzaldehyde	137		15.473						
3,4-dihydroxybenzoic acid	153		11.792	X	X	X			
3',4'-*O*-dimethylnorbelladine		288	16.700						
3'-*O*-methylnorbelladine		274	16.879						
4-hydroxybenzaldehyde	121		17.948	X	X	X			
4'-*O*-methylnorbelladine		274	15.288	X	X	X			
9-*O*-demethylhomolycorine		302	7.972						
Caffeic acid		181	18.344						
Cherylline		286	7.205						
Coclaurine		286	15.978						
Dopamine		154	3.306	X	X	X			
Ferulic acid		195	19.596						
Flexinine		288	7.461						
Galanthamine		288	4.600	X	X	X	X	X	X
Gigancrinine		288	6.593						
Gigantelline		300	15.043	X		X			
Gigantellinine		316	12.374	X		X			
Haemanthamine		302	11.170	X	X	X	X	X	X
Homolycorine		316	15.764						
Isoferulic acid		195	19.757						
Isovanillic acid		169	18.361						
Isovanillin		153	18.539						
Levodopa (L-dopa)		198	3.914						
L-tyrosine		182	4.348	X	X	X	X	X	X
Lycoramine		290	4.760	X	X	X			
Lycorine		288	3.942	X	X	X			
Narciclasine		308	18.368						
Norbelladine		260	6.918	X	X	X			
Norgalanthamine		274	4.169	X	X	X			
Obliquine		449	20.841						
Pancracine		288	6.078						

Papaverine		340	17.997	X	X	X	X	X	X
p-coumaric acid		165	19.437						
Phenylalanine		166	6.053	X	X	X	X	X	X
Sanguinine		274	3.526	X	X	X			
Tazettine		332	17.194						
Trans-cinnamic acid	147		21.256						
Tyramine		138	3.483	X	X	X	X	X	X
Vanillin		153	18.699						
Vittatine and/or crinine		272	8.894	X	X	X			

Sample IDs 1, 2, and 3 are methanolic extract of leaf and 4, 5, 6 are subsequent hexane extract of those samples respectively

Legend:
Green X: Detection and identification of the compound by Multiple Reaction Monitoring (MRM) on HPLC-MS/MS using three diagnostic MRM transitions
Yellow X: Signal detected but not sure of the identification of the compound by HPLC-MS/MS (e.g. weak signal presents through background noise, S/N ratio near of 3, qualifier ion ratios are not the same as standard, *etc.*)
Empty case: No detection

Table 6.S6. List of reported compounds in *Leucojum aestivum* leaves or shoot cultures or bulbs.

S. no.	Author	Year	Tissue	Detected Metabolites	Link/DOI
1	Georgievaa L et al.	2007	Bulb and *in vitro* shoot-clumps	galanthamine, sanguinine, narwedine, N-formylnorgalanthamine, epinorgalanthamine, epigalanthamine, homolycorine, 8-*O*-demethylhomolycorine, 11-hydroxyvitattine, lycorine, haemanthamine, hordenine, methyltyramine, ungiminorine and lycoramine	http://www.znaturforsch.com/ac/v62c/s62c0627.pdf
2	Pavlov A et al.	2007	shoot culture	galanthamine	https://doi.org/10.1016/j.procbio.2006.12.006
3	Ptak A et al.	2009	*in vitro* cultures	galanthamine, N-formylnorgalanthamine, narwedine, crinine, demethylmaritidine, trisphaeridine, anhydrolycorine, lycorine, nor-galanthamine, pluviine	https://doi.org/10.1021/np800585c
4	Berkov S et al.	2013	Leaf	galanthamine, lycorine, homolycorine, tazettine, haemanthamine/crinine and narciclasine types of 38 alkaloids	https://doi.org/10.1016/j.bse.2012.10.002
5	Ivan I et al.	2013	*in vitro* shoot	galanthamine, norgalanthamine, lycorine	https://doi.org/10.1016/j.jplph.2013.03.017
6	Spina R et al.	2021	*in vivo* and *in vitro* bulblets	galanthamine, lycorine, tyramine, pseudolycorine, tazettine, 1,2-dihydro-chlidanthine	https://doi.org/10.3390/ijms22041773

7	Tousignant L et al.	2022	Bulb	galanthamine, lycorine	https://doi.org/10.1007/s00425-021-03741-x
8	Morańska E et al.	2023	*In vitro* plant	galanthamine, demethylmaritidine, lycorine	https://doi.org/10.3390/molecules28041525
9	Karimzadegan V et al.	2024	Leaf	4'-*O*-methylnorbelladine, Lycorine, norgalanthamine, narciclasine, vittatine, 11-hydroxyvittatine	https://doi.org/10.1016/j.plaphy.2024.108612
10	Ptak A et al.	2026	*in vitro* cultures	galanthamine, vittatine, demethylmaritidine, crinine, 11-hydroxyvitattine, lycorine, epiisohaemanthamine, chlidanthine, ismine, tazettine,	https://doi.org/10.3390/molecules31020258

Table 7.S7. Residues of AKR candidates interacting with docked NADPH and narwedine or narwedine.

Gene	Ligand	Hydrophobic	H-bonds	Other
***La*AKR1**	NADPH	Ala24, Tyr54	Thr23, Ala24 (n=2), Tyr54 (n=2), Ser164 (n=2), Asn165, Ser213 (n=2), Leu215, Gly217, Lys262 (n=2), Ser263, Phe264, Asn265, Asn272 (n=2)	Salt Bridges: Asp49, Lys262, Arg268
	nornarwedine	Tyr54, Ile130	Asp219, NADPH	n.d.
	narwedine	Ile130, Val297	His117	n.d.
***La*AKR2**	NADPH	Ala24, Tyr54	Thr23, Ala24 (n=2), His117, Ser163 (n=2), Asn164, Gln185, Ser212 (n=2), Leu214, Gly215, Gly216, Lys261, Phe263, Arg267 (n=2), Asn271 (n=2)	Salt Bridges: Asp49, Lys261, Arg267
	nornarwedine	Phe28, Leu53, Tyr54, Phe129, Trp296, Asn304, Trp305	Tyr54	n.d.
	narwedine	Phe26, Phe28, Tyr54	Tyr54, Thr300	n.d.
***La*AKR3**	NADPH	Ala24, Tyr54	Thr23, Ala24 (n=2), Ser163 (n=3), Asn164 (n=2), Gln185, Ser212 (n=2), Leu214, Gly215, GLy216, Lys261 (n=2), Phe263, Ag267, Asn271 (n=2)	Salt Bridges: Asp49, Lys261, Arg267
	nornarwedine	Phe28, Trp86 (n=2), Leu118, Phe129, Leu131	Tyr54, His296	*n.d.*
	narwedine	Phe26 (n=2), Phe129	Tyr54, His296	n.d.

Table 8.S8. *La*TMT1 interactions with docked SAM and tocopherols.

Enzyme	Ligand	Interactions		
		Hydrophobic	H-bonds	Other
LaTMT1	SAM	Leu158	Met87, Gly138, Ser141, Thr157 (n=2), Leu158, Ser159, Gln162, Ala186	Salt Bridge: Asp133
	gamma-tocopherol	Leu71, Leu78, Trp79, Trp233 (n=2), Tyr260 (n=2), Phe295, Val299, Ala303, Leu312, Thr319	n.d.	n.d.
	alpha-tocopherol	Leu71, Leu72, Trp79 (n=2), Glu206, Trp233, Tyr260 (n=2), Val299, Thr319, Ala323	n.d.	n.d.

Table 9.S9. List of primers

S. No.	*Gene*	Application	Type	sequence
1	*LaΔTNMT1*	*in vitro* assays	F.	aatgaattcggatctatgacgtcggcgtcggcgacggat
2	*LaΔTNMT1*		R.	ataaagcttttactctggtttacggcatgtaatgactgcaaacttgattagattcttc
3	*LaNMT*		F.	atctgaattcggaggctcaggtatggggaaattggtggaggttcc
4	*LaNMT*		R.	acgttctagactatttctttttgaaaagaaaatgtgcaaccatccattcttctcc
5	*LaTNMT1*		F.	atcaggtaccgaattcggaggctctggtatgcgaaccccaaaaacacaaaaca
6	*LaTNMT1*		R.	atctgtcgacttaggatccctctggtttacggcatgtaatgact
7	*LaTNMT2*		F.	atcaggtaccgaattcggaggctctggtatgacgacgatgacggatgatct
8	*LaTNMT2*		R.	atcttctagattaggatccctttggcttacgacatgcaatgac
9	*LaNMT*	*in vivo* assays	F.	ggggacaagtttgtacaaaaaagcaggctatggggaaattggtggaggttccg
10	*LaNMT*		R.	ggggaccactttgtacaagaaagctgggtctaagcgtagtctggtacatcataagggtatgca tagtcaggtacgtcataaggataagcgtaatctggaacatcgtatgggtatttctttttgaaaag aaaatgtgcaac
11	*LaTMT2*		F.	ggggacaagtttgtacaaaaaagcaggctatgatgacgacgatgacggatgatct
12	*LaTMT2*		R.	ggggaccactttgtacaagaaagctgggtctaagcgtagtctggtacatcataagggtatgca tagtcaggtacgtcataaggataagcgtaatctggaacatcgtatgggtactttggcttacgac atgcaatgac
13	*LaTMT1*		F.	ggggacaagtttgtacaaaaaagcaggctatgatgcgaaccccaaaaacacaaaaca
14	*LaTMT1*		R.	ggggaccactttgtacaagaaagctgggtctaagcgtagtctggtacatcataagggtatgca tagtcaggtacgtcataaggataagcgtaatctggaacatcgtatgggtactctggtttacggc atgtaatgact
15	*LaNMT*	Localization	F.	ggggacaagtttgtacaaaaaagcaggctatggggaaattggtggaggt
16	*LaNMT*		R.	ggggaccactttgtacaagaaagctgggtctttcttttgaaaagaaaatgtgcaac
17	*LaTMT1*		F.	ggggacaagtttgtacaaaaaagcaggctatgcgaaccccaaaaacacaaaaca
18	*LaTMT1*		R.	ggggaccactttgtacaagaaagctgggtcctctggtttacggcatgtaatgact
19	*LaTMT2*		F.	ggggacaagtttgtacaaaaaagcaggctatgacgacgatgacggatgatct
20	*LaTMT2*		R.	ggggaccactttgtacaagaaagctgggtcctttggcttacgacatgcaatgac
21	*LaAKRI_EcoRI*	*In vitro* as well as invivo	F.	ggggacaagtttgtacaaaaaagcaggctgaattcatgttgagcattcctgaggtgatcc
22	*LaAKRI_SalI*		R.	ggggaccactttgtacaagaaagctgggtgtcgacctacttatcgtcgtcatccttatagtcctt atcgtcgtcatccttatagtccttgtcgtcatcgtctttgtagtcttcttctccattttcctcgaaaaa aaattcatctg
23	*LaAKRII_EcoRI*		F.	ggggacaagtttgtacaaaaaagcaggctgaattcatgttgagcattcctgaggtgatcc
24	*LaAKRII_SalI*		R.	ggggaccactttgtacaagaaagctgggtgtcgacctacttatcgtcgtcatccttatagtcctt atcgtcgtcatccttatagtccttgtcgtcatcgtctttgtagtctaattcattatctcgatttacctct tccacgaaaaaatgt
25	*LaAKRIII_EcoRI*		F.	ggggacaagtttgtacaaaaaagcaggctgaattcatgttgagcattcctgaggtgatcc
26	*LaAKRIII_SalI*		R.	ggggaccactttgtacaagaaagctgggtgtcgacctacttatcgtcgtcatccttatagtcctt atcgtcgtcatccttatagtccttgtcgtcatcgtctttgtagtctaattcattatctcgatttacctct tccacgaaaaaatgt
27	*LaN4'OMT*	qPCR	F.	gtgaagctcgtcaggattgg
28	*LaN4'OMT*		R.	ggtttctgaaagagaqcctagc
29	*LaCYP96T1*		F.	tgttatggcgaggatgaagg
30	*LaCYP96T1*		R.	acatgtcccttcaccatctg

31	*LaNMT*	F.	gcttaccactttgaggacata
32	*LaNMT*	R.	gagccactcttcgcttgtcct
33	*LaTMT1*	F.	gatcgaggaggcgcttaaat
34	*LaTNMT1*	R.	ctatcccacacccaacatcaa
35	*LaTNMT2*	F.	cggtggagctgctatctatcta
36	*LaTNMT2*	R.	gtcttgtctccaagcccattag
37	*LaNR*	F.	aacaatgcagggacagccat
38	*LaNR*	R.	gccgattcgaaattggtggc
39	*HISTONE3*	F.	acaagcctttggaagggcag
40	*HISTONE3*	R.	ggagtgaagaagccccacc
41	*LaAKR1*	F.	agcttcaacaaggagagaatcaa
42	*LaAKR1*	R.	tgtttcaactgtaactcttttgcg
43	*LaAKR2*	F.	gtgagcatggtagtaaaaagcttt
44	*LaAKR2*	R.	gaaatcattgtctccattgtcca
45	*LaAKR3*	F.	gtgagcatggtagtaaaaagcttc
46	*LaAKR3*	R.	ggaaatcattgtctccattgtgtg

Table 10.S10. MRM transitions and instrumental parameters used on HPLC-MS/MS for *in vivo* experiments

Compound name	Retention time (min)	Precursor (m/z)	Product (m/z)	Fragmentor (V)	Collision energy (V)	Polarity (ESI +/-)
3,4-dihydroxybenzaldehyde	15.501	137	119 **108** 92	114	20 26 26	Negative
3'-*O*-methylnorbelladine	17.062	274	**137** 121 109	105	18 15 40	Positive
4'-*O*,*N*-dimethylnorbelladine	16.094	288	**137** 122 94	70	14 40 40	Positive
4'-*O*-methylnorbelladine	15.879	274	**137** 122 94	105	18 40 40	Positive
11-hydroxyvittatine	4.808	288	226 **196** 153	105	26 34 40	Positive
3',4'-*O*-dimethylnorbelladine	16.904	288	**151** 135 107	100	10 40 40	Positive

Galanthamine	5.287	288	270	120	14	Positive
			225		18	
			213		22	
Haemanthamine	14.291	302	211	105	22	Positive
			196		34	
			181		30	
Lycorine	4.172	288	270	92	20	Positive
			177		20	
			147		28	
			119		40	
Narwedine	10.481	286	**229**	95	25	Positive
			225		18	
			201		26	
Nornarwedine	8.910	272	229	100	25	Positive
			201		25	
			158		25	
Norbelladine	7.408	260	**138**	86	5	Positive
			123		20	
			121		17	
Norgalanthamine	4.505	274	231	115	14	Positive
			213		18	
			198		40	
Normaritidine	N/A	274	256	100	25	Positive
			228		25	
			196		25	
Noroxomaritidine	N/A	272	244	100	25	Positive
			229		25	
			212		25	
Norpluviine	N/A	274	224	100	25	Positive
			147		25	
			119		25	
Oxomaritinamine	N/A	274	**219**	100	25	Positive
			165		25	
			136		25	
Papaverine	18.317	340	324	165	40	Positive
			202		27	
			171		40	
Tyramine	3.525	138	121	81	5	Positive
			91		20	
			77		20	
	11.785	272	226	105	26	Positive

Vittatine and/or crinine	196	34
	136	26

Notes:
Quantifier ion for each compound is **bold** and qualifier ions are not.
N/A: Not applicable (*i.e.*, reference standard not available)

Identification criteria used for compounds we have reference standards:
Retention time window (tolerance on RT): 10%
Signals with signal-to-noise ratio ≤ 3 were not considered in the analysis.
Qualifier ratio tolerance: uncertainty of 20% (relative)
Number of qualifiers used (MRM transitions monitored per compound): 3 (except lycorine (4))
ISTD used: papaverine

Table 11.S11. MRM transitions and instrumental parameters used for HPLC-MS/MS analyses in metabolite screening for *L. aestivum* leaves

Compound name	Retention time (min)	Precursor (m/z)	Product (m/z)	Fragmentor (V)	CE (V)	Polarity (ESI +/-)
3,4-dihydroxybenzaldehyde	15.473	137	119	114	20	Negative
			108		26	
			92		26	
3,4-dihydroxybenzoic acid	11.792	153	**109**	45	13	Negative
			108		29	
			91		29	
3'-*O*-methylnorbelladine	16.879	274	**137**	105	18	Positive
			121		15	
			109		40	
4-hydroxybenzaldehyde	17.948	121	120	69	18	Negative
			92		26	
			65		30	
4'-*O*-methylnorbelladine	15.288	274	**137**	105	18	Positive
			122		40	
			94		40	
9-*O*-demethylhomolycorine	7.972	302	**284**	120	22	Positive
			251		34	
			94		30	
11-hydroxyvittatine	4.440	288	226	105	26	Positive
			196		34	
			153		40	
3',4'-*O*-dimethylnorbelladine	16.700	288	**151**	100	10	Positive
			135		40	
			107		40	
Caffeic acid	18.344	181	**163**	76	5	Positive
			135		10	
			117		21	
Cherylline	7.205	286	**243**	103	18	Positive
			165		40	
			137		18	
Coclaurine	15.978	286	269	115	14	Positive
			175		20	
			107		30	
Dopamine	3.306	154	**137**	78	10	Positive
			119		18	
			91		26	

Ferulic acid	19.596	195	**177**	81	5	Positive
			145		20	
			117		21	
Flexinine	7.461	288	242	110	26	Positive
			149		34	
			147		30	
Galanthamine	4.600	288	270	120	14	Positive
			225		18	
			213		22	
Gigancrinine	6.593	288	**214**	110	34	Positive
			213		34	
			170		34	
Gigantelline	15.043	300	**257**	135	20	Positive
			194		20	
			107		40	
Gigantellinine	12.374	316	273	135	20	Positive
			192		20	
			137		20	
Haemanthamine	11.170	302	211	105	22	Positive
			196		34	
			181		30	
Homolycorine	15.764	316	300	115	30	Positive
			298		22	
			94		26	
Isoferulic acid	19.757	195	**177**	81	5	Positive
			145		20	
			117		21	
Isovanillic acid	18.361	169	151	81	10	Positive
			125		5	
			93		9	
Isovanillin	18.539	153	125	86	10	Positive
			93		13	
			65		25	
Levodopa	3.914	198	181	78	10	Positive
			152		10	
			139		14	
L-Tyrosine	4.348	182	165	83	10	Positive
			136		10	
			123		14	
Lycoramine	4.760	290	233	99	20	Positive
			215		20	

			189		24	
Lycorine	3.942	288	270	92	20	Positive
			177		20	
			147		28	
			119		40	
Narciclasine	18.368	308	**248**	82	28	Positive
			218		36	
			202		40	
Norbelladine	6.918	260	**138**	86	5	Positive
			123		20	
			121		17	
Norgalanthamine	4.169	274	231	115	14	Positive
			213		18	
			198		40	
Obliquine	20.841	449	**329**	135	26	Positive
			244		38	
			121		40	
Pancracine	6.078	288	**270**	95	18	Positive
			185		34	
			165		40	
Papaverine	17.997	340	324	165	40	Positive
			202		27	
			171		40	
p-coumaric acid	19.437	165	**147**	76	5	Positive
			119		17	
			91		20	
Phenylalanine	6.053	166	**120**	74	9	Positive
			103		29	
			77		40	
Sanguinine	3.526	274	217	85	14	Positive
			199		22	
			184		40	
Tazzetine	17.194	332	**314**	90	14	Positive
			181		30	
			153		40	
Trans-cinnamic acid	21.256	147	**103**	65	9	Negative
			77		20	
Tyramine	3.483	138	121	81	5	Positive
			91		20	
			77		20	
Vanillin	18.699	153	125	86	10	Positive

			93		13	
			65		25	
Vittatine and/or crinine	8.894	272	226	105	26	Positive
			196		34	
			136		26	

Notes: Quantifier ion for each compound is **bold** and qualifier ions are not.

Identification criteria used (FDA GFI 118, 2003):
Retention time window (tolerance on RT): 10%
Signal-to-noise: noise algorithm used = RMS ; noise used = between retention time of each compound ± 0.5 min.
Signals with signal-to-noise ratio ≤ 3 were not considered in the analysis.
Qualifier ratio tolerance: uncertainty of 20% (relative)
Number of qualifiers used (MRM transitions monitored per compound): 3 (except trans-cinnamic acid (2) and lycorine (4))
ISTD used: papaverine
Softwares used for identifications: MassHunter Qualitative Analysis 10.0 and MassHunter Quantitative Analysis (for QQQ) Version 10.0

Table 12.S12. Instrumental parameters used in Single Ion Monitoring mode on HPLC-MS/MS for in-vitro experiments

Compound name	Precursor (m/z)	Fragmentor (V)	Polarity
Norgalanthamine	274	115	Positive
Galanthamine	288	115	Positive
Nornarwedine	272	95	Positive
Narwedine	286	95	Positive

Supplementary Table 3.13. Instrumental parameters used in Product Ion mode on HPLC-MS/MS for in-vitro experiments

Compound name	Precursor (m/z)	Start mass (m/z)	End mass (m/z)	Fragmentor (V)	Collision energy (V)	Polarity
Galanthamine	288	50	290	115	20	Positive
Narwedine	286	50	290	95	20	Positive

3.9. Supplementary Figures

A Golgi-Localized N-Methyltransferase and Reversible Aldo–Keto Reductases Coordinate Dual Terminal Routes in Galanthamine Biosynthesis

Basanta Lamichhane[1], Archana Niraula[1], Natacha Merindol[1], Sarah-Eve Gélinas[1], Patrick Lagüe[2], Simon Ricard[1,3], Hugo Germain[1,3], Isabel Desgagné-Penix[1,3*]

[1]Department of Biochemistry, Chemistry, Physics and Forensic Science, Université du Québec à Trois-Rivières, Trois-Rivières, Québec, Canada

[2]Department of Biochemistry, Microbiology and Bioinformatics, Université Laval, Québec, Québec, Canada

[3]Plant Biology Research Group, Trois-Rivières, Québec, Canada

BL: Basanta.Lamichhane@uqtr.ca

AN: Archana.Niraula@uqtr.ca

NM: Natacha.Merindol@uqtr.ca

SEG: Sarah-Eve.Gelinas@uqtr.ca

SR: Simon.Ricard@uqtr.ca

PL: patrick.lague@bcm.ulaval.ca

HG: Hugo.Germain@uqtr.ca

IDP: Isabel.Desgagne-Penix@uqtr.ca

*Corresponding author's email address: Isabel.Desgagne-Penix@uqtr.ca

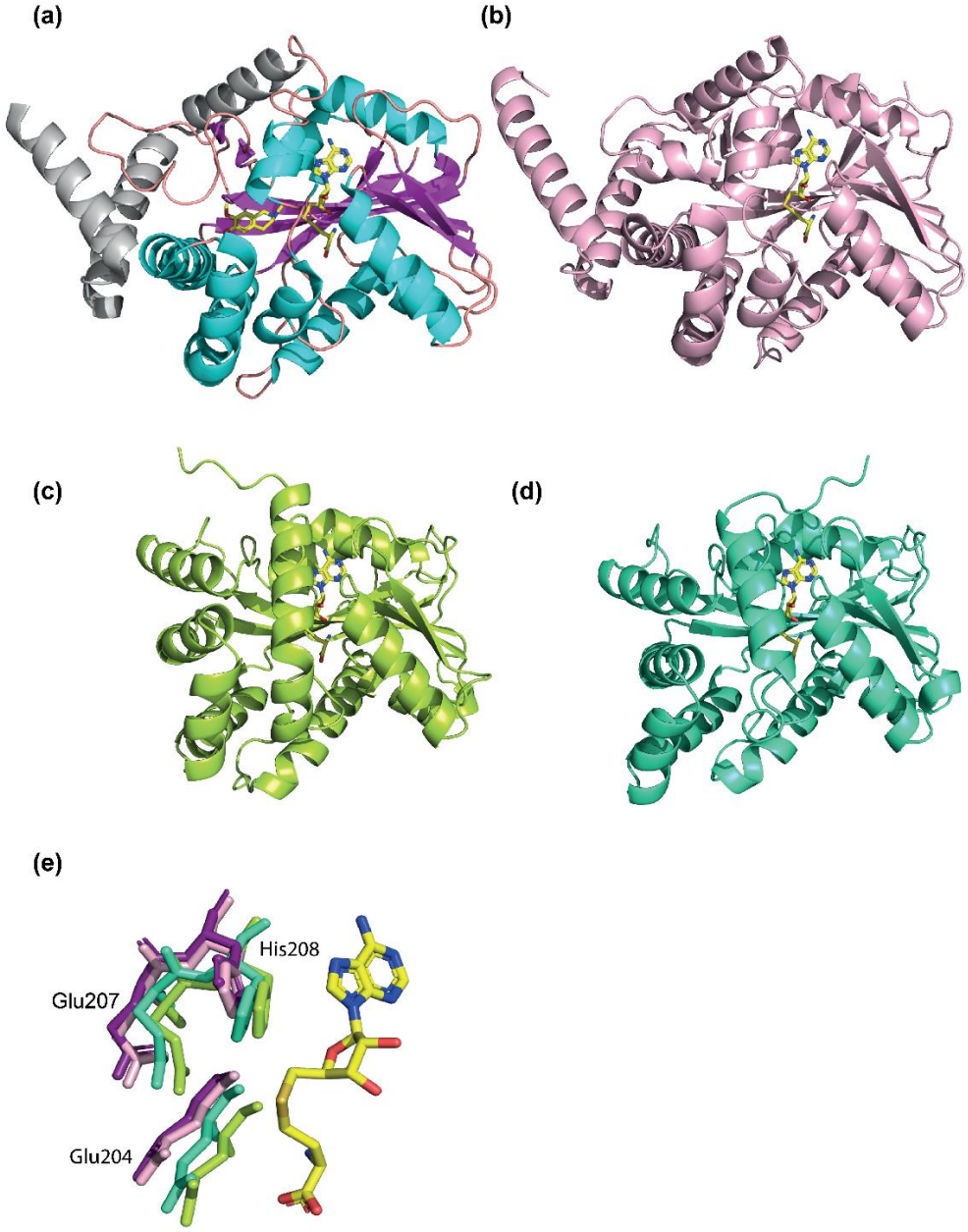


Figure 33. Structural comparison of N-methyltransferase candidates with the reference coclaurine N-methyltransferase (CNMT) from *Coptis japonica* (PDB: 6GKV).

(a) CNMT structure (PDB: 6GKV) shown in cartoon with cyan α-helices, purple β-sheets, and the flexible N-terminal region in grey. Bound ligands S-adenosylhomocysteine (SAH) and heliamine are shown as yellow sticks.(b) Predicted structure of *Leucojum aestivum* LaCNMT shown in light pink cartoon with bound SAH as yellow sticks. (c) Predicted structure of LaTNMT1 shown in lime cartoon with SAH as yellow sticks. (d) Predicted structure of LaTNMT2 shown in turquoise cartoon with SAH as yellow sticks.

All structures are shown in the same orientation for direct comparison. (e) Superposition of the putative catalytic residues Glu204, Glu207, and His208 shown as sticks in CNMT (purple), LaCNMT (pink), LaTNMT1 (lime), and LaTNMT2 (turquoise), with SAH rendered as yellow sticks. This view highlights the conservation of the catalytic triad in all candidates despite divergence in the N-terminal architecture.

Score	Expect	Method	Identities	Positives	Gaps
662 bits(1709)	0.0	Compositional matrix adjust.	317/325(98%)	322/325(99%)	0/325(0%)

```
LaAKR2  1    MLSIPEVILTKESRAMPVVGMGTAAFPFAPENTELAIINAIEIGYRHFDTASLYCSEEPL  60
LaAKR3  1    MLSIPEVILTKDSRAMPVVGMGTAAFPFAPENTELAIINAIEIGYRHFDTASLYCSEEPL  60

LaAKR2  61   GKAVVEAQKLGFIKSREELFITSKLWCNEAHPDLVIPAIKKSLRNLKMEYLDLYLIHLPF  120
LaAKR3  61   GKAVVEAQKLGFIESREELFITSKLWCNEAHPDLVIPAIKKSLRNLKMEYLDLYLIHLPF  120

LaAKR2  121  STKPGSPPFPLYEEDIAAMDMQGVWKAMEECKRLGMAKAIGVSNFTVKKLEELLPIVKMP  180
LaAKR3  121  STKPGSPPFPLYEEDIAAMDMQGVWKAMEECKRLGMAKAIGVSNFTVKKLEELLPIAKMP  180

LaAKR2  181  PQVNQVEMNPTWQQKKLMQYCNAKGIHVTAYSPLGGQEAPIFPNMVTKSEILKEIANARG  240
LaAKR3  181  PQVNQVEMNPTWQQKKLMQYCNAKGIHVTAYSPLGGQEAPIFPNMVAKSEVLKEIANARG  240

LaAKR2  241  KTVAQVSLRWVYEQGVSMVVKSFNKERMKANIEIFNWNLSEEECRMISQIPQCKRWTMET  300
LaAKR3  241  KTVAQISLRWVYEQGVSMVVKSFNKERMKANIEIFDWNLSEEECRMISQIPQCKRHTMET  300

LaAKR2  301  MISNWKSHTDDEHFFVEEVNRDNEL  325
LaAKR3  301  MISNWKSHTDDEHFFVEEVNRDNEL  325
```

Figure 34. Pairwise sequence analysis.

Pair wise sequence alignment using The Basic Local Alignment Search Tool (BLAST) for protein sequence of *La*AKR2 and *La*AKR3. Color in red denotes the alternative aminoacids between two sequences.

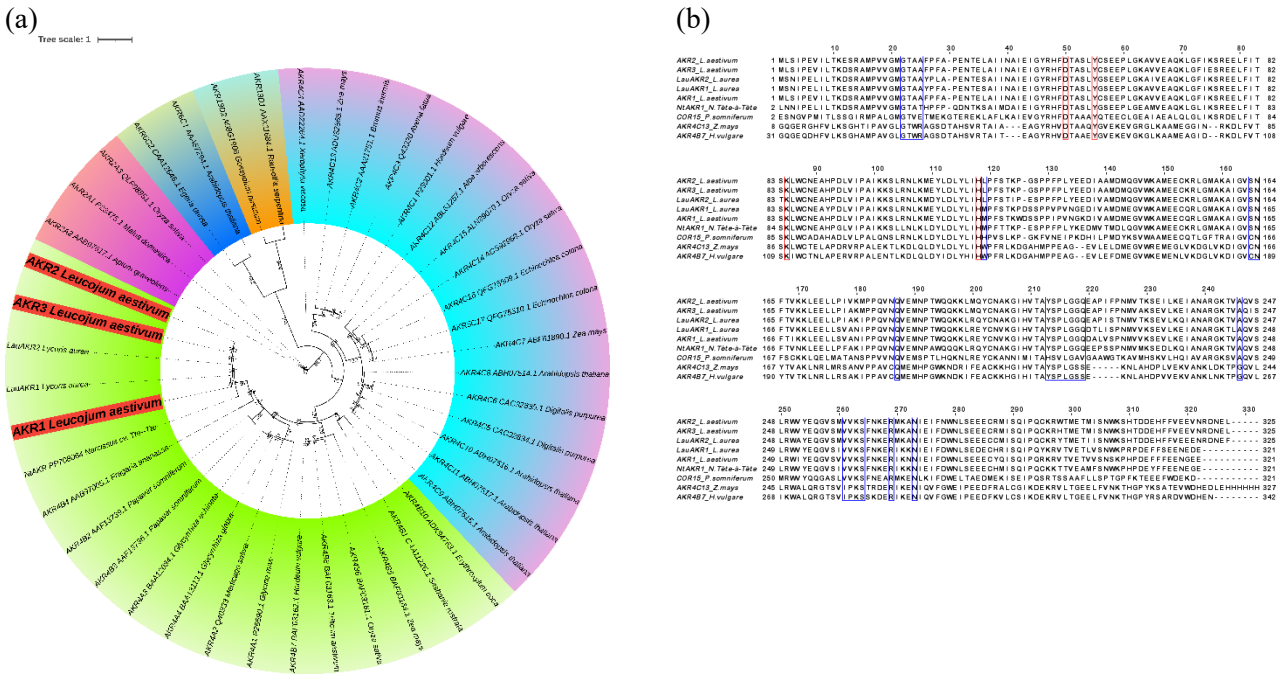
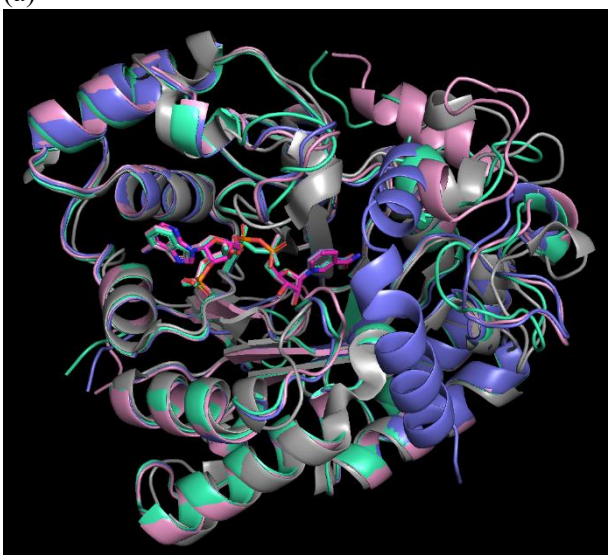


Figure 35. Evolutionary analysis by the Maximum Likelihood method and Multiple sequence analysis.

(a) The phylogeny was inferred using the Maximum Likelihood method with 1000 bootstraps. This analysis involved 43 amino acid sequences. Evolutionary analyses were conducted in IQ-Tree and viewed in ITOL software. Bold font highlighted with red are the transcripts studied in the experiment. The accessions or sequences are listed in Supplementary Table S3. (b) Multiple sequence alignment was performed with 9 sequences with residues in red box represents catalytic tetrad and in blue box are the substrate binding region predicted by conserved domain database (NCBI).

(a)



(b)

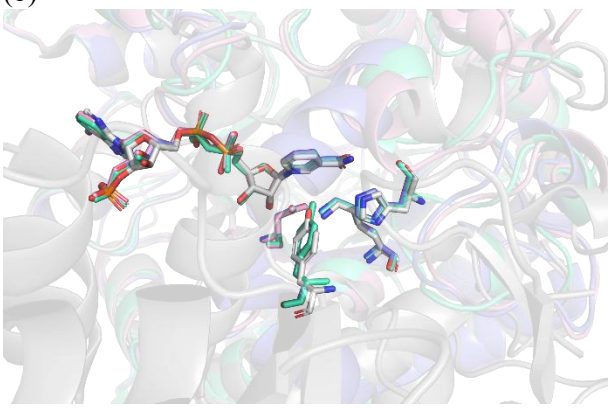


Figure 36. Structural comparison of AKR candidates.

(a) Cartoon representation of predicted structure of *La*AKR candidates superposed with crystallized AKR4C17 and NADPH (shown as pink stick) from *Echinochloa colona* (PDV: 7F7L) in grey. LaAKR1 is shown as turquoise, LaAKR2 as purple, LaAKR3 as pink. (b) Superposed Catalytic tetrad residues Asp50, Tyr55, Lys84, and His117 (left to right), with NADPH shown as sticks (7F7L grey, LaAKR1 turquoise, LaAKR2 purple, LaAKR3 as pink sticks).

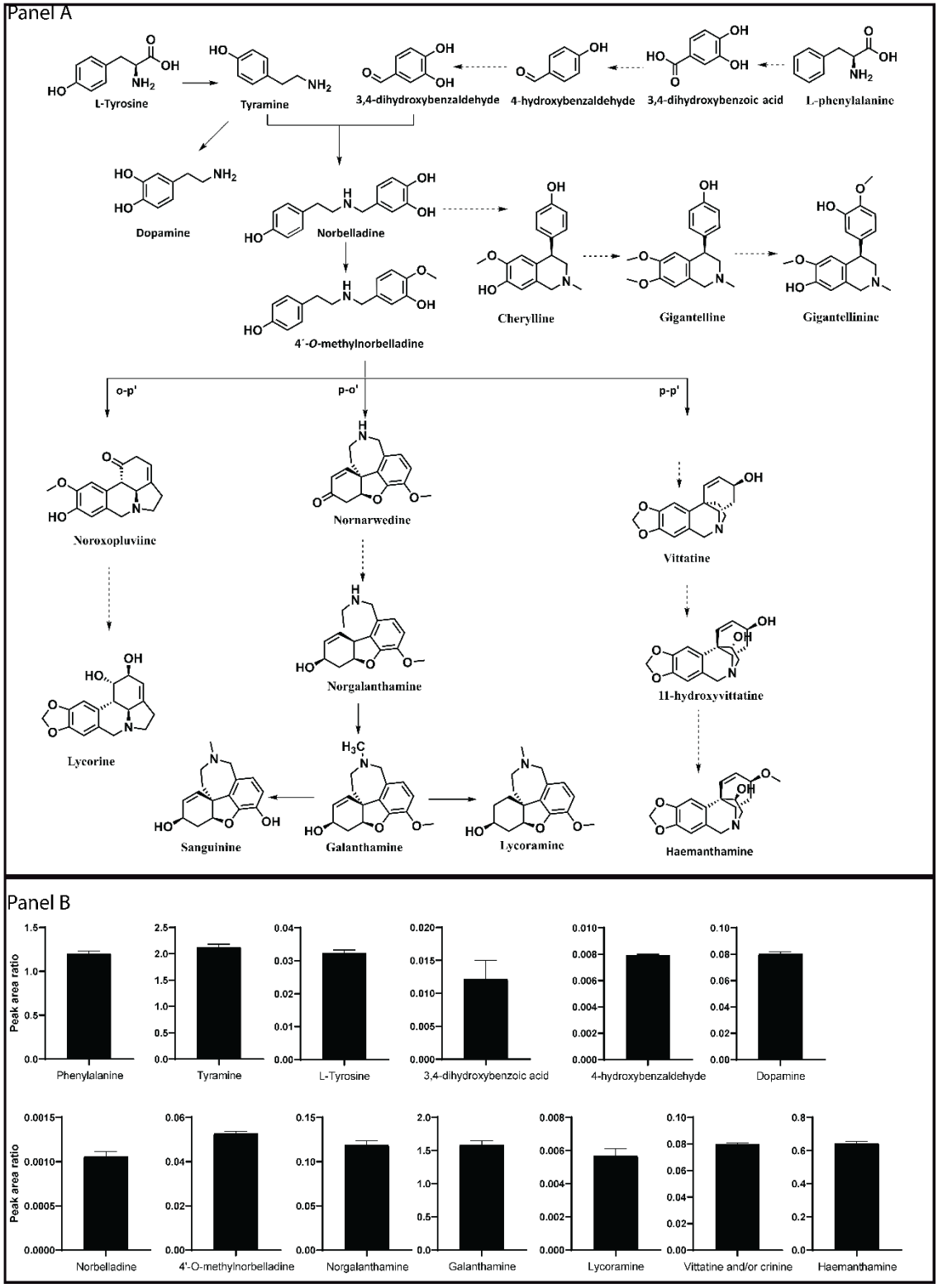


Figure 37. Metabolic screening in leaf of *L. aestivum*.

Panel A. Detected metabolites shown in predicted biosynthetic pathway where solid arrow shows single step and dotted arrow shows two or more steps. Panel B. Targeted metabolite screening of *Leucojum aestivum* leaves by LC-MS/MS in three biological replicates with peak area ratio calculated for 1ppm papaverine used as internal standard.

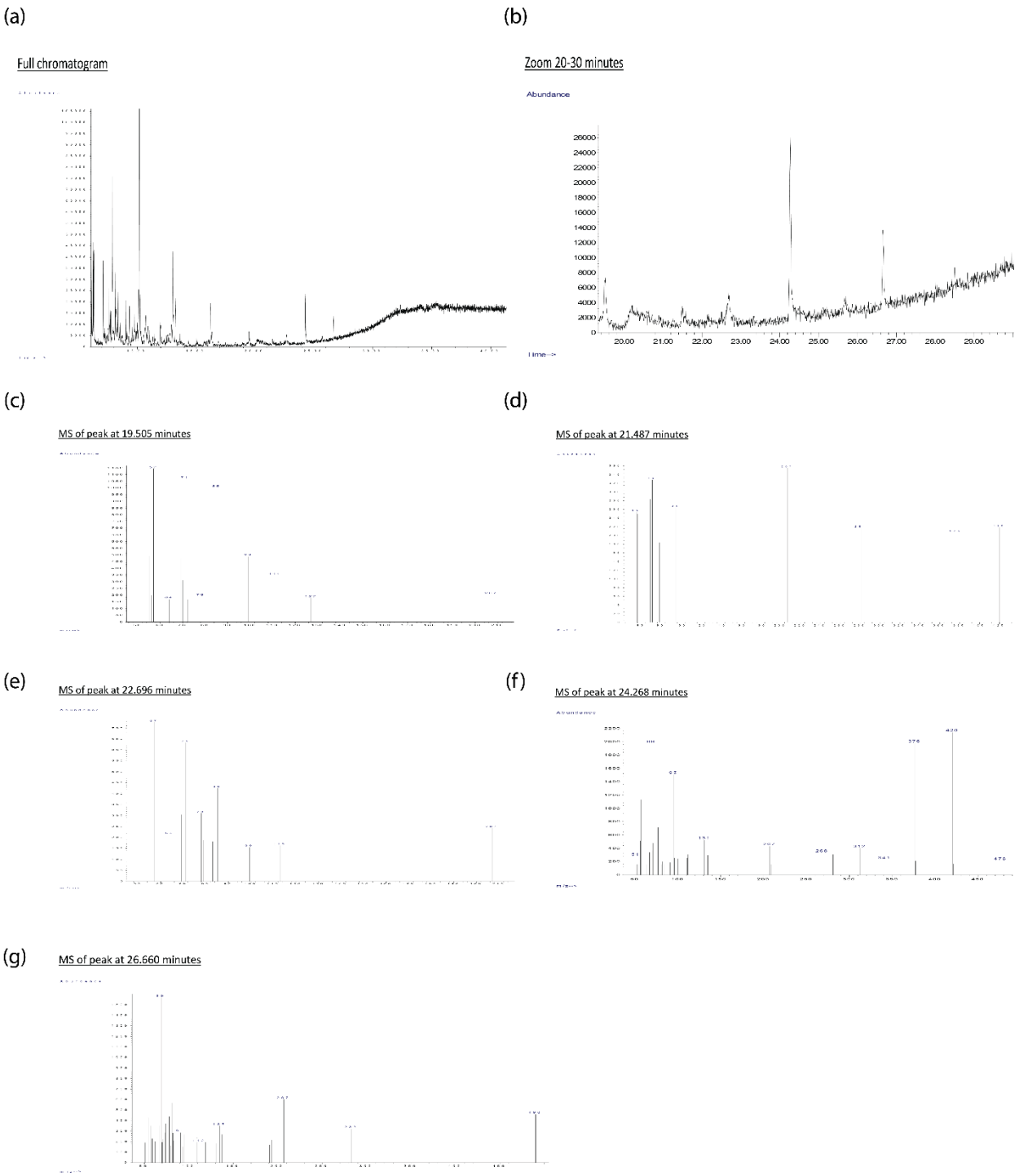


Figure 38. GC/MS of nonpolar fraction of leaf extract.

(a) Full chromatogram of GC/MS. **(b)** Zoom of chromatogram for 20-30 minutes. **(c)** Mass fragmentation of peak of mass 207 at 19.5 minutes. **(d)** Mass fragmentation of peak of mass 420 at 21.48 minutes. **(e)** Mass fragmentation of peak of mass 207 at 22.69 minutes. **(f)** Mass fragmentation of peak of mass 476 at 24.26 minutes. **(f)** Mass fragmentation of peak of mass 490 at 26.6 minutes

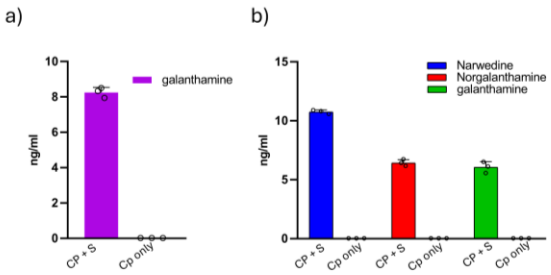


Figure 39. Enzymatic activity of dialyzed crude protein extracts.

Crude protein extracts were prepared and dialyzed four times prior to enzymatic assays. For each reaction, 10 µL of dialyzed protein extract was incubated with either norgalanthamine or nornarwedine as substrate. Product formation was quantified by LC–MS/MS. (a) Conversion of norgalanthamine to galanthamine catalyzed by the crude protein extract compared with the negative control reaction lacking protein. (b) Conversion of nornarwedine to narwedine, norgalanthamine, and galanthamine mediated by crude protein extract relative to the control sample. Bars represent mean values from replicate assays, with individual data points overlaid. Abbreviation; CP: crude protein, S: substrate

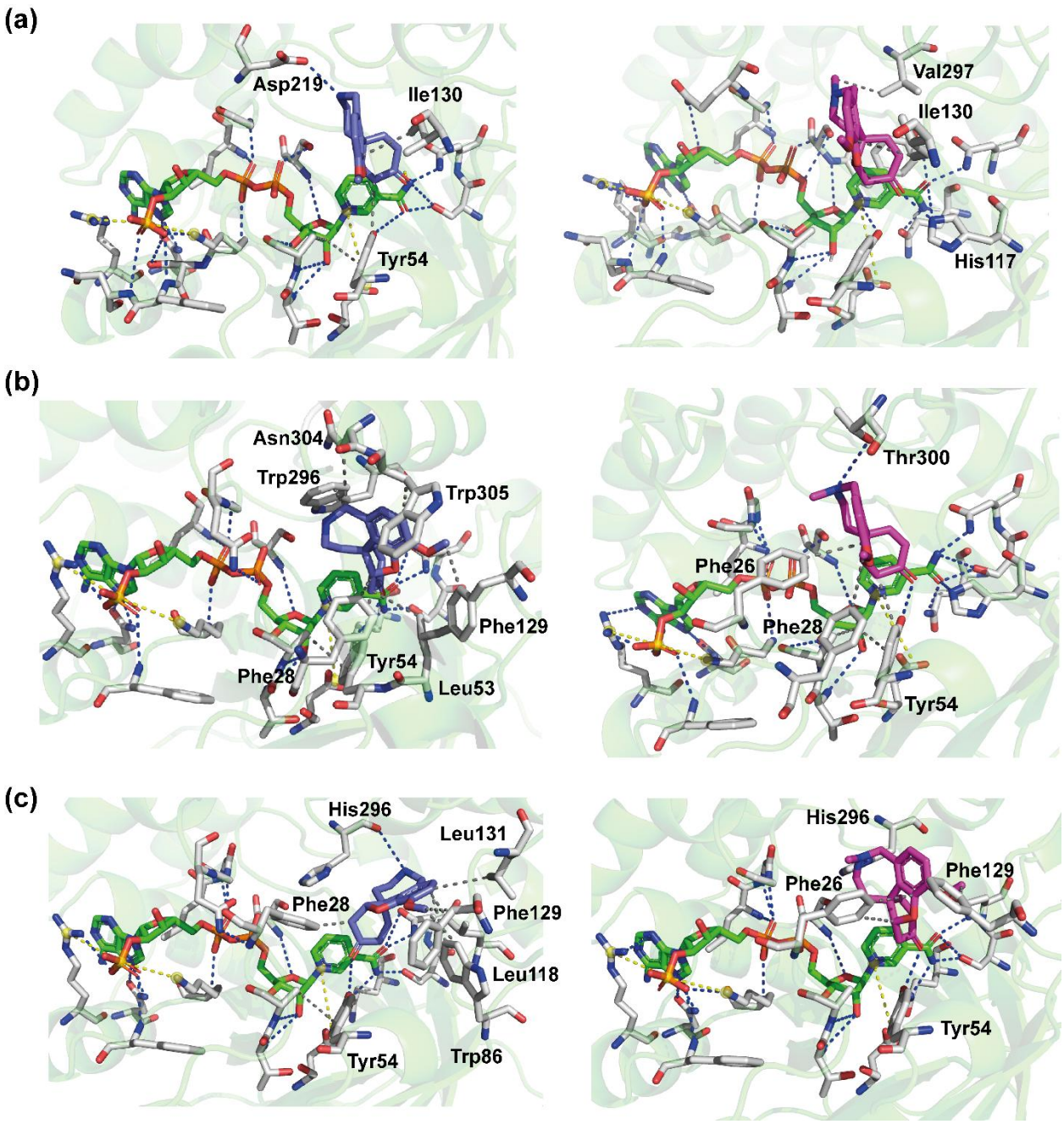


Figure 40. Active site representation for AKR candidates docked with narwedine or nornarwedine and NADPH.

(a) *La*AKR1 docked with nornarwedine (left) and narwedine (right), (b) *La*AKR2 docked with nornarwedine (left) and narwedine (right), (c) *La*AKR3 docked with nornarwedine (left) and narwedine (right). Protein is shown as a transparent cartoon, and ligand and NADPH interaction active-site residues are shown as grey sticks. NADPH is displayed as green sticks, nornarwedine as purple sticks, narwedine as pink sticks.

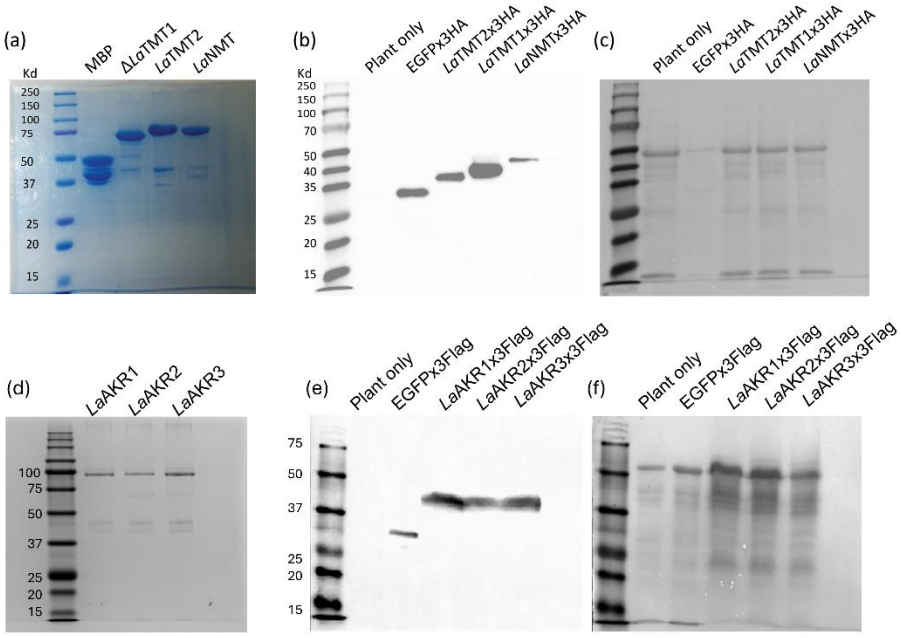


Figure 41. SDS gel and western blot

(a) SDS gel stained by Coomassie blue after running the purified MBP and its fusion proteins *La*ΔTMT1, *La*TMT2, and *La*NMT, respectively, in each well. (b) Western blot analysis illustrating the expression of C-terminal 3HA fused proteins EGFP, *La*TMT1, *La*TMT2, and *La*NMT, respectively in *N. benthamiana* leaf lysate. (c) Ponceau stained image of the blot (b). (d) SDS gel stained by Coomassie blue after running the purified MBP fusion proteins *La*AKR1, *La*AKR2, and *La*AKR3, respectively, in each well. (e) Western blot analysis illustrating the expression of C-terminal 3Flag fused proteins EGFP, *La*AKR1, *La*AKR2, and *La*AKR3, respectively in *N. benthamiana* leaf lysate. (f) Ponceau stained image of the blot (e).

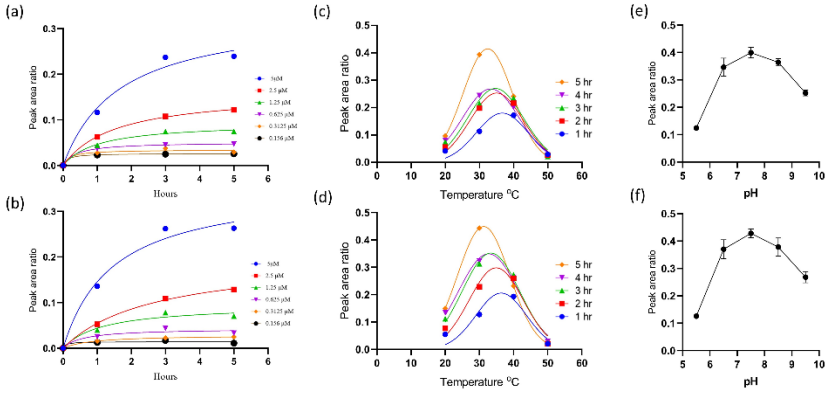


Figure 42. Optimization of enzyme concentration, temperature, pH and time for enzymatic reaction of *La*TMT2 with norgalanthamine and *N*-demethylnarwedine.

(a) Effect of enzyme concentration on the formation of galanthamine. **(b)** Effect of enzyme concentration on the formation of N-demethylnarwedine. **(c)** Effect of temperature on the formation of galanthamine. **(d)** Effect of temperature on the formation of narwedine. **(e)** Effect of pH on the formation of galanthamine. **(f)** Effect of pH on the formation of Narwedine.

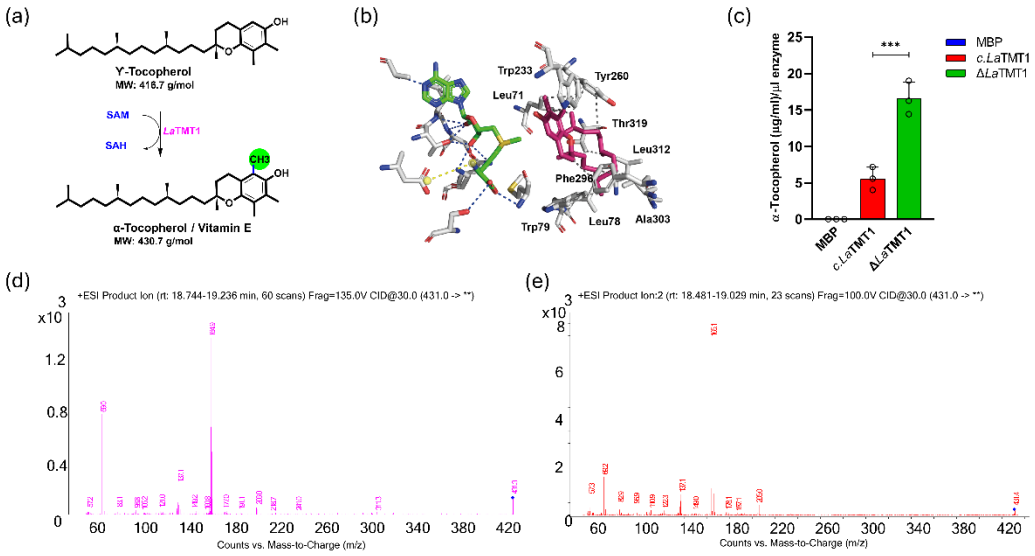


Figure 43. Biochemical characterization of LaTMT1 as a γ-tocopherol methyltransferase.

a) Schematic representation of the enzymatic methylation of γ-tocopherol to α-tocopherol (Vitamin E) catalyzed by the tocopherol methyltransferase. Added methyl group is shown by green circle and blue bond, *La*TMT1 in pink is enzyme, SAM: S-Adenosyl methionine, SAH:S-Adenosyl-L-homocysteine **b)** Molecular docking pose of γ-tocopherol (deep-pink) and SAM (green) within the predicted active site of *La*TMT1. c) Bar graph showing quantification of α-tocopherol production by ΔLaTMT1 (green), crude *La*TMT1 with signal peptide (red) compared to negative control MBP (blue) as determined by LC–MS/MS. Other negative controls included no enzyme and boiled enzyme with substrate showed no product; (***p<0.0004). d) Mass spectra showing characteristic fragmentation patterns of standard α-tocopherol (magenta color). e) Mass spectra of corresponding peak of α-tocopherol produced by *La*TMT1 in invitro reaction (red color).

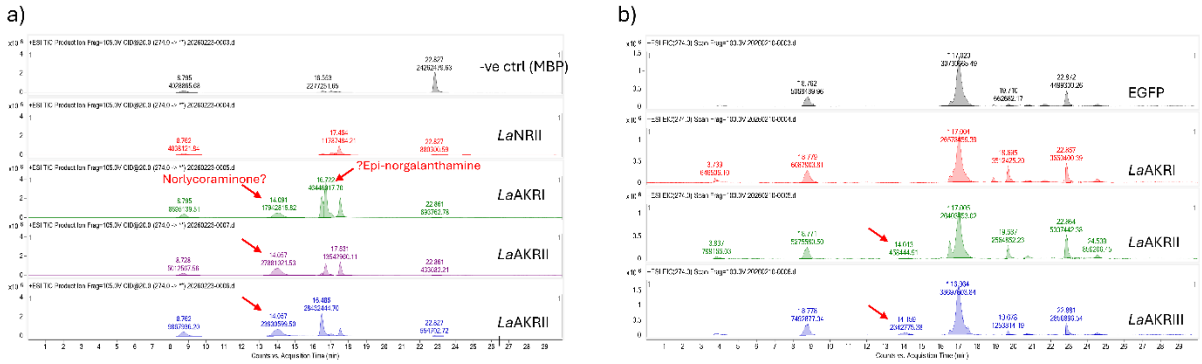


Figure 44. LC–MS/MS analysis of products formed from nornarwedine in AKR-mediated *in vivo* and *in vitro* assays.

(a) Total ion chromatograms (TICs) obtained from *in vitro* enzymatic assays using nornarwedine as substrate, showing reactions containing purified LaNRII (SDR) and the three AKR isoforms compared with MBP protein controls. (b) Extracted ion chromatograms (EICs) derived from *in vivo* transient expression assays in *Nicotiana benthamiana*, with EGFP-expressing samples serving as negative controls along with the three AKR candidates. Newly detected metabolite peaks absent in negative controls are indicated by red arrows.

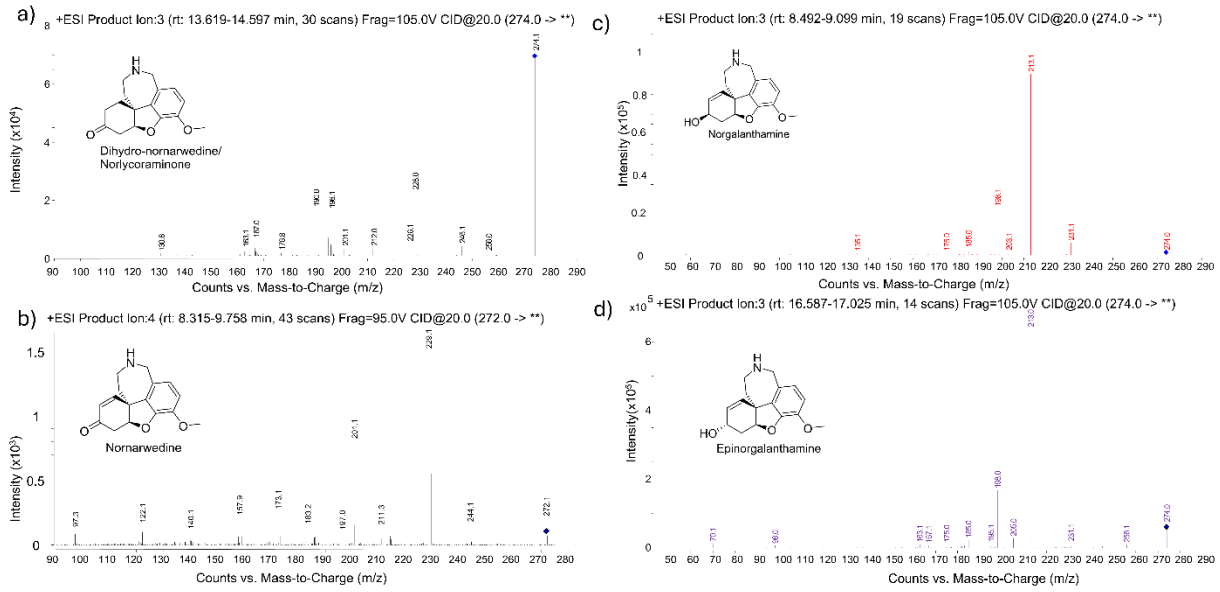


Figure 45. MS/MS fragmentation profile of the new peaks.

a) MS/MS spectra of peak obtained at almost 14-minute of mass 274. (b) MS/MS fragmentation pattern of nornarwedine standard. c) Fragmentation of peak retained at 8.795 i.e. norgalanthamine. d) Fragmentation of peak obtained at 16.7 in invitro reaction predicted to be epi-norgalanthamine.

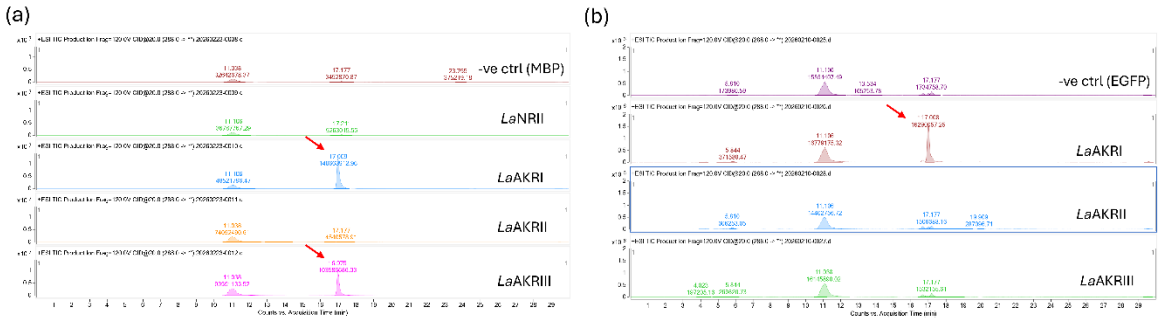


Figure 46. HPLC-MS/MS analysis of peaks produced on *in vivo* and *in vitro* enzymatic reaction of narwedine with AKRs.

a) Total ion chromatogram of *in vitro* assay using narwedine as substrate with MBP protein as negative control along with one SDR (*La*NRII) and other three AKRs. b) Total ion chromatogram of *in vivo* assay sample with EGFP as negative control along with three AKRs. New peaks absent in –ve controls are shown with red arrows.

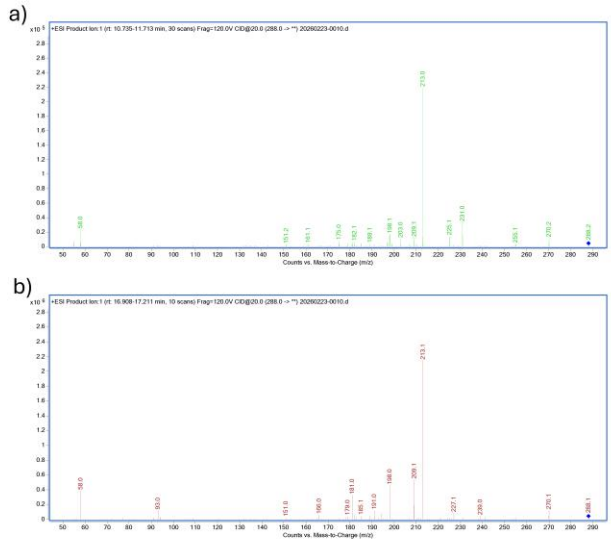


Figure 47. MS/MS fragmentation profile of the new peak.

a) Fragmentation of peak retained at 8.795 i.e. galanthamine. d) Fragmentation of new peak obtained at 16.7 in invitro reaction, predicted to be epi-galanthamine.

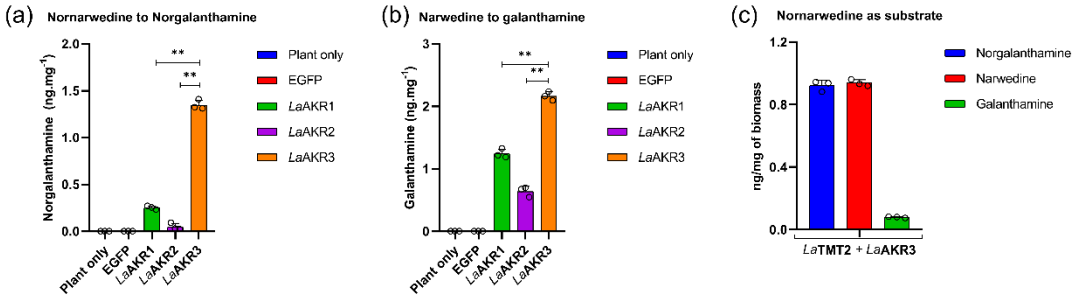


Figure 48. In planta activity of candidate genes in *Nicotiana benthamiana* upon transient expression assays.

Bar graphs represent metabolite accumulation in *N. benthamiana* leaves following *Agrobacterium*-mediated transient expression of candidate genes followed by substrate infiltration. Negative controls include non-infiltrated plants ("Plant only") and empty vector (EGFP). Metabolites were quantified by LC–MS/MS and normalized to fresh leaf biomass (ng mg^{-1} fresh weight) by removing the background. Data are presented as mean ± SD from three independent biological replicates. Statistical significance was determined using one-way ANOVA followed by Tukey's multiple-comparison test. (a) Accumulation of norgalanthamine upon expression of LaAKR isoforms with nornarwedine as substrate. b) Accumulation of galanthamine from narwedine in leaves expressing LaAKR isoforms.(c) Metabolite profiling in leaves co-expressing *La*TMT2 and *La*AKR3 with nornarwedine as substrate giving norgalanthamine, narwedine and galanthamine. Statistical significance was determined by one-way ANOVA with Tukey's multiple-comparison test (**P<0.0001).

Chapter IV

4.1 Overall Discussion

The central objective of this doctoral thesis was to elucidate genetic network/pathway and develop sustainable and practical strategies for producing pharmaceutically valuable specialized metabolites, with a particular focus on galanthamine, an FDA-approved drug for the treatment of Alzheimer's disease. At present, galanthamine is costly and its supply is constrained by reliance on extraction from wild plant populations, raising both sustainability and conservation concerns. This thesis addresses that challenge by establishing a molecular framework for galanthamine biosynthesis in *L. aestivum*, thereby providing the foundation for biotechnological alternatives to wild harvesting. Such approaches—including plant tissue culture, genetic engineering, and pathway reconstruction in heterologous hosts—represent promising routes to minimize ecological impact while ensuring a reliable supply of Amaryllidaceae alkaloids (AAs). Specifically, this work focused on the identification and functional characterization of key biosynthetic enzymes for galanthamine production, exploration of their structural and catalytic properties, and reconstitution of the pathway in *N. benthamiana*, ultimately paving the way for future metabolic engineering applications.

The AA biosynthetic pathway initiates with the condensation of tyramine and 3,4-dihydroxybenzaldehyde (3,4-DHBA) to generate norcraugsodine, followed by its reduction to norbelladine. This two-step entry point, previously elucidated in our laboratory, were mediated by norbelladine synthase (*La*NBS) and the reductase *La*NRI (Majhi et al., 2023). In this study, we characterized an alternative reductase isoform, *La*NRII, which is 98% identical to *La*NRI and retains the conserved catalytic triad. Structural modelling and docking identified key active-site residues underlying substrate recognition. Co-expression of *La*NBS and *La*NRII in *N. benthamiana* yielded low but measurable norbelladine levels, indicating that this step may be rate-limiting. *In vitro* assays with purified enzymes confirmed the condensation reaction, and thermal-unfolding analyses further supported the direct binding of 3,4-DHBA and tyramine to *La*NBS and *La*NRII.

Norbelladine is regioselectively methylated by *La*N4′*O*MT to form 4′-*O*-methylnorbelladine (4′*O*M), a central AA intermediate (Kilgore et al., 2014; Koirala et al., 2024; Liscombe et al., 2012; Su et al., 2022; Sun et al., 2018). *In vitro*, *La*N4′*O*MT exhibits strong 4′-*O*-methylation activity in the presence of Mg^{2+}, whereas Ni^{2+} broadens its catalytic profile, enabling formation of 3′,4′-*O*-

dimethylnorbelladine and single-step conversion of 3,4-DHBA to vanillin and isovanillin, demonstrating pronounced substrate and regioselective flexibility consistent with *N. papyraceus* *O*MT homologs (Koirala et al., 2024). Although vanillin typically arises from the sequential conversion of caffeic acid → ferulic acid → vanillin (Gallage et al., 2014), our data reveal that 3,4-DHBA can yield vanillin in a single enzymatic step, offering a markedly shorter biosynthetic route with metabolic engineering potential. The identification and functional characterization of *La*N4′*O*MT in *L. aestivum* thus establishes the enzyme responsible for generating 4′*O*M while also providing an alternative, streamlined entry point for vanillin biosynthesis.

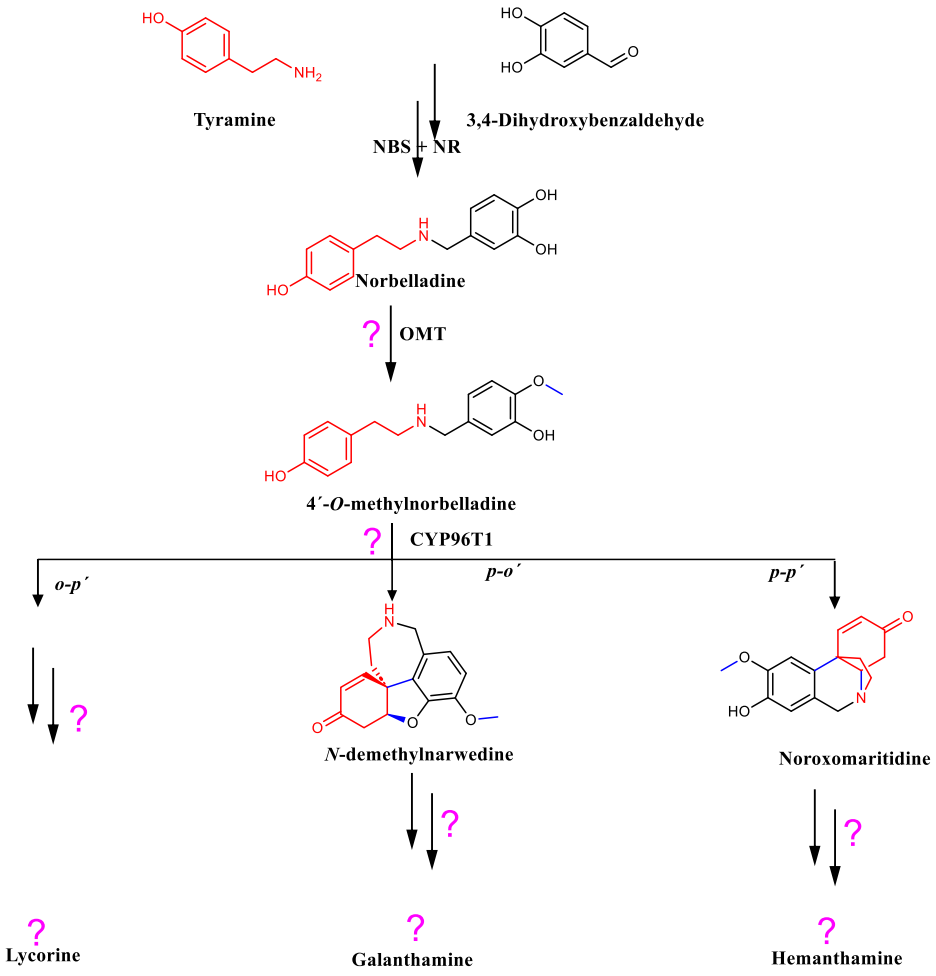


Figure 49. Elucidated known AA pathway at the start of this PhD thesis.
All the enzymes represented by pink question mark "?" was the aim of PhD

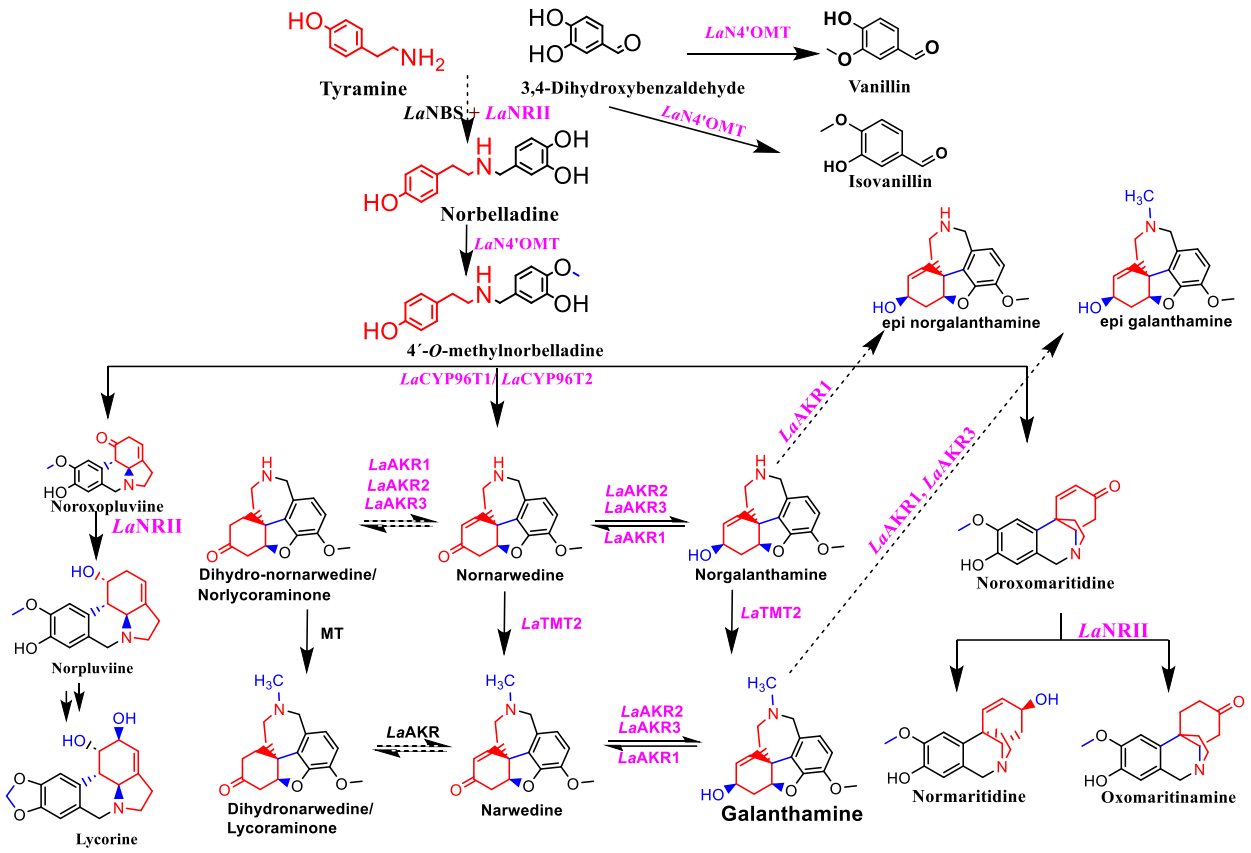


Figure 50 Elucidated AA pathway at the end of this PhD thesis.
All the enzymes in pink are identified in this study.

In AA pathway, 4′*O*M subsequently undergoes regioselective phenol coupling reactions catalyzed by cytochrome P450 (CYP) enzymes (Kilgore et al., 2016a; Mehta et al., 2024). In this study, we identified two cytochrome P450 transcripts, *LaCYP96T1* and *LaCYP96T2*, involved in generating structurally diverse AA scaffolds. Functional assays showed that these enzymes catalyze all three C–C phenol-coupling modes—*p–p′*, *p–o′*, and *o–p′*. Although the *o–p′* intermediate noroxopluviine was not detected in initial assays, the *p–o′* product *N*-demethylnarwedine and the *p–p′* product noroxomaritidine were identified, suggesting that the *o–p′* product may be short-lived. Co-expression of *La*CYP96T1 with a reductase (*La*NRII) in a heterologous *in vivo* system yielded all three reduced phenol-coupled products, including the *o–p′*-derived norpluviine. For *in vitro* validation, microsomal *La*CYP96T1 from *N. benthamiana* and purified recombinant *La*NRII from *E. coli* were combined, successfully reconstituting norpluviine biosynthesis. This provides the first *in vitro* evidence of enzymatic *o–p′* phenol coupling and subsequent reduction leading to norpluviine, defining a previously uncharacterized step in AA biosynthesis.

The reductive tailoring of phenol-coupled products carried out by a single reductase enzyme, *La*NRII, is unique finding of our study. This broad substrate acceptance positions *La*NRII as a central and highly flexible enzyme, contributing to multiple branches of the AA pathway. To our knowledge, this is the first short-chain dehydrogenase/reductase (SDR) enzyme characterized as both substrate- and product-promiscuous within a single alkaloid biosynthetic system. Reductive tailoring steps are a central and recurring feature of specialized metabolite biosynthesis across the plant kingdom, and the SDR superfamily represents one of the most widespread and functionally diverse enzyme classes mediating such transformations. In this study, *La*NRII, a 98%-identical isoform of *La*NRI, participates in the early reductive steps of AA biosynthesis and exhibits remarkable catalytic flexibility by reducing all three phenol-coupled products generated by *La*CYP96T, however, only two out of three *in vivo* replicates showed reduced *p–o′* derived norgalanthamine. The other reduced products, i.e. *p-p′* and *o-p′* were observed in larger extent based on peak area. This unusual catalytic breadth not only reinforces the role of *La*NRII as a multifunctional branch-point enzyme in AA biosynthesis but also suggests that substrate and product promiscuity within SDR scaffolds may represent an important evolutionary mechanism contributing to the structural diversification of AAs.

Alongside SDRs, aldo-keto reductases (AKRs) constitute a second major class of NAD(P)H-dependent oxidoreductases mediating reductive tailoring in plant specialized metabolism, and the present study establishes three AKR isoforms — *La*AKR1, *La*AKR2, and *La*AKR3 — as the enzymes governing the terminal reductive steps of galanthamine biosynthesis in *L. aestivum*. All three isoforms catalyzed reversible interconversions between nornarwedine and norgalanthamine, and between narwedine and galanthamine, in both NADPH-dependent (reductive) and NADP+-dependent (oxidative) directions, revealing that flux through this terminal node is bidirectional and dynamically regulated rather than constitutively committed. Within this system, *La*AKR3 functions as the predominant reductase driving forward flux toward galanthamine with the highest specific activity, while *La*AKR1 preferentially catalyzes the reverse oxidative reactions — a functional divergence that, together with the dual-substrate activity of *La*TMT2, reveals an enzymatically flexible terminal architecture in which both competing biosynthetic routes to galanthamine are simultaneously operative and interconnected. Beyond canonical reductions, the *La*AKR isoforms also displayed catalytic plasticity by generating minor stereoisomeric and

alternative-regiochemistry products — including putative norlycoraminone and epi-galanthamine — suggesting a broader contribution to AA structural diversity than their primary pathway roles would indicate.

Similarly, in the tertiary steps of AA biosynthesis, *N*-methylation plays a pivotal role in enhancing structural diversity and conferring pharmacological activity, yet the identity of the enzyme responsible for this critical modification had remained a subject of considerable debate. We identified and tested three *N*-methyltransferase candidates: *LaNMT*, a coclaurine-like NMT, and two γ-tocopherol methyltransferase homologs, *LaTMT1* and *LaTMT2*. *In vitro* assays demonstrated that *La*TMT2 efficiently methylates both nornarwedine and norgalanthamine — the two key intermediates at the competing biosynthetic branch point — with a kinetic preference for nornarwedine, while transient expression in *N. benthamiana* confirmed its superior catalytic efficiency and substrate promiscuity relative to the other MT candidates. Supported by both *in vitro* and *in vivo* evidence, *La*TMT2 emerges as the key branch-enabling *N*-methyltransferase that reconciles the previously competing models of galanthamine biosynthesis and represents a strategic target for metabolic engineering to enhance galanthamine production.

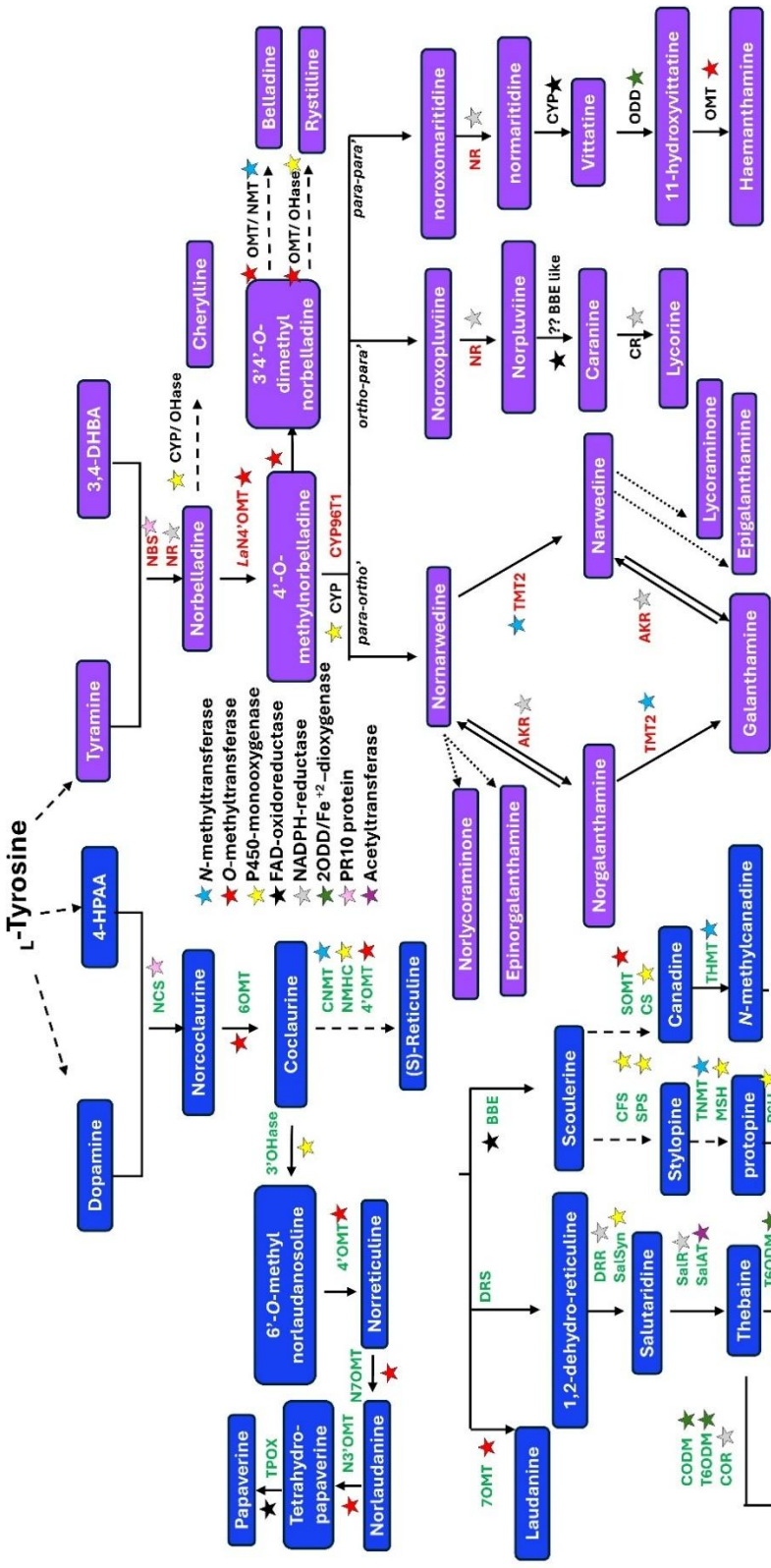


Figure 51. Biosynthetic network of BIA in blue and AA in purple with several class of enzymes for reaction.

We identified that the Amaryllidaceae pathway shares striking parallels with other alkaloid systems. Several enzymatic transformations in the AA pathway mirror those found in BIAs as predicted, suggesting recruitment from similar gene families. For example, the similarity between morphine and galanthamine biosynthesis are striking. The condensation of 3,4-dihydroxybenzaldehyde (3,4-DHBA) with tyramine to form norbelladine resembles the Pictet–Spengler condensation of 4-hydroxyphenylacetaldehyde (4-HPAA) and dopamine to yield norcoclaurine in BIA metabolism (Liscombe et al., 2005). Likewise, the 4′-*O*-methylation of norbelladine parallels the action of 4′*O*-methyltransferase in morphine biosynthesis giving (*S*)-reticuline by 3′-hydroxyl-*N*-methylcoclaurine 4′-*O*-methyltransferase (Frenzel and Zenk, 1990).

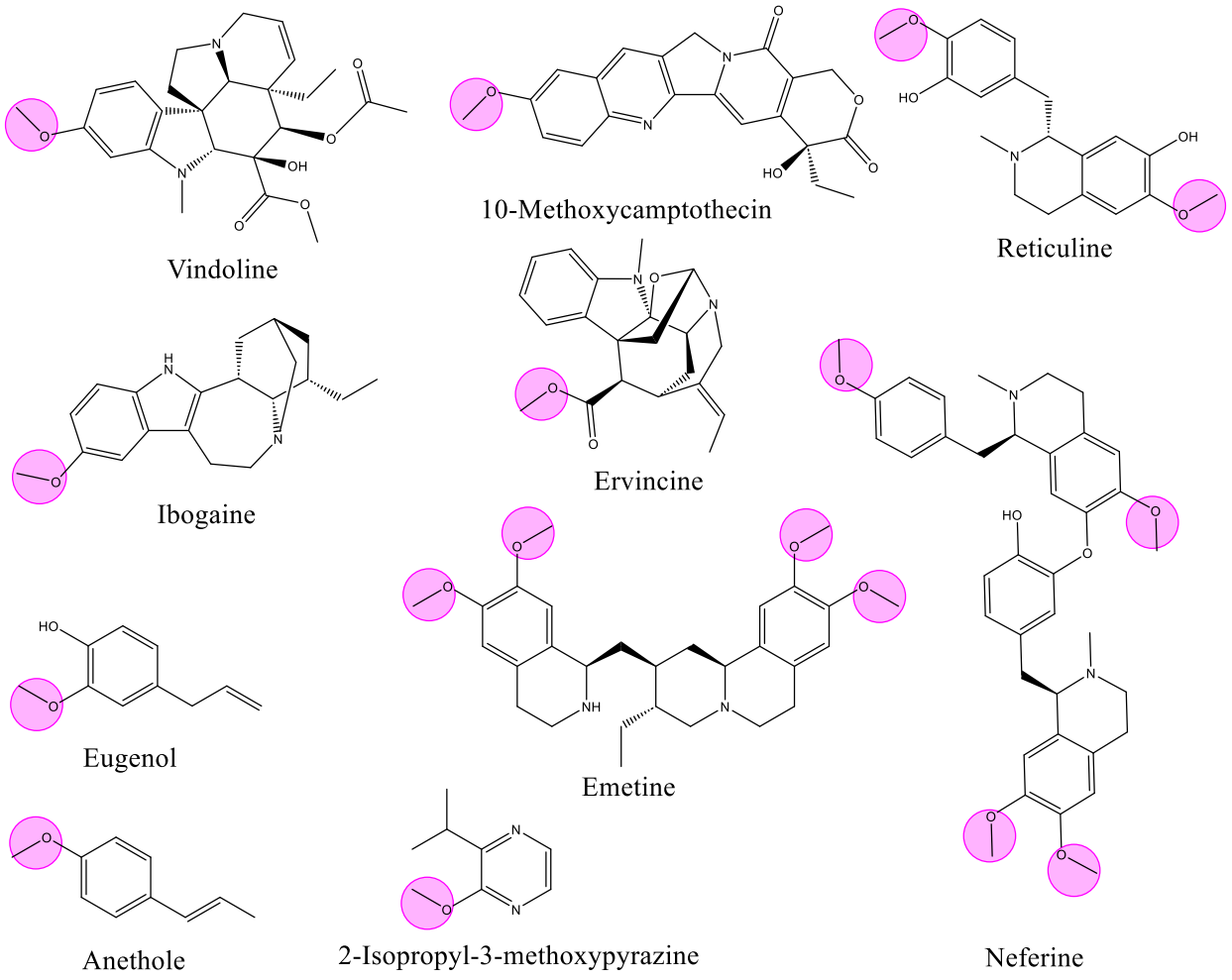


Figure 52. Structure of few O-methylated specialized metabolites catalyzed by O-methyltransferase

Several other *O*-methyltransferases in BIA like 6*O*MT, N3′OMT, 4′OMT, 7OMT perform *O* methylation to get valuable alkaloids and are all SAM dependent like *O*MTs in AA giving 4′-*O*-

methyl norbelladine from norbelladine or haemanthamine from 11-hydroxyvittatine (Figure 7, Figure 8). Similarly, enzymes like 6-*O*-methyltransferase (6*O*MT) and 7-*O*-methyltransferase (7*O*MT) are crucial for the diversity of 1-benzylisoquinolines found in *Nelumbo nucifera* (Menéndez-Perdomo and Facchini, 2020). In flavonoid biosynthesis, *O*MT is required for biosynthesis of methylated phenylpropenes, such as eugenol and trans-anethole, important aromatic compounds that determine flavour and aroma in many herbs and fruit like apple (Yauk et al., 2015). Several *O*MTs involved in the terminal tailoring steps of monoterpene indole alkaloid pathways have been functionally characterized and cloned including the vindoline-forming *O*MT from *Catharanthus roseus* (Levac et al., 2008), 10-hydroxycamptothecin *O*MT identified in *Camptotheca acuminata* (Salim et al., 2018) and the ibogaine-producing *O*MT from *Tabernanthe iboga* (Farrow et al., 2018). In addition, three *O*MTs implicated in the biosynthesis of monoterpene isoquinoline alkaloids such as emetine have been isolated from *Psychotria ipecacuanha* (Nomura and Kutchan, 2010). *O*MTs constitute a conserved and versatile enzyme family that contributes broadly to plant biology, including roles in developmental regulation, hormonal signaling networks, and specialized metabolite biosynthesis.

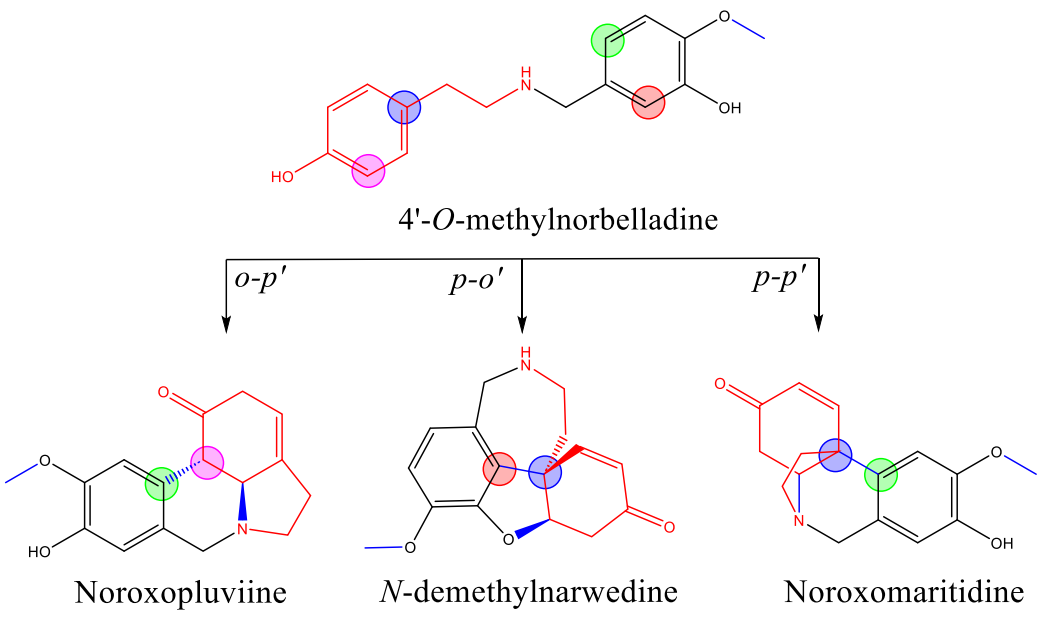


Figure 53. Structure showing intramolecular oxidative coupling of 4′-*O*-methylnorbelladine

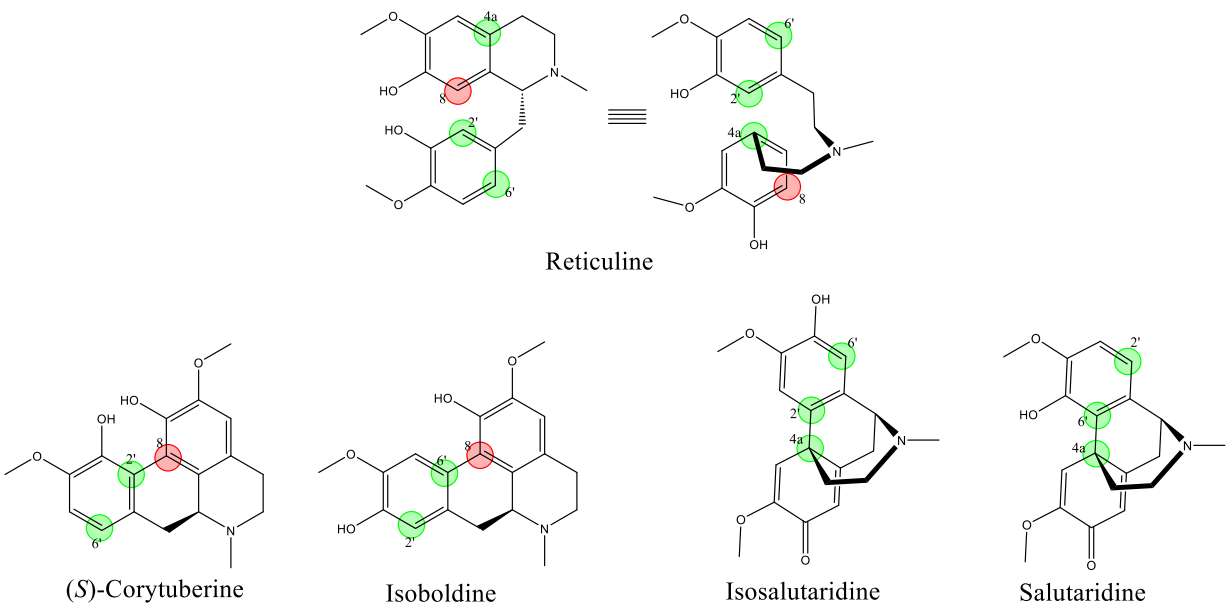


Figure 54. Structure showing intramolecular oxidative coupling of *R* and *S* reticuline

The phenol-coupling reactions catalyzed by *La*CYP96T1 and *La*CYP96T2 parallel well-characterized oxidative coupling steps in the BIA pathway (Figure 9, Figure 10). It has been elucidated that the salutaridine synthase (CYP719B1) catalyzes C–C phenol coupling in morphine biosynthesis converting (*R*)-reticuline to salutaridine (Gesell et al., 2009). Additional analogies can be drawn to other CYP-mediated C–C phenol-coupling reactions in BIAs, including the conversion of (*S*)-reticuline to the aporphine alkaloid (*S*)-corytuberine by CYP80G2 (Ikezawa et al., 2008) underscoring the mechanistic parallels between BIA and AA biosynthesis. In protoalkaloid or phenethylisoquinoline alkaloid biosynthesis, i.e., colchicine, C-C phenol coupling is a major reaction converting autumnaline to isoandrocymbine (Nasreen et al., 1996). Although not examined in this study, insights from CYP719A enzymes in *C. japonica* and *Eschscholzia californica*, which catalyze methylenedioxy bridge formation in BIA biosynthesis to give berberine (Ikezawa et al., 2003), may inform hypotheses regarding analogous methylenedioxy bridge formation during the conversion of norpluviine to caranine in the lycorine branch of AA biosynthesis.

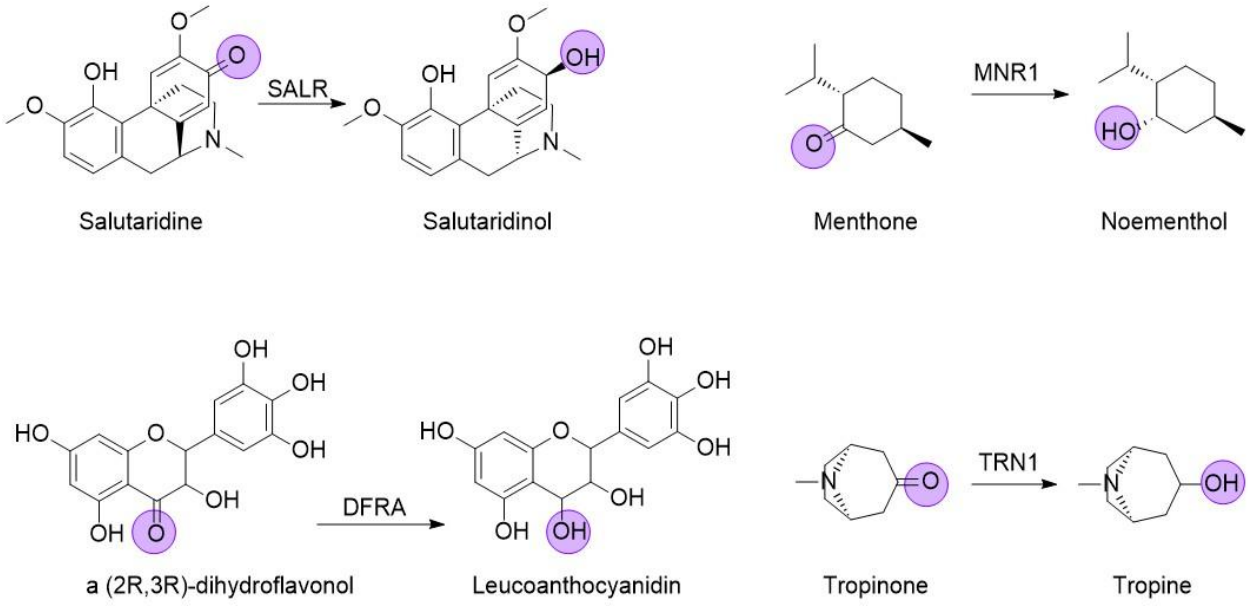


Figure 55. Structure of few specialized metabolites catalyzed by SDRs.
(SALR: Salutaridine Reductase; MNR1: neomenthol dehydrogenase; DFRA: Dihydroflavonol 4-reductase; TRN1: Tropinone reductase)

Reductive tailoring steps also converge: the reduction of *N*-demethylnarwedine in AAs closely resembles salutaridine reduction in morphinan biosynthesis, reactions typically mediated by short-chain dehydrogenases/reductases (SDRs) (Figure 11) or aldo-keto reductases (AKRs) (Figure 12). In morphine biosynthesis, for instance, stereo-specific reduction of salutaridine to salutaridinol is catalyzed by the NADPH-dependent SDR salutaridine reductase (SalR), while codeinone reductase (CoR), an AKR, catalyzes the conversion of codeinone or morphinone to codeine and morphine (Unterlinner et al., 1999; Ziegler et al., 2006). A similar role for SDRs was also demonstrated in the terminal step of noscapine biosynthesis (Chen and Facchini, 2014) and recently an AKR in galanthamine biosynthesis from *Lycoris* species has been functionally characterized (Xiang et al., 2025). Additionally, tropinone reductases (TRs), such as TR-I and TR-II, are critical in tropane alkaloid biosynthesis, converting tropinone into tropine or pseudotropine, respectively, leading to the production of important alkaloids like hyoscyamine, scopolamine, and calystegines (Robins and Walton, 1993). In phenylpropanoid metabolism, SDRs contribute to the biosynthesis of important metabolites involved in defense, pigmentation, and structural support. For example, cinnamoyl-CoA reductase (CCR) catalyzes the first committed step in monolignol biosynthesis, essential for lignin formation, while dihydroflavonol 4-reductase (DFR) participates in flavonoid biosynthesis, which contributes to antioxidant functions and plant signaling. (Beld et

al., 1989; Pan et al., 2014; Petit et al., 2007; Sattler et al., 2017). SDRs are also integral to terpenoid metabolism, as demonstrated by their involvement in menthol biosynthesis through monoterpene double-bond reductases, underscoring their role in chemical defense (Liu et al., 2021; Ringer et al., 2003). Beyond these pathways, SDRs contribute to the synthesis of other secondary metabolites such as phytoalexins and plant aroma (Kitaoka et al., 2016; Valletta et al., 2023).

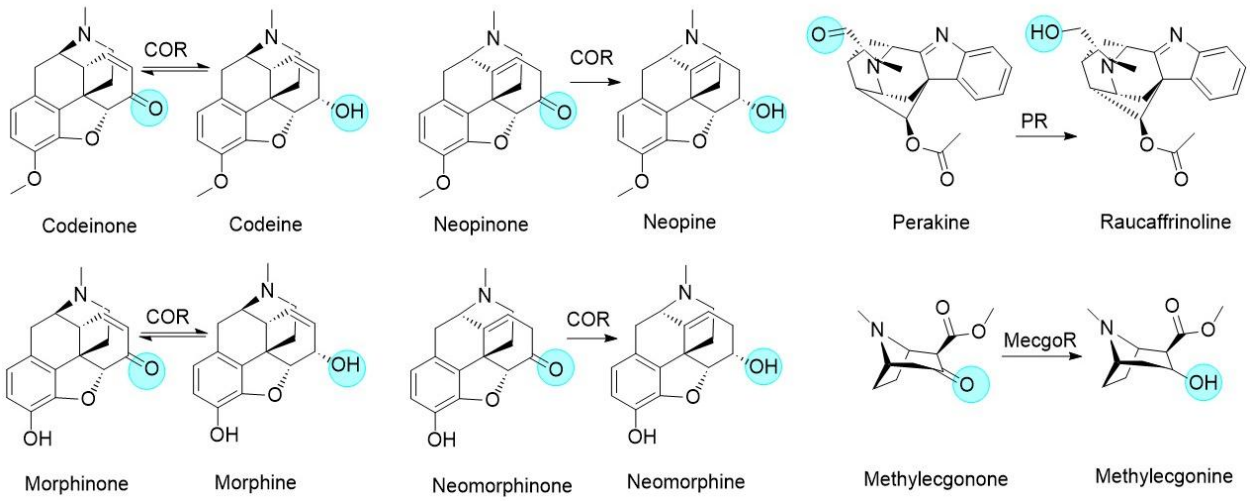


Figure 56. Structure showing aldo-keto reduction to give rise to specialized metabolites catalyzed by AKRs
COR: Codeinone reductase PR: Perakine reductase, MecgoR: Methylecgonone reductase

Divergence between AA and BIA pathways occurs at the methylation stage as coclaurine *N*-methyltransferase acts early in BIA biosynthesis unlike the *N*-methylation in the galanthamine pathway that occurs at late stage. The effective *N* methylation is carried out by similar reaction mechanism using SAM as methyl donor and some pharmaceautically valuable compounds formed by similar mechanism is illustrated (Figure 11). In MIA biosynthesis also several γ-tocopherol like *N*-methyltransferase has been characterized (Cázares-Flores et al., 2016; Levac et al., 2016; Liscombe et al., 2010).

Building upon these cross-pathway parallels, our characterization of *La*TMT2 places this enzyme within a broader emerging paradigm in plant specialized metabolism: the functional repurposing of primary metabolic enzyme scaffolds for roles in alkaloid biosynthesis.

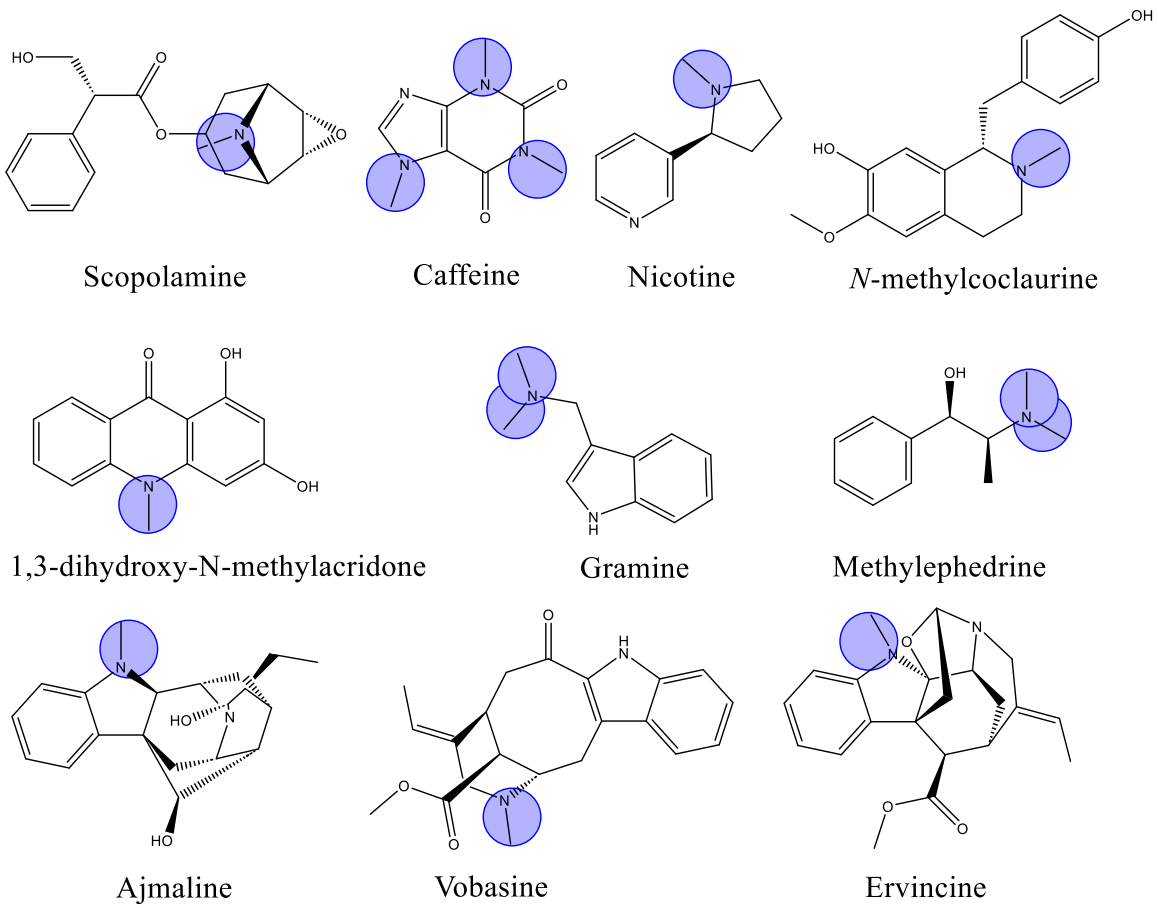


Figure 57 Structure of some N-methylated specialized metabolites catalyzed by N-methyltransferases

γ-Tocopherol methyltransferases (γ-TMTs) are classically associated with vitamin E biosynthesis, catalyzing the conversion of γ-tocopherol to α-tocopherol in plastids (Bergmüller et al., 2003; Shintani and DellaPenna, 1998). However, the discovery by Liscombe et al. that a γ-TMT homolog from Catharanthus roseus (Cr2270) catalyzes *N*-methylation of a vindoline pathway intermediate provided the first clear evidence that this enzyme scaffold had been independently recruited for alkaloid biosynthesis (Liscombe et al., 2010). Subsequent studies identified additional TMT-derived *N*-methyltransferases involved in MIA metabolism, including picrinine N-methyltransferases and organelle-targeted γ-TMT homologs (Cázares-Flores et al., 2016), indicating that this evolutionary recruitment has occurred multiple times across divergent plant lineages.

Within the Amaryllidaceae, a TMT homolog from Narcissus cv. Tête-à-Tête was recently implicated in the *N*-methylation of nornarwedine (Mehta et al., 2024), and our identification of

*La*TMT2 as an 82% similar homolog in *Leucojum aestivum* further reinforces the hypothesis that TMT-derived *N*-methyltransferases represent a conserved, lineage-specific innovation for late-stage alkaloid biosynthesis within this family. In contrast to the CNMT scaffold employed in BIA biosynthesis, the recruitment of γ-TMT homologs in Amaryllidaceae suggests that both the enzymatic identity and temporal positioning of *N*-methylation events have undergone independent evolutionary optimization across alkaloid-producing lineages. Collectively, these findings suggest that γ-TMT homologs constitute a versatile and evolvable catalytic platform whose substrate specificity can be redirected from lipophilic tocopherol derivatives toward structurally distinct hydrophilic alkaloid substrates through relatively limited structural adaptation. This functional plasticity not only provides a conceptual framework for identifying TMT-like *N*-methyltransferase candidates in other Amaryllidaceae species but also establishes a rational basis for future protein engineering efforts aimed at optimizing *La*TMT2 activity toward specific galanthamine pathway intermediates.

A key finding of this study is that the terminal node of galanthamine biosynthesis is governed not by a single committed step, but by a dynamic network of N-methyltransferase and reductase activities shaped by substrate channeling, cofactor balance, and active-site architecture. Within this network, *La*TMT2 and the *La*AKR isoforms act on overlapping substrate pools—nornarwedine, norgalanthamine, narwedine, and galanthamine—creating an interconnected system in which methylation-first and reduction-first routes operate simultaneously. Structural analyses provide a coherent molecular basis for these complementary activities: in *La*TMT2, favorable substrate orientation, short substrate-to-SAM distances (~3.2 Å), and the conserved Glu-Glu-His catalytic triad support efficient SN2 methyl transfer to both nornarwedine and norgalanthamine, explaining its broad substrate acceptance with a kinetic preference toward nornarwedine. Similarly, in *La*AKR3, optimal hydride-transfer geometry underpins efficient reduction of narwedine, whereas in *La*AKR1, a unique His117-mediated interaction appears to reorient narwedine toward preferential NADP+-dependent oxidation, suggesting that subtle active-site differences dictate reaction directionality among isoforms. Collectively, these configurations indicate that flux through the terminal galanthamine node exists as a tunable equilibrium rather than a unidirectional pathway, influenced by NADPH/NADP+ availability, relative *La*AKR isoform expression, and substrate pools generated by *La*TMT2. This dynamic enzymatic orchestration parallels the alkaloid

interconversion systems described in *P. somniferum*, extending the concept of metabolic flexibility at alkaloid branch points to the coupled methylation–reduction network that defines the terminal architecture of galanthamine biosynthesis in *L. aestivum*.

Taken together, these comparative insights highlight the extensive evolutionary and mechanistic parallels between AA, BIAs, and other specialized metabolites such as MIAs. Such cross-pathway analogies provide a powerful framework for predicting and identifying candidate genes responsible for the yet-unresolved steps in AA biosynthesis.

Subcellular localization studies revealed a sophisticated spatial architecture underpinning AA biosynthesis, consistent with the broader principle that plant specialized metabolic pathways achieve efficiency and regulatory control through compartmentalization (Figure 12). Enzymes catalyzing the early phenylpropanoid steps — *La*C4H and *La*C3′H — are anchored to the endoplasmic reticulum (ER) membrane (Karimzadegan et al., 2024), in agreement with the well-established paradigm for class II cytochrome P450 enzymes, which are universally tethered to the ER via an N-terminal transmembrane α-helix with their catalytic domains facing the cytosol (Hasemann et al., 1995). This topology is not merely structural: ER anchoring facilitates productive interaction with the membrane-embedded NADPH-dependent cytochrome P450 oxidoreductase (CPR), whose co-localization with P450s in the two-dimensional plane of the ER membrane is now recognized as a key driver of electron transfer efficiency and metabolon assembly (Laursen et al., 2016; Parage et al., 2016). Our results extend this paradigm to *La*CYP96T1 and *La*CYP96T2, which were similarly ER-anchored, consistent with their identity as membrane-bound P450s. The ER localization of multiple P450s in the pathway strongly supports the formation of a dynamic metabolon at the cytosol-ER interface, a model well-substantiated in the phenylpropanoid pathway where C4H serves as a scaffolding hub recruiting soluble enzymes such as PAL to the ER surface, enabling substrate channeling and insulating reactive intermediates from the bulk cytosol (Achnine et al., 2004; Dastmalchi et al., 2016; Jørgensen et al., 2005). Substrate channeling in such metabolons has been directly demonstrated by isotopic dilution experiments, in which labeled phenylalanine-derived intermediates did not equilibrate with exogenously supplied unlabeled substrates, revealing the direct handoff between sequentially acting enzymes (Rasmussen and Dixon, 1999). By analogy, the co-occurrence of *La*C4H, *La*C3′H, *La*CYP96T1, and *La*CYP96T2 at the ER membrane raises the testable

hypothesis that these enzymes similarly operate as a channeled complex, minimizing the loss of labile or cytotoxic intermediates to the cytosol and maximizing flux toward the final alkaloid products.

The cytosolic localization of *La*N4′OMT is consistent with the general pattern observed for soluble SAM-dependent methyltransferases in alkaloid pathways, which are recruited to the ER surface through transient protein-protein interactions rather than permanent membrane anchoring (Winkel, 2004). Enzymes of the cytochrome P450 superfamily have been proposed to serve as anchoring points on the ER membrane for the recruitment of otherwise soluble enzymes, enabling the dynamic assembly of pathway-specific metabolic complexes (Bassard et al., 2017; Jørgensen et al., 2005). The dual localization of *La*NMT in both the cytosol and ER is particularly noteworthy, as it implies a capacity to participate in reactions in both compartments — a functional flexibility that may allow *La*NMT to interact with ER-resident P450s when the metabolon is assembled, while also operating independently in the soluble phase. Such dual localization has precedent in other plant methyltransferases and may reflect a dynamic, stimulus-dependent redistribution to the ER surface, analogous to the conditional metabolon recruitment observed in cyanogenic glucoside biosynthesis(Laursen et al., 2016). NBS and NR, as nucleo-cytosolic enzymes, occupy a strategically accessible compartment: their presence in both the nucleus and cytosol is consistent with a dual role in catalysis and potentially in transcriptional regulation of pathway genes, a phenomenon increasingly recognized for metabolic enzymes that moonlight as transcriptional co-regulators in specialized metabolism (Gupta and Uversky, 2023).

The localization of *La*TMT2 to the Golgi apparatus is a striking finding that warrants careful interpretation. In alkaloid-producing plants, the Golgi and its associated vesicular trafficking machinery play well-documented roles in the subcellular sorting and vacuolar deposition of bioactive metabolites. Immuno-cytological studies in *Berberis* and *Papaver* demonstrated that biosynthetic enzymes and their alkaloid products can be compartmentalized within specialized vesicles that subsequently fuse with the central vacuole, releasing their contents for sequestration (Amann et al., 1986; Roberts, 1987). Intracellular transport of specialized metabolites involves vesicle-mediated membrane transport, membrane-transporter-mediated vacuolar sequestration, and export to the apoplast (Nour-Eldin and Halkier, 2013). The Golgi localization of *La*TMT2 may therefore reflect a role in the methylation of alkaloid intermediates destined for vacuolar storage,

a step that could influence the physicochemical properties — and hence tonoplast permeability — of the final product. Alternatively, it may indicate that *La*TMT2 acts on substrates that transit the secretory pathway, possibly glycosylated or lipid-associated alkaloid precursors. This warrants future investigation using co-localization with Golgi markers and functional analysis of *La*TMT2 in vesicle-trafficking mutant backgrounds (Xiao et al., 2025).

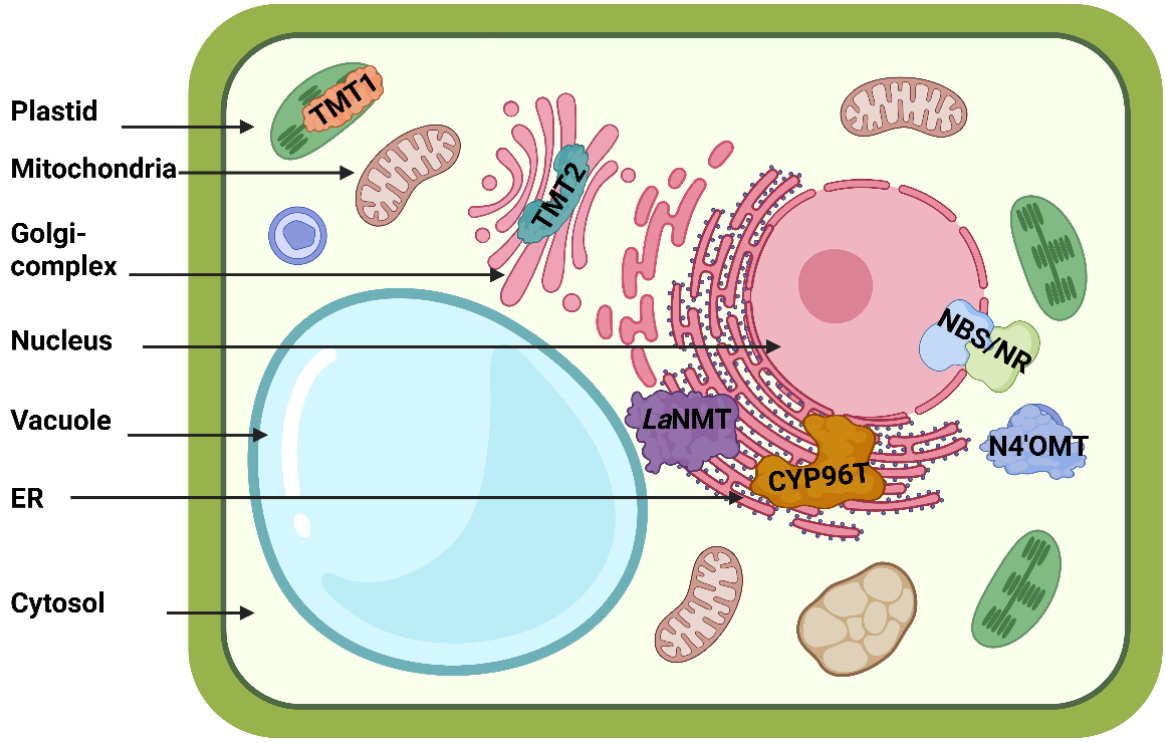


Figure 58. Schematic diagram of sub-cellular localization of the studied enzymes.
(Created in BioRender. Lamichhane, B. (2025) https://BioRender.com/undefined)

In striking contrast, *La*TMT1 localized to plastids, consistent with its proposed association with tocopherol biosynthesis. In plants, all enzymatic activities for tocopherol synthesis — including the plastidic γ-tocopherol methyltransferase (γ-TMT) — have been localized to the inner chloroplast envelope (Soll et al., 1980), and the plastid has long been established as the exclusive site of tocochromanol biosynthesis (d'Harlingue and Camara, 1985; Shintani and DellaPenna, 1998). The plastid localization of *La*TMT1 is therefore biochemically coherent and suggests that this enzyme may have been co-opted from, or retained dual catalytic activity with, the tocopherol methylation machinery — a form of enzymatic promiscuity with potential implications for the

cross-talk between primary antioxidant metabolism and specialized alkaloid biosynthesis. Collectively, these diverse localizations underscore a complex spatial orchestration of AA biosynthesis across the ER, cytosol, Golgi, and plastid. This multi-compartment architecture is not merely an anatomical curiosity: it has direct consequences for metabolite availability, enzyme efficiency, pathway flux, and the capacity of the plant to regulate and insulate each biosynthetic step in response to developmental and environmental cues.

4.2 Conclusion

This study identified and functionally characterized enzymes spanning the early, mid, and late stages of the galanthamine biosynthetic pathway, thereby providing the most comprehensive experimental reconstruction of this specialized metabolic route to date. By demonstrating that key steps, including oxidative phenol coupling, reductive transformations, and terminal *N*-methylation—can be modularly reconstituted in *N. benthamiana*, this work establishes a practical proof-of-concept for heterologous galanthamine production. Across the pathway, recurring patterns of enzymatic flexibility emerged: reductases such as *La*NRII catalyze multiple substrate transformations, *La*TMT2 efficiently methylates structurally distinct intermediates, and *La*CYP96T enzymes perform multiple regioselective C–C phenol-coupling reactions. These findings collectively reveal a dynamic and branching biosynthetic architecture characterized by catalytic plasticity, functional redundancy, and high diversification potential—features that underpin the structural richness of AAs.

Beyond its direct insights into galanthamine biosynthesis, this thesis contributes a broader conceptual framework for understanding and engineering AA pathways. The results highlight common principles of specialized metabolism: the importance of enzymatic promiscuity in generating chemical diversity, the modular nature of pathway organization, and the influence of subcellular compartmentalization on metabolic efficiency. By situating AA biosynthesis within the wider biochemical landscape defined by benzylisoquinoline and monoterpene indole alkaloids, this work establishes evolutionary and mechanistic parallels that can accelerate the discovery of missing biosynthetic enzymes across related pathways.

Taken together, this research advances the mechanistic understanding of AA assembly by resolving previously uncharacterized oxidative coupling and *N*-methylation steps, elucidating the enzymatic logic driving scaffold diversification, and revealing the compartmental choreography that directs metabolic flux. More importantly, the detailed characterization of *La*CYP96T1, *La*CYP96T2, *La*NRII, and especially the versatile, branch-enabling *La*TMT2 provides a foundational enzymatic toolkit with immediate translational relevance. These enzymes constitute actionable targets for metabolic engineering, enabling the rational optimization of precursor supply, control of branch-point reactions, and reconstruction of tailored biosynthetic routes in microbial or plant-based platforms. By uniting fundamental enzymology with applied biotechnology, this thesis lays the groundwork for sustainable, scalable, and ethically responsible production systems for galanthamine and other high-value AA—transforming long-standing biochemical uncertainties into new opportunities for green biomanufacturing and therapeutic innovation.

4.3 Perspectives

To fully leverage the biosynthetic capacity of the AA pathway, several critical research directions merit focused investigation. First, structure–function analyses of key catalytic enzymes—including *La*CYP96T1/2, *La*NRII and AKR's are essential for defining the molecular determinants governing substrate specificity, regioselectivity, and catalytic promiscuity. Approaches such as site-directed mutagenesis, domain-swapping, and high-resolution structural modeling will clarify active-site architectures and enable the rational engineering of more efficient or tailored biocatalysts for targeted pathway manipulation. Such insights will be indispensable for optimizing metabolic flux through preferred biosynthetic routes and minimizing the accumulation of undesired intermediates.

In parallel, the continued development of heterologous expression platforms offers a powerful avenue for scalable AA production. Expanding full or partial pathway reconstitution *in N. benthamiana* or engineering microbial hosts such as *Pseudomonas putida*, *Saccharomyces cerevisiae,* and *Chlamydomonas reinhardtii* will enable controlled production environments and tunable metabolic engineering strategies. Incorporating dynamic regulatory modules, compartmental targeting signals, precursor supply optimization, and cofactor regeneration systems will be particularly valuable for enhancing pathway efficiency and yield. Moreover, systems-level

analyses—including metabolomics, fluxomics, and transcriptome-guided pathway redesign—could further refine host performance and stabilize production traits.

By addressing these knowledge gaps through integrated biochemical, structural, and synthetic-biology approaches, future research will substantially deepen our mechanistic understanding of AA biosynthesis while accelerating the development of sustainable, high-yield biotechnological platforms. Such advances will not only facilitate reliable production of medicinally important alkaloids such as galanthamine but also open opportunities to generate novel analogues with improved pharmacological profiles, ultimately expanding the therapeutic landscape derived from Amaryllidaceae natural products.

4.4 References

Achnine, L., Blancaflor, E.B., Rasmussen, S. and Dixon, R.A. (2004) Colocalization of L-phenylalanine ammonia-lyase and cinnamate 4-hydroxylase for metabolic channeling in phenylpropanoid biosynthesis. *The Plant Cell* **16**, 3098-3109.

Adesanya, S., Olugbade, T., Odebiyl, O. and Aladesanmi, J. (1992) Antibacterial alkaloids in Crinum jagus. *International Journal of Pharmacognosy* **30**, 303-307.

Aghaali, Z. and Naghavi, M.R. (2024) Developing benzylisoquinoline alkaloid-enriched opium poppy via CRISPR-directed genome editing: A review. *BMC Plant Biology* **24**, 700.

Al Mamun, A., Maříková, J., Hulcová, D., Janoušek, J., Šafratová, M., Nováková, L., Kučera, T., Hrabinová, M., Kuneš, J. and Korábečný, J. (2020) Amaryllidaceae alkaloids of belladine-type from Narcissus pseudonarcissus cv. Carlton as new selective inhibitors of butyrylcholinesterase. *Biomolecules* **10**, 800.

Amann, M., Wanner, G. and Zenk, M. (1986) Intracellular compartmentation of two enzymes of berberine biosynthesis in plant cell cultures. *Planta* **167**, 310-320.

Aniszewski, T. (2015) *Alkaloids: chemistry, biology, ecology, and applications*:Elsevier.

Atanasov, A.G., Waltenberger, B., Pferschy-Wenzig, E.-M., Linder, T., Wawrosch, C., Uhrin, P., Temml, V., Wang, L., Schwaiger, S. and Heiss, E.H. (2015) Discovery and resupply of pharmacologically active plant-derived natural products: A review. *Biotechnology advances* **33**, 1582-1614.

Barken, I., Geller, J. and Rogosnitzky, M. (2008) Noscapine inhibits human prostate cancer progression and metastasis in a mouse model. *Anticancer research* **28**, 3701-3704.

Bassard, J.-E., Møller, B.L. and Laursen, T. (2017) Assembly of dynamic P450-mediated metabolons—order versus chaos. *Current molecular biology reports* **3**, 37-51.

Bastida, J., Lavilla, R. and Viladomat, F. (2006) Chemical and biological aspects of Narcissus alkaloids. *The alkaloids: chemistry and biology* **63**, 87-179.

Beaudoin, G.A. and Facchini, P.J. (2014) Benzylisoquinoline alkaloid biosynthesis in opium poppy. *Planta* **240**, 19-32.

Beld, M., Martin, C., Huits, H., Stuitje, A.R. and Gerats, A.G. (1989) Flavonoid synthesis in Petunia hybrida: partial characterization of dihydroflavonol-4-reductase genes. *Plant molecular biology* **13**, 491-502.

Benedec, D., Oniga, I., Hanganu, D., Gheldiu, A.M., Puşcaş, C., Silaghi-Dumitrescu, R., Duma, M., Tiperciuc, B., Vârban, R. and Vlase, L. (2018) Sources for developing new medicinal products: biochemical investigations on alcoholic extracts obtained from aerial parts of some Romanian Amaryllidaceae species. *BMC complementary and alternative medicine* **18**, 1-12.

Bergmüller, E., Porfirova, S. and Dörmann, P. (2003) Characterization of an Arabidopsis mutant deficient in γ-tocopherol methyltransferase. *Plant Molecular Biology* **52**, 1181-1190.

Berkov, S., Atanasova, M., Georgiev, B., Bastida, J. and Doytchinova, I. (2022) The Amaryllidaceae alkaloids: an untapped source of acetylcholinesterase inhibitors. *Phytochemistry Reviews* **21**, 1415-1443.

Boccia, M., Grzech, D., Lopes, A.A., O'Connor, S.E. and Caputi, L. (2022) Directed biosynthesis of new to nature alkaloids in a heterologous *Nicotiana benthamiana* expression host. *Frontiers in Plant Science* **13**, 919443.

Bostock, J. and Riley, H.T. (1855) *The natural history of Pliny*:HG Bohn.

Bravo, R.R., Faria, A.C., Brito-da-Costa, A.M., Carmo, H., Mladěnka, P., da Silva, D.D. and Remião, F. (2022) Cocaine: an updated overview on chemistry, detection, biokinetics, and pharmacotoxicological aspects including abuse pattern. *Toxins* **14**, 278.

Brückner, K. and Tissier, A. (2013) High-level diterpene production by transient expression in *Nicotiana benthamiana*. *Plant Methods* **9**, 46.

Cahlíková, L., Kawano, I., Řezáčová, M., Blunden, G., Hulcová, D. and Havelek, R. (2021) The Amaryllidaceae alkaloids haemanthamine, haemanthidine and their semisynthetic derivatives as potential drugs. *Phytochemistry Reviews* **20**, 303-323.

Cankar, K., Jongedijk, E., Klompmaker, M., Majdic, T., Mumm, R., Bouwmeester, H., Bosch, D. and Beekwilder, J. (2015) (+)-Valencene production in *Nicotiana benthamiana* is increased by down-regulation of competing pathways. *Biotechnology journal* **10**, 180-189.

Cázares-Flores, P., Levac, D. and De Luca, V. (2016) Rauvolfia serpentina N-methyltransferases involved in ajmaline and Nβ-methylajmaline biosynthesis belong to a gene family derived from γ-tocopherol C-methyltransferase. *The Plant Journal* **87**, 335-342.

Chen, X. and Facchini, P.J. (2014) Short-chain dehydrogenase/reductase catalyzing the final step of noscapine biosynthesis is localized to laticifers in opium poppy. *The Plant Journal* **77**, 173-184.

Chen, X., Long, X., Liao, Y. and Zheng, J. (2018) Lycorine inhibits the proliferation and promotes apoptosis of SGC-7901 gastric cancer cells by downregulating expression of cyclin D1. *Xi bao yu fen zi Mian yi xue za zhi= Chinese Journal of Cellular and Molecular Immunology* **34**, 354-358.

Chiocchio, I., Mandrone, M., Tomasi, P., Marincich, L. and Poli, F. (2021) Plant secondary metabolites: An opportunity for circular economy. *Molecules* **26**, 495.

Choi, K.-B., Morishige, T., Shitan, N., Yazaki, K. and Sato, F. (2002) Molecular cloning and characterization of coclaurinen-methyltransferase from cultured cells of Coptis japonica. *Journal of Biological Chemistry* **277**, 830-835.

Çitoğlu, G.S., Acıkara, Ö.B., Yılmaz, B.S. and Özbek, H. (2012) Evaluation of analgesic, anti-inflammatory and hepatoprotective effects of lycorine from Sternbergia fisheriana (Herbert) Rupr. *Fitoterapia* **83**, 81-87.

Cravens, A., Payne, J. and Smolke, C.D. (2019) Synthetic biology strategies for microbial biosynthesis of plant natural products. *Nature communications* **10**, 2142.

Cui, W., Iwasa, K., Sugiura, M., Takeuchi, A., Tode, C., Nishiyama, Y., Moriyasu, M., Tokuda, H. and Takeda, K. (2007) Biotransformation of phenolic 1-benzyl-N-methyltetrahydroisoquinolines in plant cell cultures followed by LC/NMR, LC/MS, and LC/CD. *Journal of natural products* **70**, 1771-1778.

d'Harlingue, A. and Camara, B. (1985) Plastid enzymes of terpenoid biosynthesis. Purification and characterization of gamma-tocopherol methyltransferase from Capsicum chromoplasts. *Journal of Biological Chemistry* **260**, 15200-15203.

Dang, T.T.T., Onoyovwi, A., Farrow, S.C. and Facchini, P.J. (2012) Biochemical genomics for gene discovery in benzylisoquinoline alkaloid biosynthesis in opium poppy and related species. In: *Methods in enzymology* pp. 231-266. Elsevier.

Dastmalchi, M., Bernards, M.A. and Dhaubhadel, S. (2016) Twin anchors of the soybean isoflavonoid metabolon: evidence for tethering of the complex to the endoplasmic reticulum by IFS and C4H. *The Plant Journal* **85**, 689-706.

Dastmalchi, M., Chang, L., Torres, M.A., Ng, K.K. and Facchini, P.J. (2018) Codeinone reductase isoforms with differential stability, efficiency and product selectivity in opium poppy. *The Plant Journal* **95**, 631-647.

de Sousa Falcão, H., Leite, J.A., Barbosa-Filho, J.M., de Athayde-Filho, P.F., de Oliveira Chaves, M.C., Moura, M.D., Ferreira, A.L., De Almeida, A.B.A., Souza-Brito, A.R.M. and de Fátima Formiga Melo Diniz, M. (2008) Gastric and duodenal antiulcer activity of alkaloids: a review. *Molecules* **13**, 3198-3223.

Deng, X., Zhao, L., Fang, T., Xiong, Y., Ogutu, C., Yang, D., Vimolmangkang, S., Liu, Y. and Han, Y. (2018) Investigation of benzylisoquinoline alkaloid biosynthetic pathway and its transcriptional regulation in lotus. *Horticulture Research* **5**.

Desgagné-Penix, I. (2021) Biosynthesis of alkaloids in Amaryllidaceae plants: A review. *Phytochemistry Reviews* **20**, 409-431.

Desgagné-Penix, I. and Facchini, P.J. (2011) Benzylisoquinoline alkaloid biosynthesis. *Plant Metabolism and Biotechnology*, 241-261.

Desgagné-Penix, I. and Facchini, P.J. (2012) Systematic silencing of benzylisoquinoline alkaloid biosynthetic genes reveals the major route to papaverine in opium poppy. *The Plant Journal* **72**, 331-344.

Dey, P., Kundu, A., Kumar, A., Gupta, M., Lee, B.M., Bhakta, T., Dash, S. and Kim, H.S. (2020) Analysis of alkaloids (indole alkaloids, isoquinoline alkaloids, tropane alkaloids). In: *Recent advances in natural products analysis* pp. 505-567. Elsevier.

Diamond, A. and Desgagné-Penix, I. (2016) Metabolic engineering for the production of plant isoquinoline alkaloids. *Plant biotechnology journal* **14**, 1319-1328.

Dong, L., Jongedijk, E., Bouwmeester, H. and Van Der Krol, A. (2016) Monoterpene biosynthesis potential of plant subcellular compartments. *New Phytologist* **209**, 679-690.

Eichhorn, J., Takada, T., Kita, Y. and Zenk, M.H. (1998) Biosynthesis of the Amaryllidaceae alkaloid galanthamine. *Phytochemistry* **49**, 1037-1047.

El Tahchy, A., Boisbrun, M., Ptak, A., Dupire, F., Chrétien, F., Henry, M., Chapleur, Y. and Laurain-Mattar, D. (2010) New method for the study of Amaryllidaceae alkaloid biosynthesis using biotransformation of deuterium-labeled precursor in tissue cultures. *Acta Biochimica Polonica* **57**.

El Tahchy, A., Ptak, A., Boisbrun, M., Barre, E., Guillou, C., Dupire, F.o., Chrétien, F.o., Henry, M., Chapleur, Y. and Laurain-Mattar, D. (2011) Kinetic study of the rearrangement of deuterium-labeled 4′-*O*-methylnorbelladine in Leucojum *aestivum* shoot cultures by mass spectrometry. Influence of precursor feeding on Amaryllidaceae alkaloid accumulation. *Journal of natural products* **74**, 2356-2361.

Elgorashi, E., Zschocke, S., Van Staden, J. and Eloff, J. (2003) The anti-inflammatory and antibacterial activities of Amaryllidaceae alkaloids. *South African Journal of Botany* **69**, 448-449.

Erb, M. and Kliebenstein, D.J. (2020) Plant secondary metabolites as defenses, regulators, and primary metabolites: the blurred functional trichotomy. *Plant physiology* **184**, 39-52.

Evidente, A., Andolfi, A., Abou-Donia, A.H., Touema, S.M., Hammoda, H.M., Shawky, E. and Motta, A. (2004) (−)-Amarbellisine, a lycorine-type alkaloid from Amaryllis belladonna L. growing in Egypt. *Phytochemistry* **65**, 2113-2118.

Facchini, P.J. and De Luca, V. (1994) Differential and tissue-specific expression of a gene family for tyrosine/dopa decarboxylase in opium poppy. *Journal of Biological Chemistry* **269**, 26684-26690.

Farrow, S.C., Kamileen, M.O., Meades, J., Ameyaw, B., Xiao, Y. and O'Connor, S.E. (2018) Cytochrome P450 and O-methyltransferase catalyze the final steps in the biosynthesis of the anti-addictive alkaloid ibogaine from Tabernanthe iboga. *Journal of Biological Chemistry* **293**, 13821-13833.

Fennell, C. and Van Staden, J. (2001) Crinum species in traditional and modern medicine. *Journal of ethnopharmacology* **78**, 15-26.

Ferdausi, A., Chang, X. and Jones, M. (2021) Transcriptomic analysis for differential expression of genes involved in secondary metabolite production in Narcissus pseudonarcissus field derived bulb and *in vitro* callus. *Industrial Crops and Products* **168**, 113615.

Fossati, E., Narcross, L., Ekins, A., Falgueyret, J.-P. and Martin, V.J. (2015) Synthesis of morphinan alkaloids in Saccharomyces cerevisiae. *PLoS One* **10**, e0124459.

Frenzel, T. and Zenk, M.H. (1990) S-Adenosyl-L-methionine: 3′-hydroxy-N-methyl-(S)-coclaurine-4′-*O*-methyl transferase, a regio-and stereoselective enzyme of the (*S*)-reticuline pathway. *Phytochemistry* **29**, 3505-3511.

Gallage, N.J., Hansen, E.H., Kannangara, R., Olsen, C.E., Motawia, M.S., Jørgensen, K., Holme, I., Hebelstrup, K., Grisoni, M. and Møller, B.L. (2014) Vanillin formation from ferulic acid in Vanilla planifolia is catalysed by a single enzyme. *Nature communications* **5**, 4037.

Gesell, A., Rolf, M., Ziegler, J., Chávez, M.L.D., Huang, F.-C. and Kutchan, T.M. (2009) CYP719B1 is salutaridine synthase, the CC phenol-coupling enzyme of morphine biosynthesis in opium poppy. *Journal of Biological Chemistry* **284**, 24432-24442.

Girard, M.-P., Karimzadegan, V., Héneault, M., Cloutier, F., Bérubé, G., Berthoux, L., Mérindol, N. and Desgagné-Penix, I. (2022) Chemical Synthesis and Biological Activities of Amaryllidaceae Alkaloid Norbelladine Derivatives and Precursors. *Molecules* **27**, 5621.

Golubova, D., Tansley, C., Su, H. and Patron, N. (2024) Engineering *Nicotiana benthamiana* as a platform for natural product biosynthesis. *Current Opinion in Plant Biology* **81**, 102611.

Griffiths, N.J. (2015) Design, Synthesis and Biological Evaluation of Narciclasine Analogues. University of Bath.
Guo, J., Gao, D., Lian, J. and Qu, Y. (2024) De novo biosynthesis of antiarrhythmic alkaloid ajmaline. *Nature Communications* **15**, 457.
Gupta, M.N. and Uversky, V.N. (2023) Moonlighting enzymes: when cellular context defines specificity. *Cellular and Molecular Life Sciences* **80**, 130.
Gurkok, T., Ozhuner, E., Parmaksiz, I., Özcan, S., Turktas, M., Ipek, A., Demirtas, I., Okay, S. and Unver, T. (2016) Functional characterization of 4′ OMT and 7OMT genes in BIA biosynthesis. *Frontiers in plant science* **7**, 98.
Hagel, J.M. and Facchini, P.J. (2005) Elevated tyrosine decarboxylase and tyramine hydroxycinnamoyltransferase levels increase wound-induced tyramine-derived hydroxycinnamic acid amide accumulation in transgenic tobacco leaves. *Planta* **221**, 904-914.
Hagel, J.M. and Facchini, P.J. (2010) Dioxygenases catalyze the O-demethylation steps of morphine biosynthesis in opium poppy. *Nature chemical biology* **6**, 273-275.
Hagel, J.M. and Facchini, P.J. (2013) Benzylisoquinoline alkaloid metabolism: a century of discovery and a brave new world. *Plant and Cell Physiology* **54**, 647-672.
Hasan, M.M., Kim, H.-S., Jeon, J.-H., Kim, S.H., Moon, B., Song, J.-Y., Shim, S.H. and Baek, K.-H. (2014) Metabolic engineering of *Nicotiana benthamiana* for the increased production of taxadiene. *Plant cell reports* **33**, 895-904.
Hasemann, C.A., Kurumbail, R.G., Boddupalli, S.S., Peterson, J.A. and Deisenhofer, J. (1995) Structure and function of cytochromes P450: a comparative analysis of three crystal structures. *Structure* **3**, 41-62.
He, M., Qu, C., Gao, O., Hu, X. and Hong, X. (2015) Biological and pharmacological activities of Amaryllidaceae alkaloids. *Rsc advances* **5**, 16562-16574.
Heinrich, M. (2010) Galanthamine from Galanthus and other Amaryllidaceae–chemistry and biology based on traditional use. *The alkaloids: chemistry and biology* **68**, 157-165.
Heinrich, M. and Teoh, H.L. (2004) Galanthamine from snowdrop—the development of a modern drug against Alzheimer's disease from local Caucasian knowledge. *Journal of ethnopharmacology* **92**, 147-162.
Helmy, M., Smith, D. and Selvarajoo, K. (2020) Systems biology approaches integrated with artificial intelligence for optimized metabolic engineering. *Metabolic engineering communications* **11**, e00149.
Henriques, A., Kerber, V. and Moreno, P. (2004) Em Farmacognosia: da planta ao medicamento. *Eds.: Simões, CMO et al* **5**.
Hiatt, A., Caffferkey, R. and Bowdish, K. (1989) Production of antibodies in transgenic plants. *Nature* **342**, 76-78.
Hnin, S.Y.Y., Nakashima, Y. and Morita, H. (2024) Substrate Flexibilities of Norbelladine Synthase and Noroxomaritidine/Norcraugsodine Reductase for Hydroxylated and/or Methoxylated Aldehydes. *Chemical and Pharmaceutical Bulletin* **72**, 507-511.
Hotchandani, T., de Villers, J. and Desgagné-Penix, I. (2019) Developmental regulation of the expression of Amaryllidaceae alkaloid biosynthetic genes in Narcissus papyraceus. *Genes* **10**, 594.
Hotchandani, T. and Desgagne-Penix, I. (2017) Heterocyclic Amaryllidaceae alkaloids: biosynthesis and pharmacological applications. *Current topics in medicinal chemistry* **17**, 418-427.
Houghton, P.J., Agbedahunsi, J.M. and Adegbulugbe, A. (2004) Choline esterase inhibitory properties of alkaloids from two Nigerian Crinum species. *Phytochemistry* **65**, 2893-2896.
Hu, J., Li, W., Liu, Z., Zhang, G. and Luo, Y. (2021) Molecular cloning and functional characterization of tyrosine decarboxylases from galanthamine-producing Lycoris radiata. *Acta Physiologiae Plantarum* **43**, 84.
Huang, X.-Q. and Dudareva, N. (2023) Plant specialized metabolism. *Current Biology* **33**, R473-R478.
Hussein, R.A. and El-Anssary, A.A. (2019) Plants secondary metabolites: the key drivers of the pharmacological actions of medicinal plants. *Herbal medicine* **1**, 13.

Ikezawa, N., Iwasa, K. and Sato, F. (2008) Molecular cloning and characterization of CYP80G2, a cytochrome P450 that catalyzes an intramolecular C–C phenol coupling of (S)-reticuline in magnoflorine biosynthesis, from cultured Coptis japonica cells. *Journal of Biological Chemistry* **283**, 8810-8821.

Ikezawa, N., Tanaka, M., Nagayoshi, M., Shinkyo, R., Sakaki, T., Inouye, K. and Sato, F. (2003) Molecular cloning and characterization of CYP719, a methylenedioxy bridge-forming enzyme that belongs to a novel P450 family, from cultured Coptis japonica cells. *Journal of Biological Chemistry* **278**, 38557-38565.

Iwasa, K. and Kim, C.W. (1997) Biotransformations of protoberberines in cell cultures of Dicentra spectablis. *Phytochemistry* **46**, 1359-1363.

Jayawardena, T.U., Merindol, N., Liyanage, N.S. and Desgagné-Penix, I. (2024) Unveiling Amaryllidaceae alkaloids: from biosynthesis to antiviral potential–a review. *Natural Product Reports*.

Jayawickreme, K., Świstak, D., Ozimek, E., Reszczyńska, E., Rysiak, A., Makuch-Kocka, A. and Hanaka, A. (2023) Pyrrolizidine alkaloids—pros and cons for pharmaceutical and medical applications. *International Journal of Molecular Sciences* **24**, 16972.

Jia, X., Luo, S., Ye, X., Liu, L. and Wen, W. (2024) Evolution of the biochemistry underpinning purine alkaloid metabolism in plants. *Philosophical Transactions B* **379**, 20230366.

Jiang, Y., Xia, B., Liang, L., Li, X., Xu, S., Peng, F. and Wang, R. (2013) Molecular and analysis of a phenylalanine ammonia-lyase gene (LrPAL2) from Lycoris radiata. *Molecular biology reports* **40**, 2293-2300.

Jiang, Y., Xia, N., Li, X., Shen, W., Liang, L., Wang, C., Wang, R., Peng, F. and Xia, B. (2011) Molecular cloning and characterization of a phenylalanine ammonia-lyase gene (LrPAL) from Lycoris radiata. *Molecular biology reports* **38**, 1935-1940.

Jiao, X., Fu, X., Li, Q., Bu, J., Liu, X., Savolainen, O., Huang, L., Guo, J., Nielsen, J. and Chen, Y. (2024) De novo production of protoberberine and benzophenanthridine alkaloids through metabolic engineering of yeast. *Nature Communications* **15**, 8759.

Jin, Z. (2007) Amaryllidaceae and Sceletium alkaloids. *Natural product reports* **24**, 886-905.

Jørgensen, K., Rasmussen, A.V., Morant, M., Nielsen, A.H., Bjarnholt, N., Zagrobelny, M., Bak, S. and Møller, B.L. (2005) Metabolon formation and metabolic channeling in the biosynthesis of plant natural products. *Current opinion in plant biology* **8**, 280-291.

Ka, S., Koirala, M., Mérindol, N. and Desgagné-Penix, I. (2020) Biosynthesis and biological activities of newly discovered Amaryllidaceae alkaloids. *Molecules* **25**, 4901.

Ka, S., Mérindol, N., Seck, I., Ricard, S., Diop, A., Boye, C.S.B., Landelouci, K., Daoust, B., Berthoux, L. and Pépin, G. (2021) Biological investigation of Amaryllidaceae alkaloid extracts from the bulbs of Pancratium trianthum collected in the Senegalese flora. *Molecules* **26**, 7382.

Karimzadegan, V., Koirala, M., Sobhanverdi, S., Merindol, N., Majhi, B.B., Gélinas, S.-E., Timokhin, V.I., Ralph, J., Dastmalchi, M. and Desgagné-Penix, I. (2024) Characterization of cinnamate 4-hydroxylase (CYP73A) and p-coumaroyl 3′-hydroxylase (CYP98A) from Leucojum *aestivum*, a source of Amaryllidaceae alkaloids. *Plant Physiology and Biochemistry* **210**, 108612.

Kianfe, B., Kühlborn, J., Tchuenguem, R., Tchegnitegni, B., Ponou, B., Groß, J., Teponno, R., Dzoyem, J., Opatz, T. and Tapondjou, L. (2020) Antimicrobial secondary metabolites from the medicinal plant Crinum glaucum A. Chev.(Amaryllidaceae). *South African Journal of Botany* **133**, 161-166.

Kilgore, M.B., Augustin, M.M., May, G.D., Crow, J.A. and Kutchan, T.M. (2016a) CYP96T1 of Narcissus sp. aff. Pseudonarcissus catalyzes formation of the Para-Para'CC phenol couple in the Amaryllidaceae alkaloids. *Frontiers in plant science* **7**, 225.

Kilgore, M.B., Augustin, M.M., Starks, C.M., O'Neil-Johnson, M., May, G.D., Crow, J.A. and Kutchan, T.M. (2014) Cloning and characterization of a norbelladine 4′-*O*-methyltransferase involved in the biosynthesis of the Alzheimer's drug galanthamine in Narcissus sp. aff. pseudonarcissus. *PloS one* **9**, e103223.

Kilgore, M.B., Holland, C.K., Jez, J.M. and Kutchan, T.M. (2016) Identification of a Noroxomaritidine Reductase with Amaryllidaceae Alkaloid Biosynthesis Related Activities. *J Biol Chem* **291**, 16740-16752.
Kilgore, M.B. and Kutchan, T.M. (2016b) The Amaryllidaceae alkaloids: biosynthesis and methods for enzyme discovery. *Phytochemistry reviews* **15**, 317-337.
Kiris, I., Basar, M.K., Sahin, B., Gurel, B., Coskun, J., Mroczek, T. and Baykal, A.T. (2021) Evaluation of the therapeutic effect of lycoramine on Alzheimer's disease in mouse model. *Current medicinal chemistry* **28**, 3449-3473.
Kishimoto, S., Sato, M., Tsunematsu, Y. and Watanabe, K. (2016) Evaluation of biosynthetic pathway and engineered biosynthesis of alkaloids. *Molecules* **21**, 1078.
Kitaoka, N., Wu, Y., Zi, J. and Peters, R.J. (2016) Investigating inducible short-chain alcohol dehydrogenases/reductases clarifies rice oryzalexin biosynthesis. *The plant journal* **88**, 271-279.
Kohnen-Johannsen, K.L. and Kayser, O. (2019) Tropane alkaloids: chemistry, pharmacology, biosynthesis and production. *Molecules* **24**, 796.
Koirala, M., Cristine Goncalves dos Santos, K., Gélinas, S.-E., Ricard, S., Karimzadegan, V., Lamichhane, B., Sameera Liyanage, N., Merindol, N. and Desgagné-Penix, I. (2023) Auxin and light-mediated regulation of growth, morphogenesis, and alkaloid biosynthesis in Crinum x powellii 'Album' callus. *Phytochemistry* **216**, 113883.
Koirala, M., Merindol, N., Karimzadegan, V., Gélinas, S.-E., Liyanage, N.S., Lamichhane, B., Tobón, M.C.G., Lagüe, P. and Desgagné-Penix, I. (2024) Kinetic and *in silico* structural characterization of norbelladine O-methyltransferase of Amaryllidaceae alkaloids biosynthesis. *Journal of Biological Chemistry* **300**.
Kornienko, A. and Evidente, A. (2008) Chemistry, biology, and medicinal potential of narciclasine and its congeners. *Chemical reviews* **108**, 1982-2014.
Kumar, A. and Kumar, S. (2024) *Secondary metabolites and biotherapeutics*:Elsevier.
Kurotani, K.-i., Hirakawa, H., Shirasawa, K., Tanizawa, Y., Nakamura, Y., Isobe, S. and Notaguchi, M. (2023) Genome sequence and analysis of *Nicotiana benthamiana*, the model plant for interactions between organisms. *Plant and Cell Physiology* **64**, 248-257.
Kutchan, T.M. and Dittrich, H. (1995) Characterization and mechanism of the berberine bridge enzyme, a covalently flavinylated oxidase of benzophenanthridine alkaloid biosynthesis in plants (∗). *Journal of Biological Chemistry* **270**, 24475-24481.
Laursen, T., Borch, J., Knudsen, C., Bavishi, K., Torta, F., Martens, H.J., Silvestro, D., Hatzakis, N.S., Wenk, M.R. and Dafforn, T.R. (2016) Characterization of a dynamic metabolon producing the defense compound dhurrin in sorghum. *Science* **354**, 890-893.
Lee, S., Park, N.-I., Park, Y., Park, K.-C., Kim, E.S., Son, Y.K., Choi, B.-S., Kim, N.-S. and Choi, I.-Y. (2024) O-and N-Methyltransferases in benzylisoquinoline alkaloid producing plants. *Genes & Genomics* **46**, 367-378.
Levac, D., Cázares, P., Yu, F. and De Luca, V. (2016) A picrinine N-methyltransferase belongs to a new family of γ-tocopherol-like methyltransferases found in medicinal plants that make biologically active monoterpenoid indole alkaloids. *Plant Physiology* **170**, 1935-1944.
Levac, D., Murata, J., Kim, W.S. and De Luca, V. (2008) Application of carborundum abrasion for investigating the leaf epidermis: molecular cloning of Catharanthus roseus 16-hydroxytabersonine-16-O-methyltransferase. *The Plant Journal* **53**, 225-236.
Li, C., Deng, C., Pan, G., Wang, X., Zhang, K., Dong, Z., Zhao, G., Tan, M., Hu, X. and Shi, S. (2020) Lycorine hydrochloride inhibits cell proliferation and induces apoptosis through promoting FBXW7-MCL1 axis in gastric cancer. *Journal of Experimental & Clinical Cancer Research* **39**, 230.
Li, C., Huang, P., Wong, K., Xu, Y., Tan, L., Chen, H., Lu, Q., Luo, C., Tam, C. and Zhu, L. (2018a) Coptisine-induced inhibition of Helicobacter pylori: elucidation of specific mechanisms by probing urease active site and its maturation process. *Journal of enzyme inhibition and medicinal chemistry* **33**, 1362-1375.

Li, L., Dai, H.-J., Ye, M., Wang, S.-L., Xiao, X.-J., Zheng, J., Chen, H.-Y., Luo, Y.-h. and Liu, J. (2012) Lycorine induces cell-cycle arrest in the G0/G1 phase in K562 cells via HDAC inhibition. *Cancer cell international* **12**, 49.

Li, R.W., Palit, P., Smith, P.N. and Lin, G.D. (2021) Amaryllidaceae alkaloids as anti-inflammatory agents targeting cholinergic anti-inflammatory pathway: mechanisms and prospects. In: *Evidence Based Validation of Traditional Medicines: A comprehensive Approach* pp. 97-116. Springer.

Li, W., Qiao, C., Pang, J., Zhang, G. and Luo, Y. (2019) The versatile O-methyltransferase LrOMT catalyzes multiple O-methylation reactions in amaryllidaceae alkaloids biosynthesis. *International journal of biological macromolecules* **141**, 680-692.

Li, W., Yang, Y., Qiao, C., Zhang, G. and Luo, Y. (2018b) Functional characterization of phenylalanine ammonia-lyase-and cinnamate 4-hydroxylase-encoding genes from Lycoris radiata, a galanthamine-producing plant. *International journal of biological macromolecules* **117**, 1264-1279.

Li, Y., Li, J., Qian, B., Cheng, L., Xu, S. and Wang, R. (2018c) De novo biosynthesis of p-coumaric acid in E. coli with a trans-cinnamic acid 4-hydroxylase from the Amaryllidaceae plant Lycoris aurea. *Molecules* **23**, 3185.

Liscombe, D.K., Louie, G.V. and Noel, J.P. (2012) Architectures, mechanisms and molecular evolution of natural product methyltransferases. *Nat Prod Rep* **29**, 1238-1250.

Liscombe, D.K., MacLeod, B.P., Loukanina, N., Nandi, O.I. and Facchini, P.J. (2005) Evidence for the monophyletic evolution of benzylisoquinoline alkaloid biosynthesis in angiosperms. *Phytochemistry* **66**, 1374-1393.

Liscombe, D.K., Usera, A.R. and O'Connor, S.E. (2010) Homolog of tocopherol C methyltransferases catalyzes N methylation in anticancer alkaloid biosynthesis. *Proceedings of the National Academy of Sciences* **107**, 18793-18798.

Liu, Q., Majdi, M., Cankar, K., Goedbloed, M., Charnikhova, T., Verstappen, F.W., De Vos, R.C., Beekwilder, J., Van der Krol, S. and Bouwmeester, H.J. (2011) Reconstitution of the costunolide biosynthetic pathway in yeast and *Nicotiana benthamiana*. *PloS one* **6**, e23255.

Liu, Q., Manzano, D., Tanić, N., Pesic, M., Bankovic, J., Pateraki, I., Ricard, L., Ferrer, A., de Vos, R. and van de Krol, S. (2014) Elucidation and in planta reconstitution of the parthenolide biosynthetic pathway. *Metabolic engineering* **23**, 145-153.

Liu, X., Bu, J., Ma, Y., Chen, Y., Li, Q., Jiao, X., Hu, Z., Cui, G., Tang, J. and Guo, J. (2021) Functional characterization of (S)–N-methylcoclaurine 3′-hydroxylase (NMCH) involved in the biosynthesis of benzylisoquinoline alkaloids in Corydalis yanhusuo. *Plant Physiology and Biochemistry* **168**, 507-515.

Liyanage, N.S., Lamichhane, B., Fantino, E., Mérindol, N., Gélinas, S.-E., Tobón, M.C.G. and Desgagné-Penix, I. (2025) Coclaurine N-methyltransferase-like enzymes drive the final biosynthetic reaction of the anti-Alzheimer's drug galanthamine in Amaryllidaceae. *Plant Physiology and Biochemistry*, 110067.

Luca, L.D. (2006) Naturally occurring and synthetic imidazoles: Their chemistry and their biological activities. *Current medicinal chemistry* **13**, 1-23.

Lv, F., Li, X. and Wang, Y. (2022) Lycorine inhibits angiogenesis by docking to PDGFRα. *Bmc Cancer* **22**, 873.

Majhi, B.B., Gélinas, S.-E., Mérindol, N., Ricard, S. and Desgagné-Penix, I. (2023) Characterization of norbelladine synthase and noroxomaritidine/norcraugsodine reductase reveals a novel catalytic route for the biosynthesis of Amaryllidaceae alkaloids including the Alzheimer's drug galanthamine. *Frontiers in Plant Science* **14**, 1231809.

Manolov, S.P., Atanasova, S.N., Ghate, M. and Ivanov, I.I. (2015) A brief review of Cherylline synthesis.

Masi, M., Di Lecce, R., Mérindol, N., Girard, M.-P., Berthoux, L., Desgagné-Penix, I., Calabrò, V. and Evidente, A. (2022) Cytotoxicity and antiviral properties of alkaloids isolated from Pancratium maritimum. *Toxins* **14**, 262.

Mehta, N., Meng, Y., Zare, R., Kamenetsky-Goldstein, R. and Sattely, E. (2024) A developmental gradient reveals biosynthetic pathways to eukaryotic toxins in monocot geophytes. *Cell* **187**, 5620-5637. e5610.
Meißner, W. (1819) Ueber ein neues Pflanzenalkali (Alkaloid). *Journal für Chemie und Physik* **25**, 377-381.
Menéndez-Perdomo, I.M. and Facchini, P.J. (2020) Isolation and characterization of two O-methyltransferases involved in benzylisoquinoline alkaloid biosynthesis in sacred lotus (Nelumbo nucifera). *Journal of Biological Chemistry* **295**, 1598-1612.
Meng, F., Zhang, S., Su, J., Zhu, B., Pan, X., Qiu, X., Cui, X., Wang, C., Niu, L. and Li, C. (2024) Characterization of two CYP80 enzymes provides insights into aporphine alkaloid skeleton formation in Aristolochia contorta. *The Plant Journal*.
Merindol, N., Belem Martins, L.L., Elfayres, G., Custeau, A., Berthoux, L., Evidente, A. and Desgagné-Penix, I. (2024) Amaryllidaceae Alkaloids Screen Unveils Potent Anticoronaviral Compounds and Associated Structural Determinants. *ACS Pharmacology & Translational Science*.
Miettinen, K., Dong, L., Navrot, N., Schneider, T., Burlat, V., Pollier, J., Woittiez, L., Van Der Krol, S., Lugan, R. and Ilc, T. (2014) The seco-iridoid pathway from Catharanthus roseus. *Nature communications* **5**, 3606.
Morris, J.S., Caldo, K.M.P., Liang, S. and Facchini, P.J. (2021) PR10/Bet v1-like Proteins as Novel Contributors to Plant Biochemical Diversity. *ChemBioChem* **22**, 264-287.
Nair, J.J. and van Staden, J. (2014) Cytotoxicity studies of lycorine alkaloids of the Amaryllidaceae. *Natural product communications* **9**, 1934578X1400900834.
Nair, J.J. and van Staden, J. (2018) Antifungal constituents of the plant family Amaryllidaceae. *Phytotherapy Research* **32**, 976-984.
Nair, J.J. and van Staden, J. (2023) Antiviral Effects of the Plant Family Amaryllidaceae. *Natural Product Communications* **18**, 1934578X231162781.
Nair, J.J., Wilhelm, A., Bonnet, S.L. and van Staden, J. (2017) Antibacterial constituents of the plant family Amaryllidaceae. *Bioorganic & medicinal chemistry letters* **27**, 4943-4951.
Nasreen, A., Rueffer, M. and Zenk, M.H. (1996) Cytochrome P-450-dependent formation of isoandrocymbine from autumnaline in colchicine biosynthesis. *Tetrahedron letters* **37**, 8161-8164.
Negishi, O. and Negishi, Y. (2017) Phenylpropanoid 2, 3-dioxygenase involved in the cleavage of the ferulic acid side chain to form vanillin and glyoxylic acid in Vanilla planifolia. *Bioscience, biotechnology, and biochemistry* **81**, 1732-1740.
Nett, R.S., Lau, W. and Sattely, E.S. (2020) Discovery and engineering of colchicine alkaloid biosynthesis. *Nature* **584**, 148-153.
Nielsen, J. and Keasling, J.D. (2016) Engineering cellular metabolism. *Cell* **164**, 1185-1197.
Nomura, T. and Kutchan, T.M. (2010) Three new O-methyltransferases are sufficient for all O-methylation reactions of ipecac alkaloid biosynthesis in root culture of Psychotria ipecacuanha. *Journal of Biological Chemistry* **285**, 7722-7738.
Nour-Eldin, H.H. and Halkier, B.A. (2013) The emerging field of transport engineering of plant specialized metabolites. *Current opinion in biotechnology* **24**, 263-270.
O'Connor, S.E. (2015) Engineering of secondary metabolism. *Annual review of genetics* **49**, 71-94.
Ober, D. and Hartmann, T. (1999) Homospermidine synthase, the first pathway-specific enzyme of pyrrolizidine alkaloid biosynthesis, evolved from deoxyhypusine synthase. *Proceedings of the National Academy of Sciences* **96**, 14777-14782.
Othman, L., Sleiman, A. and Abdel-Massih, R.M. (2019) Antimicrobial activity of polyphenols and alkaloids in middle eastern plants. *Frontiers in microbiology* **10**, 911.
Pan, H., Zhou, R., Louie, G.V., Mühlemann, J.K., Bomati, E.K., Bowman, M.E., Dudareva, N., Dixon, R.A., Noel, J.P. and Wang, X. (2014) Structural studies of cinnamoyl-CoA reductase and cinnamyl-alcohol dehydrogenase, key enzymes of monolignol biosynthesis. *The Plant Cell* **26**, 3709-3727.

Parage, C., Foureau, E., Kellner, F., Burlat, V., Mahroug, S., Lanoue, A., Duge de Bernonville, T., Londono, M.A., Carqueijeiro, I. and Oudin, A. (2016) Class II cytochrome P450 reductase governs the biosynthesis of alkaloids. *Plant physiology* **172**, 1563-1577.
Petit, P., Granier, T., d'Estaintot, B.L., Manigand, C., Bathany, K., Schmitter, J.-M., Lauvergeat, V., Hamdi, S. and Gallois, B. (2007) Crystal structure of grape dihydroflavonol 4-reductase, a key enzyme in flavonoid biosynthesis. *Journal of molecular biology* **368**, 1345-1357.
Pichersky, E. and Lewinsohn, E. (2011) Convergent evolution in plant specialized metabolism. *Annual review of plant biology* **62**, 549-566.
Plaitakis, A. and Duvoisin, R.C. (1983) Homer's moly identified as Galanthus nivalis L.: physiologic antidote to stramonium poisoning. *Clinical neuropharmacology* **6**, 1-6.
Poyraz, S., Döndaş, H.A., Döndaş, N.Y. and Sansano, J.M. (2023) Recent insights about pyrrolidine core skeletons in pharmacology. *Frontiers in Pharmacology* **14**, 1239658.
Pyne, M., Narcross, L., Fossati, E., Bourgeois, L., Burton, E., Gold, N. and Martin, V. (2016) Reconstituting plant secondary metabolism in Saccharomyces cerevisiae for production of high-value benzylisoquinoline alkaloids. In: *Methods in enzymology* pp. 195-224. Elsevier.
Rasmussen, S. and Dixon, R.A. (1999) Transgene-mediated and elicitor-induced perturbation of metabolic channeling at the entry point into the phenylpropanoid pathway. *The Plant Cell* **11**, 1537-1551.
Reed, J. (2016) Transient expression for engineering triterpenoid diversity in plants. University of East Anglia.
Reed, J. and Osbourn, A. (2018) Engineering terpenoid production through transient expression in *Nicotiana benthamiana*. *Plant cell reports* **37**, 1431-1441.
Riddle, J.M. (1985) Ancient and medieval chemotherapy for cancer. *Isis* **76**, 319-330.
Ringer, K.L., McConkey, M.E., Davis, E.M., Rushing, G.W. and Croteau, R. (2003) Monoterpene double-bond reductases of the (−)-menthol biosynthetic pathway: isolation and characterization of cDNAs encoding (−)-isopiperitenone reductase and (+)-pulegone reductase of peppermint. *Archives of Biochemistry and Biophysics* **418**, 80-92.
Roberts, M.F. (1987) Papaver latex and alkaloid storage vacuoles. In: *Plant vacuoles: their importance in solute compartmentation in cells and their applications in plant biotechnology* pp. 513-528. Springer.
Robertson, J. and Stevens, K. (2014) Pyrrolizidine alkaloids. *Natural product reports* **31**, 1721-1788.
Robins, R.J. and Walton, N.J. (1993) The biosynthesis of tropane alkaloids. In: *The alkaloids: chemistry and pharmacology* pp. 115-187. Elsevier.
Salim, V. and De Luca, V. (2013) Towards complete elucidation of monoterpene indole alkaloid biosynthesis pathway: Catharanthus roseus as a pioneer system. In: *Advances in botanical research* pp. 1-37. Elsevier.
Salim, V., Jones, A.D. and DellaPenna, D. (2018) Camptotheca acuminata 10-hydroxycamptothecin O-methyltransferase: an alkaloid biosynthetic enzyme co-opted from flavonoid metabolism. *The Plant Journal* **95**, 112-125.
Samanani, N., Liscombe, D.K. and Facchini, P.J. (2004) Molecular cloning and characterization of norcoclaurine synthase, an enzyme catalyzing the first committed step in benzylisoquinoline alkaloid biosynthesis. *The Plant Journal* **40**, 302-313.
Sattler, S.A., Walker, A.M., Vermerris, W., Sattler, S.E. and Kang, C. (2017) Structural and biochemical characterization of cinnamoyl-CoA reductases. *Plant physiology* **173**, 1031-1044.
Schenck, C.A. and Maeda, H.A. (2018) Tyrosine biosynthesis, metabolism, and catabolism in plants. *Phytochemistry* **149**, 82-102.
Schramm, S., Köhler, N. and Rozhon, W. (2019) Pyrrolizidine alkaloids: biosynthesis, biological activities and occurrence in crop plants. *Molecules* **24**, 498.
Seigler, D.S. (2012) *Plant secondary metabolism*:Springer Science & Business Media.
Shamma, M. (2012) *The isoquinoline alkaloids chemistry and pharmacology*:Elsevier.

Shang, X.F., Morris-Natschke, S.L., Liu, Y.Q., Guo, X., Xu, X.S., Goto, M., Li, J.C., Yang, G.Z. and Lee, K.H. (2018) Biologically active quinoline and quinazoline alkaloids part I. *Medicinal research reviews* **38**, 775-828.
Shen, L., Zhao, J., Xia, Y., Lu, J., Sun, J., Tang, J., Xing, H., Yin, L., Yang, Y. and Wang, C. (2024) Lycorine derivative effectively inhibits the replication of coronaviruses both *in vitro* and *in vivo*. *hLife* **2**, 75-87.
Shende, V.V., Bauman, K.D. and Moore, B.S. (2024) The shikimate pathway: gateway to metabolic diversity. *Natural product reports* **41**, 604-648.
Shintani, D. and DellaPenna, D. (1998) Elevating the vitamin E content of plants through metabolic engineering. *Science* **282**, 2098-2100.
Singh, A. and Desgagné-Penix, I. (2017) Transcriptome and metabolome profiling of Narcissus pseudonarcissus 'King Alfred'reveal components of Amaryllidaceae alkaloid metabolism. *Scientific reports* **7**, 1-14.
Singh, R., Poonam and Geetanjali (2019) Chemotaxonomic Significance of Alkaloids in Plants. In: *Biodiversity and Chemotaxonomy* pp. 121-136. Springer.
Singh, T.P. and Singh, O.M. (2018) Recent progress in biological activities of indole and indole alkaloids. *Mini reviews in medicinal chemistry* **18**, 9-25.
Soll, J., Kemmerling, M. and Schultz, G. (1980) Tocopherol and plastoquinone synthesis in spinach chloroplasts subfractions. *Archives of biochemistry and biophysics* **204**, 544-550.
Srinivasan, P. and Smolke, C.D. (2020) Biosynthesis of medicinal tropane alkaloids in yeast. *Nature* **585**, 614-619.
Stadler, R. and Zenk, M. (1993) The purification and characterization of a unique cytochrome P-450 enzyme from Berberis stolonifera plant cell cultures. *Journal of Biological Chemistry* **268**, 823-831.
Stanilova, M.I., Molle, E.D. and Yanev, S.G. (2010) Galanthamine production by Leucojum *aestivum* cultures *in vitro*. *The alkaloids: chemistry and biology* **68**, 167-270.
Strunz, G.M. and Findlay, J.A. (1985) Pyridine and piperidine alkaloids. In: *The alkaloids: chemistry and pharmacology* pp. 89-183. Elsevier.
Su, Y., Li, H.P., Zhang, M., Ding, X.W., Xu, J.H., Chen, Q. and Zheng, G.W. (2022) Regioselectivity Inversion of an O-Methyltransferase via Semi-rational Mutagenesis Combined with Metal Ion Substitution. *ChemCatChem* **14**, e202200844.
Suhadolnik, R., Fischer, A. and Zulalian, J. (1963) Biogenesis of the amaryllidaceae alkaloids. III. Phenylalanine and protocatechuic aldehyde as C6-C1 precursors of haemanthamine and lycorine. In: *Proc Chem Soc* pp. 208-212.
Sun, B., Wang, P., Wang, R., Li, Y. and Xu, S. (2018) Molecular Cloning and Characterization of a meta/para-*O*-Methyltransferase from Lycoris aurea. *International journal of molecular sciences* **19**, 1911.
Tan, C.-X., Schrader, K.K., Mizuno, C.S. and Rimando, A.M. (2011) Activity of lycorine analogues against the fish bacterial pathogen Flavobacterium columnare. *Journal of agricultural and food chemistry* **59**, 5977-5985.
Tousignant, L., Diaz-Garza, A.M., Majhi, B.B., Gélinas, S.-E., Singh, A. and Desgagne-Penix, I. (2022) Transcriptome analysis of Leucojum *aestivum* and identification of genes involved in norbelladine biosynthesis. *Planta* **255**, 1-23.
Tuzimski, T. and Petruczynik, A. (2023) New trends in the practical use of isoquinoline alkaloids as potential drugs applicated in infectious and non-infectious diseases. *Biomedicine & Pharmacotherapy* **168**, 115704.
Unterlinner, B., Lenz, R. and Kutchan, T.M. (1999) Molecular cloning and functional expression of codeinone reductase: the penultimate enzyme in morphine biosynthesis in the opium poppy Papaver somniferum. *The Plant Journal* **18**, 465-475.

Valletta, A., Iozia, L.M., Fattorini, L. and Leonelli, F. (2023) Rice phytoalexins: half a century of amazing discoveries; part I: distribution, biosynthesis, chemical synthesis, and biological activities. *Plants* **12**, 260.

van Herpen, T.W., Cankar, K., Nogueira, M., Bosch, D., Bouwmeester, H.J. and Beekwilder, J. (2010) *Nicotiana benthamiana* as a production platform for artemisinin precursors. *PLoS One* **5**, e14222.

Vargas, F.C. (2008) Plant motifs on Inca ceremonial vases from Peru*. *Botanical Journal of the Linnean Society* **82**, 313-325.

Velásquez, A.C., Chakravarthy, S. and Martin, G.B. (2009) Virus-induced gene silencing (VIGS) in *Nicotiana benthamiana* and tomato. *Journal of visualized experiments: JoVE*.

Wang, B., Kashkooli, A.B., Sallets, A., Ting, H.-M., de Ruijter, N.C., Olofsson, L., Brodelius, P., Pottier, M., Boutry, M. and Bouwmeester, H. (2016) Transient production of artemisinin in *Nicotiana benthamiana* is boosted by a specific lipid transfer protein from A. annua. *Metabolic Engineering* **38**, 159-169.

Wang, Y., Shi, Y., Li, K., Yang, D., Liu, N., Zhang, L., Zhao, L., Zhang, X., Liu, Y. and Gao, L. (2021) Roles of the 2-oxoglutarate-dependent dioxygenase superfamily in the flavonoid pathway: a review of the functional diversity of F3H, FNS I, FLS, and LDOX/ANS. *Molecules* **26**, 6745.

Wen, M., Zeng, J., Qiu, F., Zhang, F. and Liao, Z. (2024) De Novo Synthesis of Anticholinergic Hyoscyamine and Scopolamine in *Nicotiana benthamiana* Based on Elucidating Tropane Alkaloid Biosynthetic Pathway of Anisodus luridus. *Agronomy* **14**, 2460.

Wijekoon, C.P. and Facchini, P.J. (2012) Systematic knockdown of morphine pathway enzymes in opium poppy using virus-induced gene silencing. *The Plant Journal* **69**, 1052-1063.

Wilkinson, D., Murray, J.i. and Group, G.R. (2001) Galantamine: a randomized, double-blind, dose comparison in patients with Alzheimer's disease. *International journal of geriatric psychiatry* **16**, 852-857.

Wink, M. (2015) Modes of action of herbal medicines and plant secondary metabolites. *Medicines* **2**, 251-286.

Winkel, B.S. (2004) Metabolic channeling in plants. *Annu. Rev. Plant Biol.* **55**, 85-107.

Winkler, A., Hartner, F., Kutchan, T.M., Glieder, A. and Macheroux, P. (2006) Biochemical evidence that berberine bridge enzyme belongs to a novel family of flavoproteins containing a bi-covalently attached FAD cofactor. *Journal of Biological Chemistry* **281**, 21276-21285.

Xiang, M.-L., Hu, B.-Y., Qi, Z.-H., Wang, X.-N., Xie, T.-Z., Wang, Z.-J., Ma, D.-Y., Zeng, Q. and Luo, X.-D. (2022) Chemistry and bioactivities of natural steroidal alkaloids. *Natural Products and Bioprospecting* **12**, 23.

Xiang, Y., Jiang, X., Li, J., Sun, B., Liu, Z., Li, D., Wu, M., Wang, R. and Xu, S. (2025) Functional characterization of aldo-keto reductase genes from Lycoris aurea that participate in galantamine biosynthesis. *Plant Science*, 112869.

Xiao, C., Zhou, G., He, T. and Li, C. (2025) Transport of secondary metabolites in plants: Mechanistic insights and transporter engineering for crop improvement. *Plant communications* **6**.

Xu, Z., Tian, Y., Wang, J., Ma, Y., Li, Q., Zhou, Y., Zhang, W., Liu, T., Kong, L. and Wang, Y. (2024) Convergent evolution of berberine biosynthesis. *Science Advances* **10**, eads3596.

Yang, F. (2017) Chemotaxonomy Study of Plants from the Family Proteaceae Based on Its Natural Product Profile (Alkaloid).

Yauk, Y.K., Chagné, D., Tomes, S., Matich, A.J., Wang, M.Y., Chen, X., Maddumage, R., Hunt, M.B., Rowan, D.D. and Atkinson, R.G. (2015) The O-methyltransferase gene M do OMT 1 is required for biosynthesis of methylated phenylpropenes in ripe apple fruit. *The Plant Journal* **82**, 937-950.

Zandavar, H. and Babazad, M.A. (2023) Secondary metabolites: Alkaloids and flavonoids in medicinal plants. In: *Herbs and Spices-New Advances*. IntechOpen.

Zhang, Y.-M., Li, T., Xu, C.-C., Qian, J.-Y., Guo, H., Zhang, X., Zhan, Z.-J. and Lu, J.-J. (2024) Uncover the anticancer potential of lycorine. *Chinese Medicine* **19**, 121.

Ziegler, J., Brandt, W., Geißler, R. and Facchini, P.J. (2009) Removal of substrate inhibition and increase in maximal velocity in the short chain dehydrogenase/reductase salutaridine reductase involved in morphine biosynthesis. *Journal of Biological Chemistry* **284**, 26758-26767.

Ziegler, J., Voigtländer, S., Schmidt, J., Kramell, R., Miersch, O., Ammer, C., Gesell, A. and Kutchan, T.M. (2006) Comparative transcript and alkaloid profiling in Papaver species identifies a short chain dehydrogenase/reductase involved in morphine biosynthesis. *The Plant Journal* **48**, 177-192.

applied sciences

MDPI

Article

Production of Dictyostelium discoideum Hybrid Type Enzyme SteelyA in the Diatom *Phaeodactylum tricornutum*

Nicolas Sene, Basanta Lamichhane, Sarah-Eve Gélinas, Alexandre Custeau, Natacha Merindol, Fatma Meddeb-Mouelhi and Isabel Desgagné-Penix *

Department of Biochemistry, Chemistry, Physics and Forensic Science, Université du Québec à Trois-Rivières, Trois-Rivières, QC G8Z 4M3, Canada; nicolas.sene@uqtr.ca (N.S.); basanta.lamichhane@uqtr.ca (B.L.); sarah-eve.gelinas@uqtr.ca (S.-E.G.); alexandre.custeau@uqtr.ca (A.C.); fatma.meddeb@uqtr.ca (F.M.-M.)

* Correspondence: isabel.desgagne-penix@uqtr.ca

Abstract

The bioproduction of high-value molecules offers a sustainable and cost-effective alternative to traditional extraction and chemical synthesis, particularly for complex metabolites like cannabinoids (CBs), which have therapeutic potential for neurodegenerative diseases. The marine diatom *Phaeodactylum tricornutum* presents a promising chassis for CB biosyn- thesis due to its high lipid content, essential building blocks to biosynthesize CBs. In this study, we explored the feasibility of producing olivetolic acid (OA), the key CB precursor, using a hybrid-type polyketide synthase, SteelyA, from *Dictyostelium discoideum*. Unlike the native *Cannabis sativa* enzymes—tetraketide synthase and olivetolic acid cyclase—which exhibit low productivity and stability in diatoms, SteelyA was expected to offer an alterna- tive biosynthetic route. Heterologous production in *P. tricornutum* resulted in a C-terminal fragment of the SteelyA enzyme, suggesting partial expression or processing of the very high-molecular-weight (352 kDa) SteelyA protein over six months without affecting cellular growth. However, HPLC-MS analysis did not detect intracellular OA or its derivatives *in vivo* and *in vitro*, suggesting enzymatic inactivity or metabolic limitations. These negative findings highlight the need for further investigation into the metabolic and proteomic requirements for CB precursor biosynthesis in diatoms, guiding future optimization strategies for sustainable cannabinoid production.

Keywords: metabolic engineering; cannabinoids; cannabinoid precursor; microalgae; diatom bioengineering; heterologous production; high-molecular-weight protein; hybrid polyketide synthase; olivetolic acid; *Phaeodactylum tricornutum*; secondary metabolite biosynthesis; SteelyA

check for updates

Academic Editor: Luca Mazzoni

Received: 16 September 2025

Revised: 15 October 2025

Accepted: 22 October 2025

Published: 31 October 2025

Citation: Sene, N.; Lamichhane, B.; Gélinas, S.-E.; Custeau, A.; Merindol, N.; Meddeb-Mouelhi, F.; Desgagné-Penix, I. Production of *Dictyostelium discoideum* Hybrid Type Enzyme SteelyA in the Diatom *Phaeodactylum tricornutum*. *Appl. Sci.* **2025**, *15*, 11679. https://doi.org/10.3390/ app152111679

Copyright: © 2025 by the authors. Licensee MDPI, Basel, Switzerland. This article is an open access article distributed under the terms and conditions of the Creative Commons Attribution (CC BY) license (https://creativecommons.org/licenses/by/4.0/).

Annex 2; Research Paper (Co-authorship)

Plant Physiology and Biochemistry 226 (2025) 110067

Contents lists available at ScienceDirect

Plant Physiology and Biochemistry

journal homepage: www.elsevier.com/locate/plaphy

Coclaurine *N*-methyltransferase-like enzymes drive the final biosynthetic reaction of the anti-Alzheimer's drug galanthamine in *Amaryllidaceae*

Nuwan Sameera Liyanage [a], Basanta Lamichhane [a], Elisa Fantino [a], Natacha Merindol [a], Sarah-Eve Gelinas [a], Maria Camila García Tobon´ [a], Isabel Desgagne-Penix [a,b,*]

[a] *Department of Chemistry, Biochemistry and Physics, Universite du Quebec a Trois-Rivieres, Trois-Rivieres, QC, Canada* [b] *Plant Biology Research Group, Trois-, Quebec, Canada*

ARTICLEINFO

Keywords:
Alkaloids
Norgalanthamine
Specialized metabolism
Hippeastrum papilio
Leucojum aestivum
Lycoris radiata
Substrate promiscuity
Molecular docking
Environmental stress

ABSTRACT

Galanthamine, an isoquinoline alkaloid used to treat symptoms of Alzheimer's disease, is predominantly extracted from *Amaryllidaceae* plants, yet its supply remains limited. In this study, we identified, isolated, and characterized *N*-methyltransferases (NMTs) from three galanthamine-producing species: *Leucojum aestivum Lycoris radiata*, and *Hippeastrum papilio*. The transcriptomic analysis identified five unique NMT isoforms, among which *LaLrHp*NMT1, an isoform highly conserved across all three species, exhibited the highest catalytic activity. Phylogenetic and analyses revealed that these enzymes share high sequence conservation and maintain the class I methyltransferase Rossmann fold with key catalytic residues, paralleling known NMTs from benzylisoquinoline alkaloid pathways. Flexible docking simulations confirmed that norgalanthamine, a crucial precursor, fits within the enzyme's active site and interacts with conserved residues Glu204 and His208. *In vitro* and *in planta* assays demonstrated that *LaLrHp*NMT1 efficiently catalyzes the *N*-methylation of norgalanthamine to galanthamine. Site-directed mutagenesis confirmed the key role of Glu204 and the participation of Phe residues in substrate stabilization. Additional enzyme assays revealed that *LaLrHp*NMT1 is promiscuous towards various alkaloid intermediates, while subcellular localization using eGFP-tagged constructs exposed a dual distribution in the cytosol and endoplasmic reticulum, suggesting that NMT activity occurs at the cytosol–ER interface where other biosynthetic enzymes reside. Environmental stress experiments in *H. papilio* shoots culture showed significant upregulation of *NMT* expression under heat and other stress conditions associated with AA levels modulation, indicating a potential link between stress responses and alkaloid biosynthesis. These findings deepen our understanding of galanthamine biosynthesis and provide a foundation for metabolic engineering strategies aimed at improving production yields.

Annex 3; Research Paper (Co-authorship)

Kinetic and in silico structural characterization of norbelladine O-methyltransferase of Amaryllidaceae alkaloids biosynthesis

Received for publication, April 8, 2024, and in revised form, July 24, 2024 Published, Papers in Press, August 8, 2024,
https://doi.org/10.1016/j.jbc.2024.107649

Manoj Koirala[1], Natacha Merindol[1], Vahid Karimzadegan[1], Sarah-Eve Gélinas[1], Nuwan Sameera Liyanage[1], Basanta Lamichhane[1], Maria Camila García Tobón[1], Patrick Lagüe[2], and Isabel Desgagné-Penix[1,3,*]

From the [1]Department of Chemistry, Biochemistry and Physics, Université du Québec à Trois-Rivières, Trois-Rivières, Québec, Canada; [2]Department of Biochemistry, Microbiology and Bioinformatics, Laval University, Québec, Canada; [3]Plant Biology Research Group, Trois-Rivières, Québec, Canada

* For correspondence: Isabel Desgagné-Penix, Isabel.Desgagne-Penix@uqtr. ca.

Reviewed by members of the JBC Editorial Board. Edited by Sarah E. O'Connor

Amaryllidaceae alkaloids are a diverse group of alkaloids exclusively reported from the Amaryllidaceae plant family. In planta, their biosynthesis is still not fully characterized; however, a labeling study established 4^0-*O*-methylnorbelladine as the key intermediate compound of the pathway. Previous reports have characterized O-methyltransferases from several Amaryllidaceae species. Nevertheless, the formation of the different O-methylnorbelladine derivatives (3^0-*O*-methylnorbelladine, 4^0-*O*-methylnorbelladine, and 3^04^0-*O*-dimethylnorbelladine), the role, and the preferred substrates of O-methyltransferases are not clearly understood. In this study, we performed the biochemical characterization of an O-methyltransferase candidate from Narcissus papyraceus (NpOMT) *in vitro* and *in vivo*, following biotransformation of norbelladine in *Nicotiana benthamiana* having transient expression of NpOMT. Docking analysis was further used to investigate substrate preferences, as well as key interacting residues of NpOMT. Our study shows that NpOMT methylates norbelladine preferentially at the 4^0-OH position *in vitro* and in planta. Interestingly, NpOMT also catalyzed the synthesis of 3^0,4^0-*O*-dimethylnorbelladine from norbelladine and 4^0-*O*-methylnorbelladine during *in vitro* enzymatic assay. Furthermore, we show that NpOMT methylates 3,4-dihydroxybenzylaldehyde and caffeic acid in a nonregiospecific manner to produce meta/para monomethylated products. This study reveals a novel catalytic potential of an Amaryllidaceae O-methyltransferase and its ability to regioselectively methylate norbelladine in the heterologous host *N. benthamiana*.

Annex 4; Research Paper (Co-authorship)

Phytochemistry 216 (2023) 113883

Contents lists available at ScienceDirect

Phytochemistry

journal homepage: www.elsevier.com/locate/phytochem

Auxin and light-mediated regulation of growth, morphogenesis, and alkaloid biosynthesis in *Crinum* x *powellii* 'Album' callus

Manoj Koirala [a], Karen Cristine Goncalves dos Santos [a], Sarah-Eve G´elinas [a], Simon Ricard [a], Vahid Karimzadegan [a], Basanta Lamichhane [a], Nuwan Sameera Liyanage [a], Natacha Merindol [a], Isabel Desgagn´e-Penix [a,b,*]

[a] *Department of Chemistry, Biochemistry and Physics, Universit´e du Quebec a Trois-Rivieres, Trois-Rivieres, QC, Canada*
[b] *Plant Biology Research Group, Trois-Rivieres, Quebec, Canada*

ARTICLEINFO

Keywords:
Amaryllidaceae alkaloids
Stress
Transcriptomic study AAs
biosynthesis pathway
specialized metabolism
multi-omics

ABSTRACT

Crinum x *powellii* 'Album' belongs to the Amaryllidaceae medicinal plant family that produces a range of structurally diverse alkaloids with potential therapeutic properties. The optimal conditions for *in vitro* tissue growth, morphogenesis, and alkaloid biosynthesis remain unclear. Auxin and light play critical roles in regulating plant growth, development, and alkaloid biosynthesis in several *Amaryllidaceae* plants. Here, we have succeeded in showing, for the first time, that the combination of auxin and light significantly influence *C.* x *powellii* "Album" *in vitro* tissue growth, survival, and morphogenesis compared to individual treatments. Furthermore, this combination also upregulates the expression of alkaloid biosynthetic genes and led to an increase in the content of certain alkaloids, suggesting a positive impact on the defense and therapeutic potential of the calli. Our findings provide insights into the regulation of genes involved in alkaloid biosynthesis in *C.* x *powellii* "Album" callus and underline the potential of auxin and light as tools for enhancing their production in plants. This study provides a foundation for further exploration of *C.* x *powellii* "Album" calli as a sustainable source of bioactive alkaloids for pharmaceutical and agricultural applications. Furthermore, this study paves the way to the discovery of the biosynthetic pathway of specialized metabolites from *C.* x *powellii* "Album", such as cherylline and lycorine.